Using yeast to study neurodegenerative diseases: Amyloid formation as a protective mechanism and a new Alzheimer's disease model

by

Sebastian Treusch

B.S. Molecular and Cellular Biology
University of Arizona, 2004

Submitted to the Department of Biology in partial fulfillment of the requirements for the degree of

DOCTOR OF PHILOSOPHY IN BIOLOGY

at the

MASSACHUSETTS INSTITUTE OF TECHNOLOGY

June 2011

Signature of Author:_____
Sebastian Treusch
Department of Biology

Certified by:_____
Susan L. Lindquist
Professor of Biology
Thesis Supervisor

Accepted by:_____
Robert T. Sauer
Professor of Biology
Co-Chair, Biology Graduate Committee

Using yeast to study neurodegenerative diseases: Amyloid formation as a protective mechanism and a new Alzheimer's disease model

by

Sebastian Treusch

Submitted to the Department of Biology on May 6, 2011 in Partial Fulfillment of the

Requirements for the Degree of Doctor of Philosophy in Biology

Abstract

Numerous neurodegenerative diseases are pathologically characterized by idiosyncratic protein amyloid inclusions. Not surprisingly amyloid fibrils have long been proposed to be the toxic protein species in these neurodegenerative diseases. However, more recent work has begun to suggest that the formation of ordered inclusions serves a protective role and that soluble oligomers on pathway to amyloid formation cause neuronal death. In that regard, ordered protein inclusions, such as aggresomes, have also been shown to facilitate the asymmetric inheritance of protein damage during the mitoses of cells ranging from E. coli to human stem cells.

Yeast prion proteins are another group of proteins capable of adapting an amyloid conformation. The self-templating amyloid fold allows yeast prions to act as non-Mendelian elements of inheritance. We have shown that yeast prion amyloid fibrils, especially upon prion protein overexpression, localize to the IPOD (insoluble protein deposit), an ordered inclusion proximal to the vacuole, and that the majority of the prion amyloid is asymmetrically inherited upon cell division.

I used the yeast prion Rnq1 to investigate how amyloid formation contributes to proteotoxicity. Ectopic overexpression of Rnq1 was extremely toxic, but only if the endogenous Rnq1 protein had adopted its amyloid conformation. The Hsp40 co-chaperone Sis1 was able to counteract the Rnq1-induced toxicity when co-overexpressed. In collaboration with Doug Cyr's lab I showed that Sis1-mediated amyloid formation was cytoprotective and that disordered non-amyloid aggregates induced toxicity. These results provide evidence that the formation of ordered inclusions can be cytoprotective.

I further characterized Rnq1 toxicity, conducted two genome-wide screens for modifiers and found that Rnq1 induced a G2/M cell cycle arrest. Rnq1 overexpression resulted in the mislocalization of the core spindle pole body component Spc42 to the IPOD and an unduplicated spindle pole body. In mammalian cells aggresomes localize to centrosomes, the mammalian equivalent of the yeast spindle pole body. The finding that a yeast prion can

interact with a spindle pole body component represents a new connection between the IPOD and aggresomes.

Lastly, I studied a yeast model of Aβ 1-42 toxicity. Accumulation of the amyloid beta peptide is thought to be causal in both sporadic and familial Alzheimer's disease. In collaboration with Kent Matlack I developed a yeast model that expressed Aβ 1-42 in a manner recapitulating mammalian Aβ 1-42 generation and that was amenable to screens for genetic modifiers of Aβ 1-42 toxicity. The screen identified the yeast homolog of PICALM, a known Alzheimer's disease risk factor. I showed that Aβ 1-42 expression resulted in a defect in endocytosis that could be reverted by several of the genetic suppressors. In collaboration with the Caldwell lab, we showed that the genetic modifiers also modulated Aβ 1-42 toxicity in a neuronal setting, *C. elegans* glutamatergic neurons. Finally, we showed that PICALM could protect primary rat cortical neuron cultures from Aβ oligomer toxicity.

Thesis Supervisor: Susan Lindquist
Title: Professor of Biology

Acknowledgements

First of all, I would like to thank my advisor Susan Lindquist. It has been a wonderful opportunity and great honor to have been a member of her lab. I learned a tremendous amount from her, not only as a scientist and writer but also as a person. I have heard that at the end of one's graduate career there is often nothing more to be learned in one's graduate lab. That certainly is not true for Sue's lab. Not only is Sue applying her vast expertise of protein folding to an extensive range of research areas, Sue is always looking to develop and employ new technologies and methods in her lab. Sue also has created a fantastic lab environment, full of amazing, as well as supportive, people.

My thesis committee has been very supportive and has provided an immense amount of valuable feedback on my thesis projects. Iain Cheeseman, David Housman and Jonathan King have been on my committee for several years. Li-Huei Tsai joined the committee for my defense and I am excited to get her feedback, especially on the Aβ project. Being able to get advice and feedback from my committee has been crucial. I want to thank Iain and David for their advice and support as I was preparing to interview for postdoctoral positions. Iain always took the time to talk and share his insights. I especially want to thank him for his encouragement and occasionally providing me with much needed perspective.

As I mentioned, Sue's lab is full of people that have supported me during my time in her lab. First and foremost, Brooke Bevis does a wonderful and essential job managing the lab and gracefully prevents it from slowly descending into chaos. She always takes the time to listen and has personally helped me through several "grad school moments" with her encouragements and practical advice. Martin Duennwald, a former postdoc with whom I rotated prior to joining the lab, helped me to get acclimated and started in the lab. He taught me techniques used throughout my thesis and even put together a mini yeast prion journal club

for me and another graduate student. My current and former bay mates Jens Tyedmers, Chris Pacheco and Dan Termine provided formative scientific discussions and welcome distraction. Although I am somewhat glad that we did not have Pandora when Jens and I shared the bay. I am not sure if I could have handled the amount of 80s music. I also want to thank my baymates for putting up with me and providing support when things were not going so well. And that goes for numerous other lab members as well.

The Aβ project would not have possible with out the help of Haesun Han and Kent Matlack. Haesun assisted me with the genetic screen. Kent not only started the Aβ project but also provided a lot of suggestions and great conversations along the way. Shu Hamamichi did a marvelous job with the Aβ *C. elegans* experiments. He even spent additional time in Alabama to complete them before joining the Lindquist lab. Simon Alberti, a former postdoc, generated an invaluable collection of expression constructs that facilitated several yeast experiments. Bob Burger does a simply outstanding job managing the financial side of the lab. Karen Allendorfer did an outstanding job proofreading many chapters of this thesis. Sven Heinrich gave me invaluable comments and suggestions on hot to write Chapter 3. I also would like to thank all the other current and former lab members for making the Lindquist lab such a fantastic place to do science.

Andreas Hochwagen, a current Whitehead Fellow, shared his knowledge of the cell cylce with me and gifted me several key reagents. The Whitehead simply has been a fantastic place to be a graduate student. Facilities, dish washing, and IT services have been incredible. The Whitehead microarray facility has been outstanding and George Bell was a huge help in analyzing Aβ microarray data.

I want to thank my parents for their love and support. They afforded me with many great opportunities, most importantly the opportunity to be independent.

Finally, my girl friend Jen is the best thing that happened to me during graduate school. She provided constant support, propping me up countless times, but also pointed out when I was being stubborn and needed to look at things from a different side. In addition she picked out Milan, our wirehair dachshund, who in his own way has been a huge help in writing this thesis; there is something very relaxing about chasing that little bugger around the coffee table.

Table of Contents

Figure List

Chapter: Introdution

Chapter Two: Chaperone-dependent amyloid assembly protects cells from prion toxicity

Chapter Three: Dissecting the detrimental effects of prion protein overexpression and the complex routes to its detoxification

Chapter Four: A yeast model connects Alzheimer's disease modifiers to Aβ toxicity

Table List

Chapter Three: Dissecting the detrimental effects of prion protein overexpression and the complex routes to its detoxification

Chapter Four: A yeast model connects Alzheimer's disease modifiers to Aβ toxicity

Appendix One: Prion induction involves an ancient system for the sequestration of aggregated proteins and heritable changes in prion fragmentation

Chapter One:

Introduction

Much of this chapter was published as “Amyloid deposits: Protection against toxic protein species?” *Cell Cycle* Sebastian Treusch, Douglas M. Cyr and Susan Lindquist. Sections on asymmetric inheritance of protein damage and yeast models of neurodegenerative diseases are new additions.

Abstract

Neurodegenerative diseases ranging from Alzheimer's disease and polyglutamine diseases to transmissible spongiform encephalopathies are associated with the aggregation and accumulation of misfolded proteins. In several cases the intracellular and extracellular protein deposits contain a fibrillar protein species called amyloid. However, while amyloid deposits are hallmarks of numerous neurodegenerative diseases, their actual role in disease progression remains unclear. Especially perplexing is the often poor correlation between protein deposits and other markers of neurodegeneration. As a result the question remains whether amyloid deposits are the disease causing species, the consequence of cellular disease pathology or even the result of a protective cellular response to misfolded protein species. Here we highlight studies that suggest that accumulation and sequestration of misfolded protein in amyloid inclusion bodies and plaques can serve a protective function. Furthermore, we discuss how exceeding the cellular capacity for protective deposition of misfolded proteins may contribute to the formation of toxic protein species. We also highlight how yeast model systems can be employed to study the proteotoxicity of amyloidogenic proteins and proteins implicated in neurodegeneration.

Introduction

The study of neurodegenerative diseases began over a hundred years ago when Alois Alzheimer identified fibrillar structures within the postmortem brain of a patient who had exhibited progressive cognitive dysfunction and psychosis (ALZHEIMER*, et al.*

1995). It is now known that the majority of neurodegenerative diseases characterized by progressive neuronal dysfunction and loss are associated with the deposition of misfolded proteins. These misfolded proteins are frequently found in a β-sheet rich fibrillar protein conformation known as amyloid (CAUGHEY*, et al.* 2003; NELSON*, et al.* 2005) (Figure C1.1). For more than forty years amyloid deposits were thought to be causative agents in the degenerative process (ROTH*, et al.* 1966). But the tables have turned. Recent studies suggest instead that a group of still poorly defined pre-amyloid species, rather than the amyloid deposits themselves, are the true toxic conformations (KAYED*, et al.* 2003; LESNE*, et al.* 2006; SHANKAR*, et al.* 2008; WALSH*, et al.* 2002) (Figure C1.1). These soluble prefibrillar oligomers share conformational characteristics independent of the proteins primary amino acid sequences and may share a common mechanism of toxicity (KAYED*, et al.* 2003). Indeed even proteins completely unrelated to disease, such as PI3 kinase and the *E. Coli* protein HypF-N, can be induced to form such prefibrillar structures in vitro and, when they do, they are toxic when applied extracellularly to cells in culture or injected into rat brains (BAGLIONI*, et al.* 2006; BUCCIANTINI*, et al.* 2002). The intra- and extracellular conversion of misfolded proteins into highly structured and less reactive amyloid forms may reduce the levels of these toxic protein species and therefore be protective.

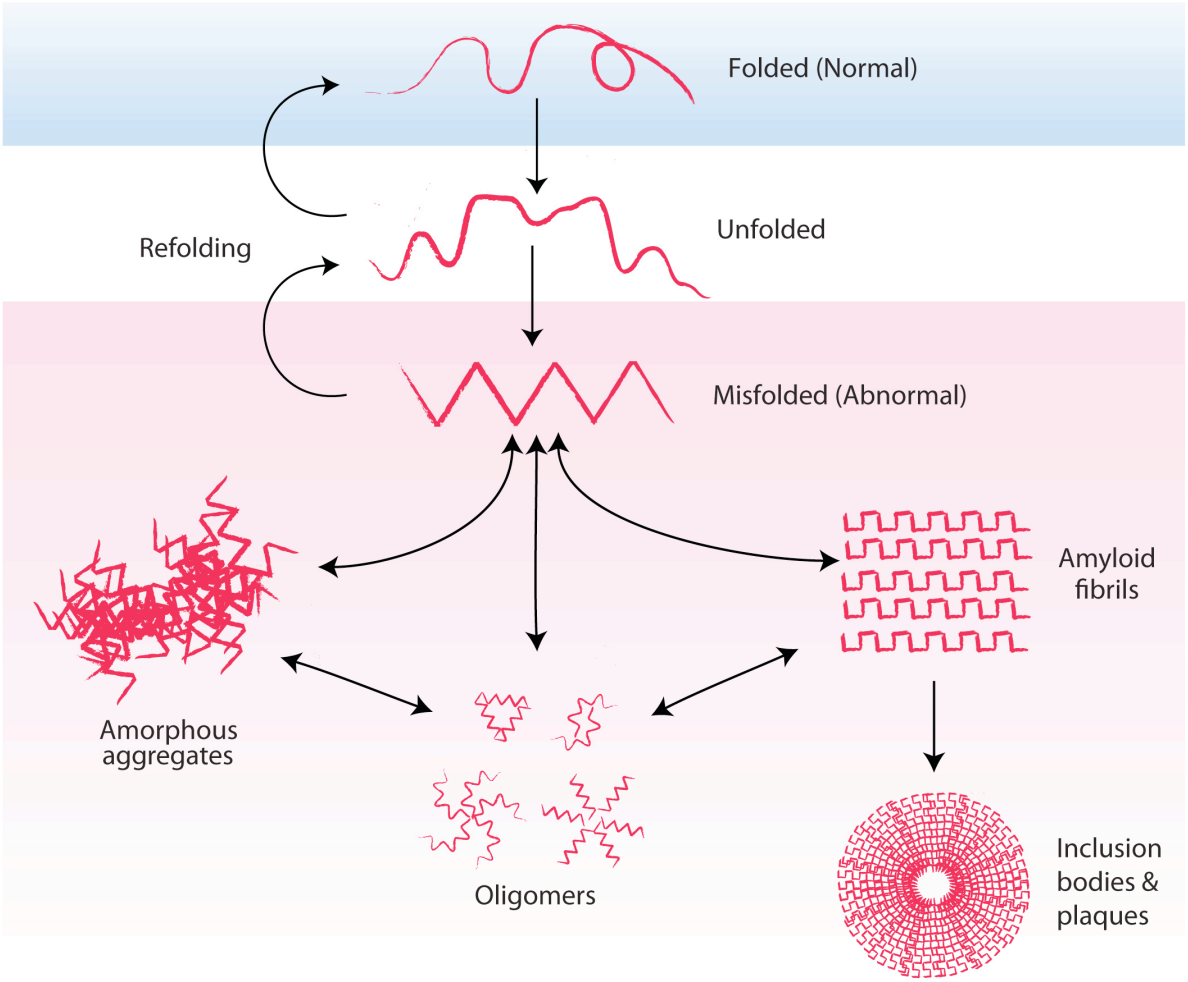

Figure C1.1 Aggregation of misfolded protein can give rise to oligomers, amorphous aggregates and inclusion bodies. The accumulation of misfolded protein leads to the formation of different protein assemblies. Prefibrillar oligomers formed by different proteins share a common structure and are thought to be the toxic protein species in diseases such as Alzheimer's and Huntington's (KAYED, *et al.* 2003; LESNE, *et al.* 2006). Oligomers are conformationaly molten and can associate to form amorphous aggregates or convert to an amyloidogenic nucleus to initiate amyloid fibril formation. Amyloid fibrils have a highly organized structure due to repeating β-sheets and are

insoluble. Amyloid fibrils are often found in intra- and extracellular inclusions such as inclusion bodies and amyloid plaques. The generation of amyloid fibers and inclusion bodies can protect cells by reducing the formation of highly interactive toxic oligomers and amorphous aggregates.

We focus on three neurodegenerative diseases, Alzheimer's, Huntington's and prion disease. We will first present studies in which the formation of inclusion bodies and amyloid plaques protects against proteotoxicity and then discuss how exceeding the cellular capacity for deposition of misfolded proteins may give rise to toxic protein species. Although these studies do not preclude detrimental effects of amyloid deposits in particular contexts (eg. obstructive vascular amyloid), they clearly show that amyloid formation can be beneficial. Furthmore, we highlight how yeast models have been used to garner insight into how the misfolded proteins central to these neurodegenerative diseases lead to cellular defects and ultimately death.

Pathological features associated with neurodegenerative diseases

The protein deposits found in Alzheimer's, Huntington's and prion disease are formed by completely unrelated proteins. They accumulate in distinct brain regions and have highly characteristic morphologies that form the basis of histological diagnosis. Neurodegeneration also affects distinct regions of the brain in each diseases, reflecting disease specific vulnerability of particular neurons (ELLISON*, et al.* 2004). However, in all three diseases the correlation between the localization of neurodegeneration and protein deposition is weak.

Alzheimer's disease (AD), the most common cause of dementia, most severely affects the temporal pole, hippocampus and amygdala (DUYCKAERTS*, et al.* 2003). AD is characterized by the accumulation of two very different proteins, each with a distinct

distribution. Aβ (amyloid β) peptide accumulates extracellularly in amyloid plaques while hyperphosphorylated tau, a microtubule binding protein, accumulates intracellularly in neurofibrillary tangles. A definitive pathological diagnosis of AD requires the detection of both types of aggregation. Aβ may accumulate in different plaque forms. Neuritic plaques, also referred to as classic or cored plaques, contain a dense amyloid core surrounded in turn by a ring of abnormal cellular processes and a rim of diffuse amyloid (DUYCKAERTS*, et al.* 2003; ELLISON*, et al.* 2004). In these neuritic plaques tau accumulation can also be present in dystrophic neurites surrounding the amyloid core.

It has been hypothesized that Aβ accumulation is the primary cause of pathogenesis in AD, yet there is a weak correlation between Aβ plaque density and the severity of dementia (ELLISON*, et al.* 2004). For example, brain samples of aged patients without clinical dementia can display abundant Aβ plaques (ELLISON*, et al.* 2004). To some extent this may be the consequence of Aβ accumulating in plaques without any associated neuritic degeneration (such as "burned-out" and "diffuse plaques"). Tau-containing neurofibrillary tangles correlate better with clinical severity of AD than Aβ plaques, but even here, the question remains whether tau aggregation itself is toxic or if it is the result of a protective mechanism (BRETTEVILLE*, et al.* 2008; CONGDON*, et al.* 2008; GOTZ*, et al.* 2008; HERNANDEZ*, et al.* 2008).

Huntington's disease (HD), classified as a hyperkinetic movement disorder, tends to affect brain regions distinct from those affected by Alzheimer's disease. HD is characterized by atrophy of the cerebral cortex, globus pallidus and striatum, specifically

with loss of medium spiny neurons within the neostriatum (CUMMINGS*, et al.* 2000; ROSS 2003; ZOGHBI*, et al.* 2000). HD is caused by CAG repeat expansions in the *huntingtin* gene, which lead to the accumulation of polyglutamine-expanded Huntingtin protein within intranuclear inclusion bodies or neurites (ELLISON*, et al.* 2004). The density of intranuclear inclusions correlates positively with the CAG repeat length present in the *huntingtin* gene (HEDREEN*, et al.* 2003). However neuronal vulnerability does not correspond to the cellular concentration of Huntingtin protein nor the distribution of Huntingtin inclusions (GUTEKUNST*, et al.* 1999). In fact there is a distinct dissociation of inclusion distribution and the selective pattern of striatal neuron loss, as few to no inclusions are detected in the vulnerable striatal neurons (KUEMMERLE*, et al.* 1999).

Prion diseases or spongiform encephalopathies can present in numerous ways, such as sporadic versus variant Creutzfeldt-Jakob disease (CJD). While the prion disease subtypes all involve the accumulation of a proteinase-K resistant form of the prion protein PrP (PrPres), they each affect different brain regions and involve distinct patterns of PrP aggregation (ELLISON*, et al.* 2004). Sporadic CJD causes spongiform change in the neuropil of the cerebral cortex, subcortical grey matter and cerebellar molecular layer (BUDKA*, et al.* 2003). The brainstem and spinal cord do not exhibit spongiform change although PrP deposits can be present. PrPres deposits in sporadic CJD are found in synaptic, perivacuolar, perineuronal and plaque-like patterns (BUDKA*, et al.* 2003). However neuronal loss correlates with microglial activation and axonal damage, but not with local deposition of PrPres. In contrast, variant CJD, caused by the consumption of meat from cows with Bovine Spongiform Encephalopathy, leads to the

presence of a large number of florid plaques in the cerbral and cerebellar cortex (IRONSIDE*, et al.* 2003). Florid plaques have a dense amyloid core, a pale radiating fibrillar periphery and are surrounded by a halo of spongiform change. Interestingly, spongiform change in variant CJD is most pronounced in the basal ganglia, which contain relatively few amyloid plaques (IRONSIDE*, et al.* 2003).

In summary, while the particular misfolded proteins vary in these diseases, in all three cases protein deposits are a poor indicator of neuronal loss. This makes it plausible that structured protein deposits help cells cope with misfolded proteins. In turn, the failure of particular neurons to create such deposits may cause their disease specific vulnerability.

Protein deposition as a cellular response to misfolded proteins

One of the first indications that protein inclusions may protect cells from toxic misfolded proteins came from a study investigating the response of tissue culture cells to either proteasome inhibitors or to overexpression of proteins targeted to the proteasome. The Kopito laboratory established that exceeding the proteasome's capacity to cope with misfolded proteins, by either perturbation, leads to the accumulation of stable aggregates at a distinct structure adjacent to the centrosome (JOHNSTON*, et al.* 1998). This structure was termed the aggresome to emphasize that its formation is a common cellular response to the presence of aggregated misfolded protein.

The aggresome is highly structured deposit of insoluble protein surrounded by a cage formed by the intermediate filament protein vimentin. Most strikingly, aggresomes are actively formed near the centrosome through dynein-dependent retrograde transport of protein aggregates along microtubules (GARCIA-MATA*, et al.* 1999; JOHNSTON*, et al.* 2002; JOHNSTON*, et al.* 1998). Far from being amorphous protein accumulations, aggresomes are formed through an active and conserved cellular process, that appears to serve a vital purpose: sweeping the cytoplasm clear of potentially toxic aggregates of misfolded proteins (KOPITO 2000).

In yeast, misfolded proteins can accumulate in two distinct compartments, the JUNQ (juxta-nuclear quality control compartment) and the IPOD (insoluble protein deposit) (KAGANOVICH*, et al.* 2008). The JUNQ forms mostly upon inhibition of the proteasome and contains poly-ubiquitinated proteins targeted for proteasomal degradation. The IPOD co-localizes with the pre-autophagosomal structure at the vacuole and contains amyloidogenic proteins, such as yeast prions as well as ectopically expressed mutant huntingtin exon one (both discussed below) (KAGANOVICH*, et al.* 2008; TYEDMERS*, et al.* 2010). Furthermore, a variant of mutant huntingtin exon one that does not localize to the IPOD can associate with the spindle pole body, the yeast equivalent of the centrosome (WANG*, et al.* 2009). This microtubule-dependent aggregation has been taken as evidence for aggresome formation in yeast. However, it remains unclear how the yeast quality control compartments, JUNQ and IPOD, relate to mammalian aggresomes (MATHUR*, et al.* 2010).

Asymmetric Inheritance of Damaged Proteins

Further support for the notion that protein inclusions serve a protective function has come from a different direction. In yeast oxidatively damaged proteins are retained in progenitor cells during mitosis (AGUILANIU*, et al.* 2003). While dispersed throughout the cytosol in young cells, oxidatively damaged proteins accumulate in aggregates during replicative aging. The segregation of these aggregates partially determines the life span and fitness of the progeny (ERJAVEC*, et al.* 2007). In *Escherichia coli* aggregates consisting of damaged proteins also are retained in the progenitor cells and contribute to the aging of those cells (LINDNER*, et al.* 2008).

In human embryonic stem cells polyubiquitinylated proteins were not only contained in aggresome-like deposits but also were inherited asymmetrically (FUENTEALBA*, et al.* 2008). Furthermore, tissue culture cells containing aggresomes of mutant huntingtin underwent mitoses during which only one of the daughter cells inherited the accumulated protein damage (RUJANO*, et al.* 2006). Most convincing are the findings from the examination of epithelial crypts of the small intestine of ataxia type 3 patients (RUJANO*, et al.* 2006). Similar to HD, this protein folding disease is caused by a polyglutamine expansion, albeit in the ataxin-3 protein instead of huntingtin. In these epithelial crypts, long-lived stem cells were devoid of ataxin-3 polyglutamine inclusions. On the contrary, short-lived terminally differentiated cells did contain polyglutamine inclusions (RUJANO*, et al.* 2006). These studies indicate that the deposition of damaged and misfolded proteins in aggresomes enables mitotic cells to asymmetrically segregate the accumulated damage to the cell with the shorter life

expectancy. This evolutionarily conserved mechanism allows one of the mitotic cells to start with a clean slate, ensuring its fitness and increasing its life expectancy (ERJAVEC*, et al.* 2007; RUJANO*, et al.* 2006). These studies show that, at least in mitotic cells, the intracellular formation of inclusion bodies serves a protective function. Furthermore, while protein damage has consistently been associated with neurodegeneration in aging individuals, these studies also suggest that, to an extent, aging is the accumulation of protein damage.

Protein deposition as a protective mechanism

A host of studies involving proteins linked to neurodegenerative diseases and other amyloidogenic proteins have investigated the role of inclusion and plaque formation in pathogenicity. The case is perhaps strongest for Huntington's disease, for which it has been postulated that inclusions cause toxicity due to the sequestration of proteins critical for cell homeostasis (PREISINGER*, et al.* 1999). Indeed, inclusions formed by mutant Huntingtin protein have been shown to sequester glyceraldehydes-3-phosphate dehydrogenase, to impair transcription due to sequestration of the transcriptional coactivator CREB binding protein, and to interfere with the function of the ubiquitin-proteasome system (BENCE*, et al.* 2001; BURKE*, et al.* 1996; NUCIFORA*, et al.* 2001). However smaller oligomeric species and loosely packed amorphous aggregates may be more prone to interact with and sequester proteins than densely packed amyloid deposits.

Indeed, several studies suggest that the formation of tightly packed Huntingtin deposits is beneficial for cell survival. The Greenberg lab demonstrated that transfection of mutant *huntingtin* into primary striatal neurons induced the formation of inclusions (SAUDOU*, et al.* 1998). The inclusions formed resembled protein deposits found in the brains of Huntington patients, as they were intranuclear and ubiquitinylated. But inclusions were not sufficient to induce apoptosis. On the contrary, inhibiting the ubiquitinylation of mutant Huntingtin prevented the formation of inclusions and actually increased cell death (SAUDOU*, et al.* 1998).

In a complementary study, the Finkbeiner group used time-lapse microscopy to follow the fate of individual *huntingtin* transfected neurons. The majority of neurons died without the formation of inclusion bodies and the formation of an inclusion body actually increased the probability of neuron survival (ARRASATE*, et al.* 2004). The formation of inclusion bodies directly correlated with a decrease in soluble Huntingtin, suggesting that inclusion bodies protect neurons by decreasing levels of soluble toxic isoforms of Huntingtin (ARRASATE*, et al.* 2004). Inclusion body formation could also serve a protective function by increasing the autophagic degradation of the aggregated protein species (TAYLOR*, et al.* 2003). Inclusions of mutant Huntingtin directly induce autophagy through sequestration of mTOR, a negative regulator of autophagy, and autophagy not only reduces the levels of aggregated but also soluble mutant huntingtin (RAVIKUMAR*, et al.* 2004; WILLIAMS*, et al.* 2008).

Together, these studies suggest that compounds elevating the formation of inclusion bodies, such as aggresomes, could lessen cellular pathology. On the other

hand compounds antagonizing the toxicity of mutant huntingtin by reducing its aggregation have been identified (EHRNHOEFER, *et al.* 2006). On the surface, this appears to conflict with the notion that promoting inclusions may be beneficial, but both, solubilization and inclusion body formation, may diminish the levels of toxic oligomers, the more critical species in pathogenesis. In fact, in a HD model a compound could prevent huntingtin-mediated proteasome dysfunction by promoting inclusion formation (BODNER, *et al.* 2006).

Although the characteristic protein deposits are found extracellularly in AD and prion disease, not intracellularly as in HD, here too studies suggest that structured protein deposits are less toxic than other conformers. As for HD, amyloid assembly may serve a beneficial function by shifting the equilibrium away from more toxic conformers, such as prefibrillar oligomers (KAYED, *et al.* 2003; LESNE, *et al.* 2006; WALSH, *et al.* 2002).

In a collaborative effort, the Kelly and Dillin laboratories investigated the roles of the aging process and the heat shock response in the formation of proteotoxic species in a *Caenorhabiditis elegans* model of AD. The intracellular expression of Aβ resulted in the formation of Aβ aggregates, but these aggregates did not correlate with toxicity (COHEN, *et al.* 2006). RNAi mediated repression of the insulin/IGF-1 receptor DAF-2, resulting in increased life span, reduced Aβ-mediated toxicity while slightly increasing the amount of Aβ aggregates. This protection depended on both *daf-16* and *hsf-1*. Interestingly, repression of DAF-16 reduced the number of high molecular weight Aβ aggregates, while repression of HSF-1 increased it. The Kelly and Dillin laboratories concluded that two dichotomous cellular pathways counteract Aβ toxicity: The HSF-1 pathway controls

disaggregation, while the DAF-16 pathway transforms toxic Aβ oligomers into larger Aβ aggregates of lower toxicity (COHEN, *et al.* 2006).

In a separate study by the Mucke group, a point mutation within Aβ, the Arctic mutation (Aβ E22G), influenced the rate at which Aβ assembled into amyloid fibers. *In vitro* and in transgenic mice, the Artic mutation enhanced formation of neuritic amyloid plaques and diminished non-amyloid Aβ assemblies (CHENG, *et al.* 2007). As non-amyloid Aβ assemblies correlated with behavioral and neuronal deficits in these transgenic mice, the promotion of Aβ amyloid fibril formation, without a coinciding increase in oligomeric Aβ, may be beneficial.

Most recently, in a follow-up study of a clinical trial, the immunization of AD patients with the full length Aβ peptide exhibited reduced Aβ immunostaining and amyloid plaques (HOLMES, *et al.* 2008). Unfortunately, immunization neither slowed nor stopped the progression of neurodegeneration. As immunization with Aβ peptide may not have reduced the levels of toxic oligomeric Aβ species, the authors suggest, that immunization specifically against oligomeric Aβ species may be more successful at halting neurodegeneration.

Plaque formation may also prove beneficial in the case of prion disease. PrPres isoforms, the protease resistant forms of PrP that include amyloid, are not toxic on their own. Mice that do not express their own PrP protein (Prn-$p^{0/0}$) are completely resistant to the intracerebral injection of even very high doses PrPres (BUELER, *et al.* 1993). Equally striking, mice producing a secreted form of PrP, GPI anchor-less PrP, accumulated massive plaque-like amyloid deposits, yet had no clinical manifestations of prion disease

(CHESEBRO, *et al.* 2005). Some brain lesions were present, but there was less neurodegeneration associated with these amyloid plaques than with diffuse wild type PrPres deposits. These results were especially significant as transgenic mice had up to 40% more PrPres in comparison to mice with WT PrP (CHESEBRO, *et al.* 2005). Using human tissue samples, the Barron laboratory showed that the accumulation of certain forms of PrPres failed to result in spongiform degeneration. Brain extracts from two cases of familial prion disease were used to test the transmission of disease to transgenic mice. One of the samples exhibited PrPres deposits and spongiform change, while the other presented with PrPres deposits and no spongiform change. Brain extract from the patient without spongiform degeneration did not result in disease transmission but elicited PrPres deposition in large multicentric plaques. Therefore, PrPres would appear to be rendered nonpathogenic by its sequestration in amyloid plaques (PICCARDO, *et al.* 2007).

Lessons on protective aggregation from a yeast model

Yeast prion proteins, just as PrP, can adopt self-perpetuating conformational states. In yeast, however, prions do not cause disease, but rather serve as heritable genetic elements, perpetuated by the transfer of the prion template from mother to daughter cell (SHORTER, *et al.* 2005). The heritable protein conformation of the yeast prions is amyloid in nature and, as for Aβ, Huntingtin and PrP, amyloid formation by the yeast prion proteins proceeds through intermediate oligomeric protein species (CHITI, *et al.* 2006; SERIO, *et al.* 2000). In fact, the observation that prefibrillar oligomers are

intermediates in amyloid formation was first made for the yeast prion protein Sup35 (SERIO, *et al.* 2000; SHORTER, *et al.* 2004). Oligomers formed by the yeast prion protein Sup35 share structural features with the oligomers formed by disease-related amyloidogenic proteins, including recognition by anti-oligomeric antibodies and interaction with specific small compounds (SHORTER, *et al.* 2004; WANG, *et al.* 2008). Thus the study of yeast prions can provide insight into amyloid formation and cellular responses to the presence of amyloid.

The yeast prion [*RNQ+*] is formed by the Rnq1 protein (The cytoplasmic inheritance of yeast prions is designated by [ ]). Rnq is nonessential and has no known biological function, except when it is in prion state (SONDHEIMER, *et al.* 2000). In this case the [*RNQ+*] prion interacts with other amyloidogenic proteins *in vivo* and enables them to adopt their amyloid conformation. For example, [*RNQ+*] facilitates the *de novo* induction of the [*PSI+*] prion state by enhancing the amyloid conversion of the yeast prion protein Sup35 (DERKATCH, *et al.* 2001).

We recently reported that moderate ectopic overexpression of Rnq1 is extremely toxic if endogenous Rnq1 is in the [*RNQ+*] prion conformation (DOUGLAS, *et al.* 2008). While overexpression of Rnq1 did result in the formation of amyloid inclusions, as assessed by Thioflavin-T staining, semi-denaturing agarose gels and *in vitro* seeding assays, the amyloid conformation did not represent the toxic species. In fact, co-expression of an Hsp40 chaperone, Sis1, known to interact with the prion form of Rnq1 (SONDHEIMER, *et al.* 2001), suppressed the toxicity elicited by Rnq1 overexpression by promoting Rnq1 assembly into amyloid. Mutants of Rnq1, impaired in their interaction

with the chaperone and their ability to readily form amyloid, exhibited enhanced toxicity. Chaperones have been shown to antagonize toxicity associated with protein misfolding before, but in those cases overexpressed chaperones either decreased protein aggregation (CUMMINGS*, et al.* 1998) or appeared to have no observable effect on protein aggregation (WARRICK*, et al.* 1999). This study presents the first instance in which a chaperone antagonizes the toxicity of a misfolding protein by facilitating its deposition into an amyloid inclusion. It clearly demonstrates that actively promoting the formation of inclusion bodies and even amyloid plaques may prove beneficial in protein misfolding pathologies.

Formation of toxic protein species due to non-productive templating

While the formation of aggresomes and extracellular amyloid plaques appears to serve a protective function, they could be associated with toxicity if their assembly is overwhelmed by the amount of protein damage or impeded by other molecular and cellular factors. As shown by the Kampinga group, aggresome formation by mutant huntingtin in tissue culture cells did not affect the cellular progression through mitosis. However, when the mutant huntingtin formed scattered secondary inclusions, the completion of mitosis was delayed or even failed completely (RUJANO*, et al.* 2006). The Kampinga group speculated that these secondary inclusions, distinct from aggresomes, form when the process of aggresome formation is saturated (RUJANO*, et al.* 2006). These results are reminiscent of our studies in which overexpression of the yeast prion protein Rnq1 resulted in toxicity when it exceeded the cellular capacity to efficiently assemble

the prion protein into amyloid. The toxicity of Rnq1 overexpression was exacerbated by factors interfering with amyloid assembly, such as repression of Sis1, the chaperone required for Rnq1 amyloid formation, or mutations within Rnq1, which reduce its interaction with the chaperone (DOUGLAS*, et al.* 2008).

Importantly, Rnq1 overexpression only resulted in toxicity if the endogenous Rnq1 protein was in its [*RNQ+*] prion conformation, making the otherwise benign prion state a prerequisite for Rnq1 mediated toxicity. Interestingly, the Rnq1 prion state is also required for toxicity of mutant huntingtin exon 1 in yeast models of Huntington's disease (MERIIN*, et al.* 2002). While the Rnq1 prion conformation usually acts as a template for the conversion of soluble Rnq1 protein conformers into benign amyloid conformers, we hypothesize that this process can also result in the formation of toxic protein species. We refer to this as non-productive templating, which occurs when the cellular capacity to facilitate amyloid formation is exceeded or impeded (Figure C1.2).

The notion of non-productive templating offers a unifying explanation for the observation that amyloid formation is sometimes associated with toxicity even when the amyloid form itself is benign. We discuss two cases in point: As mentioned earlier, the expression of GPI-anchorless PrP resulted in the formation of amyloid plaques but was not overtly toxic. However, when GPI-anchorless PrP was expressed together with WT PrP, deposits of both amyloid and non-amyloid PrPres formed and the clinical manifestations of scrapie disease were enhanced (CHESEBRO*, et al.* 2005). It has been suggested that PrPres subverts a stress protective function of PrP into an apoptotic signal (RAMBOLD*, et al.* 2008). The toxic signal elicited is dependent on the presence of

PrPres and the expression of GPI-anchored PrP (RAMBOLD, *et al.* 2008). PrPres may influence the folding state of the GPI-anchored PrP through incomplete templating and thus cause the induction of a toxic signal.

The second case in point involves the fungal prion [Het-s]. Non-productive templating can explain how the [Het-s] prion mediates heterokaryon incompatibility in the fungus *Podospora anserina* (COUSTOU-LINARES, *et al.* 2001). Heterokaryon incompatability, a type of programmed cell death, results when two cells with incompatible geneotypes, *het-s* and *het-S*, fuse to form a mixed cytoplasm. The two alleles encode distinct sequence variants of the Het-s protein. One, HET-s, is able to form the [Het-s] prion, where as the other, HET-S, cannot adopt an amyloid conformation. The prion form of the HET-s allele by itself is completely benign. However, if the HET-S allele is expressed in the presence of the [Het-s] prion form it results in cell death. The interaction of HET-s protein with the [Het-s] prion form leads to the templated formation of additional non-toxic prion amyloid. On the other hand, we speculated that non-productive templating of the HET-S protein variant, which cannot form amyloid, by the [Het-s] prion form leads to the formation of a toxic misfolded species resulting in cell death (Figure C1.2).

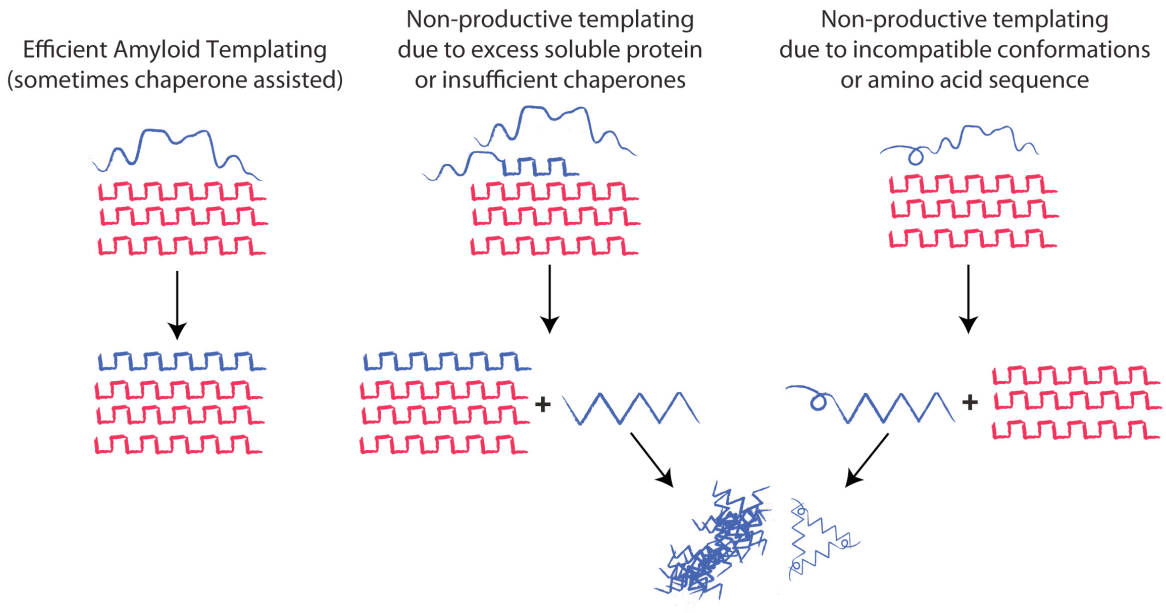

Figure C1.2 Amyloid and Non-productive templating.

Amyloid fibrils grow by causing protein of the same amino-acid sequence to adopt the same amyloid conformation. This is referred to as amyloid templating and involves the efficient addition of monomer or oligomeric species to the amyloid fiber, which maybe assisted by specific chaperones (e.g. Rnq1 and the Hsp40 Sis1, Sup35NM and Hsp104 (SHORTER, *et al.* 2004)). If the amount of substrate exceeds the cellular capacity for amyloid conversion or if amino acid sequences are incompatible, the interaction with the amyloid fibrils may give rise to other abnormal conformational species, which may go on to form toxic oligomers and amorphous aggregates (Rnq1, PrP and Het-s/S). We refer to this as non-productive templating.

Yeast models of neurodegenerative diseases

Studying the neurodegenerative diseases discussed is encumbered by their late onset and complex etiology. Several mouse models of neurodegenerative diseases have been developed, but often it takes several combinatorial genetic alterations, such as mutations, deletions, and transgene insertions, to produce a phenotype mimicking the human disease (OAKLEY*, et al.* 2006). Our lab has developed mouse models of human prion diseases, such as Fatal Familial Insomnia, that more precisely recapitulate the mutations thought to be causal in these diseases (JACKSON*, et al.* 2009). But although mouse models provide a tremendous tool for studying these diseases it can take up to a year for these mice to develop disease phenotypes (JACKSON*, et al.* 2009).

In addition to the more common methods of studying neurodegenerative diseases, our lab has taken the unique approach of studying the proteotoxicity of disease-associated proteins in the yeast *S. cerevisiae* (KHURANA*, et al.* 2010). As a eukaryotic organism, yeast shares a wealth of cell biological features with mammalian organisms. Cellular organelles such as the nucleus, mitochondria, the endoplasmic reticulum, endocytic vesicles and degradative compartments are present in yeast. Additionally, cellular processes such as autophagy, the cell cycle, and proteasomal protein degradation are conserved between yeast and higher eukaryotic organisms. Most importantly, the protein folding machinery, in part chaperones like Hsp40s and Hsp70s, is very highly conserved between all eukaryotic organisms.

As previously mentioned, HD has been modeled in yeast through the expression of the mutant huntingtin exon one containing different lengths of polyglutamine

expansions (MERIIN, *et al.* 2002). As in the human disease, yeast expressing mutant huntingtin exon one displayed aggregation dependent on the length of the polyglutamine expansion. Expression of mutant huntingtin exon one containing a stretch of 72 or more glutamines caused a growth defect in yeast and lead to the sequestration of multiple ERAD components (DUENNWALD, *et al.* 2008; MERIIN, *et al.* 2002). Importantly, overexpression of ERAD proteins Npl4 and Ufd1 not only ameliorated mutant huntingtin toxicity in yeast but also in mammalian neuron-like cells (DUENNWALD, *et al.* 2008).

Several aspects of Parkinson's disease and related synucleinopathies have also been recapitulated in yeast (COOPER, *et al.* 2006; OUTEIRO, *et al.* 2003). Parkinson's disease, such as other synucleinopathies, is characterized by the presence of α-synuclein containing Lewy Bodies. α -synuclein is a small lipid-binding protein and its moderate expression in yeast results in localization to the plasma membrane. Increased expression of α-synuclein gave rise to the formation of α-synuclein foci and diminished cell growth (OUTEIRO, *et al.* 2003). Subsequent studies revealed that α-synuclein impairs ER to Golgi trafficking and that the α-synuclein foci contain stalled vesicles (COOPER, *et al.* 2006). A genetic screen for modifiers of α-synuclein toxicity identified several genes that not only modulated toxicity in yeast; their homologs decreased α-synuclein toxicity in other model systems such a *C. elegans* and rat primary neurons (COOPER, *et al.* 2006). Furthermore, this yeast model was used to conduct a small molecule screen for compounds capable of counteracting α-synuclein toxicity. Again the identified compounds not only suppressed α-synuclein toxicity in yeast, but also in other model

organisms (SU, *et al.* 2009). In addition, the compounds could counteract the toxicity of rotenone, a mitochondrial poison that elicits Parkinson-like defects (SU, *et al.* 2009).

More recently, toxicity of TDP-43 has been modeled in yeast (JOHNSON, *et al.* 2008). Aggregation of TDP-43, a ubiquitously expressed nuclear DNA binding protein, in cytoplasmic inclusions is associated with amyotrophic lateral sclerosis (ALS) and frontal temporal lobar degeneration with ubiquitin-positive inclusions (FTLD-U) (NEUMANN, *et al.* 2006). Expression of TDP-43 in yeast resulted in toxicity and recapitulated the cytoplasmic aggregation observed in the human diseases (JOHNSON, *et al.* 2008). A subsequent yeast screen for modifiers of TDP-43 toxicity identified Pbp1, the yeast ortholog of the human *ATAXIN-2* gene, poly-glutamine expansions in which cause the neurodegenerative disease spinocerebellar ataxia type 2 (SCA2) (ELDEN, *et al.* 2010). Subsequent sequencing analyses of human patients revealed that intermediate poly-glutamine expansions in *ATAXIN-2* showed a significant association with ALS, suggesting that ATAXIN-2 is a risk factor for ALS (ELDEN, *et al.* 2010).

Conclusion

The protein deposits that are the hallmark of neurodegenerative diseases are now seen in a different light. Formerly viewed as the cause of cellular dysfunction and neuronal loss, intracellular protein deposits, especially, are the product of a regulated cellular process enabling cells to cope with the accumulation of misfolded and damaged proteins. This notion is supported by studies demonstrating that the deposition of damaged and misfolded proteins in inclusions enables mitotic cells, ranging from the

unicellular organism *Escherichia coli* to human embryonic stem cells, to asymmetrically segregate the accumulated damage to the daughter cell with the shorter life expectancy (AGUILANIU*, et al.* 2003; ERJAVEC*, et al.* 2007; FUENTEALBA*, et al.* 2008; LINDNER*, et al.* 2008; RUJANO*, et al.* 2006). Based on our results in yeast, we suggest that inefficiencies in inclusion body and plaque formation, arising with accumulating protein damage, can result in the inception of toxic protein species due to non-productive templating. Further studies are needed to elucidate which types of protein deposits in the individual diseases are protective and how their formation circumvents the formation of more toxic species, such as prefibrillar oligomers.

In addition to studies of endogenous amyloidogenic proteins, such as yeast prion proteins, yeast has proven to be a fertile ground for elucidating the mechanisms of proteotoxicity elicited by neurodegenerative disease associated proteins (KHURANA*, et al.* 2010). The cellular toxicities induced by mutant huntingtin, α-synuclein and TDP-43 have been modeled in yeast. In each case these studies in yeast have helped to reveal how particular misfolding proteins cause toxicity in mammalian cells. In the future, yeast-based small molecule screens may yield compounds that can directly counteract the misfolding and toxicity of these disease-associated proteins (SU*, et al.* 2009).

Acknowledgements

We would like to thank Peter Douglas, Vikram Khurana, Kent Matlack and Chris Pacheco for critical reading of the manuscript. We also thank Tom DiCesare for help with the

illustrations. This work was supported by the National Institutes of Health (D.M.C. and S.L.) and a Howard Hughes Medical Institute Investigatorship (to S.L.).

References

Aguilaniu, H., Gustafsson, L., Rigoulet, M., & Nystrom, T. (2003) Asymmetric Inheritance of Oxidatively Damaged Proteins During Cytokinesis. *Science* 299(5613):1751-1753.

Alzheimer, A., Stelzmann, R.A., Schnitzlein, H.N., & Murtagh, F.R. (1995) An English Translation of Alzheimer's 1907 Paper, "Uber Eine Eigenartige Erkankung Der Hirnrinde". *Clin Anat* 8(6):429-431.

Arrasate, M., Mitra, S., Schweitzer, E.S., Segal, M.R., & Finkbeiner, S. (2004) Inclusion Body Formation Reduces Levels of Mutant Huntingtin and the Risk of Neuronal Death. *Nature* 431(7010):805-810.

Baglioni, S., Casamenti, F., Bucciantini, M., Luheshi, L.M., Taddei, N., Chiti, F., Dobson, C.M., & Stefani, M. (2006) Prefibrillar Amyloid Aggregates Could Be Generic Toxins in Higher Organisms. *J Neurosci* 26(31):8160-8167.

Bence, N.F., Sampat, R.M., & Kopito, R.R. (2001) Impairment of the Ubiquitin-Proteasome System by Protein Aggregation. *Science* 292(5521):1552-1555.

Bodner, R.A., Outeiro, T.F., Altmann, S., Maxwell, M.M., Cho, S.H., Hyman, B.T., McLean, P.J., Young, A.B., Housman, D.E., & Kazantsev, A.G. (2006) Pharmacological Promotion of Inclusion Formation: A Therapeutic Approach for Huntington's and Parkinson's Diseases. *Proc Natl Acad Sci U S A* 103(11):4246-4251.

Bretteville, A. & Planel, E. (2008) Tau Aggregates: Toxic, Inert, or Protective Species? *J Alzheimers Dis* 14(4):431-436.

Bucciantini, M., Giannoni, E., Chiti, F., Baroni, F., Formigli, L., Zurdo, J., Taddei, N., Ramponi, G., Dobson, C.M., & Stefani, M. (2002) Inherent Toxicity of Aggregates Implies a Common Mechanism for Protein Misfolding Diseases. *Nature* 416(6880):507-511.

Budka, H., Head, M.W., Ironside, J.W., Gambetti, P., Parchi, P., Zeidler, M., & Tagliavini, F. (2003) Sporadic Creutzfeldt-Jakob Disease. *Neurodegeneration: The Molecular Pathology of Dementia and Movement Disorders*, ed Dickson D (ISN Neuropath Press, Basel), pp 287-297.

Bueler, H., Aguzzi, A., Sailer, A., Greiner, R.A., Autenried, P., Aguet, M., & Weissmann, C. (1993) Mice Devoid of Prp Are Resistant to Scrapie. *Cell* 73(7):1339-1347.

Burke, J.R., Enghild, J.J., Martin, M.E., Jou, Y.S., Myers, R.M., Roses, A.D., Vance, J.M., & Strittmatter, W.J. (1996) Huntingtin and Drpla Proteins Selectively Interact with the Enzyme Gapdh. *Nat Med* 2(3):347-350.

Caughey, B. & Lansbury, P.T. (2003) Protofibrils, Pores, Fibrils, and Neurodegeneration: Separating the Responsible Protein Aggregates from the Innocent Bystanders. *Annu Rev Neurosci* 26:267-298.

Cheng, I.H., Scearce-Levie, K., Legleiter, J., Palop, J.J., Gerstein, H., Bien-Ly, N., Puolivali, J., Lesne, S., Ashe, K.H., Muchowski, P.J., & Mucke, L. (2007) Accelerating Amyloid-Beta Fibrillization Reduces Oligomer Levels and Functional Deficits in Alzheimer Disease Mouse Models. *J Biol Chem* 282(33):23818-23828.

Chesebro, B., Trifilo, M., Race, R., Meade-White, K., Teng, C., LaCasse, R., Raymond, L., Favara, C., Baron, G., Priola, S., Caughey, B., Masliah, E., & Oldstone, M. (2005) Anchorless Prion Protein Results in Infectious Amyloid Disease without Clinical Scrapie. *Science* 308(5727):1435-1439.

Chiti, F. & Dobson, C.M. (2006) Protein Misfolding, Functional Amyloid, and Human Disease. *Annu Rev Biochem* 75:333-366.

Cohen, E., Bieschke, J., Perciavalle, R.M., Kelly, J.W., & Dillin, A. (2006) Opposing Activities Protect against Age-Onset Proteotoxicity. *Science* 313(5793):1604-1610.

Congdon, E.E. & Duff, K.E. (2008) Is Tau Aggregation Toxic or Protective? *J Alzheimers Dis* 14(4):453-457.

Cooper, A.A., Gitler, A.D., Cashikar, A., Haynes, C.M., Hill, K.J., Bhullar, B., Liu, K., Xu, K., Strathearn, K.E., Liu, F., Cao, S., Caldwell, K.A., Caldwell, G.A., Marsischky, G., Kolodner, R.D., Labaer, J., Rochet, J.C., Bonini, N.M., & Lindquist, S. (2006) Alpha-Synuclein Blocks Er-Golgi Traffic and Rab1 Rescues Neuron Loss in Parkinson's Models. *Science* 313(5785):324-328.

Coustou-Linares, V., Maddelein, M.L., Begueret, J., & Saupe, S.J. (2001) In Vivo Aggregation of the Het-S Prion Protein of the Fungus Podospora Anserina. *Mol Microbiol* 42(5):1325-1335.

Cummings, C.J., Mancini, M.A., Antalffy, B., DeFranco, D.B., Orr, H.T., & Zoghbi, H.Y. (1998) Chaperone Suppression of Aggregation and Altered Subcellular Proteasome Localization Imply Protein Misfolding in Sca1. *Nat Genet* 19(2):148-154.

Cummings, C.J. & Zoghbi, H.Y. (2000) Trinucleotide Repeats: Mechanisms and Pathophysiology. *Annu Rev Genomics Hum Genet* 1:281-328.

Derkatch, I.L., Bradley, M.E., Hong, J.Y., & Liebman, S.W. (2001) Prions Affect the Appearance of Other Prions: The Story of [*Pin(+)*]. *Cell* 106(2):171-182.

Douglas, P.M., Treusch, S., Ren, H.Y., Halfmann, R., Duennwald, M.L., Lindquist, S., & Cyr, D.M. (2008) Chaperone-Dependent Amyloid Assembly Protects Cells from Prion Toxicity. *Proc Natl Acad Sci U S A* 105(20):7206-7211.

Duennwald, M.L. & Lindquist, S. (2008) Impaired Erad and Er Stress Are Early and Specific Events in Polyglutamine Toxicity. *Genes Dev* 22(23):3308-3319.

Duyckaerts, C. & Dickson, D. (2003) Neuropathology of Alzheimer's Disease. *Neurodegeneration: The Molecular Pathology of Dementia and Movement Disorders*, ed Dickson D (ISN Neuropath Press, Basel), pp 47-65.

Ehrnhoefer, D.E., Duennwald, M., Markovic, P., Wacker, J.L., Engemann, S., Roark, M., Legleiter, J., Marsh, J.L., Thompson, L.M., Lindquist, S., Muchowski, P.J., & Wanker, E.E. (2006) Green Tea (-)-Epigallocatechin-Gallate Modulates Early Events in Huntingtin Misfolding and Reduces Toxicity in Huntington's Disease Models. *Hum Mol Genet* 15(18):2743-2751.

Elden, A.C., Kim, H.J., Hart, M.P., Chen-Plotkin, A.S., Johnson, B.S., Fang, X., Armakola, M., Geser, F., Greene, R., Lu, M.M., Padmanabhan, A., Clay-Falcone, D., McCluskey, L., Elman, L., Juhr, D., Gruber, P.J., Rub, U., Auburger, G., Trojanowski, J.Q., Lee, V.M., Van Deerlin, V.M., Bonini, N.M., & Gitler, A.D. (2010) Ataxin-2 Intermediate-Length Polyglutamine Expansions Are Associated with Increased Risk for Als. *Nature* 466(7310):1069-1075.

Ellison, D., Love, S., Chimelli, L., Harding, B.N., Lowe, J., & Vinters, H.V. (2004) *Neuropathology: A Reference Text of Cns Pathology* (MOSBY, St Louis) Second Ed.

Erjavec, N., Larsson, L., Grantham, J., & Nystrom, T. (2007) Accelerated Aging and Failure to Segregate Damaged Proteins in Sir2 Mutants Can Be Suppressed by Overproducing the Protein Aggregation-Remodeling Factor Hsp104p. *Genes Dev* 21(19):2410-2421.

Fuentealba, L.C., Eivers, E., Geissert, D., Taelman, V., & De Robertis, E.M. (2008) Asymmetric Mitosis: Unequal Segregation of Proteins Destined for Degradation. *Proc Natl Acad Sci U S A* 105(22):7732-7737.

Garcia-Mata, R., Bebok, Z., Sorscher, E.J., & Sztul, E.S. (1999) Characterization and Dynamics of Aggresome Formation by a Cytosolic Gfp-Chimera. *J Cell Biol* 146(6):1239-1254.

Gotz, J., Ittner, L.M., Fandrich, M., & Schonrock, N. (2008) Is Tau Aggregation Toxic or Protective: A Sensible Question in the Absence of Sensitive Methods? *J Alzheimers Dis* 14(4):423-429.

Gutekunst, C.A., Li, S.H., Yi, H., Mulroy, J.S., Kuemmerle, S., Jones, R., Rye, D., Ferrante, R.J., Hersch, S.M., & Li, X.J. (1999) Nuclear and Neuropil Aggregates in Huntington's Disease: Relationship to Neuropathology. *J Neurosci* 19(7):2522-2534.

Hedreen, J.C. & Roos, R.A.C. (2003) Huntington's Disease. *Neurodegeneration: The Molecular Pathology of Dementia and Movement Disorders*, ed Dickson D (ISN Neuropath Press, Basel), pp 229-241.

Hernandez, F. & Avila, J. (2008) Tau Aggregates and Tau Pathology. *J Alzheimers Dis* 14(4):449-452.

Holmes, C., Boche, D., Wilkinson, D., Yadegarfar, G., Hopkins, V., Bayer, A., Jones, R.W., Bullock, R., Love, S., Neal, J.W., Zotova, E., & Nicoll, J.A. (2008) Long-Term Effects of Abeta42 Immunisation in Alzheimer's Disease: Follow-up of a Randomised, Placebo-Controlled Phase I Trial. *Lancet* 372(9634):216-223.

Ironside, J.W., Head, M.W., & Will, R.G. (2003) Variant Creutzfeldt-Jakob Disease. *Neurodegeneration: The Molecular Pathology of Dementia and Movement Disorders*, ed Dickson D (ISN Neuropath Press, Basel), pp 310-317.

Jackson, W.S., Borkowski, A.W., Faas, H., Steele, A.D., King, O.D., Watson, N., Jasanoff, A., & Lindquist, S. (2009) Spontaneous Generation of Prion Infectivity in Fatal Familial Insomnia Knockin Mice. *Neuron* 63(4):438-450.

Johnson, B.S., McCaffery, J.M., Lindquist, S., & Gitler, A.D. (2008) A Yeast Tdp-43 Proteinopathy Model: Exploring the Molecular Determinants of Tdp-43 Aggregation and Cellular Toxicity. *Proc Natl Acad Sci U S A* 105(17):6439-6444.

Johnston, J.A., Illing, M.E., & Kopito, R.R. (2002) Cytoplasmic Dynein/Dynactin Mediates the Assembly of Aggresomes. *Cell Motil Cytoskeleton* 53(1):26-38.

Johnston, J.A., Ward, C.L., & Kopito, R.R. (1998) Aggresomes: A Cellular Response to Misfolded Proteins. *J Cell Biol* 143(7):1883-1898.

Kaganovich, D., Kopito, R., & Frydman, J. (2008) Misfolded Proteins Partition between Two Distinct Quality Control Compartments. *Nature* 454(7208):1088-1095.

Kayed, R., Head, E., Thompson, J.L., McIntire, T.M., Milton, S.C., Cotman, C.W., & Glabe, C.G. (2003) Common Structure of Soluble Amyloid Oligomers Implies Common Mechanism of Pathogenesis. *Science* 300(5618):486-489.

Khurana, V. & Lindquist, S. (2010) Modelling Neurodegeneration in Saccharomyces Cerevisiae: Why Cook with Baker's Yeast? *Nat Rev Neurosci* 11(6):436-449.

Kopito, R.R. (2000) Aggresomes, Inclusion Bodies and Protein Aggregation. *Trends Cell Biol* 10(12):524-530.

Kuemmerle, S., Gutekunst, C.A., Klein, A.M., Li, X.J., Li, S.H., Beal, M.F., Hersch, S.M., & Ferrante, R.J. (1999) Huntington Aggregates May Not Predict Neuronal Death in Huntington's Disease. *Ann Neurol* 46(6):842-849.

Lesne, S., Koh, M.T., Kotilinek, L., Kayed, R., Glabe, C.G., Yang, A., Gallagher, M., & Ashe, K.H. (2006) A Specific Amyloid-Beta Protein Assembly in the Brain Impairs Memory. *Nature* 440(7082):352-357.

Lindner, A.B., Madden, R., Demarez, A., Stewart, E.J., & Taddei, F. (2008) Asymmetric Segregation of Protein Aggregates Is Associated with Cellular Aging and Rejuvenation. *Proc Natl Acad Sci U S A* 105(8):3076-3081.

Mathur, V., Taneja, V., Sun, Y., & Liebman, S.W. (2010) Analyzing the Birth and Propagation of Two Distinct Prions, [Psi+] and [Het-S](Y), in Yeast. *Mol Biol Cell* 21(9):1449-1461.

Meriin, A.B., Zhang, X., He, X., Newnam, G.P., Chernoff, Y.O., & Sherman, M.Y. (2002) Huntington Toxicity in Yeast Model Depends on Polyglutamine Aggregation Mediated by a Prion-Like Protein Rnq1. *J Cell Biol* 157(6):997-1004.

Nelson, R., Sawaya, M.R., Balbirnie, M., Madsen, A.O., Riekel, C., Grothe, R., & Eisenberg, D. (2005) Structure of the Cross-Beta Spine of Amyloid-Like Fibrils. *Nature* 435(7043):773-778.

Neumann, M., Sampathu, D.M., Kwong, L.K., Truax, A.C., Micsenyi, M.C., Chou, T.T., Bruce, J., Schuck, T., Grossman, M., Clark, C.M., McCluskey, L.F., Miller, B.L., Masliah, E., Mackenzie, I.R., Feldman, H., Feiden, W., Kretzschmar, H.A., Trojanowski, J.Q., & Lee, V.M. (2006) Ubiquitinated Tdp-43 in Frontotemporal Lobar Degeneration and Amyotrophic Lateral Sclerosis. *Science* 314(5796):130-133.

Nucifora, F.C., Jr., Sasaki, M., Peters, M.F., Huang, H., Cooper, J.K., Yamada, M., Takahashi, H., Tsuji, S., Troncoso, J., Dawson, V.L., Dawson, T.M., & Ross, C.A. (2001) Interference by Huntingtin and Atrophin-1 with Cbp-Mediated Transcription Leading to Cellular Toxicity. *Science* 291(5512):2423-2428.

Oakley, H., Cole, S.L., Logan, S., Maus, E., Shao, P., Craft, J., Guillozet-Bongaarts, A., Ohno, M., Disterhoft, J., Van Eldik, L., Berry, R., & Vassar, R. (2006) Intraneuronal

Beta-Amyloid Aggregates, Neurodegeneration, and Neuron Loss in Transgenic Mice with Five Familial Alzheimer's Disease Mutations: Potential Factors in Amyloid Plaque Formation. *J Neurosci* 26(40):10129-10140.

Outeiro, T.F. & Lindquist, S. (2003) Yeast Cells Provide Insight into Alpha-Synuclein Biology and Pathobiology. *Science* 302(5651):1772-1775.

Piccardo, P., Manson, J.C., King, D., Ghetti, B., & Barron, R.M. (2007) Accumulation of Prion Protein in the Brain That Is Not Associated with Transmissible Disease. *Proc Natl Acad Sci U S A* 104(11):4712-4717.

Preisinger, E., Jordan, B.M., Kazantsev, A., & Housman, D. (1999) Evidence for a Recruitment and Sequestration Mechanism in Huntington's Disease. *Philos Trans R Soc Lond B Biol Sci* 354(1386):1029-1034.

Rambold, A.S., Muller, V., Ron, U., Ben-Tal, N., Winklhofer, K.F., & Tatzelt, J. (2008) Stress-Protective Signalling of Prion Protein Is Corrupted by Scrapie Prions. *Embo J* 27(14):1974-1984.

Ravikumar, B., Vacher, C., Berger, Z., Davies, J.E., Luo, S., Oroz, L.G., Scaravilli, F., Easton, D.F., Duden, R., O'Kane, C.J., & Rubinsztein, D.C. (2004) Inhibition of Mtor Induces Autophagy and Reduces Toxicity of Polyglutamine Expansions in Fly and Mouse Models of Huntington Disease. *Nat Genet* 36(6):585-595.

Ross, C.A. (2003) Introduction to Trinucleotide Repeat Disorders. *Neurodegeneration: The Molecular Pathology of Dementia and Movement Disorders*, ed Dickson D (ISN Neuropath Press, Basel), pp 226-228.

Roth, M., Tomlinson, B.E., & Blessed, G. (1966) Correlation between Scores for Dementia and Counts of 'Senile Plaques' in Cerebral Grey Matter of Elderly Subjects. *Nature* 209(5018):109-110.

Rujano, M.A., Bosveld, F., Salomons, F.A., Dijk, F., van Waarde, M.A., van der Want, J.J., de Vos, R.A., Brunt, E.R., Sibon, O.C., & Kampinga, H.H. (2006) Polarised Asymmetric Inheritance of Accumulated Protein Damage in Higher Eukaryotes. *PLoS Biol* 4(12):e417.

Saudou, F., Finkbeiner, S., Devys, D., & Greenberg, M.E. (1998) Huntingtin Acts in the Nucleus to Induce Apoptosis but Death Does Not Correlate with the Formation of Intranuclear Inclusions. *Cell* 95(1):55-66.

Serio, T.R., Cashikar, A.G., Kowal, A.S., Sawicki, G.J., Moslehi, J.J., Serpell, L., Arnsdorf, M.F., & Lindquist, S.L. (2000) Nucleated Conformational Conversion and the Replication of Conformational Information by a Prion Determinant. *Science* 289(5483):1317-1321.

Shankar, G.M., Li, S., Mehta, T.H., Garcia-Munoz, A., Shepardson, N.E., Smith, I., Brett, F.M., Farrell, M.A., Rowan, M.J., Lemere, C.A., Regan, C.M., Walsh, D.M., Sabatini, B.L., & Selkoe, D.J. (2008) Amyloid-Beta Protein Dimers Isolated Directly from Alzheimer's Brains Impair Synaptic Plasticity and Memory. *Nat Med* 14(8):837-842.

Shorter, J. & Lindquist, S. (2004) Hsp104 Catalyzes Formation and Elimination of Self-Replicating Sup35 Prion Conformers. *Science* 304(5678):1793-1797.

Shorter, J. & Lindquist, S. (2005) Prions as Adaptive Conduits of Memory and Inheritance. *Nat Rev Genet* 6(6):435-450.

Sondheimer, N. & Lindquist, S. (2000) Rnq1: An Epigenetic Modifier of Protein Function in Yeast. *Mol Cell* 5(1):163-172.

Sondheimer, N., Lopez, N., Craig, E.A., & Lindquist, S. (2001) The Role of Sis1 in the Maintenance of the [Rnq+] Prion. *Embo J* 20(10):2435-2442.

Su, L.J., Auluck, P.K., Outeiro, T.F., Yeger-Lotem, E., Kritzer, J.A., Tardiff, D.F., Strathearn, K.E., Liu, F., Cao, S., Hamamichi, S., Hill, K.J., Caldwell, K.A., Bell, G.W., Fraenkel, E., Cooper, A.A., Caldwell, G.A., McCaffery, J.M., Rochet, J.C., & Lindquist, S. (2009) Compounds from an Unbiased Chemical Screen Reverse Both Er-to-Golgi Trafficking Defects and Mitochondrial Dysfunction in Parkinson's Disease Models. *Dis Model Mech* 3(3-4):194-208.

Taylor, J.P., Tanaka, F., Robitschek, J., Sandoval, C.M., Taye, A., Markovic-Plese, S., & Fischbeck, K.H. (2003) Aggresomes Protect Cells by Enhancing the Degradation of Toxic Polyglutamine-Containing Protein. *Hum Mol Genet* 12(7):749-757.

Tyedmers, J., Treusch, S., Dong, J., McCaffery, J.M., Bevis, B., & Lindquist, S. (2010) Prion Induction Involves an Ancient System for the Sequestration of Aggregated Proteins and Heritable Changes in Prion Fragmentation. *Proc Natl Acad Sci U S A* 107(19):8633-8638.

Walsh, D.M., Klyubin, I., Fadeeva, J.V., Cullen, W.K., Anwyl, R., Wolfe, M.S., Rowan, M.J., & Selkoe, D.J. (2002) Naturally Secreted Oligomers of Amyloid Beta Protein Potently Inhibit Hippocampal Long-Term Potentiation in Vivo. *Nature* 416(6880):535-539.

Wang, H., Duennwald, M.L., Roberts, B.E., Rozeboom, L.M., Zhang, Y.L., Steele, A.D., Krishnan, R., Su, L.J., Griffin, D., Mukhopadhyay, S., Hennessy, E.J., Weigele, P., Blanchard, B.J., King, J., Deniz, A.A., Buchwald, S.L., Ingram, V.M., Lindquist, S., & Shorter, J. (2008) Direct and Selective Elimination of Specific Prions and Amyloids by 4,5-Dianilinophthalimide and Analogs. *Proc Natl Acad Sci U S A* 105(20):7159-7164.

Wang, Y., Meriin, A.B., Zaarur, N., Romanova, N.V., Chernoff, Y.O., Costello, C.E., & Sherman, M.Y. (2009) Abnormal Proteins Can Form Aggresome in Yeast: Aggresome-Targeting Signals and Components of the Machinery. *FASEB J* 23(2):451-463.

Warrick, J.M., Chan, H.Y., Gray-Board, G.L., Chai, Y., Paulson, H.L., & Bonini, N.M. (1999) Suppression of Polyglutamine-Mediated Neurodegeneration in Drosophila by the Molecular Chaperone Hsp70. *Nat Genet* 23(4):425-428.

Williams, A., Sarkar, S., Cuddon, P., Ttofi, E.K., Saiki, S., Siddiqi, F.H., Jahreiss, L., Fleming, A., Pask, D., Goldsmith, P., O'Kane, C.J., Floto, R.A., & Rubinsztein, D.C. (2008) Novel Targets for Huntington's Disease in an Mtor-Independent Autophagy Pathway. *Nat Chem Biol* 4(5):295-305.

Zoghbi, H.Y. & Orr, H.T. (2000) Glutamine Repeats and Neurodegeneration. *Annu Rev Neurosci* 23:217-247.

Chapter Two:

Chaperone-dependent amyloid assembly protects cells from prion toxicity

This work was previously published in *PNAS.*

Authors: Peter M. Douglas[*], Sebastian Treusch[*], Hong-Yu Ren, Randal Halfmann, Martin L. Duennwald, Susan Lindquist and Douglas M. Cyr. [*]These authors made equal contributions to this work.

Abstract

Protein conformational diseases are associated with the aberrant accumulation of amyloid protein aggregates, but whether amyloid formation is cytotoxic or protective is unclear. To address this issue we investigated a normally benign amyloid formed by the yeast prion [*RNQ*$^{+}$]. Surprisingly, modest overexpression of Rnq1 protein was deadly, but only when preexisting Rnq1 was in the [*RNQ*$^{+}$] prion conformation. Molecular chaperones protect against protein aggregation diseases, and are generally believed to do so by solubilizing their substrates. The Hsp40 chaperone, Sis1, suppressed Rnq1 proteotoxicity, but instead of blocking Rnq1 protein aggregation, it stimulated conversion of soluble Rnq1 to [*RNQ*$^{+}$] amyloid. Furthermore, interference with Sis1-mediated [*RNQ*$^{+}$] amyloid formation exacerbated Rnq1 toxicity. These and other data establish that even subtle changes in the folding homeostasis of an amyloidogenic protein can create a severe proteotoxic gain-of-function phenotype and that chaperone-mediated amyloid assembly can be cytoprotective. The possible relevance of these findings to other phenomena, including prion-driven neurodegenerative diseases and heterokaryon incompatibility in fungi is discussed.

Introduction

Alzheimer's disease, transmissible spongiform encephalopathies and polyglutamine diseases are representatives of a large group of neurodegenerative disorders that are associated with the misfolding and conversion of particular proteins into amyloid (CARRELL*, et al.* 1997). Amyloids form in response to many perturbations in

protein homeostasis, namely mutations in the amino acid sequence of a disease-related protein, expansion of simple sequence elements in disease genes, elevated protein levels and age-associated cell stress (CHITI, *et al.* 2006). Amyloid fibrils share a cross-β structural motif, in which β-strands run perpendicular to the long fiber axis, and accumulate in intracellular and extracellular inclusions (CAUGHEY, *et al.* 2003; NELSON, *et al.* 2005). Fibril formation requires that a misfolded protein expose a pleated β-surface that is capable of serving as a template and hydrogen bonding partner with an extra β-strand (CARRELL, *et al.* 1997). Biochemical parameters for classification of protein aggregates as amyloid include resistance to solubilization by the detergent SDS and the ability to bind indicator dyes such as thioflavin-T (CHITI, *et al.* 2006).

Amyloid deposits in the brain are a hallmark of protein conformational disease, but often there is only a poor correlation between the detection of amyloid fibrils and other markers of neurodegeneration (HAASS, *et al.* 2007). Thus, there is still intense debate about whether amyloids are the causative toxic protein species in neurodegenerative diseases. In fact, recent, still controversial, work suggests that amyloids might be benign or cytoprotective and that difficult-to-characterize soluble oligomeric conformers are the toxic species of disease causing proteins (CHENG, *et al.* 2007; KAYED, *et al.* 2003; SHORTER, *et al.* 2005).

Cells buffer proteotoxic events related to intracellular protein misfolding via chaperone-mediated partitioning of non-native conformers between pathways for proper folding, inclusion body formation, and degradation (ROSS, *et al.* 2005). Molecular chaperones also play a critical role in the propagation of yeast prions, which are

examples of intracellular amyloids that in general are not inherently toxic (LINDQUIST 1997; WICKNER 1994). However, the conversion of active soluble Sup35 and Ure2 into their prion states [*PSI*$^{+}$] and [*URE3*], respectively, inactivates these proteins (LINDQUIST 1997; WICKNER 1994). Yeast prion formation occurs spontaneously, at a low frequency, and the prion state is then perpetuated through the templating of newly synthesized prion proteins by preexisting amyloid-like prions (CHIEN, *et al.* 2004). Templated prion proteins then undergo stable changes in structure and function to enter an amyloid-like state that is propagated and passed from mother cells to their daughters in a molecular chaperone-dependent manner (CHIEN, *et al.* 2004). Yeast prions thereby constitute cytoplasmically transmitted, protein-based elements of inheritance that are dominant in genetic crosses (prions are denoted by brackets, italics and capital letters to reflect these properties).

The yeast prion [*RNQ*$^{+}$] is determined by the conformational state of the Rnq1 protein, which contains a C-terminal asparagine- and glutamine-rich prion domain and an N-terminal non-prion forming domain (DERKATCH, *et al.* 2000; SONDHEIMER, *et al.* 2000). The native form of Rnq1 has no known normal biological function and is non-essential. Yet, the [*RNQ*$^{+}$] prion can have important effects on yeast cells because it influences certain other proteins to convert to amyloid-like states (MERIIN, *et al.* 2002; OSHEROVICH, *et al.* 2001; TANEJA, *et al.* 2007). For example, [*RNQ*$^{+}$] prions are required for the initial conversion of native Sup35 to the [*PSI*$^{+}$] state. Indeed [*RNQ*$^{+}$] constitutes the cytoplasmically inherited factor known as [*PIN*$^{+}$] (PSI inducible) and is the only known yeast prion that is commonly found in wild strains (DERKATCH, *et al.* 2001; NAKAYASHIKI, *et*

al. 2005). [*RNQ*$^{+}$] prions also cause the exon 1 fragment of huntingtin protein, containing glutamine repeats, to become toxic in yeast (MERIIN*, et al.* 2002). Thus, [*RNQ*$^{+}$] prions can interact with other amyloid-forming proteins and thereby help drive their conversion into benign or toxic amyloid-like species.

Results

Overexpression of Rnq1 is toxic in [*RNQ*$^{+}$] cells

We recently discovered that moderate (i.e. ~5 to 10-fold) overexpression of Rnq1 from the GAL1 promoter was severely toxic in cells that harbored the [*RNQ*$^{+}$] prion (Figure C2.1a; top, growth of serially diluted liquid cultures on agar; bottom, protein levels detected by Western blotting). This was surprising because Rnq1 overexpression was not toxic when endogenous Rnq1 was in the [*rnq*-] non-prion conformation. Nor was it toxic in cells carrying a deletion of the *RNQ1* gene, Δ*rnq1 (*Figure C2.1a). Cell growth defects observed were more extreme than any we have observed with other misfolded proteins in yeast (COOPER*, et al.* 2006; DUENNWALD*, et al.* 2006). At this modest level of Rnq1 overexpression approximately 25% of [*RNQ*$^{+}$] cells were dead within 4hrs, as determined by percentage of colony forming units and dye exclusion (data not shown). Toxicity was accompanied by the accumulation of Rnq1 aggregates that stained with the common amyloid diagnostic dye thioflavin T (Figure C2.1b). Rnq1 overexpression was found to be toxic in [*RNQ*$^{+}$] laboratory strains (W303, 74D-694, BY23 and BY4741), clinical strains (YJM269, YJM421,YJM436 and YJM653), a fermentation

strain (Y12) and wine strains (I14,T73 and WE372)(Taipale and Lindquist, unpublished observations). Thus, Rnq1 toxicity is pervasive and not strain specific.

Although not quite as deadly, a C-terminal Rnq1-YFP fusion protein behaved similarly to untagged Rnq1 and exhibited the same pattern of toxicity: toxic in [*RNQ*$^{+}$] cells, but not in [*rnq*-] or Δ*rnq1* cells. This allowed us to correlate changes in toxicity with changes in protein distribution (Figure C2.1c and Supplemental Figure C2.1). Rnq1-YFP was distributed throughout the cytosol in [*rnq*-] or Δ*rnq1* cells. Using low- and high-copy plasmids that express Rnq1-YFP at different levels, we found that toxicity positively correlated with the degree of overexpression (Supplemental Figure C2.1a). Western of cell lysates separated by SDD-AGE (semidenaturing-detergent-agarose gel electrophoresis) demonstrated that in [*RNQ*$^{+}$], but not [*rnq*-] cells, Rnq1-YFP assembled into a SDS-resistant high molecular weight species typical of amyloid assemblies of yeast prions (KRYNDUSHKIN*, et al.* 2003) (Figure C2.1d and Supplemental Figure C2.1b). Yet, a pool of soluble Rnq1-YFP, which ran at the position of a monomer on SDD-AGE gels, was also present in [*RNQ*$^{+}$] cells.

Growth of [*RNQ*$^{+}$] cells overexpressing just the non-prion-forming domain or just the prion-forming domain of Rnq1, amino acids 1-153 and 154-405, respectively, was not hindered (Supplemental Figure C2.1c). When the prion-forming domain is expressed on its own, it assembles into an SDS-resistant species that runs as an amyloid on SDD-AGE gels (Supplemental Figure C2.1d). Therefore, the mechanism for Rnq1 toxicity does not appear related to the accumulation of large quantities of [*RNQ*$^{+}$]-like amyloid per se.

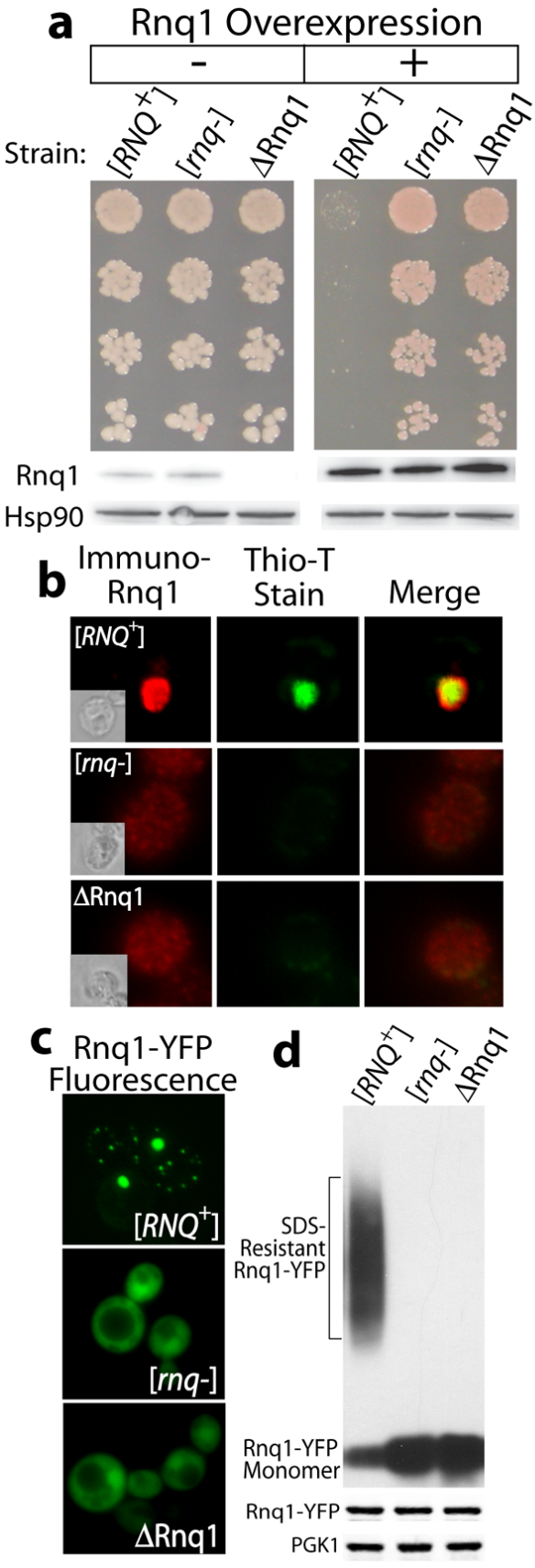
a
Rnq1 Overexpression
-
+
Strain:
[RNQ+]
[rnq-]
ΔRnq1
[RNQ+]
[rnq-]
ΔRnq1
Rnq1
Hsp90
b
Immuno-Rnq1
Thio-T Stain
Merge
[RNQ+]
[rnq-]
ΔRnq1
c
Rnq1-YFP Fluorescence
[RNQ+]
[rnq-]
ΔRnq1
d
[RNQ+]
[rnq-]
ΔRnq1
SDS-Resistant Rnq1-YFP
Rnq1-YFP Monomer
Rnq1-YFP
PGK1

Figure C2.1: Overexpression of Rnq1 is toxic to [*RNQ*$^{+}$] cells.

(a) The effect of Rnq1 overexpression on yeast cell viability in the presence and absence of the [*RNQ*$^{+}$] prion. **(b)** Thioflavin-T staining of Rnq1 in [*RNQ*$^{+}$], [*rnq*-] and *ΔRnq1* cells. Fixed yeast were decorated with α-Rnq1 sera that was detected with a fluorescent secondary antibody. The same cells were simultaneously stained with the amyloid indicator dye, thioflavin-T. **(c)** Visualization of the aggregation state of Rnq1-YFP by fluorescence microscopy. **(d)** The assembly status of Rnq1-YFP as determined by SDD-AGE. The lower panels represent Western blots of cell extracts probed with the indicated antibodies.

The toxicity of Rnq1 overexpression in the presence of the [*RNQ*$^{+}$] prion might seem similar to the toxicity of overexpressed Sup35 in the presence of its prion [*PSI*$^{+}$]. Overexpression of Sup35 is toxic in [*PSI*$^{+}$] cells as it drives too much of the essential Sup35 protein into an inactive amyloid conformation (DERKATCH, *et al.* 1997). In contrast, Rnq1 toxicity cannot be due to an inhibition of Rnq1 function as deletion of the gene encoding Rnq1 has no detectable effect on yeast growth under hundreds of conditions tested (T.F. Outeiro and S.L., unpublished data). Furthermore, in contrast to Sup35, expression of Rnq1's non-prion domain does not rescue the toxicity caused by Rnq1 overexpression (data not shown).

The Hsp40 Sis1 can suppress Rnq1 toxicity

Sis1, an essential Hsp40 chaperone, is required for the propagation of the [*RNQ*$^{+}$] prion state (SONDHEIMER, *et al.* 2001). Sis1 specifies Hsp70 function and is required for protein synthesis, protein folding and cell stress protection (FAN, *et al.* 2004; ZHONG, *et al.* 1996). Overexpressing Sis1 by as little as 3-fold strongly suppressed Rnq1 toxicity (Figure C2.2a). To examine whether other chaperones were capable of suppressing Rnq1 toxicity, an expression library of 4954 yeast genes was screened (COOPER, *et al.* 2006). Sis1 was the only chaperone in this library able to protect from Rnq1 toxicity (data not shown). This library includes, among many other chaperones, Ydj1, a member of the large Hsp40 family that is closely related to Sis1. It also includes Hsp70 Ssa1 (Hsp70) and Hsp104, which assist in shearing [*RNQ*$^{+}$] prions to form seeds required for

propagation of the [*RNQ*$^{+}$] state (ARON*, et al.* 2007) . Therefore, the effect of Sis1 on the toxicity of Rnq1 overexpression is unique.

Sis1 not only promotes [*RNQ*$^{+}$] prion formation, but it remains stably bound to the prion in a 1:1 complex (LOPEZ*, et al.* 2003). This could provide an explanation for the toxicity of overexpressed Rnq1: elevation of [*RNQ*$^{+}$] prion levels could kill cells by sequestering Sis1 away from its essential substrates. But this explanation is unlikely as cells in which Sis1 is depleted by nearly 100 fold grow for extended time periods and exhibit delayed lethality (LUKE*, et al.* 1991). In contrast, cells start to die within 4h of the induction of Rnq1 overexpression.

To directly eliminate the possibility that cell death is due to sequestration of Sis1 we deleted the domain of Sis1 that is required for interaction with the prion, the glycine- and phenylalanine-rich (G/F) region (LOPEZ*, et al.* 2003). A Sis1 ΔG/F variant fails to promote the propagation of [*RNQ*$^{+}$], but can carry out Sis1's essential functions. We overexpressed Sis1 ΔG/F, and found that unlike Sis1, it could not suppress Rnq1 toxicity.

Sis1-mediated amyloid formation protects from Rnq1 toxicity

The toxicity produced by overexpression of Rnq1 represents a dominant gain-of-function that requires endogenous Rnq1 protein to be in a [*RNQ*$^{+}$] prion conformation. It may be Sis1's ability to facilitate [*RNQ*$^{+}$] prion propagation that ameliorates Rnq1 toxicity. Indeed, the suppression of Rnq1 toxicity by Sis1 overexpression was accompanied by a substantial increase in the formation of SDS-resistant [*RNQ*$^{+}$] amyloid

(Figure C2.2b). This seemed to be accompanied by a decrease in the pool of unassembled SDS-sensitive Rnq1. We have found, however, that although SDD-AGE is a reliable method for quantitatively detecting SDS-resistant species it is not reliable for SDS-soluble species. To examine SDS-soluble species we employed gel filtration chromatography. As shown in Figure C2.2c, a large pool of unassembled Rnq1-YFP accumulated upon Rnq1-YFP overexpression (Figure C2.2c, compare top and middle chromatographs). Suppression of Rnq1 toxicity by Sis1 correlated with a dramatic decrease in unassembled Rnq1-YFP pools and a corresponding increase in the pools of assembled forms (Figure C2.2c, compare middle and bottom chromatographs). These results suggest that cytotoxic Rnq1 conformers accumulate when levels of Rnq1 protein exceed the cells capacity to efficiently promote the template-driven formation of the SDS-resistant [*RNQ*$^{+}$] prion species. To test this hypothesis we asked if Rnq1 toxicity would be exacerbated when the efficiency of [*RNQ*$^{+}$] amyloid assembly was reduced.

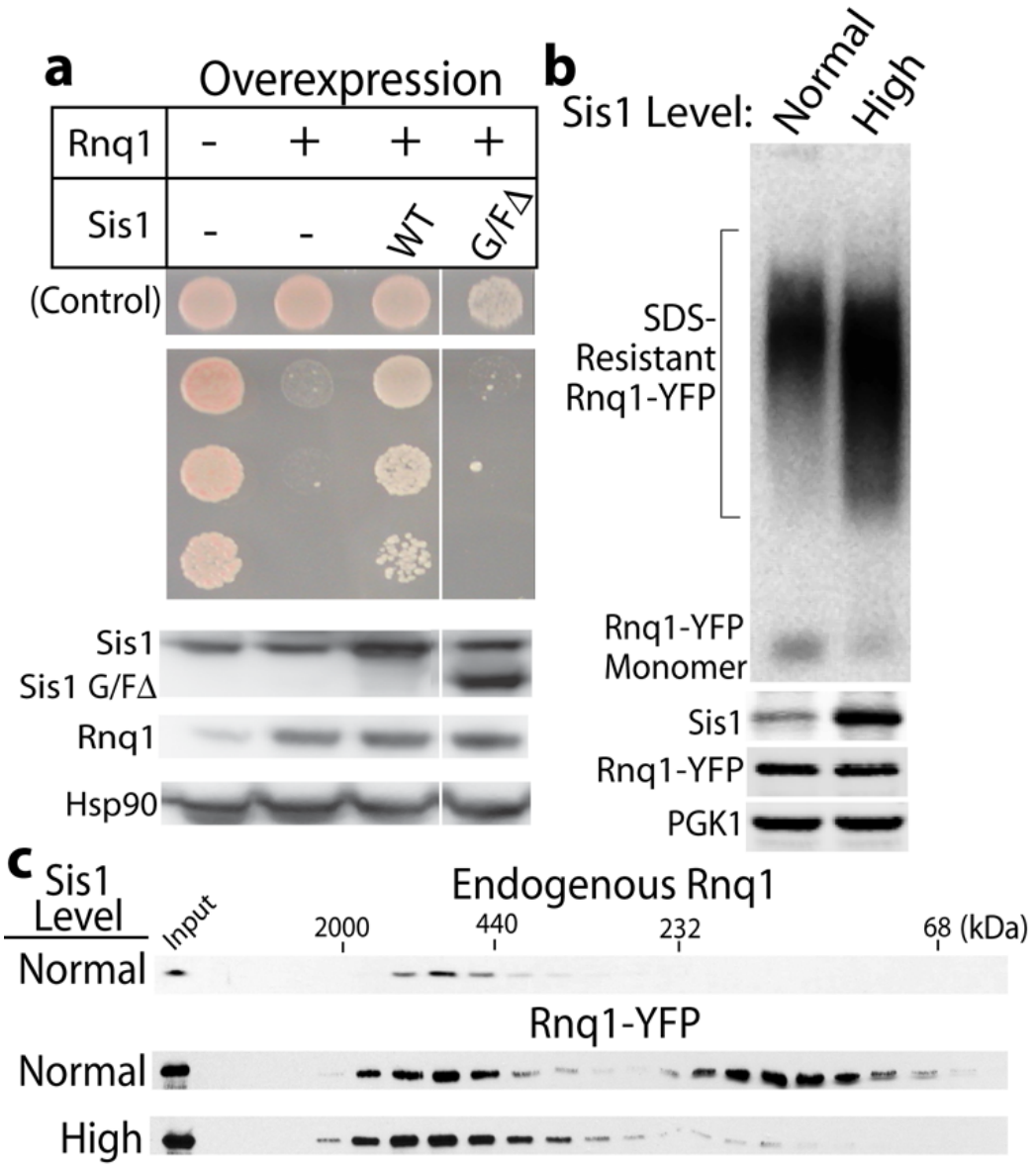

Figure C2.2: Sis1 overexpression protects against Rnq1 toxicity.

(a) The effect of Sis1 or Sis1ΔG/F overexpression on Rnq1 toxicity. The control lane shows the strains grown under non-inducing conditions. **(b)** The effect of Sis1 overexpression on the formation of SDS-resistant [*RNQ*$^{+}$] conformers as determined by SDD-AGE. **(c)** Gel filtration analysis of intracellular pools of endogenous versus overexpressed Rnq1-YFP.

Identification of the Sis1 binding site in Rnq1

First, we identified and mutated the chaperone-binding motif that Sis1 uses to interact with Rnq1. A peptide array was created that contained 25 residue N-acetylated peptides spanning the entire Rnq1 amino acid sequence. This array was incubated with purified Sis1, washed, and Sis1-interacting peptides were identified by Western blot after transfer of bound chaperone to nitrocellulose (Supplemental Figure C2.2a). Tight binding of Sis1 was only observed with a few neighboring Rnq1 peptides and these were located in the non-prion forming domain.

The amino acid sequence of this region is conserved in all known Rnq1 homologues and contains a classic, hydrophobic chaperone-binding motif, LGKLALL (Figure C2.3a and Supplemental Figure C2.2b) (RUDIGER*, et al.* 1997). Hsp40 proteins stimulate the binding of their Hsp70 co-chaperones to specific substrates. Indeed, Sis1 stimulated binding of its Hsp70 co-chaperone, Ssa1, to the peptides containing this motif in an ATP-dependent manner (Figure C2.3b). Thus, Sis1 forms a functional chaperone: substrate complex with peptides containing this chaperone-binding motif.

Next, to reduce the efficiency of Sis1's interaction with [*RNQ*$^{+}$], we replaced hydrophobic leucine residues in the Rnq1 chaperone-binding motif with alanines (L91A, L94A, and L97A). As demonstrated by co-immunoprecipitation, the capacity of Rnq1-GFP to interact with Sis1, was strongly, but not completely, reduced by these mutations (Figure C2.3c and data not shown).

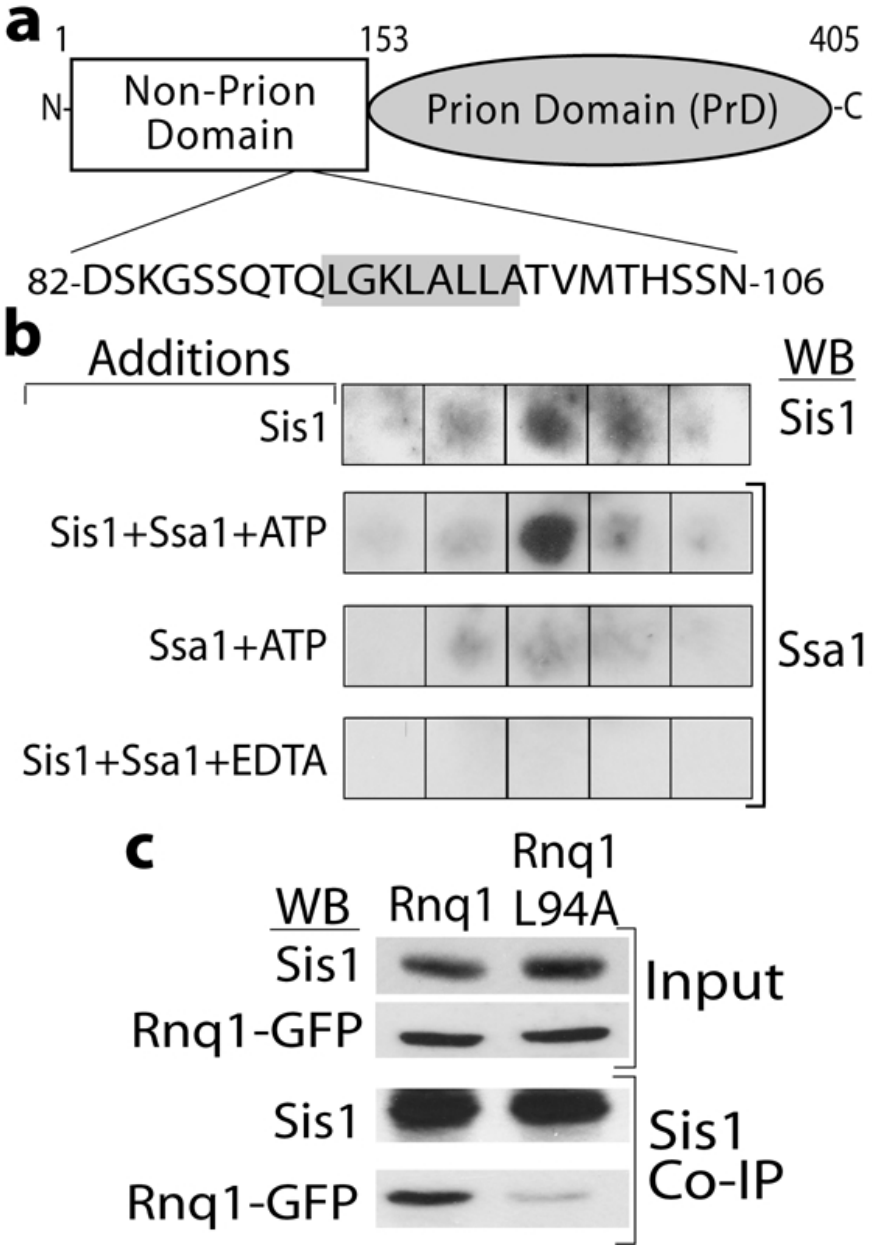

Figure C2.3: Sis1 binding to a conserved chaperone-binding motif in the non-prion domain of Rnq1.

(a) A schematic showing the domain structure of Rnq1. The underlined region in non-prion domain of Rnq1 represents a chaperone binding motif identified via screening a cellulose peptide array (see Supplemental Figure C2.2). **(b)** Sis1 dependent binding of

Hsp70 Ssa1 to the peptide in the Rnq1 peptide array that is bound most strongly by Sis1. **(c)** Mutation L94A in the chaperone-binding motif reduces the ability of Sis1 to form co-immunoprecipitable complexes with Rnq1-GFP in [*RNQ*$^{+}$] cells. Rnq1-GFP was expressed using the CUP1 promoter. Levels of the indicated proteins in **c** were visualized by Western blot analysis (WB).

Mutations in the Sis1 binding site of Rnq1 interfere with [*RNQ*$^{+}$] amyloid assembly

To determine if the Rnq1 chaperone-binding motif mutants were defective in assembly of [*RNQ*$^{+}$] amyloid, we expressed them as Rnq1-GFP fusions from an extra-chromosomal plasmid in cells expressing wild type Rnq1 in its prion state. The L91A, L94A, and L97A mutations were expressed at levels similar to those of wild type Rnq1 using the CUP1 promoter, but they had a reduced capacity to form fluorescent foci (Supplemental Figure C2.2c). An L45A mutation, which is also located in the non-prion forming domain, but lies outside of the chaperone-binding motif, had no detectable effect on the assembly of [*RNQ*$^{+}$] prions (Supplemental Figure C2.2c). Further, a time course analysis by SDD-AGE (Figure C2.4a) and pulse-chase (Supplemental Figure C2.2d) revealed that the rate at which newly synthesized Rnq1-GFP protein was converted into SDS-resistant conformers *in vivo* was reduced several fold by the L94A mutation in comparison to the wild-type protein. In addition, *in vitro*, purified Rnq1 L94A could be templated by prion "seeds" present in [*RNQ*$^{+}$] cell extracts to form SDS-resistant species (Figure C2.4b). However, it was templated and converted to an SDS-resistant form with lower efficiency than the wild-type Rnq1 protein.

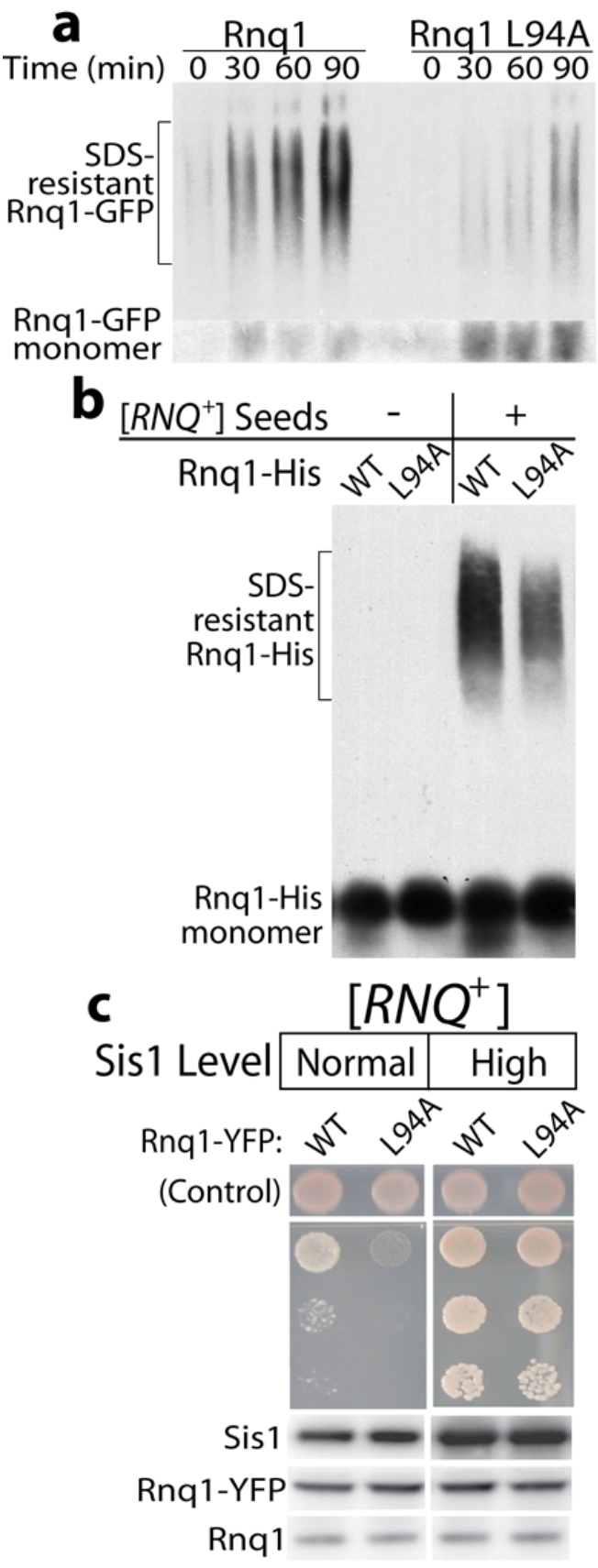
a
Rnq1
Rnq1 L94A
Time (min)
0 30 60 90
0 30 60 90
SDS-resistant Rnq1-GFP
Rnq1-GFP monomer
b
[RNQ+] Seeds
-
+
Rnq1-His
WT
L94A
WT
L94A
SDS-resistant Rnq1-His
Rnq1-His monomer
c
[RNQ+]
Sis1 Level
Normal
High
Rnq1-YFP:
WT
L94A
WT
L94A
(Control)
Sis1
Rnq1-YFP
Rnq1

Figure C2.4: Mutations in the chaperone-binding motif of Rnq1 reduce the efficiency of [*RNQ*$^{+}$] amyloid assembly.

(a) Kinetics of Rnq1-GFP L94A assembly into SDS-resistant aggregates in [*RNQ*$^{+}$] yeast determined by SDD-AGE. Rnq1-GFP fusions were expressed using the CUP1 promoter. **(b)** [*RNQ*$^{+}$] seed dependent assembly of purified Rnq1-His and Rnq1-His L94A into SDS-resistant amyloid. **(c)** Growth of 5 fold serial dilutions of [*RNQ*$^{+}$] strains in which WT or L94A Rnq1 was overexpressed from the GAL1 promoter. Where indicated, Sis1 was overexpressed from the GPD promoter. Lower panels show the relative expression level of the specified proteins as determined by Western blot.

Finally, we asked whether the impairment of Rnq1 amyloid assembly increased the toxicity of Rnq1 overexpression. As we hypothesized, Rnq1 L94A was more toxic than Rnq1 WT when overexpressed in [*RNQ*$^{+}$] cells (Figure C2.4c). A triple mutant, Rnq1 L94A-L96A-L97A, was even more toxic than Rnq1 L94A (data not shown). As expected from the fact that the Rnq1 L94A mutation impaired, but did not eliminate interaction with Sis1, overexpression of Sis1 3-fold was still able to suppress the toxicity of the mutant protein (Figure C2.4c).

Thus far, we have shown that interfering with the assembly of Rnq1 into the [*RNQ*$^{+}$] amyloid state is extremely toxic. Toxicity occurs when Rnq1 expression is higher than normal (Figure C2.1 and C2.2) or when mutations in Rnq1 interfere with the efficiency of Sis1 interaction (Figure C2.3 and C2.4). In addition, depletion of Sis1 from the cytosol reduces the efficiency of [*RNQ*$^{+}$] prion assembly and exacerbates Rnq1 toxicity (Supplemental Figure C2.3). These collective data indicate that the efficient conversion of native Rnq1 into its SDS-resistant amyloid form prevents the accumulation of a toxic Rnq1 conformer.

Suppression of Rnq1 toxicity by Sis1 requires [*RNQ* $^{+}$] prion assembly

Rnq1 L94A exhibits a higher propensity than Rnq1 WT to form SDS-soluble aggregates when [*RNQ*$^{+}$] assembly is impeded via depletion of Sis1 (Supplemental Figure C2.3). The inability of cells to maintain Rnq1 L94A in a soluble state correlates with the enhanced toxicity of the L94A mutant. In this sense Rnq1 L94A is similar to alleles of amyloidogenic proteins whose subtle defects in folding kinetics cause devastating

protein conformational diseases (CARRELL, *et al.* 1997). Thus, we wondered if Rnq1 L94A would assume a toxic conformation in the absence of templating by [*RNQ*$^{+}$] prion seeds. Indeed, overexpression of Rnq1 L94A, but not Rnq1 WT, was toxic in [*rnq*-] strains (Figure C2.5a). Hence, a small amino acid substitution can cause Rnq1 to be toxic even in the absence of [*RNQ*$^{+}$] amyloid formation.

Sis1-dependent [*RNQ*$^{+}$] amyloid formation appears to protect cells from toxicity caused by overexpression of Rnq1. If amyloid formation is a critical aspect of Sis1's ability to suppress Rnq1 toxicity, then Sis1 overexpression should not protect [*rnq*-] cells from Rnq1 L94A mediated death as these cells lack the [*RNQ*$^{+}$] prion seeds required for amyloid assembly. Indeed, overexpression of Sis1, which binds Rnq1 L94A with reduced efficiency, protected [*RNQ*$^{+}$], but not [*rnq*-] strains, from Rnq1 L94A toxicity. This finding further confirms that Rnq1 toxicity is not caused by sequestration of Sis1 into [*RNQ*$^{+}$] prion complexes. Furthermore, the presence of the [*RNQ*$^{+}$] prion assembly pathway and Sis1 overexpression are both required for the suppression of Rnq1 toxicity.

<u>Rnq1 L94A does not form prion amyloids in [*rnq*-] cells</u>

To rule out the possibility that Rnq1 L94A assembled into [*RNQ*$^{+}$] prions spontaneously in [rnq-] cells we compared its assembly status to that of Rnq1 WT in [*rnq*-] strains (Figure C2.5b-e). In [*rnq*-] cells, Rnq1 L94A exhibited a higher propensity than Rnq1 WT to coalesce into foci (Figure C2.5b). Gel-filtration chromatography showed that Rnq1 L94A formed high molecular weight aggregates in these cells (Supplemental Figure C2.4). Notably, these aggregates were not SDS-resistant and

(Figure C2.5c) were unable to bind the amyloid indicator thioflavin-T (Figure C2.5d). Thus, Rnq1 toxicity is not related to the accumulation of excess pools of [*RNQ*$^{+}$] amyloid and may be caused by a SDS-soluble Rnq1 species.

As small prion seeds in the form of detergent soluble prefibrillar species could have escaped detection by SDD-AGE and thioflavin-T staining, we applied another test for the existence of such forms of Rnq1 L94A in [*rnq*-] cell extracts (Figure C2.5e). Prion seeds in cell extracts can be sensitively detected through their ability to catalyze the conversion of exogenously added native prion protein into SDS resistant amyloid. Prion seeds were readily detected in lysates of [*RNQ*$^{+}$] cells overexpressing Rnq1 L94A (Figure C2.4b). However, extracts of [*rnq*-] cells that contained toxic levels of Rnq1 L94A failed to seed assembly of purified His-Rnq1 or His-Rnq1-L94A into SDS-resistant amyloid (Figure C2.5e).

The Rnq1 L94A assemblies in [*rnq*-] cells fail to meet three classification standards of [*RNQ*$^{+}$] amyloid. They are SDS-soluble, they do not stain with Thioflavin-T, and they do not seed polymerization of soluble Rnq1 protein. Rnq1 L94A is more lethal than Rnq1 and can assume a toxic conformation in the absence of [*RNQ*$^{+}$] templates. Rescue from Rnq1 L94A toxicity requires Sis1 overexpression and active propagation of the [*RNQ*$^{+}$] prion. Therefore, it appears that the conversion of Rnq1 L94A to [*RNQ*$^{+}$] amyloid prevents the accumulation of toxic Rnq1 conformer whose true nature remains obscure.

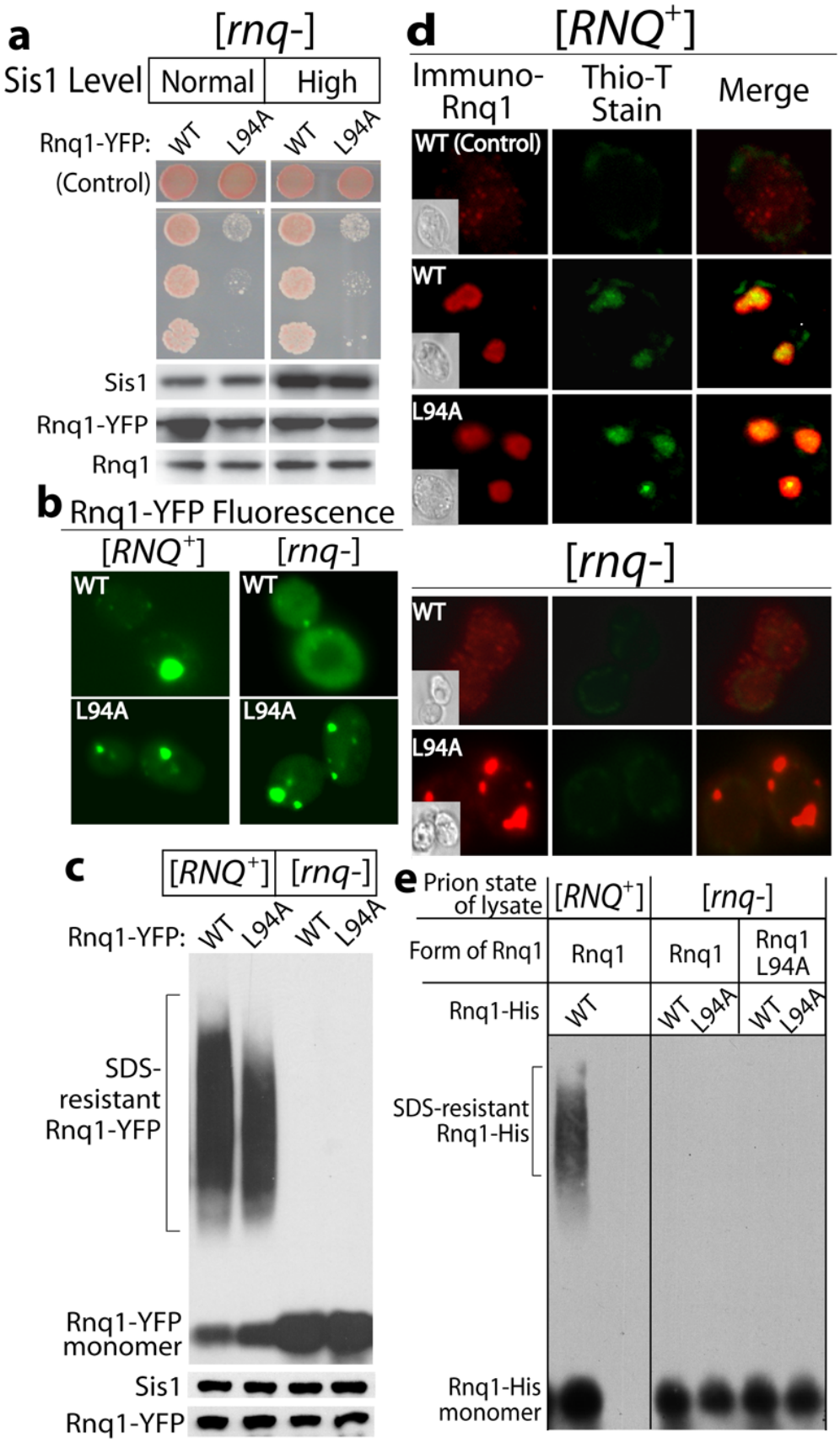
a
[rnq-]
Sis1 Level
Normal
High
Rnq1-YFP:
WT
L94A
WT
L94A
(Control)
Sis1
Rnq1-YFP
Rnq1
b
Rnq1-YFP Fluorescence
[RNQ+]
[rnq-]
WT
WT
L94A
L94A
c
[RNQ+]
[rnq-]
Rnq1-YFP:
WT
L94A
WT
L94A
SDS-resistant Rnq1-YFP
Rnq1-YFP monomer
Sis1
Rnq1-YFP
d
[RNQ+]
Immuno-Rnq1
Thio-T Stain
Merge
WT (Control)
WT
L94A
[rnq-]
WT
L94A
e
Prion state of lysate
[RNQ+]
[rnq-]
Form of Rnq1
Rnq1
Rnq1
Rnq1 L94A
Rnq1-His
WT
WT
L94A
WT
L94A
SDS-resistant Rnq1-His
Rnq1-His monomer

Figure C2.5: Rnq1 L94A toxicity and assembly status in [rnq-] yeast.

(a) Growth of 5 fold serial dilutions of [*rnq*-] strains in which WT or L94A Rnq1 was overexpressed from the GAL1 promoter. Sis1 was overexpressed from the GPD promoter. **(b)** Fluorescent foci formed by Rnq1-YFP and Rnq1-YFP L94A in [*RNQ*$^{+}$] and [*rnq*-] cells. **(c)** SDD-AGE analysis of aggregates formed by Rnq1-YFP and Rnq1-YFP L94A in [*RNQ*$^{+}$] and [*rnq*-] cells. **(d)** Thioflavin-T staining of untagged Rnq1 and Rnq1 L94A in [*RNQ*$^{+}$] and [*rnq*-] cells. Fixed yeast were decorated with α-Rnq1 sera that was detected with a fluorescent secondary antibody. The same cells were simultaneously stained with the amyloid indicator dye, thioflavin-T. **(e)** Cell extracts from [*rnq*-] cells overexpressing either Rnq1 or Rnq1 L94A were incubated with purified Rnq1-His or Rnq1-His L94A. The assembly status of purified Rnq1-His was determined by SDD-AGE. As a control, the assembly status of purified Rnq1-His incubated with [*RNQ*$^{+}$] cell extract was also determined. Lower panels in (**a**) and (**b**) are Western blots of cell extracts.

Discussion

Our data suggest a model in which efficient chaperone-dependent conversion of soluble Rnq1 into SDS-resistant [*RNQ*$^{+}$] amyloid is critical to prevent the formation of other toxic Rnq1 conformers. We demonstrate that toxic Rnq1 conformers accumulate in a non-amyloid form when [*RNQ*$^{+}$] assembly is made inefficient by multiple means. We propose that non-productive templating of Rnq1 monomers by [*RNQ*$^{+}$] seeds predisposes Rnq1 to leave the amyloid pathway and accumulate as a toxic species, whose exact nature is not yet clear. Templating of native proteins to form amyloid is a basic feature of amyloidogenesis and we suggest that inefficiencies in this process contribute to the proteotoxicity associated with certain protein conformational diseases. This templating model explains how amyloid formation can serve a protective function while the [*RNQ*$^{+}$] prion state is a prerequisite for toxicity of the Rnq1 WT protein.

One of Sis1's functions in [*RNQ*$^{+}$] prion propagation appears to be promoting the shearing of [*RNQ*$^{+}$] amyloid fibers into smaller pieces, thereby creating new surfaces to more efficiently seed the assembly of the prion (ARON*, et al.* 2007). This reaction also requires Hsp104 and Hsp70. Hence, binding of Sis1 to the non-prion forming domain of full-length Rnq1 may help facilitate this shearing process. However, since overexpression of Hsp70 and Hsp104 do not suppress Rnq1 toxicity, Sis1 may have additional functions in [*RNQ*$^{+}$] prion propagation that do not overlap with those of other chaperones. Sis1 stably associates with assembled [*RNQ*$^{+}$] conformers in a 1:1 molar ratio (LOPEZ*, et al.* 2003). Therefore, Sis1's binding to the non-prion forming domain has

the potential to stabilize [*RNQ*$^{+}$] prions in a conformation that is optimal for efficient amyloid fibril growth.

Many neurodegenerative diseases involve the accumulation of intracellular and/or extracellular amyloid protein aggregates. In the past, these amyloid aggregates were thought to be the cytotoxic, disease-causing protein conformer. However, recent studies have begun to question this view. As one striking example in mice, deletion of the GPI-anchor of the prion protein, PrP, leads to massive extracellular amyloid plaque formation in mice injected with infective scrapie, but causes no overt clinical manifestations of scrapie (CHESEBRO, *et al.* 2005). Furthermore it has been suggested that neurodegenerative diseases are caused by the ability of very different proteins to adopt common toxic non-amyloid conformers such as protofibrils or soluble oligomers (CAUGHEY, *et al.* 2003; HAASS, *et al.* 2007). Hence, amyloid formation may serve to convert oligomeric amyloid precursors into a highly stable non-toxic form (PICCARDO, *et al.* 2007).

While amyloid itself is not toxic, its interaction with soluble protein forms could give rise to pathogenic species via non-productive templating. Case in point, when GPI-anchorless PrP was expressed together with PrP WT, it accelerated scrapie disease and resulted in increased deposits of both amyloid and non-amyloid proteinase-K resistant PrP (PrPres) (CHESEBRO, *et al.* 2005). Similarly, in yeast the toxicity of Huntington exon 1 depends on the [*RNQ*$^{+}$] prion state (DUENNWALD, *et al.* 2006; MERIIN, *et al.* 2002). This concept may even extend to the heterokaryon incompatibility mediated by the [Het-s] prion in *Podospora anserina* (COUSTOU-LINARES, *et al.* 2001). HET-s in its prion form only

leads to cell death when co-expressed with the HET-S allele that cannot form amyloid. Templating of the non-amyloidogenic HET-S protein by [Het-s] prion seeds could lead to the formation of a toxic species, while templating of HET-s protein would result in the non-toxic prion amyloid species.

The aggregation state and toxicity of aggregation-prone proteins is strongly modulated by host factors such as Hsp70 and its associated co-chaperones, but the mechanisms for chaperone function in this process is just being defined (Cyr*, et al.* 2002). Molecular chaperones generally act to antagonize protein aggregation; yet, our observations that chaperone-dependent assembly of amyloid conformers can be cytoprotective provide a different view of the cytoprotective effects of chaperones in neurodegenerative disease. Thus, molecular chaperones can antagonize protein toxicity in conformational disorders by two different mechanisms: they can solubilize misfolded proteins or aid in sequestering them into benign, amyloid-like species. The most central aspect of antagonizing toxicity of misfolded proteins appears to be preventing accumulation of the detergent soluble misfolded species rather than preventing the formation of amyloid conformers.

Acknowledgements

Work in the laboratories of DMC and SL is supported by the NIH. SL is an Investigator of the Howard Hughes Medical Institute. PD is supported by a predoctoral fellowship from the American Heart Association. RH is supported by a NSF predoctoral training grant. Many thanks to Jessica Brown, Daniel Summers, and James Shorter for

helpful discussions and to Karen Allendoerfer for critical reading of the manuscript. Elizabeth Craig (UW-Madison, Wisconsin) kindly provided the Sis1 ΔG/F construct and Sis1 anti-sera.

Author contributions

I characterized Rnq1 toxicity and its suppression by Sis1. Peter Douglas performed the Rnq1-Sis1 peptide binding array and created Rnq1 mutants. Together we characterized the toxicity and properties of these Rnq1 mutants. Randal Halfmann carried out the Rnq1 seeding experiments. Martin Duennwald supervised me when I started this project during my rotation in the Lindquist lab. Susan Lindquist and I wrote the paper receiving feedback and comments from the other authors.

References

Aron, R., Higurashi, T., Sahi, C., & Craig, E.A. (2007) J-Protein Co-Chaperone Sis1 Required for Generation of [Rnq(+)] Seeds Necessary for Prion Propagation. *EMBO J* 26 (16):3794-3803.

Carrell, R.W. & Lomas, D.A. (1997) Conformational Disease. *Lancet* 350(9071):134-138.

Caughey, B. & Lansbury, P.T. (2003) Protofibrils, Pores, Fibrils, and Neurodegeneration: Separating the Responsible Protein Aggregates from the Innocent Bystanders. *Annu Rev Neurosci* 26:267-298.

Cheng, I.H., Scearce-Levie, K., Legleiter, J., Palop, J.J., Gerstein, H., Bien-Ly, N., Puolivali, J., Lesne, S., Ashe, K.H., Muchowski, P.J., & Mucke, L. (2007) Accelerating Amyloid-Beta Fibrillization Reduces Oligomer Levels and Functional Deficits in Alzheimer Disease Mouse Models. *J Biol Chem* 282(33):23818-23828.

Chesebro, B., Trifilo, M., Race, R., Meade-White, K., Teng, C., LaCasse, R., Raymond, L., Favara, C., Baron, G., Priola, S., Caughey, B., Masliah, E., & Oldstone, M. (2005) Anchorless Prion Protein Results in Infectious Amyloid Disease without Clinical Scrapie. *Science* 308(5727):1435-1439.

Chien, P., Weissman, J.S., & DePace, A.H. (2004) Emerging Principles of Conformation-Based Prion Inheritance. *Annu Rev Biochem* 73:617-656.

Chiti, F. & Dobson, C.M. (2006) Protein Misfolding, Functional Amyloid, and Human Disease. *Annu Rev Biochem* 75:333-366.

Cooper, A.A., Gitler, A.D., Cashikar, A., Haynes, C.M., Hill, K.J., Bhullar, B., Liu, K., Xu, K., Strathearn, K.E., Liu, F., Cao, S., Caldwell, K.A., Caldwell, G.A., Marsischky, G., Kolodner, R.D., Labaer, J., Rochet, J.C., Bonini, N.M., & Lindquist, S. (2006) Alpha-Synuclein Blocks Er-Golgi Traffic and Rab1 Rescues Neuron Loss in Parkinson's Models. *Science* 313(5785):324-328.

Coustou-Linares, V., Maddelein, M.L., Begueret, J., & Saupe, S.J. (2001) In Vivo Aggregation of the Het-S Prion Protein of the Fungus Podospora Anserina. *Mol Microbiol* 42(5):1325-1335.

Cyr, D.M., Hohfeld, J., & Patterson, C. (2002) Protein Quality Control: U-Box-Containing E3 Ubiquitin Ligases Join the Fold. *Trends Biochem Sci* 27(7):368-375.

Derkatch, I.L., Bradley, M.E., Hong, J.Y., & Liebman, S.W. (2001) Prions Affect the Appearance of Other Prions: The Story of [Pin(+)]. *Cell* 106(2):171-182.

Derkatch, I.L., Bradley, M.E., Masse, S.V., Zadorsky, S.P., Polozkov, G.V., Inge-Vechtomov, S.G., & Liebman, S.W. (2000) Dependence and Independence of [Psi(+)] and [Pin(+)]: A Two-Prion System in Yeast? *Embo J* 19(9):1942-1952.

Derkatch, I.L., Bradley, M.E., Zhou, P., Chernoff, Y.O., & Liebman, S.W. (1997) Genetic and Environmental Factors Affecting the De Novo Appearance of the [Psi+] Prion in Saccharomyces Cerevisiae. *Genetics* 147(2):507-519.

Duennwald, M.L., Jagadish, S., Giorgini, F., Muchowski, P.J., & Lindquist, S. (2006) A Network of Protein Interactions Determines Polyglutamine Toxicity. *Proc Natl Acad Sci U S A* 103(29):11051-11056.

Eaglestone, S.S., Ruddock, L.W., Cox, B.S., & Tuite, M.F. (2000) Guanidine Hydrochloride Blocks a Critical Step in the Propagation of the Prion-Like Determinant [Psi(+)] of Saccharomyces Cerevisiae. *Proc Natl Acad Sci U S A* 97(1):240-244.

Fan, C.Y., Lee, S., Ren, H.Y., & Cyr, D.M. (2004) Exchangeable Chaperone Modules Contribute to Specification of Type I and Type Ii Hsp40 Cellular Function. *Mol Biol Cell* 15(2):761-773.

Haass, C. & Selkoe, D.J. (2007) Soluble Protein Oligomers in Neurodegeneration: Lessons from the Alzheimer's Amyloid Beta-Peptide. *Nat Rev Mol Cell Biol* 8(2):101-112.

Kayed, R., Head, E., Thompson, J.L., McIntire, T.M., Milton, S.C., Cotman, C.W., & Glabe, C.G. (2003) Common Structure of Soluble Amyloid Oligomers Implies Common Mechanism of Pathogenesis. *Science* 300(5618):486-489.

Kryndushkin, D.S., Alexandrov, I.M., Ter-Avanesyan, M.D., & Kushnirov, V.V. (2003) Yeast [Psi+] Prion Aggregates Are Formed by Small Sup35 Polymers Fragmented by Hsp104. *J Biol Chem* 278(49):49636-49643.

Lindquist, S. (1997) Mad Cows Meet Psi-Chotic Yeast: The Expansion of the Prion Hypothesis. *Cell* 89(4):495-498.

Lopez, N., Aron, R., & Craig, E.A. (2003) Specificity of Class Ii Hsp40 Sis1 in Maintenance of Yeast Prion [Rnq(+)]. *Mol Biol Cell* 14(3):1172-1181.

Luke, M.M., Sutton, A., & Arndt, K.T. (1991) Characterization of Sis1, a Saccharomyces Cerevisiae Homologue of Bacterial Dnaj Proteins. *J Cell Biol* 114(4):623-638.

Meriin, A.B., Zhang, X., He, X., Newnam, G.P., , Y.O., & Sherman, M.Y. (2002) Huntington Toxicity in Yeast Model Depends on Polyglutamine Aggregation Mediated by a Prion-Like Protein Rnq1. *J Cell Biol* 157(6):997-1004.

Nakayashiki, T., Kurtzman, C.P., Edskes, H.K., & Wickner, R.B. (2005) Yeast Prions [Ure3] and [Psi+] Are Diseases. *Proc Natl Acad Sci U S A* 102(30):10575-10580.

Nelson, R., Sawaya, M.R., Balbirnie, M., Madsen, A.O., Riekel, C., Grothe, R., & Eisenberg, D. (2005) Structure of the Cross-Beta Spine of Amyloid-Like Fibrils. *Nature* 435(7043):773-778.

Osherovich, L.Z. & Weissman, J.S. (2001) Multiple Gln/Asn-Rich Prion Domains Confer Susceptibility to Induction of the Yeast [Psi(+)] Prion. *Cell* 106(2):183-194.

Piccardo, P., Manson, J.C., King, D., Ghetti, B., & Barron, R.M. (2007) Accumulation of Prion Protein in the Brain That Is Not Associated with Transmissible Disease. *Proc Natl Acad Sci U S A* 104(11):4712-4717.

Ross, C.A. & Poirier, M.A. (2005) Opinion: What Is the Role of Protein Aggregation in Neurodegeneration? *Nat Rev Mol Cell Biol* 6(11):891-898.

Rudiger, S., Germeroth, L., Schneider_Mergener, J., & Bukau, B. (1997) Substrate Specificity of the Dnak Chaperone Determined by Screening Cellulose-Bound Peptide Libraries. *EMBO Journal* 16(7):1501-1507.

Shorter, J. & Lindquist, S. (2005) Prions as Adaptive Conduits of Memory and Inheritance. *Nat Rev Genet* 6(6):435-450.

Shorter, J. & Lindquist, S. (2006) Destruction or Potentiation of Different Prions Catalyzed by Similar Hsp104 Remodeling Activities. *Mol Cell* 23(3):425-438.

Sondheimer, N. & Lindquist, S. (2000) Rnq1: An Epigenetic Modifier of Protein Function in Yeast. *Mol Cell* 5(1):163-172.

Sondheimer, N., Lopez, N., Craig, E.A., & Lindquist, S. (2001) The Role of Sis1 in the Maintenance of the [Rnq+] Prion. *Embo J* 20(10):2435-2442.

Taneja, V., Maddelein, M., Talarek, N., Saupe, S., & Liebman, S.W. (2007) A Non-Q/N-Rich Prion Domain of a Foreign Prion, [Het-S], Can Propagate as a Prion in Yeast. *Molecular Cell* 27:67-77.

Wickner, R.B. (1994) [Ure3] as an Altered Ure2 Protein: Evidence for a Prion Analog in Saccharomyces Cerevisiae. *Science* 264(5158):566-569.

Zhong, T., Luke, M.M., & Arndt, K.T. (1996) Transcriptional Regulation of the Yeast Dnaj Homologue Sis1. *J Biol Chem* 271(3):1349-1356.

Materials and Methods

Strains and Plasmids: W303, *MATa can1-100 ade2-1, his3-11,15 leu2-3,112 ura3-1 trp1-1*; W303*Δrnq1*, *MATa can1-100 ade2-1 his3-11,15 leu2-3,112 ura3-1 trp1-1 Δrnq1:KanMX4*; 74D-694, *MATa ade1-14 trp1-289 his3Δ-300 ura3-52 leu2-3,112*; BY4741, MATa his3Δ1 leu2Δ0 met15Δ0 ura3Δ0; W303*Δsis1*, *MATa ade2-1 his3-11,15*

leu2-3,112 ura3-1 trp1-1 ssd1-d2 sis1::HIS pRS316-SIS1. All the above strains harbored Rnq1 in its [RNQ^{+}] form and the generation of isogenic [*rnq*-] strains was accomplished via sequential passage of cells on plates containing 3 mM guanidinium-HCl (EAGLESTONE, *et al.* 2000). BY, W303 and 74D-694 strains were utilized to take advantage of the different markers or gene deletions. Identical results were obtained in studies carried out with both of these strains, so Rnq1 toxicity is not strain specific.

Strains were transformed with plasmids and cultured in synthetic media as previously described (CAPLAN, *et al.* 1991). Plasmids that express the indicated protein under control of the GAL1 promoter include pRS416-*RNQ1*, pRS416-*RNQ1-YFP*, pRS426-*RNQ1-YFP* and pYES3-*SIS1*, termed pGAL1-*SIS1*. All Rnq1 truncations were expressed as YFP fusions under control of the GAL1 promoter using the pRS416 plasmid. Plasmids that express *RNQ1* under control of the CUP1 promoter include pRS316-*RNQ1-GFP*, pRS315-*RNQ1-GFP*. The strains used were not sensitive to 500 µM $CuSO_4$. The glyceraldehyde-3-phosphate dehydrogenase (GPD) promoter controlled expression of SIS1 in pRS414-*SIS1* and pRS414-*sis1Δg/f*. The QuikChange site-directed mutagenesis kit (Stratagene) was used to create the indicated point mutations in *RNQ1.* The pDEST17 vector was used to express His-Rnq1 WT and L94A in BL21AI cells.

Analysis of Rnq1 cytotoxicity: W303 strains harboring pRS416-*RNQ1* or pRS416-*RNQ1-YFP* were grown overnight in synthetic drop-out media containing 2 % raffinose before 5-fold serial dilutions were spotted on plates containing either 2 % galactose or glucose. Alternatively, strains that harbored pRS316-*RNQ1-GFP* or pRS315-*RNQ1-GFP* were

cultured overnight in synthetic media containing glucose before serial dilutions were spotted on agarose plates that contained 500 µM $CuS0_4$. Plates were incubated for 3-5 days at 30 ºC and then photographed.

Screening of a Rnq1 peptide array: A 25mer Rnq1 cellulose bound peptide array was prepared by automated spot synthesis and screened essentially as described by (RUDIGER*, et al.* 1997). The 25mer Rnq1 cellulose bound peptide array was prepared by automated spot synthesis (Jerini Peptide Technologies). The array was screened according the manufactures instructions with 100 nM Sis1 or Hsp70 Ssa1 in the presence or absence of 1 mM EDTA or Mg-ATP. Bound chaperones were transferred to a nitrocellulose membrane and the peptide spots were identified by Western blot. Hsp70 Ssa1 bound a number of different peptides that contained clusters of hydrophobic amino acids (data not shown), yet peptides 27-30 were the only peptides that Sis1 bound reproducibly with high affinity. In addition, peptide 28, which contains residues 82-106 of Rnq1, was the only peptide that was bound by Hsp70 Ssa1 in a Sis1 and ATP dependent manner (Figure C2.3b).

Pulse-chase analysis of [*RNQ*$^+$] prion formation: Pulse labeling of yeast to analyze the kinetics of Rnq1 assembly in 74D-694 cultures was performed essentially as described by (LUKE*, et al.* 1991). 74D-694 cultures were grown overnight in synthetic media and then diluted and starved in methionine free media. Log phase cultures were first supplemented with 50 µM $CuS0_4$ to induce Rnq1-GFP or Rnq1-GFP L94A expression for 1

hr before the addition of Trans^{35}S-label (100 μCi/ml). Cultures were labeled for 10 min, then 1 mg/ml of cold methionine was added and cells were washed. Cultures were incubated for the indicated time period at 30°C before samples were collected. Cell lysis was achieved by glass bead disruption in a buffer composed of 50 mM Hepes pH 7.4, 150 mM NaCl, 1 mM EDTA, 0.1% Tween-20, 2 mM phenylmethysulfonyl fluoride and a protease inhibitor cocktail mixture. Cell debris was removed and the resulting lysate was spun at 4 ºC at 165,000 × g for 45 min in a TLA-100 rotor (Beckman Coulter). Rnq1-GFP present in the supernatant and pellet fractions was then immuneprecipitated with α-GFP (Roche) in the presence of 0.1% SDS. ^{35}S-labeled proteins in immuneprecipitates were resolved by SDS-PAGE and detected by autoradiography.

Analysis of [*RNQ*$^{+}$] prion formation by fluorescence microscopy: Assembly of Rnq1-GFP into fluorescent foci that represent prion amyloids was preformed essentially as described by (FAN*, et al.* 2004). To examine the assembly of newly synthesized Rnq1 into of [*RNQ*$^{+}$] prions Rnq1-GFP expression was induced from the CUP1 promoter by the addition of 50 μM $CuSO_4$ to log-phase cultures and live cells were photographed 1 hr later. To examine the aggregation pattern of Rnq1, Rnq1-GFP or Rnq1-YFP under condition where growth defects are observed, protein expression under control of the CUP1 or GAL1 promoter was induced by the addition of either 500 μM $CuSO_4$ or 2 % galactose, respectively, and 4 hrs later live cells were photographed.

Indirect immunofluorescence of Rnq1 and thioflavin-T staining of Rnq1 aggregates were performed as follows. Log phase cells harboring pRS416-*RNQ1* that

were cultured in synthetic raffinose media were supplemented with 2 % galactose for 4 hrs to induce expression of either Rnq1 or Rnq1 L94A. Cells were fixed with 4% formaldehyde for 1 hr and washed twice in buffer containing 1.2 M sorbitol before being converted to spheroplasts via 45 min incubations at 30ºC in the presence of 5 mg/ml zymolyase-20T. Cells were then permeabilized in phosphate buffer saline (PBS) containing 0.1% Triton X-100 for 5 min. Cells were washed and incubated with PBS that contained 0.001% Thioflavin-T for 10 min. Next, thioflavin-T stained cells were washed 4 times and incubated in PBS containing 1.0% BSA and 0.025% Triton X-100. Blocked cells were then incubated with polyclonal rabbit α-Rnq1 (1:50 dilution) for 1 hr and then washed 4 times. Cells were then decorated with goat α-rabbit conjugated Texas Red (1:1000) second antibody (Molecular Probes). Decorated cells were spotted on glass slides and photographed with a Nikon fluorescence microscope and images were processed with Metamorph and Adobe Photoshop Software.

Semi-denaturing detergent agarose gel electrophoresis (SDD-AGE): Rnq1 assembly into SDS-resistant [*RNQ*$^{+}$] prions was monitored by SDD-AGE as previously described (KRYNDUSHKIN*, et al.* 2003) with the following exceptions. Cells were lysed in buffer containing 2% SDS, 5% glycerol, 75 mM Tris-HCl pH 6.8, 2 mM EDTA, 8% 2-mercaptoethanol, 0.05% coomassie blue, 2 mM phenylmethysulfonyl fluoride and a protease inhibitor cocktail (Roche). Proteins resolved by the 1.5% agarose gel were electrophoretically transferred to PVDF in a submerged transfer apparatus for 1.5 hrs at

24 V. PVDF membranes were then decorated with α-GFP and bands were visualized with ECL reagent.

Rnq1 co-immunoprecipitation: Expression of Rnq1-GFP in log phase cells harboring the indicated form of pRS316-Rnq1-GFP was induced by supplementation with 50 μM $CuSO_4$. Cell extracts were prepared 1 hr later under the non-denaturing conditions described above for the pulse-chase analysis. Cell debris was removed by centrifugation and the resulting supernatant was supplemented with either α-Sis1 or α-GFP. Samples were incubated at 4ºC for 1 hr before being supplemented with pre-blocked protein G agarose beads. After 1 hr, the beads were isolated by centrifugation and washed 3 times with lysis buffer. Immuneprecipitated proteins were resolved by SDS-PAGE and detected by western blot.

Size Exclusion Chromatography: [*RNQ*$^+$] or [*rnq*-] cells were grown overnight in synthetic media at 30°C. Rnq1-YFP expression was induced by the addition of 2 % galactose for 4 hrs prior to the collection of 100 OD units of cells. Proteins in extracts created with a non-denaturing lysis buffer were resolved on a Superose 12S sizing column (Pharmacia). Indicated proteins in column fractions were detected by Western blot.

Rnq1 toxicity and [*RNQ*$^+$] assembly in Sis1 depleted cells: A strain in which Rnq1-GFP expression was controlled by the CUP1 promoter and Sis1 expression was controlled the

GAL1 promoter was constructed by transforming W303*Δsis1* with pRS315-*Rnq1-GFP* and pGAL1-*SIS1*. To examine [*RNQ*$^{+}$] toxicity at different Sis1 levels, strains were generated by the plasmid shuffle technique (BOEKE*, et al.* 1987) and then grown on synthetic drop-out plates containing 2% galactose. A single colony was picked, diluted into sterile H_20 and 5-fold serial dilutions were spotted onto plates containing either galactose or glucose in the presence of 500 µM $CuSO_4$. To examine the effect that depletion of Sis1 had on [*RNQ*$^{+}$] assembly, transformants grown on galactose plates were transferred to liquid media containing either glucose or galactose and cultured overnight at 30ºC. Cells were then diluted and grown an additional 12 hrs. Rnq1-GFP expression was then induced by the addition of 500 µM $CuSO_4$ and the formation of SDS-resistant [*RNQ*$^{+}$] particles was measured by SDD-AGE. To demonstrate that Sis1 depleted cells were still capable of [*RNQ*$^{+}$] prion assembly, Sis1 levels were restored by spotting cells cultured in glucose media back onto synthetic galactose plates. After the restoration of Sis levels, [*RNQ*$^{+}$] assembly was monitored as described by SDD-AGE.

Seeded polymerization of purified Rnq1: Purified Rnq1-His was added to lysates of the indicated strains. Assembly was monitored by SDD-AGE. Also see (SHORTER*, et al.* 2006).

His-Rnq1 WT and L94A were expressed from pDEST17 vector in BL21AI cells for 4 hrs at 30 ºC followed by lysis in a buffer that contained 6 M guanidium-HCl and 100 mM potassium phospate buffer pH 7.0. His-Rnq1 was purified by standard techniques on Ni-NTA agarose that was washed with 8 M urea and 100 mM potassium phosphate buffer pH 7.0. His-Rnq1 was eluted with the same buffer at pH 3.0, concentrated by methanol

precipitation and stored at -80 °C. Prior to use His-Rnq1 was resuspended in 6 M guanidium-HCl and filtered through a Microcon YM-100 spin-column. Yeast extracts containing [*RNQ*$^{+}$] seeds were prepared as follows. The indicated form of Rnq1 was expressed from the GAL1 promoter for 4 hrs. Cells were isolated by centrifugation and extracts were created by bead disruption in buffer composed of 40 mM Hepes, pH 7.5, 150 mM KCL, 2 mM DTT, 5% glycerol, 8 mM PMSF, 10 mg/ml aprotinin, and 10 mg/ml leupeptin. An aliquot of purified Rnq1 was adjusted to a final concentration of 5 µM in cell lysate and incubated at 25 ºC for 30 min, without agitation. Samples were then analyzed by SDD-AGE as described above.

Boeke, J.D., Trueheart, J., Natsoulis, G., & Fink, G.R. (1987) 5-Fluoroorotic Acid as a Selective Agent in Yeast Molecular Genetics. *Methods in Enzymology* 154:164-175.

Caplan, A.J. & Douglas, M.G. (1991) Characterization of Ydj1: A Yeast Homologue of the Bacterial Dnaj Protein. *J Cell Biol* 114(4):609-621.

Eaglestone, S.S., Ruddock, L.W., Cox, B.S., & Tuite, M.F. (2000) Guanidine Hydrochloride Blocks a Critical Step in the Propagation of the Prion-Like Determinant [Psi(+)] of Saccharomyces Cerevisiae. *Proc Natl Acad Sci U S A* 97(1):240-244.

Fan, C.Y., Lee, S., Ren, H.Y., & Cyr, D.M. (2004) Exchangeable Chaperone Modules Contribute to Specification of Type I and Type Ii Hsp40 Cellular Function. *Mol Biol Cell* 15(2):761-773.

Kryndushkin, D.S., Alexandrov, I.M., Ter-Avanesyan, M.D., & Kushnirov, V.V. (2003) Yeast [Psi+] Prion Aggregates Are Formed by Small Sup35 Polymers Fragmented by Hsp104. *J Biol Chem* 278(49):49636-49643.

Luke, M.M., Sutton, A., & Arndt, K.T. (1991) Characterization of Sis1, a Saccharomyces Cerevisiae Homologue of Bacterial Dnaj Proteins. *J Cell Biol* 114(4):623-638.

Rudiger, S., Germeroth, L., Schneider_Mergener, J., & Bukau, B. (1997) Substrate Specificity of the Dnak Chaperone Determined by Screening Cellulose-Bound Peptide Libraries. *EMBO Journal* 16(7):1501-1507.

Shorter, J. & Lindquist, S. (2006) Destruction or Potentiation of Different Prions Catalyzed by Similar Hsp104 Remodeling Activities. *Mol Cell* 23(3):425-438.

Supplemental Figures

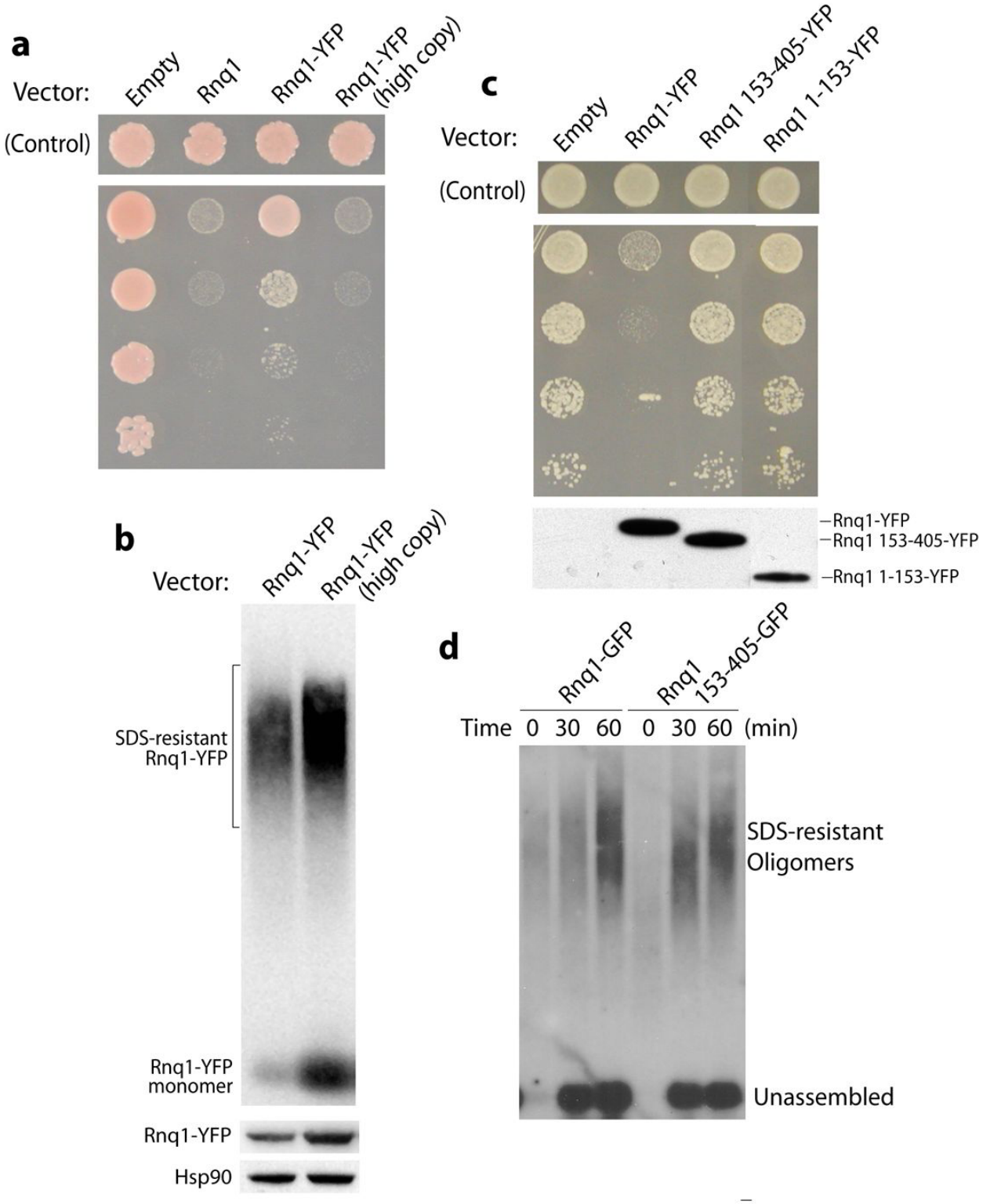

Supplemental Figure C2.1: Factors influencing Rnq1 toxicity include the expression level and presence of a carboxy-terminal tag.

(a) Comparison of the toxicity of untagged Rnq1 to Rnq1-YFP that is expressed at different levels. **(b)** SDD-AGE analysis of the assembly status of Rnq1-YFP expressed from low and high copy expression vectors. The bottom panel represents Western blots depicting Rnq1-YFP levels in the indicated extracts. **(c)** The effect on growth of [*RNQ*$^{+}$] yeast caused by overexpression of full length and truncated Rnq1-YFP fusion. Rnq1 1-153 corresponds to the Rnq1 N-terminal non-prion forming domain. Rnq1 153-405 corresponds to the Rnq1 C-terminal prion-forming domain. Spots that contain 10-fold serial dilutions of indicated yeast strains were positioned horizontally across the plate. The lower panel is a western blot of cell extracts that express the indicated YFP fusion with GFP anti-sera. **(d)** SDS-resistance of Rnq1-GFP or PrD-GFP fusions expressed under control of the CUP1 promoter as analyzed by SDD-AGE.

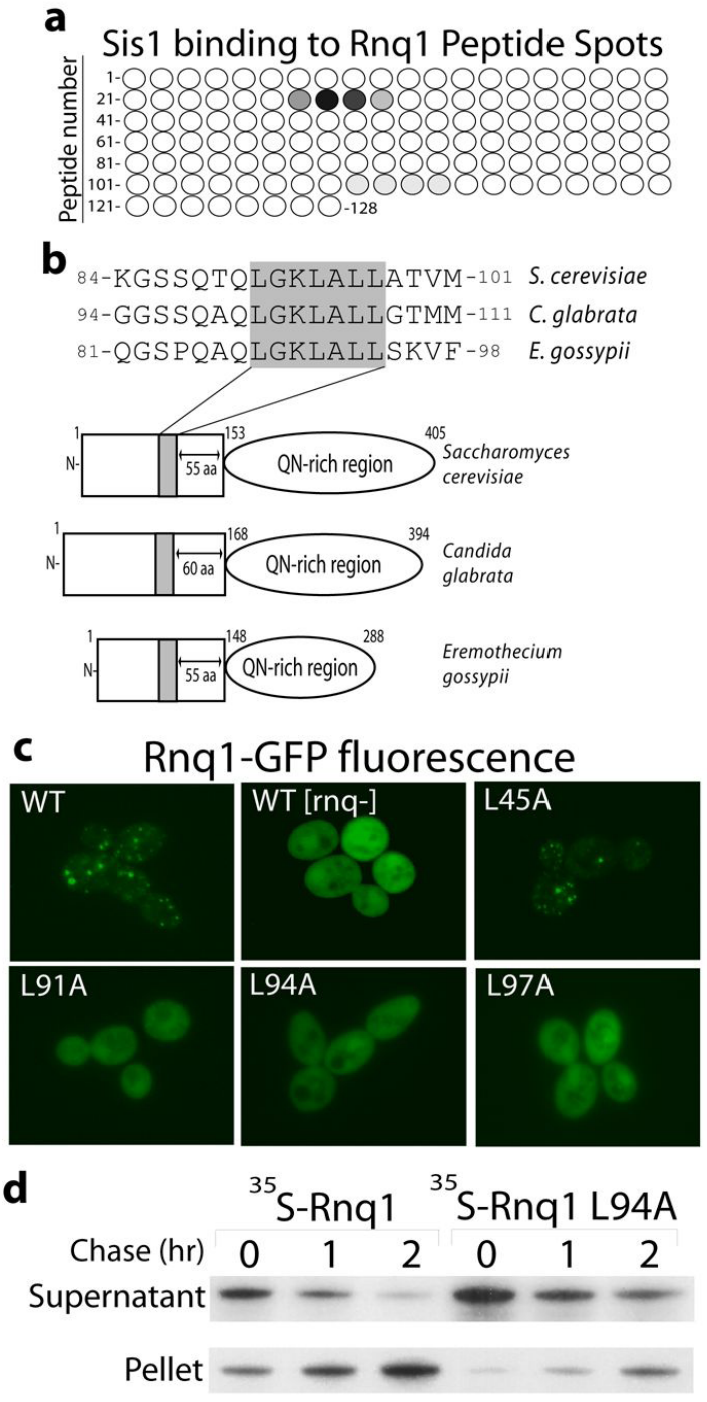

Supplemental Figure C2.2: Mutation of the chaperone-binding motif slows the rate of Rnq1 assembly into [*RNQ*$^{+}$] prions.

(a) Peptide spots in a 25-residue Rnq1 peptide array that were bound by purified Sis1. Shown is a schematic of the Rnq1 peptide array in which circles represent the peptide spots starting at amino acid 1 of Rnq1 and sequentially shift in register by 3 amino acids until the terminal peptide. Filled circles represent peptide spots where Sis1 binding could be detected as significant levels above background. The darkness of the spots correlates with the intensity of Sis1 binding signal. **(b)** Comparison of the Sis1 binding site in Rnq1 with similar regions in the two known Rnq1 homologs from *C. glabrata* and *E. gossypii*. The hydrophobic core within the peptide identified in **b** is conserved between species both in sequence as well as in proximity to the carboxy-terminal, Q/N rich prion-forming domain. The term aa is an abbreviation for amino acid. **(c)** Fluorescence microscopy of live [*RNQ*$^{+}$] cells after the indicated form of Rnq1-GFP was expressed for 1 hr. Rnq1-GFP is under the control of the CUP1 promoter. Expression was induced using 50 μM $CuSO_4$. **(d)** Pulse-Chase analysis of the assembly of nascent Rnq1 into pelletable [*RNQ*$^{+}$] prions. [*RNQ*$^{+}$] cells were labeled with ^{35}S-translabel. At the indicated times cells were lysed and fractionated by centrifugation with an airfuge. Rnq1-GFP present in supernatant and pellet fractions of cell extracts was then isolated by immuneprecipitation with α-GFP sera.

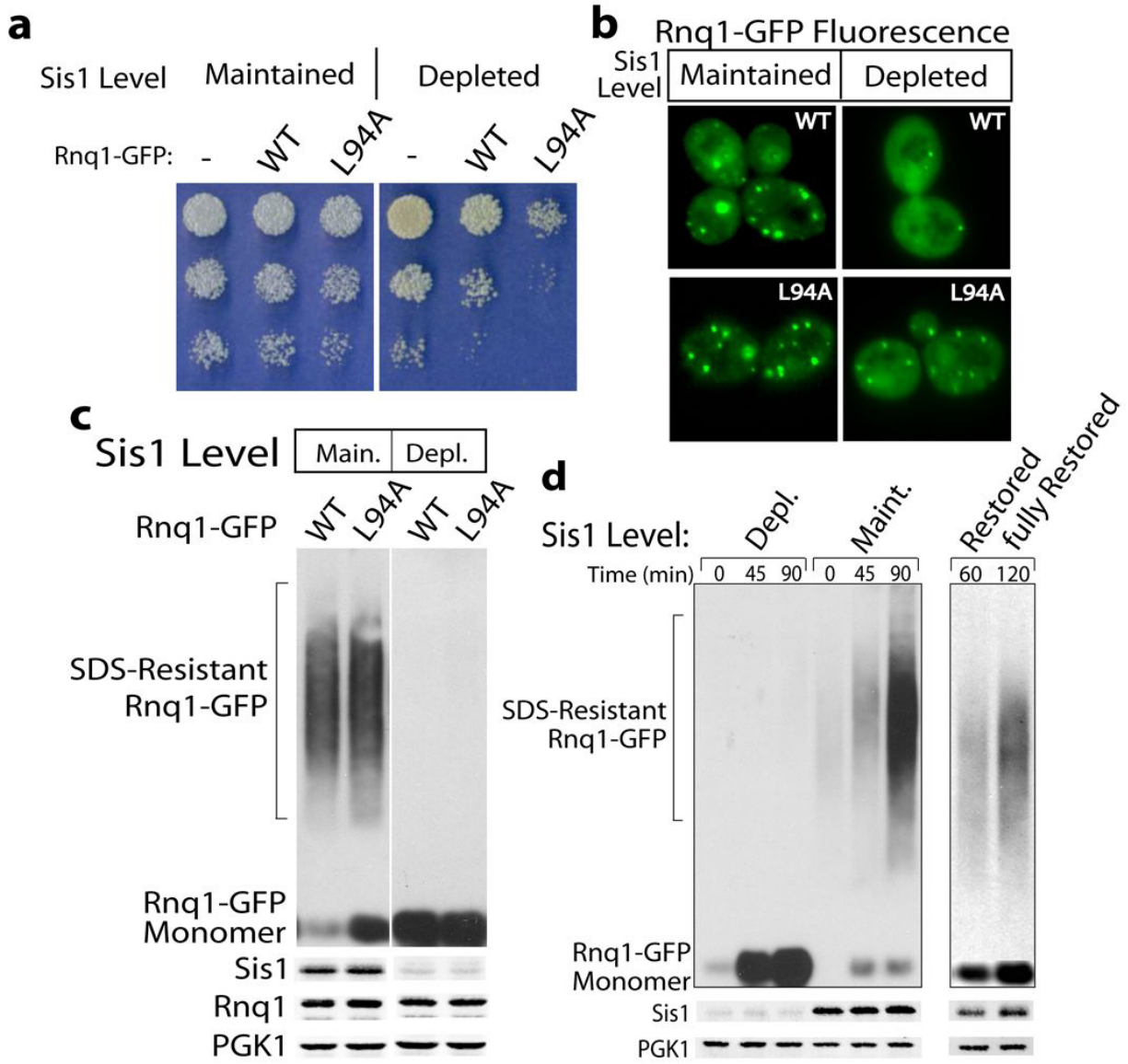

Supplemental Figure C2.3: Depletion of Sis1 hinders assembly of nascent Rnq1-GFP into SDS-resistant [*RNQ*$^{+}$] aggregates.

(a) The influence of Rnq1-GFP and Rnq1-GFP L94A overexpression on cell viability when Sis1 levels are maintained or depleted. A [*RNQ*$^{+}$] *Δsis1* strain that harbored pGAL1-*SIS1* was grown on plates that contained galactose or glucose as the carbon source to maintain Sis1 at close to normal or to deplete Sis1 levels. The same approach was

previously used to characterize the effect of Sis1 depletion on cell growth (LUKE, *et al.* 1991). Rnq1-GFP and Rnq1-GFP L94A were expressed from the CUP1 promoter in the presence of 500 µM $CuSO_4$. Rnq1-GFP expression the CUP1 promoter produces a lower concentration of protein than the GAL1 promoter (ROMANOS, *et al.* 1992) . Thus, the growth defects observed when Rnq1-GFP is expressed from the CUP1 are not as severe as when Rnq1-GFP is overexpressed from the GAL1 promoter (compare Supplemental Figure C2.1a to Figure S3a). Sis1 was depleted from a D*sis1* strain, which was maintained by a pGAL1-*SIS1* plasmid, by shifting the strain from galactose to glucose medium. Consistent with a previous report (LUKE, *et al.* 1991), the near complete depletion of Sis1 did not cause yeast to exhibit growth defects on its own, but it did exacerbate Rnq1-GFP cytotoxicity. Further, this effect was far more severe for the L94A mutant than for wild-type Rnq1. **(b)** Coalescence of Rnq1-GFP and Rnq1-GFP L94A into foci in Sis1 depleted cells. **(c)** SDD-AGE analysis of Rnq1-GFP and Rnq1-GFP L94A assembly into SDS-resistant conformers at normal and low Sis1 levels. The lower panels depict levels of the indicated proteins as determined by Western blot. These data demonstrate that the foci formed by Rnq1 L94A under toxic conditions are sensitive to SDS-treatment, and thus, do not appear to represent [*RNQ*$^{+}$] prions. **(d)** Restoration of [*RNQ*$^{+}$] prion formation in Sis1 depleted cells upon reintroduction of normal Sis1 expression. Bottom panels depict Sis1 and PGK levels in the indicated extracts as determined by Western blot. Data in panel (d) indicate that defects in the assembly of Rnq1 and Rnq1 L94A into SDS-resistant species observed upon depletion of Sis1, are not resultant from curing [*RNQ*$^{+}$] prion seeds from cells.

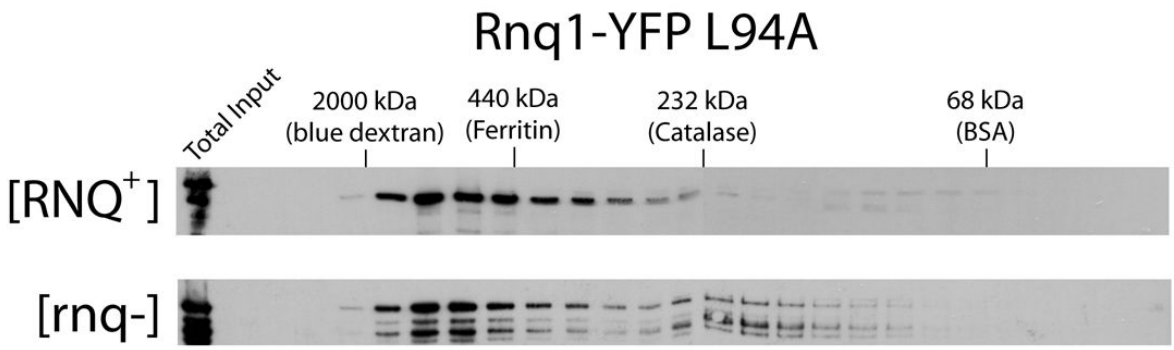

Supplemental Figure C2.4: Analysis of the mobility of Rnq1 L94A in extracts from [*RNQ*$^{+}$] and [*rnq*-] strains by gel filtration chromatography.

Rnq1-YFP L94A was expressed from the GAL1 promoter for 4 hrs in the indicated strain**.** Extracts were prepared under native buffer conditions and loaded onto a Superose 12S column. The mobility of Rnq1-YFP L94A was determined with Western blot of column fractions with anti-GFP sera.

Chapter Three:

Toxic overexpression of the prion Rnq1 causes a cell cycle arrest by sequestering the spindle pole body component Spc42

Abstract

The accumulation of intrinsically disordered proteins in aggregates is associated with a variety of human diseases. Indeed, intrinsic protein disorder is an important determinant of the gain-of-function proteotoxicity of overexpressed proteins. The yeast prion protein Rnq1 is intrinsically disordered and profoundly toxic when overexpressed in strains carrying the [*RNQ*$^{+}$] prion amyloid conformation. Here, we demonstate that Rnq1 toxicity results in a Mad2-mediated mitotic cell cycle arrest. Rnq1 overexpression results in the formation of a monopolar spindle due to a defect in the duplication of the spindle pole body, the yeast centrosome. We found that increased levels of Rnq1 induced the mis-localization of the core spindle pole body component Spc42 to the IPOD (insoluble protein deposit). Moderate overexpression of Spc42 suppressed Rnq1 toxicity confirming that the effect of Rnq1 on Spc42 localization is responsible for its toxicity. Our work illustrates how intrinsically disordered proteins can result in proteotoxicity due to illicit interactions with essential proteins. The IPOD appears to be the yeast equivalent of the centrosome-associated aggresomes of higher eukaryotes and our findings provide the first link between the IPOD and the spindle pole body.

Introduction

Amyloids are β-sheet-rich fibrous structures that can be formed by proteins with many different amino acid sequences (CHITI*, et al.* 2006). Their formation is associated with a wide variety of human diseases (ROSS*, et al.* 2005). Yet, with the exception of the systemic amyloidoses, amyloids are no longer thought to be the primary source of

toxicity (KAYED, *et al.* 2003; TREUSCH, *et al.* 2009). Rather, it is the propensity of these amyloidogenic proteins to form soluble oligomers that provides a common thread underlying their gain of function toxicities. Furthermore, these proteins are often intrinsically disordered. Intrinsic protein disorder is the best predictor of gene dosage sensitivity and may enable detrimental mass-action-driven interaction promiscuity (VAVOURI, *et al.* 2009). Indeed, the toxicity of artificial β-sheet proteins is mediated by their ability to interact with disordered proteins that occupy essential hub positions in cellular protein networks (OLZSCHA, *et al.* 2011).

Yeast provides a particularly interesting class of proteins for studying the cellular impacts of intrinsically disordered proteins. Yeast prion proteins are intrinsically disordered proteins that can stably exist in soluble or self-perpetuating amyloid conformations (SHORTER, *et al.* 2005; WICKNER, *et al.* 2004). Once a prion protein adopts an amyloid state its self-templating properties allow it to function as a cytoplasmically inherited protein-based genetic element (CHIEN, *et al.* 2004; COX, *et al.* 2003; LIEBMAN, *et al.* 1999; SHORTER, *et al.* 2005; TUITE, *et al.* 2003; WICKNER, *et al.* 2007).

Seven yeast prions have been identified (ALBERTI, *et al.* 2009; DU, *et al.* 2008; NEMECEK, *et al.* 2009; PATEL, *et al.* 2009; SONDHEIMER, *et al.* 2000; WICKNER 1994) and evidence indicates that several other yeast proteins are capable of forming amyloid-based prions (ALBERTI, *et al.* 2009). These prion proteins are characterized by the presence of a "prion domain", enriched in asparagine and glutamine amino acid residues, which is intrinsically disordered but can adopt an amyloid conformation (CHIEN, *et al.* 2004; SHORTER, *et al.* 2005; WICKNER, *et al.* 2007).

Rnq1 contains such a prion domain (SONDHEIMER, *et al.* 2000) and its [*RNQ*$^{+}$] prion state enables the formation of other prions (DERKATCH, *et al.* 2001; DERKATCH, *et al.* 2000; OSHEROVICH, *et al.* 2001; TANEJA, *et al.* 2007). (Prion status is denoted by brackets, italics and capital letters to reflect a prion's dominant, non-Mendelian genetic properties.) [*RNQ*$^{+}$] also enables the glutamine-expanded exon one fragment of huntingtin to adopt a toxic conformation when expressed in yeast (MERIIN, *et al.* 2002). In part Rnq1 may influence the aggregation of other proteins based on its localization to the IPOD (insoluble protein deposit) (KAGANOVICH, *et al.* 2008; TYEDMERS, *et al.* 2010).

In yeast, misfolded proteins can accumulate at two distinct sites, the JUNQ (juxta-nuclear quality control compartment) and the IPOD (KAGANOVICH, *et al.* 2008). The JUNQ forms mostly upon inhibition of the proteasome and contains poly-ubiquitinated proteins targeted for proteasomal degradation. The IPOD co-localizes with the pre-autophagosomal structure at the vacuole and holds amyloidogenic proteins, such as yeast prions and ectopically expressed mutant huntingtin fragments (KAGANOVICH, *et al.* 2008; TYEDMERS, *et al.* 2010).

Both JUNQ and IPOD share features with the aggresome of higher eukaryotes. Aggresomes are highly structured protein deposits that are actively formed near centrosomes through dynein-dependent retrograde transport of protein aggregates along microtubules (GARCIA-MATA, *et al.* 1999; JOHNSTON, *et al.* 2002; JOHNSTON, *et al.* 1998). Neither, JUNQ nor IPOD, has been shown to associate with the spindle pole body (SPB), the yeast equivalent of the centrosome.

We have previously reported that overexpression of Rnq1 is benign in cells whose endogenous Rnq1 is in the soluble state, but is extremely toxic if the endogenous protein is in the [*RNQ*$^{+}$] state (DOUGLAS*, et al.* 2008). Rnq1 toxicity is an intriguing model for amyloid and protein disorder associated gain-of-fucntion proteotoxicity, as deletion of *RNQ1* has no effect on cell growth. Intriguingly, the amyloid form of Rnq1 was not the toxic species, but rather Rnq1 amyloid formation was protective. Enhancing Rnq1 amyloid formation by co-overexpression of the Hsp40 co-chaperone Sis1, which co-assembles with the amyloid, restored cell growth. In complementary experiments, Rnq1 mutants with a decreased ability to interact with Sis1 exhibited increased toxicity and formed non-amyloid aggregates. Hence, amorphous non-amyloid aggregates or oligomeric species formed by this intrinsically disordered protein caused the associated toxicity (DOUGLAS*, et al.* 2008).

Here we investigated the mechanism by which Rnq1 overexpression results in toxicity. We conducted two genome-wide screens for suppressors of Rnq1 toxicity and examined the gene expression profile elicited by Rnq1 overexpression. Rnq1 toxicity results in a mitotic cell cycle arrest and a monopolar mitotic spindle. We show that Rnq1 overexpression causes the mislocalization of the core spindle pole body component Spc42. Rnq1 toxicity preempts SPB duplication and triggers cell cycle arrest.

Results

RNQ1 and *HSP104* are the only non-essential genes strictly required for Rnq1 toxicity and the [*RNQ*$^{+}$] prion state

To characterize Rnq1 toxicity, we conducted two unbiased genome-wide screens for genetic suppressors. First, we screened the two haploid deletion libraries, Mat a and Mat α (WINZELER, *et al.* 1999), for non-essential genes that are required for Rnq1-induced toxicity. These libraries contain deletions of all the non-essential yeast ORFs and, importantly, were generated independently using two [*RNQ*$^{+}$] strains (WINZELER, *et al.* 1999). Of the deletions that suppressed Rnq1 toxicity, only 69 were found in both libraries suggesting that most putative suppressors resulted from spontaneous loss of the Rnq1 prion. Indeed, after prion reintroduction into these strains, only twelve deletions were still capable of suppressing Rnq1 toxicity. These included, as expected, the two non-essential genes previously known to be required for the [*RNQ*$^{+}$] prion state: *RNQ1* itself and *HSP104*. The AAA+ ATPase Hsp104, which shears amyloid to generate heritable prion seeds, is required for prion inheritance (COX, *et al.* 2003; TAGUCHI, *et al.* 2010).

To definitively show that the effect on Rnq1 toxicity was due to the deletions, we re-created the identified deletions in two distinct yeast strains, BY and W303. Aside from the *HSP104* and *RNQ1* deletions, only three of the re-created deletions, *ksp1Δ*, *pml39Δ* and *spf1Δ,* had a modest effect on Rnq1 toxicity (Table C3.1 & Supplemental Figure C3.1). While our screen did not identify genes required for Rnq1 toxicity, it suggests that no non-essential gene, aside from Hsp104 and Rnq1, is individually required for the maintenance of the [*RNQ*$^{+}$] prion state. This result is supported by a recently published screen that used [*PSI*$^{+}$] induction as a readout of the Rnq1 prion state (MANOGARAN, *et al.* 2010). In addition, as no deletion could specifically abrogate Rnq1

toxicity the toxicity is not mediated by a Rnq1 modulated gain-of-function of a non-essential gene.

Overexpression of a diverse group of genes can suppress Rnq1 toxicity

We have previously shown that Sis1 overexpression can alleviate Rnq1 toxicity by facilitating amyloid formation (DOUGLAS*, et al.* 2008). Hence, we screened a yeast overexpression library to identify further genes that modulate Rnq1 toxicity. The plasmid-based overexpression library contains yeast ORFs controlled by the inducible *GAL1* promoter and has been previously used to identify modifiers of toxicity induced by expression of alpha-synuclein (COOPER*, et al.* 2006; GITLER*, et al.* 2009), a protein implicated in Parkinson's disease.

We identified 20 putative hits whose overexpression suppressed Rnq1 toxicity. Nine of the twenty genes had no effect on *GAL1*-driven YFP expression (Supplemental Figure C3.2), showing that their suppression of Rnq1 toxicity is not due to their repression of *GAL1*-mediated gene expression (Table C3.1). The Hsp40 Sis1, which we had identified as a suppressor previously (DOUGLAS*, et al.* 2008) was among the nine validated suppressors. The other screen hits were *GPG1*, *HRR25*, *MSA1*, *NSP1*, *NVJ1*, *SPC29*, *THI2* and *YNL208w*. The screen hit *GPG1*, which has recently been shown to antagonize prion formation (ISHIWATA*, et al.* 2009), suppressed the toxicity created by Rnq1 overexpression as strongly as *SIS1* (Figure C3.1a). Overall the suppressors were not enriched in any particular functional categories, although three have functions connecting them loosely to the cell cycle (*HRR25*, *MSA1* & *SPC29*). Notably, however,

the suppressors were enriched for proteins with prion domains (Table C3.2) (ALBERTI, *et al.* 2007).

Suppressor identified in:	Standard Name	Functional Annotation
Deletion screen	*KSP1*	Ser/thr protein kinase; nuclear translocation required for haploid filamentous growth
	PML39	Protein required for nuclear retention of unspliced pre-mRNAs
	SPF1	P-type ATPase, ion transporter of the ER membrane involved in ER function and Ca2+ homeostasis
Overexpression screen	*GPG1*	Proposed gamma subunit of the heterotrimeric G protein; overproduction causes prion curing
	HRR25	Protein kinase involved in regulating diverse events including vesicular trafficking, DNA repair, and chromosome segregation
	MSA1	Activator of G1-specific transcription factors; involved in regulation of the timing of cell cycle initiation
	NSP1	Essential component of the nuclear pore complex, which mediates nuclear import and export
	NVJ1	Nuclear envelope protein, involved in nuclear microautophagy
	SIS1	Type II HSP40 co-chaperone that interacts with the HSP70 protein Ssa1p
	SPC29	Inner plaque spindle pole body (SPB) component; required for SPB duplication
	THI2	Zinc finger protein of the Zn(II)2Cys6 type, probable transcriptional activator of thiamine biosynthetic genes
	YNL208w	Protein of unknown function

Table C3.1: Suppressors of Rnq1 toxicity identified in screens of the deletion and overexpression libraries. Functional Annotations are based on the *Saccharomyces* Genome Database.

Proteins with prion-like domains do not affect Rnq1 amyloid formation

Amyloid formation can be protective and overexpression of proteins with prion-like domains has been shown to increase the induction of [*PSI*$^{+}$] (DERKATCH*, et al.* 2001; DERKATCH*, et al.* 2004; OSHEROVICH*, et al.* 2001). Thus, we next asked whether the genes identified as overexpression suppressors of Rnq1 toxicity affected Rnq1 amyloid formation. We used semi-denaturing agarose gels to analyze the lysates of cells expressing both Rnq1 and individual suppressors (BAGRIANTSEV*, et al.* 2006; HALFMANN*, et al.* 2008). In these semi-denaturing gels, the detergent-resistant amyloid species formed by prion proteins run as broad high-molecular-weight bands. Detergent-sensitive species, such as prefibrillar oligomers and disordered aggregates, are dissolved and run as bands corresponding to the size of the particular protein monomer. As suggested by the flow cytometry analysis (Supplemental Figure C3.2), by standard SDS-PAGE based western blotting the suppressors had no effect on levels of overexpressed Rnq1 (Figure C3.1b). Sis1 overexpression, as we reported previously, increased Rnq1 amyloid conformation (Figure C3.1b) (DOUGLAS*, et al.* 2008). In contrast, Gpg1 decreased the amount of amyloid and increased the amount of soluble Rnq1. The suppressors with prion-like domains, Hrr25, Nsp1 and YNL208w, did not affect Rnq1 amyloid formation (Figure C3.1b).

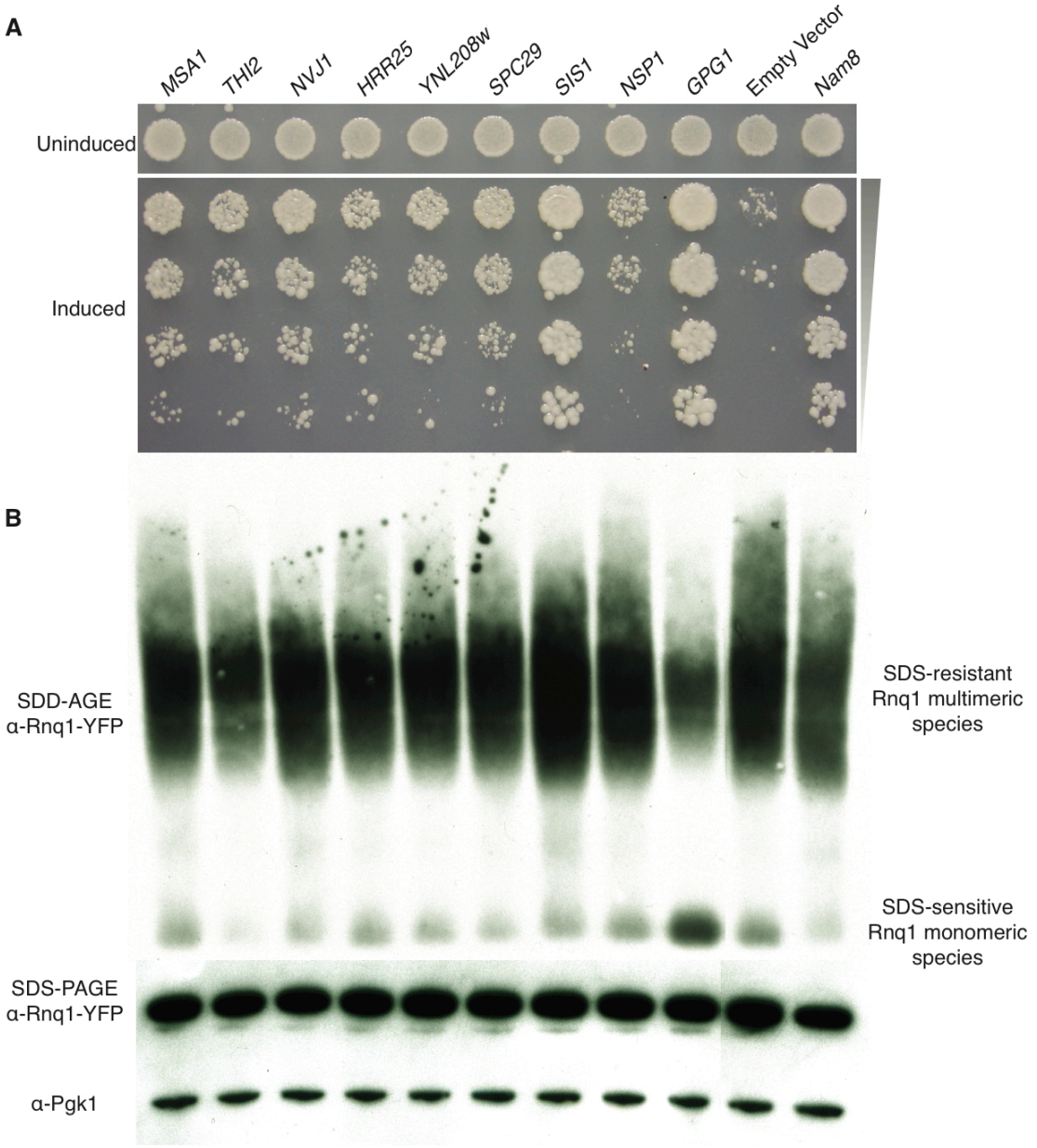

Figure C3.1: Overexpression suppressors of Rnq1 toxicity.

(A) Strains expressing individual genes that suppress Rnq1 toxicity and that do not affect *GAL1*-mediated expression were serially diluted and spotted on a non-inducing control plate and an inducing assay plate. *NAM8,* which decreases *GAL1*-mediated expression, served as a positive control for rescue**. (B)** SDD-AGE analysis of the effect of the OE screen hits on Rnq1-YFP amyloid formation. *SIS1* increased

the formation of SDS-resistant Rnq1-YFP species; *GPG1* decreased it. Rnq1-YFP expression levels were examined in the same samples by standard SDS-PAGE, followed by western blot analysis. We probed for the housekeeping protein Pgk1 to ensure equal sample loading. Samples were induced for six hours.

Suppressors with prion-like domains co-localize with Rnq1 inclusions

Next, we asked if the suppressors alter Rnq1 toxicity by direct associations with Rnq1. We created C-terminal cerulean fusions of the screen hits and examined their localization with respect to the Rnq1-YFP fusion. *GAL1*-mediated Rnq1-YFP expression in a [*RNQ*$^{+}$] background results in the formation of a single focus proximal to the vacuole, consistent with localization to the IPOD compartment (KAGANOVICH*, et al.* 2008). Sis1, as expected based on its tight interaction with [*RNQ*$^{+}$] species (SONDHEIMER*, et al.* 2001), localized to Rnq1-YFP inclusions (Figure C3.2a). Gpg1, which lacks prion-like characteristics, was found in very small foci that partially co-localized with Rnq1-YFP deposits (Figure C3.2a). The formation of these Gpg1 foci also occurred in a [*rnq*-] background and as such was independent of Rnq1 amyloid formation (data not shown). Suppressors without prion-like domains, aside from Sis1 and Gpg1, did not co-localize with Rnq1-YFP deposits. The suppressors containing prion-like domains co-localized with the Rnq1-YFP inclusions (Figure C3.2b). In contrast to Ggp1, the localization of suppressors of with prion-like domains to an inclusion was dependent on the [*RNQ*$^{+}$] prion, as they displayed diffuse fluorescence in a [*rnq*-] background (Table C3.2). These results suggest that proteins with prion domains suppress Rnq1 toxicity by interacting with Rnq1 and preventing it from making other toxic interactions.

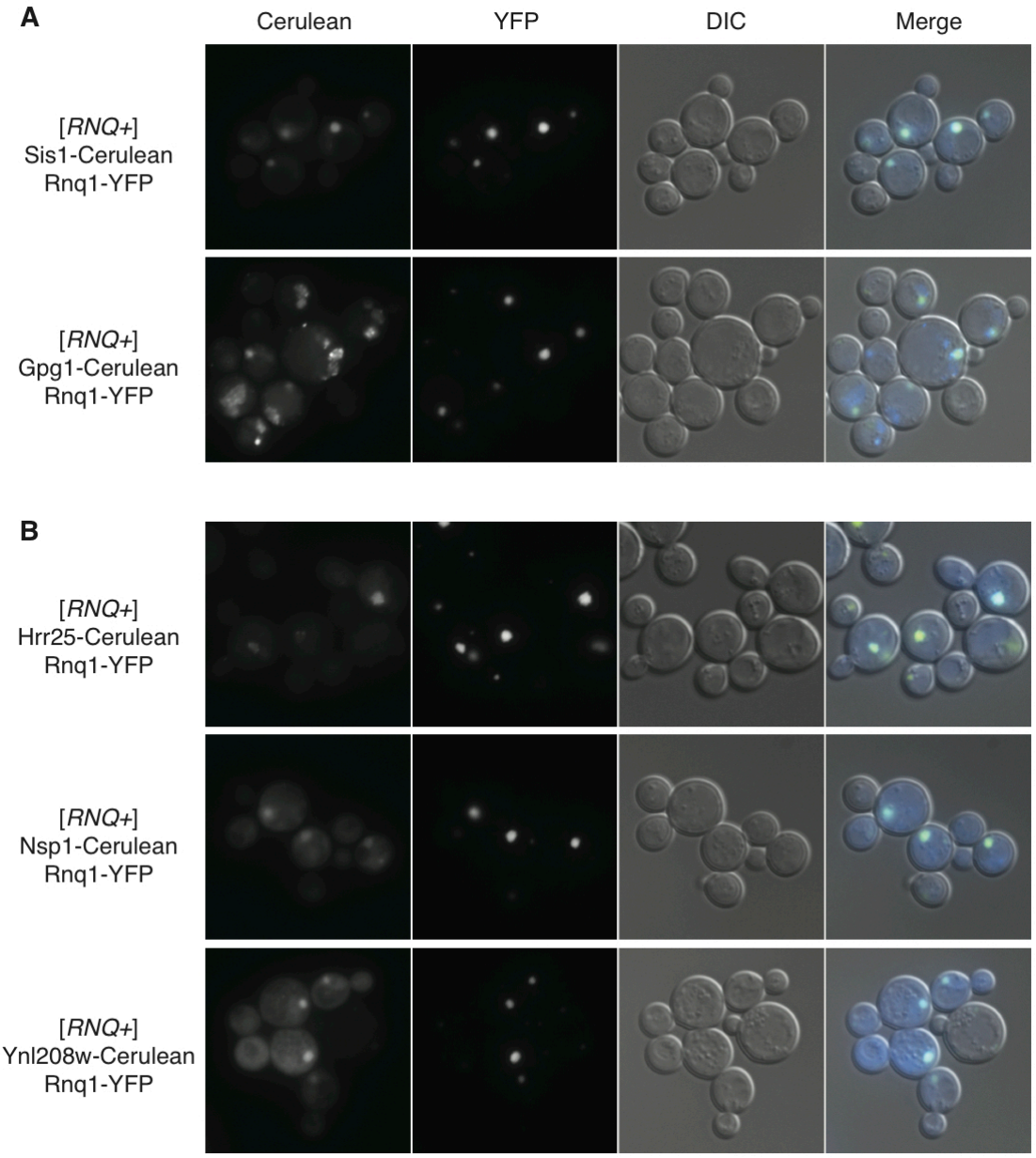

Figure C3.2: Co-localization of OE screen hits with Rnq1.

(A) We tested if Sis1 and Gpg1, which both affect Rnq1 amyloid formation, co-localize with Rnq1-YFP inclusion. Co-localization was assayed using N-terminal Cerulean Gpg1 and Sis1 fusions in conjunction with Rnq1-YFP. Sis1 co-localizes very well with Rnq1. Gpg1 forms small foci, in both [*RNQ*$^{+}$] and [*rnq*-] strain backgrounds, which partially co-

localize with Rnq1. (**B)** Next, we examined the localization of the remaining screen hits including the screen hits containing prion domains. OE screen hits with prion domains, Hrr25, Nsp1 and YNL208w, co-localized with Rnq1. Screen hits without prion domains did not co-localize with Rnq1-YFP inclusions.

Screen hit	Contains prion domain	Co-localization with Rnq-YFP in [*RNQ*$^{+}$]	Foci formation in [*rnq*-] cells
KSP1	+	-	-
PML39	-	-	-
SPF1	-	-	-
GPG1	-	+	+
HRR25	+	+	-
MSA1	-	-	-
NSP1	+	+	-
NVJ1	-	-	-
SIS1	-	+	-
SPC29	-	-	-
THI2	-	-	-
YNL208w	+	+	-

Table C3.2: Overexpression screen hits with prion-like domains co-localize with Rnq1-YFP aggregates. Four of the hits from the deletion and overexpression screens contain prion domains. The three proteins with prion domains identified in the overexpression screen, Hrr25, Nsp1 and Ynl208w, co-localized with Rnq1 inclusions.

Rnq1 toxicity results in down-regulation of cytokinetic genes

Next, we performed microarray-based gene expression analysis to elucidate the transcriptional response triggered by Rnq1 toxicity. As Rnq1 overexpression is toxic in a [*RNQ*$^{+}$] background, but shows no effect in a [*rnq*-] background, we analyzed the effect of Rnq1 overexpression on gene expression in two isogenic strains that differed solely in their Rnq1 prion state. We expressed Rnq1 from a single copy plasmid under control of the *GAL1* promoter in the [*RNQ*$^{+}$] and [*rnq*-] backgrounds for four, six and eight hours before harvesting the cells and isolating their RNA.

Interestingly, only a few genes were differentially expressed between the two strains (Supplemental Table C3.1). As might be expected, Rnq1 overexpression resulted in the elevated transcription of several chaperones and stress related proteins (Table C3.3), but did not trigger a complete heat shock response. In addition to chaperones known to influence yeast prion amyloid formation, *GPG*1 and *BTN2* were up-regulated upon Rnq1 toxicity (Supplemental Table C3.1). As mentioned and in part shown above, Gpg1 overexpression can antagonize amyloid formation (ISHIWATA*, et al.* 2009). Similarly, Btn2 overexpression has been shown to counteract inheritance of [*URE3*], the prion form of Ure2, and to co-localize with both Sup35 and Rnq1 prion deposits (KRYNDUSHKIN*, et al.* 2008).

While the genes up-regulated in response to Rnq1 toxicity indicate a response to protein folding stress, a large fraction of down-regulated genes is involved in cytokinesis. Together with the fact that several suppressors have cellular functions

related to the cell cycle, this suggests that Rnq1 toxicity maybe related to a defect in cell cycle completion (Table C3.3).

Categories of genes changed 2-fold upon Rnq1 overexpression					
	GO-term	Cluster frequency	Background frequency	P-value	Gene(s)
Up after 6h	protein folding	3/8, 37.5%	88/7167, 1.2%	0.00201	HSP104, SIS1, SSA4
Down after 6h	cytokinesis, completion of separation	4/13, 30.8%	11/7167, 0.2%	4.90E-08	CTS1, DSE2, DSE4, SCW11
Up after 8h	protein folding	4/23, 17.4%	88/7167, 1.2%	0.01368	HSP26, HSP104, SIS1, SSA4
Down after 8h	cytokinesis, completion of separation	5/27, 18.5%	11/7167, 0.2%	1.98E-08	CTS1, DSE1, DSE2, DSE4, SCW11
	hexose transport	3/27, 11.1%	24/7167, 0.3%	0.00778	HXT3, HXT6, HXT7

Table C3.3: Categories of genes changed 2-fold upon Rnq1 overexpression.

Genes that changed more than 2-fold in the [*RNQ*$^{+}$] strain in comparison to the [*rnq*-] strain were analyzed for GO-term enrichment.

Rnq1 overexpression causes cell cycle arrest in mitosis

Based on the gene expression data, we next tested whether Rnq1 toxicity caused defects in cell cycle progression. When Rnq1 was overexpressed for eight hours in the [*RNQ*$^{+}$] background, many cells arrested with large buds, i.e. presented as dumbbell-shaped cells (Figure C3.3a), indicative of a cell cycle arrest (HARDWICK 1998; NYBERG*, et al.* 2002). To define the precise arrest point we next measured DNA content using flow cytometry. Switching mid-log cultures from non-inducing raffinose media to inducing galactose media had the effect of roughly synchronizing the cultures in G1 as the cells adjusted to the new carbon source. In contrast to [*rnq*-] cultures, [*RNQ*$^{+}$] cultures overexpressing Rnq1 became enriched in cells with 2N DNA content (Figure C3.3b & Supplemental Table C3.2). We further delineated the Rnq1 induced arrest by examining cells carrying a Hof1-GFP fusion. Hof1, which regulates actomyosin ring dynamics and septin localization, is specifically degraded at the end of mitosis (BLONDEL*, et al.* 2005). In cells arrested due to overexpression of Rnq1, Hof1-GFP accumulated at the bud neck, demonstrating that these cells arrested before the initiation of cytokinesis (Figure C3.3c).

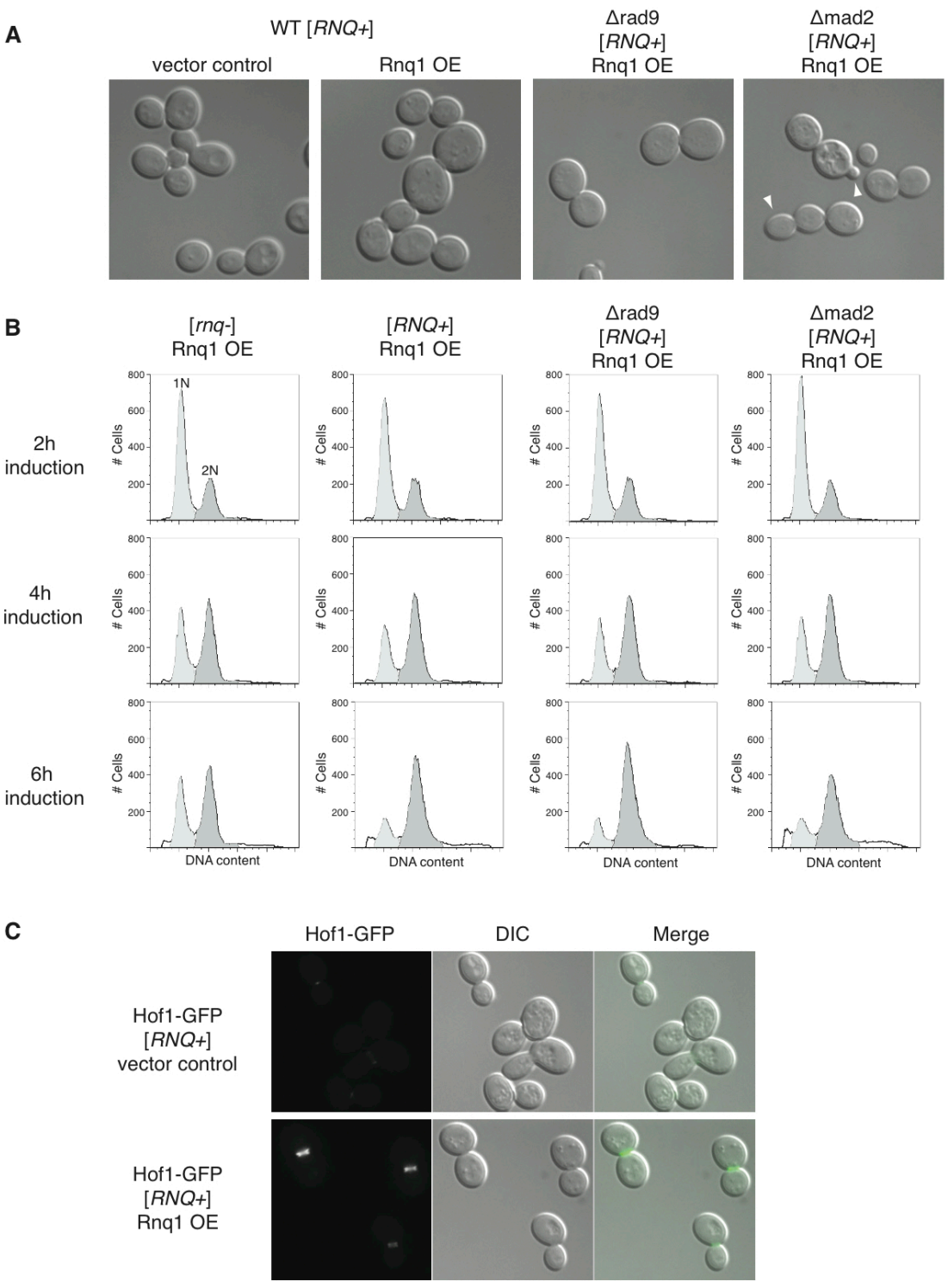

Figure C3.3: Rnq1 overexpression induces a *MAD2*-dependent cell cycle arrest.

(A) Rnq1 overexpression in a [*RNQ*$^{+}$] background results in a cell-cycle arrest at the G2/M transition, i.e. cells arrest just prior to cytokinesis and take on a dumbbell shape. Deletion of *RAD9*, component of the DNA damage checkpoint, has no effect on the Rnq1-induced arrest. On the contrary, deletion of *MAD2*, component of the spindle checkpoint, allows cells to "escape" arrest and to start rebudding. Arrowheads indicate rebudded cells.

(B) Cell cycle profiles of cells overexpressing Rnq1 reveal that Rnq1 toxicity coincides with an increase in cells with 2N DNA content beginning at 4h post induction. In the *MAD2* deletion the right-hand shoulder of the 2N peak is considerably extended at 6h. This is indicative of cells being able to "escape" arrest and to rebud.

(C) Hof1p facilitates cytokinesis and is degraded once cytokinesis is completed. Cells arrested due to Rnq1 overexpression accumulate Hof1 (bottom panel), detected using a Hof1-GFP fusion, illustrating that these cells arrested just prior to cytokinesis.

A large budded cell cycle arrest can be triggered by either DNA damage or the spindle checkpoint. To determine which of these two cell cycle phenomena contributes to the Rnq1-induced arrest, we examined gene Rnq1 toxicity in strains deleted for either the DNA damage, *rad9*Δ (WEINERT*, et al.* 1988), or the spindle checkpoint, *mad2*Δ (HARDWICK*, et al.* 1999), were abrogated. In the absence of damage to DNA or the spindle apparatus, deletion of these two genes has no effect on cell cycle progression. Overexpression of Rnq1 in *rad9*Δ cells resulted in the accumulation of dumbbell-shaped cells (Figure C3.3a) and DNA-content profiles identical to the ones observed with wild type [RNQ^{+}] cells (Figure C3.3b). In contrast, *mad2*Δ cells revealed an increase in cells with a DNA content higher than 2N (Figure C3.3b). Light microscopy showed that many of the *mad2*Δ cells arrested upon Rnq1 overexpression had begun to rebud. In wild type [*RNQ+*] cells, only 8.6% (STDev 2.6) of arrested cells began rebud, while in *mad2*Δ cells, 22.4% (STDev 2.7) formed additional buds. This indicates that Rnq1 overexpression specifically triggers the spindle checkpoint that then mediates the observed cell cycle arrest.

Rnq1 toxicity results in arrest with a monopolar spindle

To elucidate how Rnq1 triggers the spindle checkpoint, we assessed spindle formation by immuno-staining cells overexpressing Rnq1 for tubulin. [*rnq*-] cells displayed a range of spindle morphologies as expected for unsynchronized cells dividing normally (Figure C3.4a). In contrast, [RNQ^{+}] cells that had arrested due to Rnq1 over-

expression showed an aster of microtubules localized proximal to the bud neck (Figure C3.4a). This is indicative of cells arresting with a monopolar spindle.

The spindle pole body (SPB) is the microtubule organizing center (MTOC), the budding yeast equivalent of the centrosome (JASPERSEN, *et al.* 2004). A monopolar spindle can be caused by a defect in SPB duplication or a failure in separation after duplication (JASPERSEN, *et al.* 2004). The SPB spans the nuclear envelope and is duplicated during the G1 phase of the cell cycle. While duplication itself occurs early in the cell cycle, defects in duplication are not detected until the absence of a functional bipolar spindle triggers the spindle checkpoint (JASPERSEN, *et al.* 2004).

We used cryo electron microscopy (EM) to determine if the arrest with a monopolar spindle was caused by a failure in SPB duplication or in the separation of the duplicated SPBs. Cells overexpressing Rnq1, whose endogenous protein was in the [*rnq*-] conformation developed regular elongated spindles (Figure C3.4b). In contrast, [*RNQ*$^{+}$] cells contained microtubule asters originating from a single unduplicated SPB (Figure C3.4b). This suggests that Rnq1 toxicity impedes SPB duplication, potentially by sequestration of SPB components or aberrant interaction with the duplicating SPB itself.

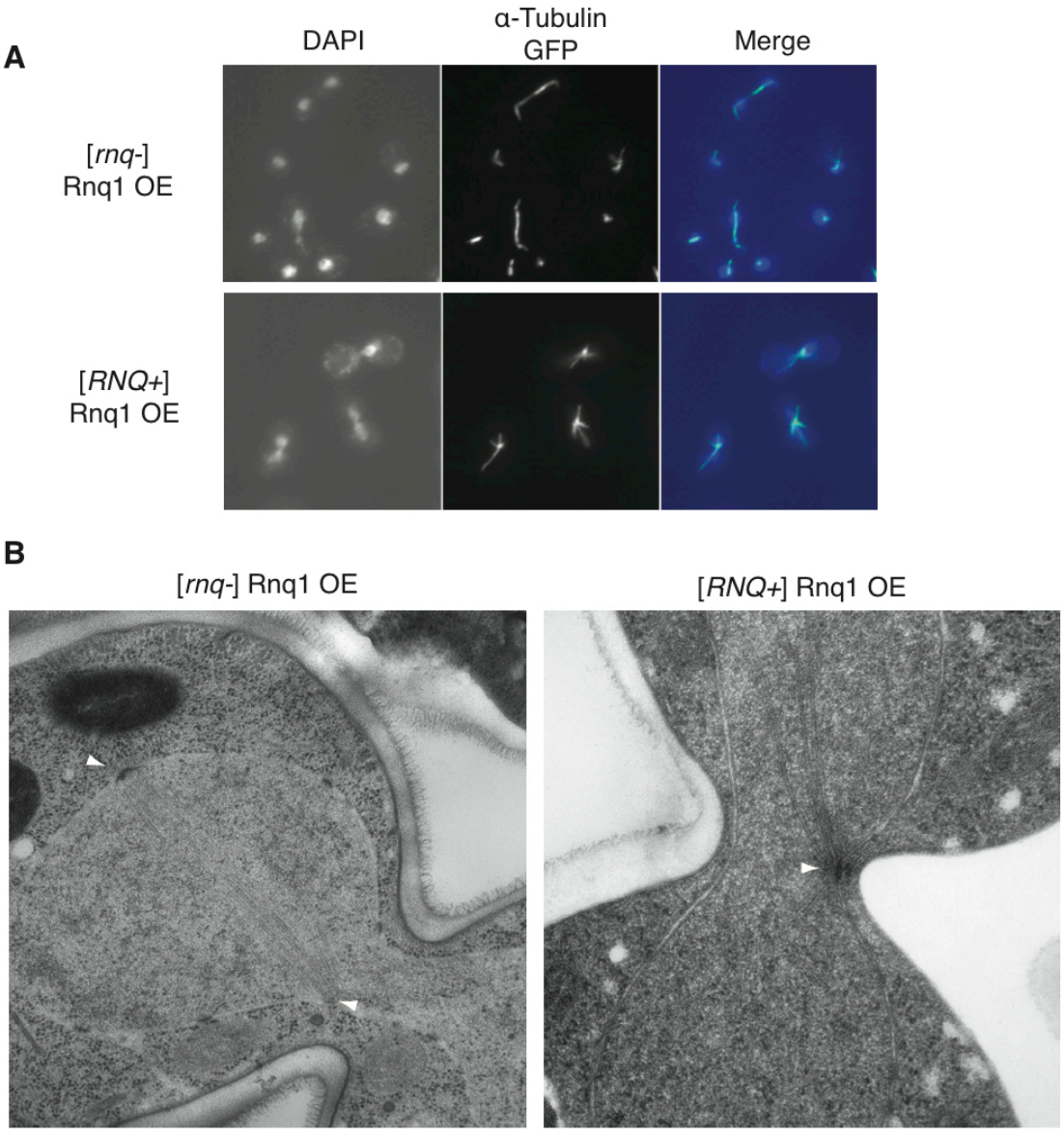

Figure C3.4: Rnq1 toxicity results in arrest with a monopolar spindle.

(A) Tubulin immunostaining of cells overexpressing Rnq1 reveals that [*rnq*-] cells formed regular spindles, whereas [*RNQ*$^{+}$] cells arrested with a monopolar spindle.

(B) Cryo electron microscopy revealed that [*RNQ*$^{+}$] cells arrested with an unduplicated spindle pole body. Arrowheads indicate spindle pole bodies. The observed spindle pole body morphologies were consistent with those previously observed for mutants of the core spindle body component Spc42.

Rnq1 overexpression causes mislocalization of Spc42

Architecturally, the SPB consists of three plaques: an outer plaque facing the cytoplasm, a central plaque spanning the nuclear membrane, and an inner plaque facing the nucleoplasm (JASPERSEN*, et al.* 2004). We examined the localization of spindle body components belonging to each of these structural elements using strains in which the endogenous genes were GFP-tagged (HOWSON*, et al.* 2005): The outer plaque components Cnm67, Nud1 and Spc72; the inner and outer plaque component Spc97; and the central plaque components Spc29, Spc42 and Spc110 (JASPERSEN*, et al.* 2004). In [*rnq*-] cells, these proteins localized to two bright foci representing the properly duplicated spindle pole bodies (see Figure C3.5b). In arrested [RNQ^{+}] cells, most of the SPB components localized to a single focus, the unduplicated SPB. In contrast, Spc42 localized to the unduplicated SPB and also localized to a separate fainter deposit within the mother cell (Figure C3.5a).

The faint deposit formed by Spc42 was reminiscent of prion protein aggregates deposited at the IPOD (TYEDMERS*, et al.* 2010) suggesting that Spc42 localized to the inclusion formed by Rnq1. We tested for Rnq1::Spc42 co-localization using a mCherry-tagged Rnq1 construct in combination with the Spc42-GFP fusion strain. The Rnq1-mCherry fusion was still able to induce arrest in [RNQ^{+}] cells and, indeed, co-localized with Spc42 deposits in the arrested cells (Figure C3.5b). We also asked if Rnq1-mCherry co-localized with other SPB components and found that only Spc42 co-localized with Rnq1 (Figure C3.5b) indicating that the effect of Rnq1 is specific to Spc42.

Spc42 is a highly phosphorylated coiled coil protein that is assembled into a crystal-like structure at the core of the SPB (BULLITT, *et al.* 1997). Interestingly, the macrostructure of Spc42 is reminiscent of the highly organized structure of amyloid fibers. However, it is unlikely that the interaction of Rnq1 and Spc42 is amyloid based. We have previously shown that the Rnq1 mutant L94A can induce toxicity in the absence of the [*RNQ*$^{+}$] prion state and without the formation of amyloid species (DOUGLAS, *et al.* 2008). We tested the effect of the Rnq1 L94A mutant and found that it also induced cell cycle arrest and Spc42 mislocalization in a [*rnq*-] background (Figure C3.5c). Hence, non-amyloid assemblies of Rnq1 caused cytotoxicity by inducing the mislocalization of Spc42.

Elevated expression of Spc42 suppresses Rnq1 toxicity

The highly specific mislocalization of Spc42 that is produced by Rnq1 over-expression provides a logical explanation for the Rnq1-induced defect in SPB duplication. Indeed, the morphologies of the unduplicated spindle pole bodies in Rnq1 arrested cells observed by EM were strikingly similar to those seen in cells with Spc42 mutations (Figure C3.4b) (DONALDSON, *et al.* 1996). Furthermore, as described above the SPB component Spc29 was one of the overexpression suppressors identified in our screen. Spc29 directly interacts with Spc42 in the central plaque of the SPB and is thought to recruit Spc42 during SPB duplication (ADAMS, *et al.* 1999; ELLIOTT, *et al.* 1999). Spc29 overexpression likely counteracts the ability of Rnq1 to misdirect Spc42 by directing it to its proper localization.

SPC42 itself was not part of the library used for our overexpression screen (which encompassed ~90% of the known yeast ORFs). Regardless, we would not have identified Spc42 as a suppressor as its overexpression using the *GAL1* promoter is profoundly toxic on its own (DONALDSON*, et al.* 1996). Therefore, as a final test of the root cause of Rnq1 toxicity, we cloned Spc42 and expressed it and other SPB components under the control of the constitutive *SUP35* promoter, which produces a more moderate level of overexpression. When expressed from the same promoter, Spc29 partially restored cell growth. Expression of other SPB components, including Spc72 and Spc97, had no effect. Expression of Spc42, however, strongly suppressed toxicity (Figure C3.6). Therefore, Rnq1 overexpression in [*RNQ*$^{+}$] cells causes a mis-localization of Spc42 to Rnq1 non-amyloid inclusions thereby diminishing the amount of soluble Spc42 needed for SPB duplication and causing a cell cycle arrest.

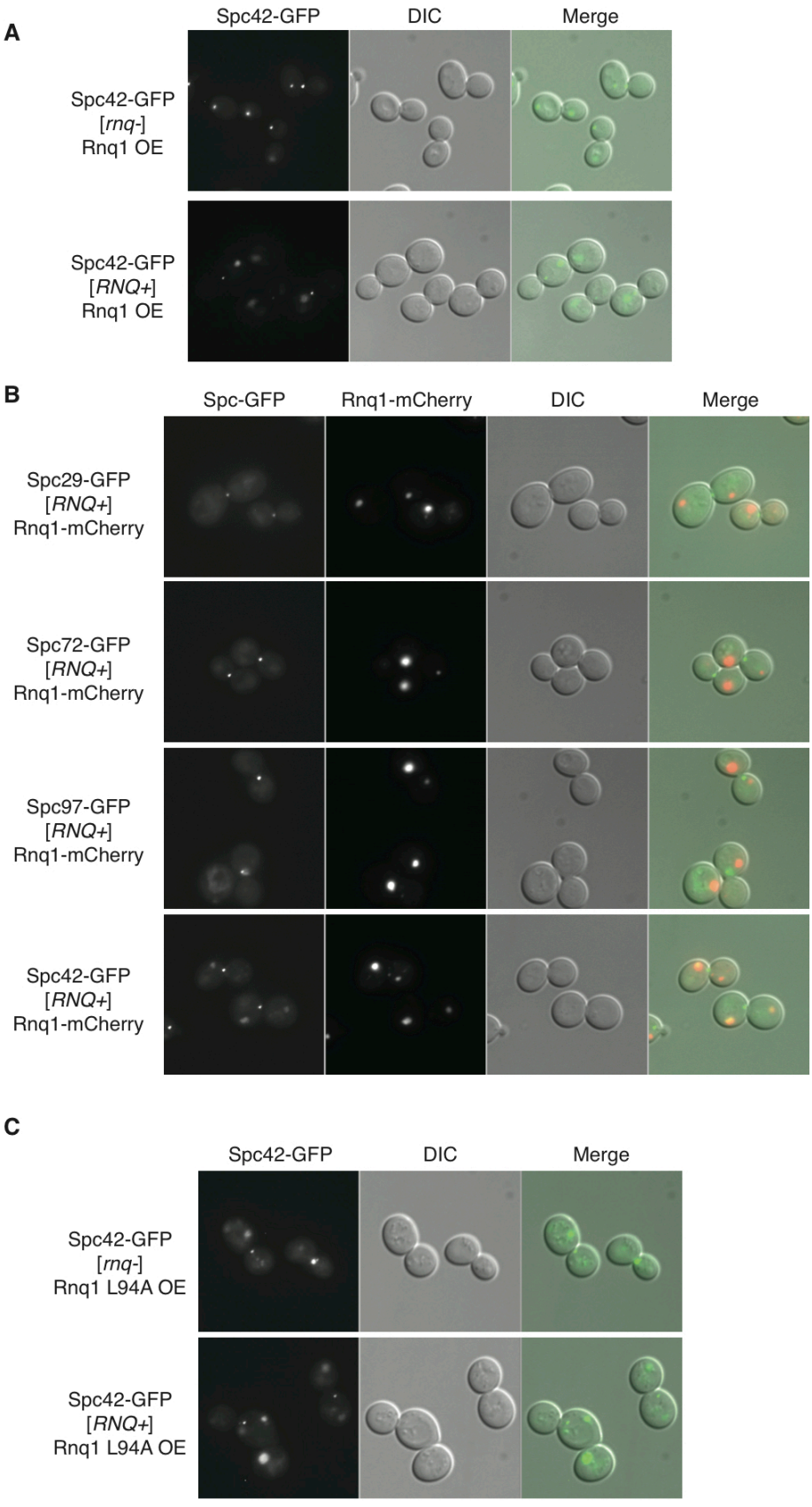
A
Spc42-GFP
DIC
Merge
Spc42-GFP
[rnq-]
Rnq1 OE
Spc42-GFP
[RNQ+]
Rnq1 OE
B
Spc-GFP
Rnq1-mCherry
DIC
Merge
Spc29-GFP
[RNQ+]
Rnq1-mCherry
Spc72-GFP
[RNQ+]
Rnq1-mCherry
Spc97-GFP
[RNQ+]
Rnq1-mCherry
Spc42-GFP
[RNQ+]
Rnq1-mCherry
C
Spc42-GFP
DIC
Merge
Spc42-GFP
[rnq-]
Rnq1 L94A OE
Spc42-GFP
[RNQ+]
Rnq1 L94A OE

Figure C3.5: Rnq1 overexpression induces mislocalization of Spc42 to inclusions.

(A) We examined how Rnq1 overexpression affected the localization of Spc42-GFP. While Spc42-GFP in control cells is found in one or two small bright foci, representing individual spindle pole bodies, it was found in one small bright focus and a larger fainter inclusion in cells subject to Rnq1 toxicity.

(B) Next, we asked if the faint Spc42-GFP deposits found in Rnq1 overexpressing prion-plus cells coincided with Rnq1 inclusions. We induced Rnq1 toxicity using a Rnq1-mCherry fusion and found that Spc42-GFP localized to the inclusions formed by Rnq1-mCherry. This Rnq1 induced change in localization appears to be specific to Spc42, as other spindle body components (Spc29, Spc72 and Spc97) did not co-localize with Rnq1.

(C) Overexpression of the Rnq1 L94A mutant causes Spc42 mislocalization and cell cycle arrest. The Rnq1 mutant L94A is toxic even in prion-minus cells, where it forms non-amyloid aggregates (DOUGLAS*, et al.* 2008). The Rnq1 L94A mutant caused Spc42 mislocalization and the formation of dumbbell-shaped cells in both [*rnq*-] and [RNQ^{+}] cells, indicating that the interaction of Rnq1 and Spc42 is not amyloid based.

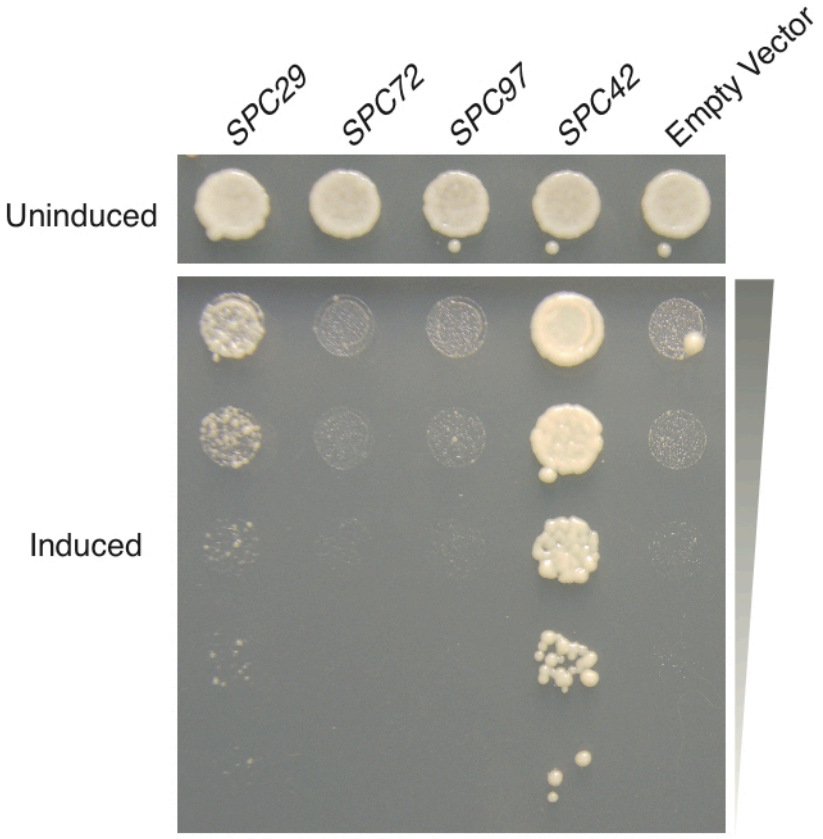

Figure C3.6: Elevated expression of Spc42 can suppress Rnq1 toxicity.

Moderate overexpression of Spc42 completely suppressed Rnq1 toxicity. Ectopic Spc72 and Spc97 expression had no effect on Rnq1 toxicity. Spc29, one of the OE screen hits, partially suppressed toxicity. Spc29 recruits Spc42 to the duplicating spindle pole body and likely can counteract the mislocalization of Spc42 induced by Rnq1.

Discussion

Cells constantly struggle to maintain protein homeostasis, targeting misfolded proteins for chaperone-mediated refolding, proteasomal degradation or inclusion body formation (ROSS, *et al.* 2005). The formation of inclusions appears to present the last line in the cellular defense against proteotoxicity as inclusions such as aggresomes form once proteasomal capacity has been exceeded (JOHNSTON, *et al.* 1998; KAGANOVICH, *et al.* 2008). Aggresomes are actively formed near the centrosome through dynein-dependent retrograde transport of protein aggregates along microtubules (GARCIA-MATA, *et al.* 1999; JOHNSTON, *et al.* 2002; JOHNSTON, *et al.* 1998). Inclusion body formation serves to "sweep" the cytoplasm of potentially toxic misfolded protein species preventing them from aberrantly interacting with other proteins (KOPITO 2000) and also appears to play an important role in facilitating the asymmetric inheritance of protein damage during cell division (FUENTEALBA, *et al.* 2008; RUJANO, *et al.* 2006).

In yeast, misfolded proteins accumulate at two distinct sites. Ubiquitinated proteins are targeted to a juxtanuclear quality control compartment, termed JNQ, whereas amyloidogenic proteins are target to the IPOD (KAGANOVICH, *et al.* 2008). Both compartments have features of aggresomes, but the IPOD has been likened to aggresomes as protein targeting to this structure is mediated by the actin cytoskeleton (GANUSOVA, *et al.* 2006) and the IPOD plays a role in the asymmetric inheritance of amyloidogenic proteins (KRYNDUSHKIN, *et al.* 2008; TYEDMERS, *et al.* 2010). Yet, aggresomes form in proximity to centrosomes, the mammalian MTOC, and no link between the IPOD and the SPB had been reported (MATHUR, *et al.* 2010). A fragment of mutant huntingtin

exon 1, 103QP, has been shown to co-localize with the yeast SPB and to form an aggresome-like structure (WANG*, et al.* 2009), but no connection between the IPOD and the SPB was observed.

We used the intrinsically disordered and amyloidogenic protein Rnq1 to model gain-of-function proteotoxicity in yeast. Rnq1 toxicity resulted in a down-regulation of genes involved in cytokinesis and subsequent experiments showed that Rnq1 toxicity resulted in a Mad2-dependent cell cylce arrest. [*RNQ*$^{+}$] cells overexpressing Rnq1 arrested with a monopolar spindle and an unduplicated SPB. We found that Rnq1 induced mis-localization of the core SPB component Spc42 to the IPOD. Moderate overexpression of Spc42 and the overexpression screen hit Spc29 counteracted the defect induced by Rnq1. The interaction of Rnq1 of Spc42 is not amyloud based as a Rnq1 mutant capable of forming non-amyloid aggregates in a [*rnq*-] background also resulted in the toxic mislocalization of Spc42. Consequently, non-amyloid aggregates, which may associate with amyloid species at the IPOD in [*RNQ*$^{+}$] cells, are the proteotoxic species in the case of Rnq1 (Figure C3.7). Our findings represent a novel connection between centrosome-associated aggresomes and their apparent yeast-equivalent, the IPOD. Especially, as Rnq1 has been shown to affect targeting of other amyloidogenic or damaged proteins to the IPOD (DERKATCH*, et al.* 2000; TYEDMERS*, et al.* 2010).

It appears that MTOCs, centrosomes and SPBs, play a role in the sensing and the subsequent asymmetric inheritance of protein damage. Centrosome–associated aggresomes did not affect mitotic cell division, yet the presence of multiple non-

aggresomal inclusions strongly impaired mitosis (RUJANO*, et al.* 2006). Furthermore, heat shock induces the aggresome-like deposition of protein aggregates at centrosomes (BARRAU*, et al.* 1978; VIDAIR*, et al.* 1996) and causes defects in cell cycle progression (HUT*, et al.* 2005). Similarly, mutants of heat shock factor 1, which coordinates the cellular response to heat stress, result in a G2/M arrest and defects in SPB duplication at elevated temperatures (MORANO*, et al.* 1999; ZARZOV*, et al.* 1997). As centrosomes and SPBs are themselves asymmetrically inherited (MACARA*, et al.* 2008) they could facilitate the asymmetric inheritance of associated protein inclusions. Furthermore, excessive protein damage, such as heat shock or Rnq1 overexpression, may interfere with MTOC function to ensure that mitosis does not proceed before the asymmetric inheritance of the protein damage in question is secured.

Overexpression of Rnq1 certainly represents an extreme case of proteotoxicity, especially as cells generally cannot overcome the defect in SPB duplication that it elicits (CHIAL*, et al.* 1999; JASPERSEN*, et al.* 2004). We tested if Spc42 localization was affected by other proteotoxic stresses such as heat shock or growth in the presence of menadione or paraquat (AGUILANIU*, et al.* 2003; TYEDMERS*, et al.* 2010). Although these conditions did to some extent result in cell cycle arrests and aberrant Spc42-GFP localization (data not shown), these phenotypes were not as striking and not as easily classified as the arrest caused by Rnq1. Certainly, more sensitive tools to monitor Spc42 assembly into the SPB core and Spc42's interaction with misfolding intrinsically disordered proteins are needed to determine if Spc42 can act as sensor of protein damage.

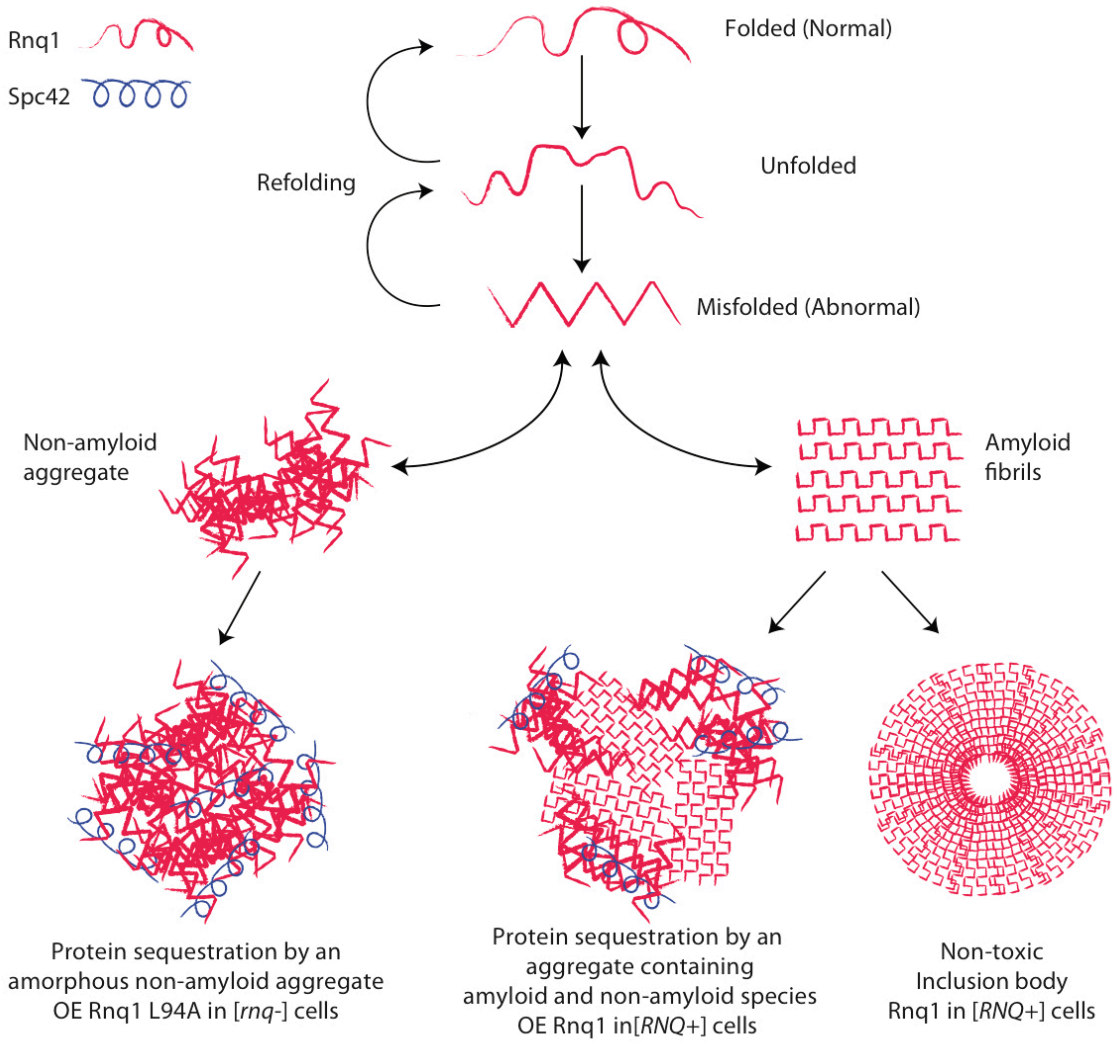

Figure C3.7: Model of Rnq1 toxicity.

As an intrinsically disordered protein Rnq1 transitions between folded, unfolded and misfolded protein conformations. In the presence of [*RNQ*$^{+}$] prion seeds it will adopt the templated amyloid conformation. Overexpression of Rnq1 exceeding the capacity for amyloid formation results in the formation of non-amyloid aggregates capable of sequestering Spc42 away from its proper localization at the SPB.

In addition to the cell biological characterization of Rnq1 toxicity, we conducted two genome-wide screens for genes that could suppress Rnq1 toxicity. Importantly, these screens also served to indentify genes involved in yeast prion maintenance. Formerly Rnq1 prion status was determined by the rate of [PSI^+] induction, but toxicity induced by Rnq1 overexpression provides a robust and more direct assessment of Rnq1 prion status. We found that no non-essential gene, aside from Hsp104 and Rnq1, is absolutely required for the maintenance of the Rnq1 prion. Our overexpression screen yielded Gpg1, which can antagonize prion formation of several yeast prions (ISHIWATA*, et al.* 2009), and genes with prion-like domains, which co-localized with Rnq1 inclusions. The latter likely reduce toxicity by interacting with Rnq1 aggregates and forming a "shield" that limits Rnq1's ability to induce mislocalization of Spc42.

We found that in addition to chaperones known to be protein stress responsive, *GPG1* and *BTN*2 were up-regulated upon Rnq1 overexpression in [RNQ^+] cells. Btn2 has been shown to influence the inheritance of the [*URE3*] prion and to co-localize with the prion forms of Sup35 and Rnq1. While Btn2 co-localized with Rnq1, its overexpression did not affect [RNQ^+] maintenance (KRYNDUSHKIN*, et al.* 2008), suggesting why we did not identify it as a suppressor in our overexpression screen. Btn2 mediates late endosome-Golgi sorting (KAMA*, et al.* 2007) and has been postulated to influence prion inheritance by facilitating the formation of aggresome-like inclusions (KRYNDUSHKIN*, et al.* 2008). Gpg1 is the proposed gamma subunit of the heterotrimeric G protein (HARASHIMA*, et al.* 2002). Yet, Gpg1 shares no homology with other G protein gamma subunits and its functional annotation is based on yeast two hybrid interactions with other G protein

components. The up-regulation of both *BTN*2 and *GPG1* may represent an uncharacterized cellular response to certain types of proteotoxicity. Indeed, their expression patterns correlate with those of chaperones involved in protein folding (*BTN2*, 7.72e-08) and response to temperature stimulus (*GPG1*, 7.16e-04) (HIBBS*, et al.* 2007). It will be interesting to see how these two proteins function in concert with chaperones such as Hsp104 and Sis1 to counteract the toxicity of intrinsically disordered proteins and to modulate yeast prion formation.

References

Adams, I.R. & Kilmartin, J.V. (1999) Localization of Core Spindle Pole Body (Spb) Components During Spb Duplication in Saccharomyces Cerevisiae. *J Cell Biol* 145(4):809-823.

Aguilaniu, H., Gustafsson, L., Rigoulet, M., & Nystrom, T. (2003) Asymmetric Inheritance of Oxidatively Damaged Proteins During Cytokinesis. *Science* 299(5613):1751-1753.

Alberti, S., Gitler, A.D., & Lindquist, S. (2007) A Suite of Gateway Cloning Vectors for High-Throughput Genetic Analysis in Saccharomyces Cerevisiae. *Yeast* 24(10):913-919.

Alberti, S., Halfmann, R., King, O., Kapila, A., & Lindquist, S. (2009) A Systematic Survey Identifies Prions and Illuminates Sequence Features of Prionogenic Proteins. *Cell* 137(1):146-158.

Bagriantsev, S.N., Kushnirov, V.V., & Liebman, S.W. (2006) Analysis of Amyloid Aggregates Using Agarose Gel Electrophoresis. *Methods Enzymol* 412:33-48.

Barrau, M.D., Blackburn, G.R., & Dewey, W.C. (1978) Effects of Heat on the Centrosomes of Chinese Hamster Ovary Cells. *Cancer Res* 38(8):2290-2294.

Blondel, M., Bach, S., Bamps, S., Dobbelaere, J., Wiget, P., Longaretti, C., Barral, Y., Meijer, L., & Peter, M. (2005) Degradation of Hof1 by Scf(Grr1) Is Important for Actomyosin Contraction During Cytokinesis in Yeast. *EMBO J* 24(7):1440-1452.

Bullitt, E., Rout, M.P., Kilmartin, J.V., & Akey, C.W. (1997) The Yeast Spindle Pole Body Is Assembled around a Central Crystal of Spc42p. *Cell* 89(7):1077-1086.

Chial, H.J. & Winey, M. (1999) Mechanisms of Genetic Instability Revealed by Analysis of Yeast Spindle Pole Body Duplication. *Biol Cell* 91(6):439-450.

Chien, P., Weissman, J.S., & DePace, A.H. (2004) Emerging Principles of Conformation-Based Prion Inheritance. *Annu Rev Biochem* 73:617-656.

Chiti, F. & Dobson, C.M. (2006) Protein Misfolding, Functional Amyloid, and Human Disease. *Annu Rev Biochem* 75:333-366.

Cooper, A.A., Gitler, A.D., Cashikar, A., Haynes, C.M., Hill, K.J., Bhullar, B., Liu, K., Xu, K., Strathearn, K.E., Liu, F., Cao, S., Caldwell, K.A., Caldwell, G.A., Marsischky, G., Kolodner, R.D., Labaer, J., Rochet, J.C., Bonini, N.M., & Lindquist, S. (2006) Alpha-Synuclein Blocks Er-Golgi Traffic and Rab1 Rescues Neuron Loss in Parkinson's Models. *Science* 313(5785):324-328.

Cox, B., Ness, F., & Tuite, M. (2003) Analysis of the Generation and Segregation of Propagons: Entities That Propagate the [Psi+] Prion in Yeast. *Genetics* 165(1):23-33.

Derkatch, I.L., Bradley, M.E., Hong, J.Y., & Liebman, S.W. (2001) Prions Affect the Appearance of Other Prions: The Story of [Pin(+)]. *Cell* 106(2):171-182.

Derkatch, I.L., Bradley, M.E., Masse, S.V., Zadorsky, S.P., Polozkov, G.V., Inge-Vechtomov, S.G., & Liebman, S.W. (2000) Dependence and Independence of [*Psi(+)*] and [*Pin(+)*]: A Two-Prion System in Yeast? *EMBO J* 19(9):1942-1952.

Derkatch, I.L., Uptain, S.M., Outeiro, T.F., Krishnan, R., Lindquist, S.L., & Liebman, S.W. (2004) Effects of Q/N-Rich, Polyq, and Non-Polyq Amyloids on the De Novo Formation of the [Psi+] Prion in Yeast and Aggregation of Sup35 in Vitro. *Proc Natl Acad Sci U S A* 101(35):12934-12939.

Donaldson, A.D. & Kilmartin, J.V. (1996) Spc42p: A Phosphorylated Component of the S. Cerevisiae Spindle Pole Body (Spd) with an Essential Function During Spb Duplication. *J Cell Biol* 132(5):887-901.

Douglas, P.M., Treusch, S., Ren, H.Y., Halfmann, R., Duennwald, M.L., Lindquist, S., & Cyr, D.M. (2008) Chaperone-Dependent Amyloid Assembly Protects Cells from Prion Toxicity. *Proc Natl Acad Sci U S A* 105(20):7206-7211.

Du, Z., Park, K.W., Yu, H., Fan, Q., & Li, L. (2008) Newly Identified Prion Linked to the Chromatin-Remodeling Factor Swi1 in Saccharomyces Cerevisiae. *Nat Genet* 40(4):460-465.

Elliott, S., Knop, M., Schlenstedt, G., & Schiebel, E. (1999) Spc29p Is a Component of the Spc110p Subcomplex and Is Essential for Spindle Pole Body Duplication. *Proc Natl Acad Sci U S A* 96(11):6205-6210.

Fuentealba, L.C., Eivers, E., Geissert, D., Taelman, V., & De Robertis, E.M. (2008) Asymmetric Mitosis: Unequal Segregation of Proteins Destined for Degradation. *Proc Natl Acad Sci U S A* 105(22):7732-7737.

Ganusova, E.E., Ozolins, L.N., Bhagat, S., Newnam, G.P., Wegrzyn, R.D., Sherman, M.Y., & Chernoff, Y.O. (2006) Modulation of Prion Formation, Aggregation, and Toxicity by the Actin Cytoskeleton in Yeast. *Mol Cell Biol* 26(2):617-629.

Garcia-Mata, R., Bebok, Z., Sorscher, E.J., & Sztul, E.S. (1999) Characterization and Dynamics of Aggresome Formation by a Cytosolic Gfp-Chimera. *J Cell Biol* 146(6):1239-1254.

Gitler, A.D., Chesi, A., Geddie, M.L., Strathearn, K.E., Hamamichi, S., Hill, K.J., Caldwell, K.A., Caldwell, G.A., Cooper, A.A., Rochet, J.C., & Lindquist, S. (2009) Alpha-Synuclein Is Part of a Diverse and Highly Conserved Interaction Network That Includes Park9 and Manganese Toxicity. *Nat Genet* 41(3):308-315.

Halfmann, R. & Lindquist, S. (2008) Screening for Amyloid Aggregation by Semi-Denaturing Detergent-Agarose Gel Electrophoresis. *J Vis Exp* (17).

Harashima, T. & Heitman, J. (2002) The Galpha Protein Gpa2 Controls Yeast Differentiation by Interacting with Kelch Repeat Proteins That Mimic Gbeta Subunits. *Mol Cell* 10(1):163-173.

Hardwick, K.G. (1998) The Spindle Checkpoint. *Trends Genet* 14(1):1-4.

Hardwick, K.G., Li, R., Mistrot, C., Chen, R.H., Dann, P., Rudner, A., & Murray, A.W. (1999) Lesions in Many Different Spindle Components Activate the Spindle Checkpoint in the Budding Yeast Saccharomyces Cerevisiae. *Genetics* 152(2):509-518.

Hibbs, M.A., Hess, D.C., Myers, C.L., Huttenhower, C., Li, K., & Troyanskaya, O.G. (2007) Exploring the Functional Landscape of Gene Expression: Directed Search of Large Microarray Compendia. *Bioinformatics* 23(20):2692-2699.

Howson, R., Huh, W.K., Ghaemmaghami, S., Falvo, J.V., Bower, K., Belle, A., Dephoure, N., Wykoff, D.D., Weissman, J.S., & O'Shea, E.K. (2005) Construction, Verification and Experimental Use of Two Epitope-Tagged Collections of Budding Yeast Strains. *Comp Funct Genomics* 6(1-2):2-16.

Hut, H.M., Kampinga, H.H., & Sibon, O.C. (2005) Hsp70 Protects Mitotic Cells against Heat-Induced Centrosome Damage and Division Abnormalities. *Mol Biol Cell* 16(8):3776-3785.

Ishiwata, M., Kurahashi, H., & Nakamura, Y. (2009) A G-Protein Gamma Subunit Mimic Is a General Antagonist of Prion Propagation in Saccharomyces Cerevisiae. *Proc Natl Acad Sci U S A* 106(3):791-796.

Jaspersen, S.L. & Winey, M. (2004) The Budding Yeast Spindle Pole Body: Structure, Duplication, and Function. *Annu Rev Cell Dev Biol* 20:1-28.

Johnston, J.A., Illing, M.E., & Kopito, R.R. (2002) Cytoplasmic Dynein/Dynactin Mediates the Assembly of Aggresomes. *Cell Motil Cytoskeleton* 53(1):26-38.

Johnston, J.A., Ward, C.L., & Kopito, R.R. (1998) Aggresomes: A Cellular Response to Misfolded Proteins. *J Cell Biol* 143(7):1883-1898.

Kaganovich, D., Kopito, R., & Frydman, J. (2008) Misfolded Proteins Partition between Two Distinct Quality Control Compartments. *Nature* 454(7208):1088-1095.

Kama, R., Robinson, M., & Gerst, J.E. (2007) Btn2, a Hook1 Ortholog and Potential Batten Disease-Related Protein, Mediates Late Endosome-Golgi Protein Sorting in Yeast. *Mol Cell Biol* 27(2):605-621.

Kayed, R., Head, E., Thompson, J.L., McIntire, T.M., Milton, S.C., Cotman, C.W., & Glabe, C.G. (2003) Common Structure of Soluble Amyloid Oligomers Implies Common Mechanism of Pathogenesis. *Science* 300(5618):486-489.

Kopito, R.R. (2000) Aggresomes, Inclusion Bodies and Protein Aggregation. *Trends Cell Biol* 10(12):524-530.

Kryndushkin, D.S., Shewmaker, F., & Wickner, R.B. (2008) Curing of the [Ure3] Prion by Btn2p, a Batten Disease-Related Protein. *EMBO J* 27(20):2725-2735.

Liebman, S.W. & Derkatch, I.L. (1999) The Yeast [Psi+] Prion: Making Sense of Nonsense. *J Biol Chem* 274(3):1181-1184.

Macara, I.G. & Mili, S. (2008) Polarity and Differential Inheritance--Universal Attributes of Life? *Cell* 135(5):801-812.

Manogaran, A.L., Fajardo, V.M., Reid, R.J., Rothstein, R., & Liebman, S.W. (2010) Most, but Not All, Yeast Strains in the Deletion Library Contain the [Pin(+)] Prion. *Yeast* 27(3):159-166.

Mathur, V., Taneja, V., Sun, Y., & Liebman, S.W. (2010) Analyzing the Birth and Propagation of Two Distinct Prions, [Psi+] and [Het-S](Y), in Yeast. *Mol Biol Cell* 21(9):1449-1461.

Meriin, A.B., Zhang, X., He, X., Newnam, G.P., , Y.O., & Sherman, M.Y. (2002) Huntington Toxicity in Yeast Model Depends on Polyglutamine Aggregation Mediated by a Prion-Like Protein Rnq1. *J Cell Biol* 157(6):997-1004.

Morano, K.A., Santoro, N., Koch, K.A., & Thiele, D.J. (1999) A Trans-Activation Domain in Yeast Heat Shock Transcription Factor Is Essential for Cell Cycle Progression During Stress. *Mol Cell Biol* 19(1):402-411.

Nemecek, J., Nakayashiki, T., & Wickner, R.B. (2009) A Prion of Yeast Metacaspase Homolog (Mca1p) Detected by a Genetic Screen. *Proc Natl Acad Sci U S A* 106(6):1892-1896.

Nyberg, K.A., Michelson, R.J., Putnam, C.W., & Weinert, T.A. (2002) Toward Maintaining the Genome: DNA Damage and Replication Checkpoints. *Annu Rev Genet* 36:617-656.

Olzscha, H., Schermann, S.M., Woerner, A.C., Pinkert, S., Hecht, M.H., Tartaglia, G.G., Vendruscolo, M., Hayer-Hartl, M., Hartl, F.U., & Vabulas, R.M. (2011) Amyloid-Like Aggregates Sequester Numerous Metastable Proteins with Essential Cellular Functions. *Cell* 144(1):67-78.

Osherovich, L.Z. & Weissman, J.S. (2001) Multiple Gln/Asn-Rich Prion Domains Confer Susceptibility to Induction of the Yeast [Psi(+)] Prion. *Cell* 106(2):183-194.

Patel, B.K., Gavin-Smyth, J., & Liebman, S.W. (2009) The Yeast Global Transcriptional Co-Repressor Protein Cyc8 Can Propagate as a Prion. *Nat Cell Biol* 11(3):344-349.

Ross, C.A. & Poirier, M.A. (2005) Opinion: What Is the Role of Protein Aggregation in Neurodegeneration? *Nat Rev Mol Cell Biol* 6(11):891-898.

Rujano, M.A., Bosveld, F., Salomons, F.A., Dijk, F., van Waarde, M.A., van der Want, J.J., de Vos, R.A., Brunt, E.R., Sibon, O.C., & Kampinga, H.H. (2006) Polarised Asymmetric Inheritance of Accumulated Protein Damage in Higher Eukaryotes. *PLoS Biol* 4(12):e417.

Shorter, J. & Lindquist, S. (2005) Prions as Adaptive Conduits of Memory and Inheritance. *Nat Rev Genet* 6(6):435-450.

Sondheimer, N. & Lindquist, S. (2000) Rnq1: An Epigenetic Modifier of Protein Function in Yeast. *Mol Cell* 5(1):163-172.

Sondheimer, N., Lopez, N., Craig, E.A., & Lindquist, S. (2001) The Role of Sis1 in the Maintenance of the [Rnq+] Prion. *EMBO J* 20(10):2435-2442.

Taguchi, H. & Kawai-Noma, S. (2010) Amyloid Oligomers: Diffuse Oligomer-Based Transmission of Yeast Prions. *FEBS J* 277(6):1359-1368.

Taneja, V., Maddelein, M.L., Talarek, N., Saupe, S.J., & Liebman, S.W. (2007) A Non-Q/N-Rich Prion Domain of a Foreign Prion, [Het-S], Can Propagate as a Prion in Yeast. *Mol Cell* 27(1):67-77.

Treusch, S., Cyr, D.M., & Lindquist, S. (2009) Amyloid Deposits: Protection against Toxic Protein Species? *Cell Cycle* 8(11):1668-1674.

Tuite, M.F. & Cox, B.S. (2003) Propagation of Yeast Prions. *Nat Rev Mol Cell Biol* 4(11):878-890.

Tyedmers, J., Treusch, S., Dong, J., McCaffery, J.M., Bevis, B., & Lindquist, S. (2010) Prion Induction Involves an Ancient System for the Sequestration of Aggregated Proteins and Heritable Changes in Prion Fragmentation. *Proc Natl Acad Sci U S A* 107(19):8633-8638.

Vavouri, T., Semple, J.I., Garcia-Verdugo, R., & Lehner, B. (2009) Intrinsic Protein Disorder and Interaction Promiscuity Are Widely Associated with Dosage Sensitivity. *Cell* 138(1):198-208.

Vidair, C.A., Huang, R.N., & Doxsey, S.J. (1996) Heat Shock Causes Protein Aggregation and Reduced Protein Solubility at the Centrosome and Other Cytoplasmic Locations. *Int J Hyperthermia* 12(5):681-695.

Wang, Y., Meriin, A.B., Zaarur, N., Romanova, N.V., Chernoff, Y.O., Costello, C.E., & Sherman, M.Y. (2009) Abnormal Proteins Can Form Aggresome in Yeast: Aggresome-Targeting Signals and Components of the Machinery. *FASEB J* 23(2):451-463.

Weinert, T.A. & Hartwell, L.H. (1988) The Rad9 Gene Controls the Cell Cycle Response to DNA Damage in Saccharomyces Cerevisiae. *Science* 241(4863):317-322.

Wickner, R.B. (1994) [Ure3] as an Altered Ure2 Protein: Evidence for a Prion Analog in Saccharomyces Cerevisiae. *Science* 264(5158):566-569.

Wickner, R.B., Edskes, H.K., Ross, E.D., Pierce, M.M., Shewmaker, F., Baxa, U., & Brachmann, A. (2004) Prions of Yeast Are Genes Made of Protein: Amyloids and Enzymes. *Cold Spring Harb Symp Quant Biol* 69:489-496.

Wickner, R.B., Edskes, H.K., Shewmaker, F., & Nakayashiki, T. (2007) Prions of Fungi: Inherited Structures and Biological Roles. *Nat Rev Microbiol* 5(8):611-618.

Winzeler, E.A., Shoemaker, D.D., Astromoff, A., Liang, H., Anderson, K., Andre, B., Bangham, R., Benito, R., Boeke, J.D., Bussey, H., Chu, A.M., Connelly, C., Davis, K., Dietrich, F., Dow, S.W., El Bakkoury, M., Foury, F., Friend, S.H., Gentalen, E., Giaever, G., Hegemann, J.H., Jones, T., Laub, M., Liao, H., Liebundguth, N., Lockhart, D.J., Lucau-Danila, A., Lussier, M., M'Rabet, N., Menard, P., Mittmann, M., Pai, C., Rebischung, C., Revuelta, J.L., Riles, L., Roberts, C.J., Ross-MacDonald, P., Scherens, B., Snyder, M., Sookhai-Mahadeo, S., Storms, R.K., Veronneau, S., Voet, M., Volckaert, G., Ward, T.R., Wysocki, R., Yen, G.S., Yu, K., Zimmermann, K., Philippsen, P., Johnston, M., & Davis, R.W. (1999) Functional Characterization of the S. Cerevisiae Genome by Gene Deletion and Parallel Analysis. *Science* 285(5429):901-906.

Zarzov, P., Boucherie, H., & Mann, C. (1997) A Yeast Heat Shock Transcription Factor (Hsf1) Mutant Is Defective in Both Hsc82/Hsp82 Synthesis and Spindle Pole Body Duplication. *J Cell Sci* 110 (Pt 16):1879-1891.

Material and Methods:

Strains and Plasmids: W303 MAT a and α, can1-100, ade2-1, his3-11,15 leu2-3,112, ura3-1, trp1-1 and BY4741 MAT a, his3Δ1, leu2Δ0, met15Δ0, ura3Δ0, and Y7092 Mat α, can1Δ::STE2pr-Sp_his5, lyp1Δ,his3Δ1, leu2Δ0, ura3Δ0, met15Δ0,LYS2+ (TONG, *et al.* 2006). As well as strains from the GFP library, which are based on the BY background and contain a GFP tag integrated using the His3 marker (HOWSON, *et al.* 2005). Deletion strains were recreated following previously published methods and primers (WINZELER, *et al.* 1999). The strains harbored Rnq1 in its [*RNQ+*] form and the generation of isogenic [*rnq*-] strains was accomplished via sequential passage of cells on plates containing 3 mM guanidinium-HCl (EAGLESTONE, *et al.* 2000). Strains were transformed with plasmids and cultured in synthetic media as previously described (CAPLAN, *et al.* 1991). Plasmids that express the indicated protein under control of the *GAL1* promoter include pRS416-*RNQ1* (WT and L94A), pRS416-*RNQ1-YFP*, pRS426-*RNQ1-YFP*, pAG416-*RNQ1-mCherry*, pRS305-*RNQ1,* pRS305-*YFP* and pBY011 (CEN, URA3, AmpR, *GAL* regulated) overexpression library constructs (COOPER, *et al.* 2006). Plasmids that utilizing the *SUP35* promoter include pAG415 constructs containing *SPC29, SPC42, SPC72,* and *SPC97*. Cerulean fusions of the screen hits were generated using overexpression library clones, gateway cloning and a pAG415 N-terminal Cerulean vector (ALBERTI, *et al.* 2007).

Analysis of Rnq1 cytotoxicity: To measure the effect of the re-created deletions, indicated deletions strains carrying pRS426-*RNQ1-YFP* were assayed. The

overexpression screen was carried out in a BYxW303 diploid. Strains tested carried an integrated pRS305-*RNQ1* construct and the indicated constructs from the overexpression library. Spc42 rescue was assayed using BY Spc42-GFP strains harboring pRS416-*RNQ1* and spindle pole body components on a *SUP35* promoter controlled pAG415 plasmid. We observed similar rescue of Rnq1 toxicity by Spc29 and Spc42 in the BY and W303 backgrounds. For all these assays strains were grown overnight in synthetic drop-out media containing 2 % glucose before 5-fold serial dilutions were spotted on plates containing either 2 % galactose or glucose. Plates were incubated for 2-3 days at 30 ºC and then photographed.

Semi-denaturing detergent agarose gel electrophoresis (SDD-AGE): Rnq1 assembly into SDS-resistant [RNQ+] prions was monitored by SDD-AGE as previously described (HALFMANN*, et al.* 2008). Cells were lysed in buffer containing 50mM Hepes pH7.5, 150mM NaCl, 2.5 mM EDTA, 1% Triton X-100, 30mM NEM, 1mM PMSF and a protease inhibitor cocktail (Roche) using glass beads. Lysates were spun clear of debris and mixed with 2x sample buffer (1xTAE, 10% glycerol, 2% SDS, bromophenol blue). Samples were run on a the 1.5% agarose gel containing 1x TAE and 0.1% SDS in running buffer with the same concentrations of TAE and SDS. The gel was blotted onto Hybond-C membrane and then probed with α-GFP. Bands were visualized with ECL reagent.

Cell cycle profiling: Freshly streaked cells were grown overnight at 30 ºC in synthetic media lacking uracil and containing 2% raffinose. Cells were diluted to an

OD 600 of 0.2 and grown for an additional 3h in the raffinose media. Cells were then washed and Rnq1 expression was induced for the indicated time intervals in media lacking uracil and containing 2% galactose. After induction cells were spun down in 15ml screw cap tubes and resuspended in 3ml dH20. The cells were fixed through the addition of 7 ml of 95% EtOH and overnight incubation at 4 °C whilst rotating. After fixation cells were spun down and resuspended in 5ml 50mM sodium citrate (pH 7.4). Cells were spun down again, resuspended in 1 ml of 50mM sodium citrate containing 0.25 mg/ml boiled RNase A (QIAGEN) and incubated at 50 °C for one hour. 50ul of 20 mg/ml Proteinase K (Invitrogen) were added before an additional 1h incubation at 50° C. After this incubation 1 ml of 50mM sodium citrate containing 16 ug/ml propidium iodide was added before cells were incubated overnight at 4 °C. DNA content of these cells was measure using on a Caliber II flow cytometer and the resulting Data were analyzed using FlowJo software.

Immunostaining: Strains were pregrown in raffinose media over night and then induced in galactose media for 8 hours (5ml OD600 0.2). Cells were spun down and resuspended in 1ml 3.7% formaldehyde (37% formaldehyde in 0.1M KPi (potassium phosphate buffer) pH6.4) after removal of supernatant. Cells were fixed over night at 4 °C. After the fixation cells were washed three time in 1ml 0.1M KPi pH 6.4 and then resuspended in 1ml 1.2M sorbitol-citrate buffer (1L: 218.6g sorbitol, 17.40g anyhydorus K2HPO4, 7g citric acid; filter sterilize). Cells were spun down again and resuspended in 200ul of digestion mix (200ul 1.2M sorbitol-citrate, 20ul glusolase and 2ul 10mg/ml zymolase). Cells were incubated in the digestion

mix for 45min at 30 °C. During the incubation 5ul 0.1% polylysine was added to each well of a 30 well slide (Thermo ER-212W). After 5min of incubation the slides was washed with distilled water and allowed to air dry completely. Digested cells were spun down at 3,000 rpm for 3min and gently resuspended in 1ml sorbitol-citrate. Cells were spun down again and then resuspended in a volume of sorbitol citrate dependent on cell pellet size (15-50ul). 5ul of cells was added to each well and incubated for 10min. Cells were removed from the side of the well using a vacuum tip. If the cell density was low, as revealed by light microscopy, more cells were added. The slides were then incubated in ice-cold methanol for 3min, followed by 10sec in ice-cold acetone. Acetone was shook off and slides air-dried. 4ul of 1:200 anti-tubulin antibody (kind gift of the Hochwagen lab) in PBS/BSA (1% BSA, 0.04M K2HPO4, 0.01M KH2PO4, 0.15M NaCl, 0.1% NaN3; for 100ml: 1g BSA, 4ml 1M K2HPO4, 1ml 1M KH2PO4, 15ml 1M NaCl, 1ml 10% NaN3, sterilized water to 100ml) were added to each well. Slide was incubated over night at room temperature in a wet chamber. After the incubation the antibody was removed using a vacuum tip and each well was washed 3 times with PBS/BSA. Then 4ul of the secondary antibody, 1:100 anti-mouse FITC, was added to each well and incubated for 2 hours. Subsequently, each well was washed 4 times with PBS/BSA. 1ul of DAPI-MOUNT was added to each well prior to adding the coverslip and sealing the slide with nail polish.

Images were taken on a Zeiss Aviovert. Final images were assembled from the different channels (GFP and DAPI) in Adobe Photoshop. Brightness and contrast were adjusted equally for all images.

Deletion library screen for suppressors of Rnq1 toxicity: The Mat a and alpha deletion libraries contain independently generated deletions of roughly all the non-essential yeast gene arrayed in 96-well format (WINZELER, *et al.* 1999). We transformed the libraries with the pRS426-*RNQ1-YFP* construct and screened for strains with improved growth in comparison to the parental BY strain. Transformation and screening was carried out as described previously (TYEDMERS, *et al.* 2008). The screen resulted in 526 putative hits in the Mat a library and 426 putative hits in the Mat alpha library. 69 were found in both libraries. We used the synthetic genetic array (SGA) strain 7092 (TONG, *et al.* 2006) to reintroduce the [RNQ+] state in each of these deletions. We mated a [*RNQ+*] SGA strain carrying the pRS426-*RNQ1-YFP* construct to the set of 69 deletions. We then selected for diploids, sporulated them, selected for haploids carrying the deletion and the Rnq1-YFP construct, and then tested the extent of Rnq1 toxicity in said haploids. Twelve deletion strains still exhibited suppression of Rnq1 toxicity after this prion reintroduction or could not be analyzed in this fashion due to mating defects.

We recreated these twelve deletions in BY and W303 using previously published primer sets (WINZELER, *et al.* 1999) and tested their ability to suppress Rnq1 toxicity.

Overexpression library screen for suppressors of Rnq1 toxicity: The overexpression library screened contains ~5800 full-length sequence verified yeast ORFs in the galactose-inducible Gateway expression plasmid pBY011 (CEN, URA3, AmpR) (COOPER, *et al.* 2006). The library is arrayed in 96-well format. Plasmid DNA was prepared by pin inoculation into deep well 96-well plates containing 1.8ml LB-

AMP, growth over night at 37 °C and 96-well mini preps using a Qiagen BioRobot 8000. Library DNA was transformed into the BY strain to create a library of yeast strains carrying the inducible overexpression constructs. Transformations were carried out using a standard lithium acetate transformation protocol adapted for a 96-well format. We mated a W303 strain carrying an integrated pRS305-*RNQ1* construct to the library. Post mating we selected for diploids carrying both the library plasmid and the Rnq1 integration and then examined their growth on galactose plates inducing both the expression of the library clone and Rnq1. 62 putative suppressors were identified after 2-4 days of growth at 30 °C. These putative hits were retested in the diploid screening strain and a haploid strain. The effects of twenty of these suppressors reproduced. We eliminated hits that have known effects on GAL induction. To further exclude false-positive suppressors we used flow cytometry to measure the expression of YFP in their presence. The identity of suppressors was verified by sequencing.

Flow cytometry: A W303 strain carrying YFP integrated at the *LEU2* locus was transformed with the putative Rnq1 toxicity suppressors. The resulting strains were grown in glucose media in a 96 well format, diluted into galactose-containing inducing media [5ul culture added to 120ul media], and incubated over night at 30 °C with mild shaking. These overnight cultures were diluted 20fold into water and YFP levels were measured using a Guava flow cytometer. Each strain was measured 3 times and 5000 cells were counted each time. The whole experiment was repeated

3 times. Values are averages of these 3 experiments and reported in percent of the vector control strain YFP levels.

Fluorescence Microscopy: Co-localization of Rnq1 and screen hits was examined in BY strains expressing Rnq1-YFP and N-terminal Cerulean fusions of suppressors. Strains were grown in raffinose media overnight and expression of Rnq1 and the screen hits was induced in galactose media for 4h prior to microscopy.

To study the Rnq1-induced cell arrest cells again were pre-grown in raffinose media but then induced in galactose media for at least 8h. The effect of Rnq1 on the localization of Hof1-GFP and Spc42-GFP, as well as other spindle pole body components, was tested in GFP library strains (HOWSON, *et al.* 2005). Co-localization of Rnq1-mCherry with spindle pole body components was examined in the same fashion.

Microscopy was conducted using a Zeiss Axiovert microscope. Brightness and contrast were adjusted equally for all images.

Alberti, S., Gitler, A.D., & Lindquist, S. (2007) A Suite of Gateway Cloning Vectors for High-Throughput Genetic Analysis in Saccharomyces Cerevisiae. *Yeast* 24(10):913-919.

Caplan, A.J. & Douglas, M.G. (1991) Characterization of Ydj1: A Yeast Homologue of the Bacterial Dnaj Protein. *J Cell Biol* 114(4):609-621.

Cooper, A.A., Gitler, A.D., Cashikar, A., Haynes, C.M., Hill, K.J., Bhullar, B., Liu, K., Xu, K., Strathearn, K.E., Liu, F., Cao, S., Caldwell, K.A., Caldwell, G.A., Marsischky, G., Kolodner, R.D., Labaer, J., Rochet, J.C., Bonini, N.M., & Lindquist, S. (2006) Alpha-Synuclein Blocks Er-Golgi Traffic and Rab1 Rescues Neuron Loss in Parkinson's Models. *Science* 313(5785):324-328.

Eaglestone, S.S., Ruddock, L.W., Cox, B.S., & Tuite, M.F. (2000) Guanidine Hydrochloride Blocks a Critical Step in the Propagation of the Prion-Like Determinant [Psi(+)] of Saccharomyces Cerevisiae. *Proc Natl Acad Sci U S A* 97(1):240-244.

Halfmann, R. & Lindquist, S. (2008) Screening for Amyloid Aggregation by Semi-Denaturing Detergent-Agarose Gel Electrophoresis. *J Vis Exp* (17).

Howson, R., Huh, W.K., Ghaemmaghami, S., Falvo, J.V., Bower, K., Belle, A., Dephoure, N., Wykoff, D.D., Weissman, J.S., & O'Shea, E.K. (2005) Construction, Verification and Experimental Use of Two Epitope-Tagged Collections of Budding Yeast Strains. *Comp Funct Genomics* 6(1-2):2-16.

Tong, A.H. & Boone, C. (2006) Synthetic Genetic Array Analysis in Saccharomyces Cerevisiae. *Methods Mol Biol* 313:171-192.

Tyedmers, J., Madariaga, M.L., & Lindquist, S. (2008) Prion Switching in Response to Environmental Stress. *PLoS Biol* 6(11):e294.

Winzeler, E.A., Shoemaker, D.D., Astromoff, A., Liang, H., Anderson, K., Andre, B., Bangham, R., Benito, R., Boeke, J.D., Bussey, H., Chu, A.M., Connelly, C., Davis, K., Dietrich, F., Dow, S.W., El Bakkoury, M., Foury, F., Friend, S.H., Gentalen, E., Giaever, G., Hegemann, J.H., Jones, T., Laub, M., Liao, H., Liebundguth, N., Lockhart, D.J., Lucau-Danila, A., Lussier, M., M'Rabet, N., Menard, P., Mittmann, M., Pai, C., Rebischung, C., Revuelta, J.L., Riles, L., Roberts, C.J., Ross-MacDonald, P., Scherens, B., Snyder, M., Sookhai-Mahadeo, S., Storms, R.K., Veronneau, S., Voet, M., Volckaert, G., Ward, T.R., Wysocki, R., Yen, G.S., Yu, K., Zimmermann, K., Philippsen, P., Johnston, M., & Davis, R.W. (1999) Functional Characterization of the S. Cerevisiae Genome by Gene Deletion and Parallel Analysis. *Science* 285(5429):901-906.

Supplemental Information

(beginning on next page)

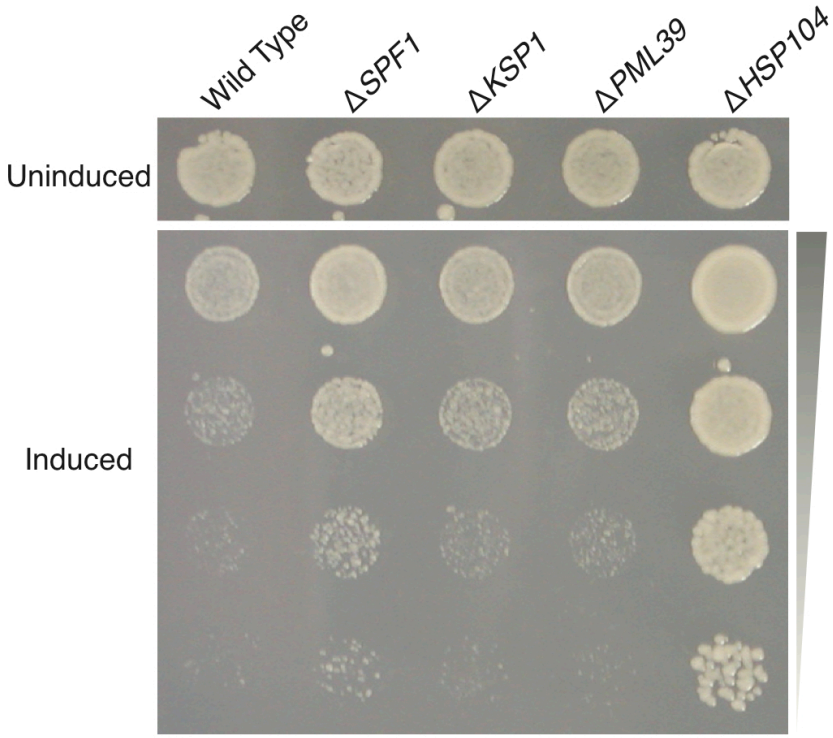

Supplemental Figure C3.1: Deletions that suppress Rnq1 toxicity.

The Mat a and α deletion libraries were screened for deletions able to suppress Rnq1 toxicity. Several deletions were identified in both libraries. These were mated and sporulated to reintroduce the [*RNQ*$^{+}$] state and then retested for Rnq1 toxicity suppression. Deletions, that still suppressed Rnq1 toxicity after re-introduction of the prion state, were recreated in BY and W303 strains. The recreated BY deletions suppressing Rnq1 toxicity are shown.

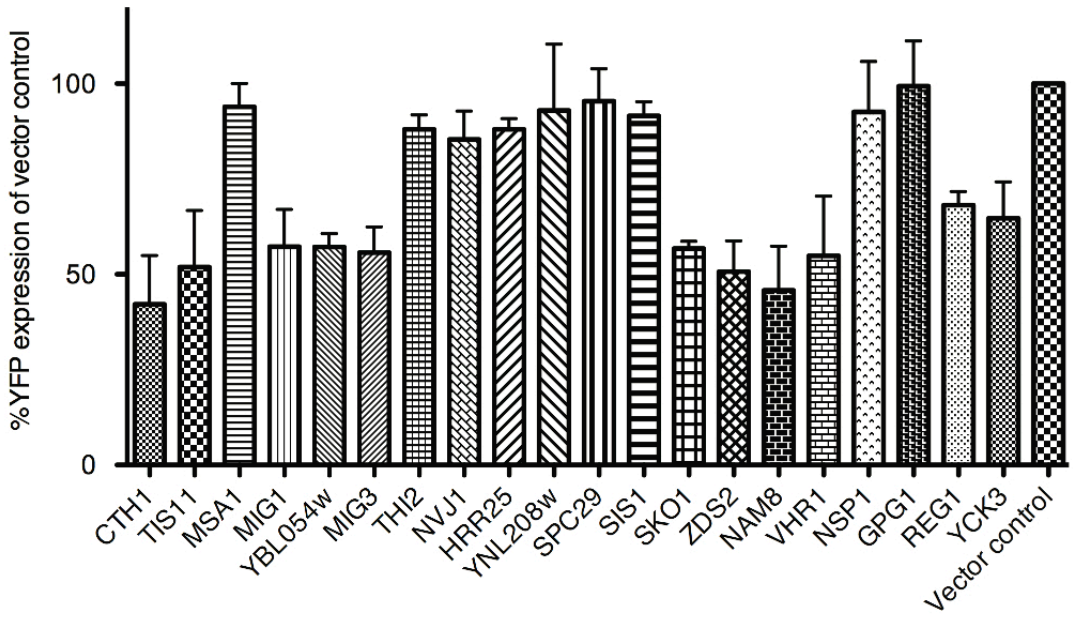

Supplemental Figure C3.2: Effect of OE screen hits on *GAL1*-mediated YFP expression. An overexpression library was screened for suppressors of Rnq1 toxicity. This library contains individual ORFs under control of the inducible *GAL1* promoter, which also controls the overexpression of Rnq1. We eliminated false positive hits that affect expression from the *GAL1* promoter by determining their effect on *GAL1*-mediated expression of YFP using flow cytometry.

Genes changed 2-fold upon Rnq1 overexpression			
Up after 6h	Down after 6h	Up after 8h	Down after 8h
ARG1	ALD4	BTN2	ALD4
FMP16	CRP1	DBF2	CTS1
HSP104	CTS1	FBP1	DSE1
MBF1	DSE2	FMP16	DSE2
SIS1	DSE4	GND2	DSE4
SSA4	EGT2	GPG1	EGT2
YDL038C	GSY2	HSP104	FET3
YGP1	HO	HSP12	FIT2
	HPF1	HSP26	GSY1
	PHO84	IDP2	HTA2
	PRY3	MBF1	HXT3
	REE1	NCA3	HXT6
	SCW11	PCK1	HXT7
		PIR3	INO1
		RPL32	LSP1
		SFC1	MRP1
		SIS1	PDH1
		SSA4	PHO84
		YGP1	PLB2
		YJL144W	PRY3
		YLR040C	PSA1
		YPS3	RGI1
		YRO2	SCW11
			SIM1
			SIT1
			SUN4
			YDR133C

Supplemental Table C3.1: Genes up- or down-regulated upon Rnq1 overexpression. Rnq1 was overexpressed in [*rnq*-] and [*RNQ*$^{+}$] strains. Shown are genes that changed more than 2-fold in the [*RNQ*$^{+}$] strain in comparison to the [*rnq*-] strain. Genes are grouped by time point and directionality of the change in their expression. We also measured gene expression after four hours of Rnq1 overexpression, but at that point we found no significant changes in gene expression.

Sample & Time of Rnq1 induction	DNA Content % 1N	% 2N
[*rnq*-] 0h	42.1	52.6
[*rnq*-] 2h	66.8	30.4
[*rnq*-] 4h	40.8	54.5
[*rnq*-] 6h	38.4	54.2
[*RNQ*$^{+}$] 0h	44.8	51.4
[*RNQ*$^{+}$] 2h	65.7	31.3
[*RNQ*$^{+}$] 4h	32.4	62.8
[*RNQ*$^{+}$] 6h	19.4	69.9
Δrad9 [*RNQ*$^{+}$] 0h	42.9	53.1
Δrad9 [*RNQ*$^{+}$] 2h	64.9	31.9
Δrad9 [*RNQ*$^{+}$] 4h	33.3	62.3
Δrad9 [*RNQ*$^{+}$] 6h	16.7	77.8
Δmad2 [*RNQ*$^{+}$] 0h	51.5	42.5
Δmad2 [*RNQ*$^{+}$] 2h	70.5	27
Δmad2 [*RNQ*$^{+}$] 4h	35.7	60.6
Δmad2 [*RNQ*$^{+}$] 6h	22.1	60.6

Supplemental Table C3.2: Quantification of cell cycle profiling of strain overexpressing Rnq1.

In [*RNQ*$^{+}$] strains Rnq1 overexpression results in an increased number of cells with 2N DNA content. This suggests that Rnq1 overexpression results in a cell cycle arrest between S-phase and G1.

Chapter Four:

A yeast model provides a mechanistic connection between Aβ Toxicity, endocytic trafficking and Alzheimer's Disease risk factors

Manuscript submitted to *Science*. Authors: Sebastian Treusch, Shusei Hamamichi, Kent E.S. Matlack, Jessica L. Goodman, Haesun Han, Chee Yeun Chung, Valeriya Baru, Joshua M. Shulman, Antonio Parrado, Malin Lindhagen-Persson, Eric M. Reiman, Denis A. Evans, David A. Bennett, Anders Olofsson, Philip L. DeJager, Rudolph E. Tanzi, Kim A. Caldwell, Guy A. Caldwell and Susan Lindquist

Abstract

Aβ (amyloid beta peptide) is a key contributor to Alzheimer's disease. We modeled Aβ toxicity in yeast by directing the peptide to the secretory compartment and performed an unbiased genome-wide screen for toxicity modifiers. The screen identified *PICALM*, a highly validated genetic risk factor for sporadic AD. *PICALM*, and other genetic hits with diverse cellular functions, modulated Aβ toxicity in the glutamatergic neurons of *C. elegans*. Further, *PICALM* protected cultured rat cortical neurons against exogenously applied Aβ oligomers, cross-validating different approaches for inducing Aβ toxicity. Aβ caused defects in clathrin-mediated endocytosis and receptor trafficking. *PICALM* and other hits partially corrected it. Our work establishes a direct link between Aβ, endocytosis, and human AD risk factors and provides a new route to deciphering mechanisms underlying AD.

Introduction

The incidence of neurodegenerative diseases will rise precipitously as the world's population ages (HEBERT*, et al.* 2003). Discovering how to mitigate these diseases is complicated by their late onset and complex etiology. Hence, model organisms are a necessity for elucidating the molecular underpinnings of these pathologies and developing therapeutic strategies. Yeast cells lack the highly specialized processes of neuronal cells and the intricacies of cell:cell communication that modulate many different aspects of neuropathology. They therefore provide a "living test tube" to assess, in an isolated cellular context, the intrinsic pathogenic properties of disease-associated polypeptides. When these impinge on common features of eukaryotic cell

biology (KHURANA, *et al.* 2010), yeast offers unequaled genetic tools for the discovery of toxicity modifiers and their mechanisms of action.

We previously generated a yeast model for the toxicity of α-synuclein (α-syn) (OUTEIRO, *et al.* 2003), a protein whose aggregation is a hallmark of Parkinson's Disease (PD), dementia with Lewy Bodies, and Multiple Systems Atrophy. α-syn caused multiple defects in Rab-regulated vesicle trafficking (COOPER, *et al.* 2006; GITLER, *et al.* 2008), a finding since corroborated in several neuronal studies (THAYANIDHI, *et al.* 2010; WINSLOW, *et al.* 2010). It also caused defects in mitochondrial function, a hallmark of PD. An unbiased genome-wide yeast screen identified genes of diverse function that suppress α-syn toxicity in yeast as well as in dopaminergic neurons of both nematodes and rat primary cultures (GITLER, *et al.* 2009). *PARK9*, whose mutation causes parkinsonism with dementia, was one of these modifiers and experiments in yeast established that it protects cells from manganese exposure, a risk factor in Parkinsonism (GITLER, *et al.* 2009). High-throughput yeast screens identified small molecules that protect neurons not only from α-syn but also from rotenone, a mitochondrial poison that can result in PD-like symptoms (SU, *et al.* 2009). Thus, α-syn impinges on vulnerabilities common to all eukaryotic cells, to which particular neurons are simply more sensitive.

Here we report findings with a yeast model of the cellular toxicity induced by the Aβ peptide. According to the amyloid cascade hypothesis, Aβ is causal in both sporadic and familial AD (HARDY, *et al.* 2002). Extracellular amyloid plaques and oligomeric species of Aβ are a hallmark of post mortem AD brains. Intracellular Aβ forms, perhaps representing an earlier stage of pathogenesis, have also been identified (KNOBLOCH, *et*

al. 2007; WALSH*, et al.* 2000). Oligomeric species of Aβ, broadly believed to be the most toxic forms of the peptide, can be detected with a conformation-specific antibody (KAYED*, et al.* 2003). This antibody also recognizes toxic oligomeric forms of several other amyloidogenic proteins associated with neurodegenerative diseases, but not their monomeric or amyloid forms. Strikingly, the antibody recognizes oligomeric intermediates that form during the assembly of a yeast prion protein Sup35, but not its monomeric or amyloid forms (KAYED*, et al.* 2003; SHORTER*, et al.* 2004). Since these proteins share no amino acid sequence homology, these findings suggest that the toxic misfolding of Aβ might represent an ancient type of protein-misfolding problem that confronts many eukaryotic cells.

A definitive diagnosis of AD requires the presence of both Aβ plaques and neurofibrillary tangles of tau, a microtubule-binding protein (LAFERLA 2010). Yet, Aβ appears to act upstream, leading not only to tau pathology (ITTNER*, et al.* 2010; LEWIS*, et al.* 2001; ROBERSON*, et al.* 2007; VOSSEL*, et al.* 2010), but other pathological features of AD, including memory impairment and cell death (ITTNER*, et al.* 2010; VOSSEL*, et al.* 2010). Indeed, targeting Aβ oligomers by passive immunization with the anti-oligomer antibody NAB61 improves learning and memory in an AD mouse model (LEE*, et al.* 2006). While connections between Aβ and tau are steadily being unraveled, connections between Aβ and AD risk factors identified in genome-wide association studies (GWAS) remain uncertain. Herein, we establish a platform for discovering and analyzing genetic modifiers of Aβ toxicity that has already provided mechanistic insights and might aid the development of new therapeutic strategies.

Results

A yeast model of Aβ toxicity

In the nervous system the most toxic form of Aβ, Aβ 1-42, is generated by successive proteolytic cleavage of APP, the transmembrane amyloid precursor protein, by the β- and γ-secretases (SELKOE, *et al.* 2007; THINAKARAN, *et al.* 2008). APP processing primarily occurs in the secretory network, with the release of Aβ into the trans-Golgi, endosomal compartments and extracellular space. There, it interacts with the plasma membrane and is subject to endocytosis (THINAKARAN, *et al.* 2008). To recapitulate the multi-compartment trafficking of Aβ in a yeast cell, we fused an ER targeting signal that is processed with high efficiency to the N-terminus of the human Aβ 1-42 sequence (ssAβ 1-42, supplementary methods on line). With neither an ER retention sequence, nor any other amino acids remaining after cleavage of the targeting sequence, the peptide will transit through the secretory pathway and be released from the cell. Critically, however, the yeast cell wall will restrain its diffusion, allowing Aβ 1-42 to interact with the plasma membrane and be subject to endocytosis.

The expression of ssAβ 1-42 from a high-copy plasmid, using a galactose-inducible (*GAL1*) promoter, decreased growth when yeast cells were shifted from glucose to galactose (Figure C4.1A). ssAβ 1-40, an APP cleavage product that is less toxic to neurons and in various AD models (LUHESHI, *et al.* 2007), was also less toxic in yeast. BPTI, a small protein commonly used to study secretion, and even a BPTI variant known to misfold in the ER were much less toxic (KOWALSKI, *et al.* 1998). The ER resident protein Pdi1 slowed growth minimally.

We next constructed stable screening strains by integrating multiple copies of the ssAβ 1-42 construct into the genome. We selected strains exhibiting intermediate levels of toxicity to enable the identification of enhancers and suppressors in the same screen and to allow analysis of Aβ induced cellular defects under circumstances where they are still amenable to amelioration (Figure C4.1B). These strains produced a peptide of the expected size for Aβ 1-42, along with higher molecular weight Aβ oligomers (Figure C4.1C and Supplemental Figure C4.1). We confirmed the localization of Aβ to the secretory system by immunostaining (Figure C4.1F and Supplemental Figure C4.2).

Soluble Aβ oligomers are increasingly recognized as the most detrimental Aβ species in AD (KAYED, *et al.* 2003; LI, *et al.* 2009). We detected oligomeric species of Aβ using the above-mentioned NAB61 antibody (Figure C4.1D) (LEE, *et al.* 2006). These species disappeared upon boiling in LDS (Supplemental Figure C4.1). We further verified the presence of oligomeric Aβ species using an indirect ELISA assay (Figure C4.1E), based on a monoclonal IgM anti-Aβ antibody (OMAB) specific for soluble Aβ oligomers (LINDHAGEN-PERSSON, *et al.* 2010). Oligomer levels were much lower in the strain with a single, non-toxic, copy of ssAβ 1-42 and undetectable in vector-only controls.

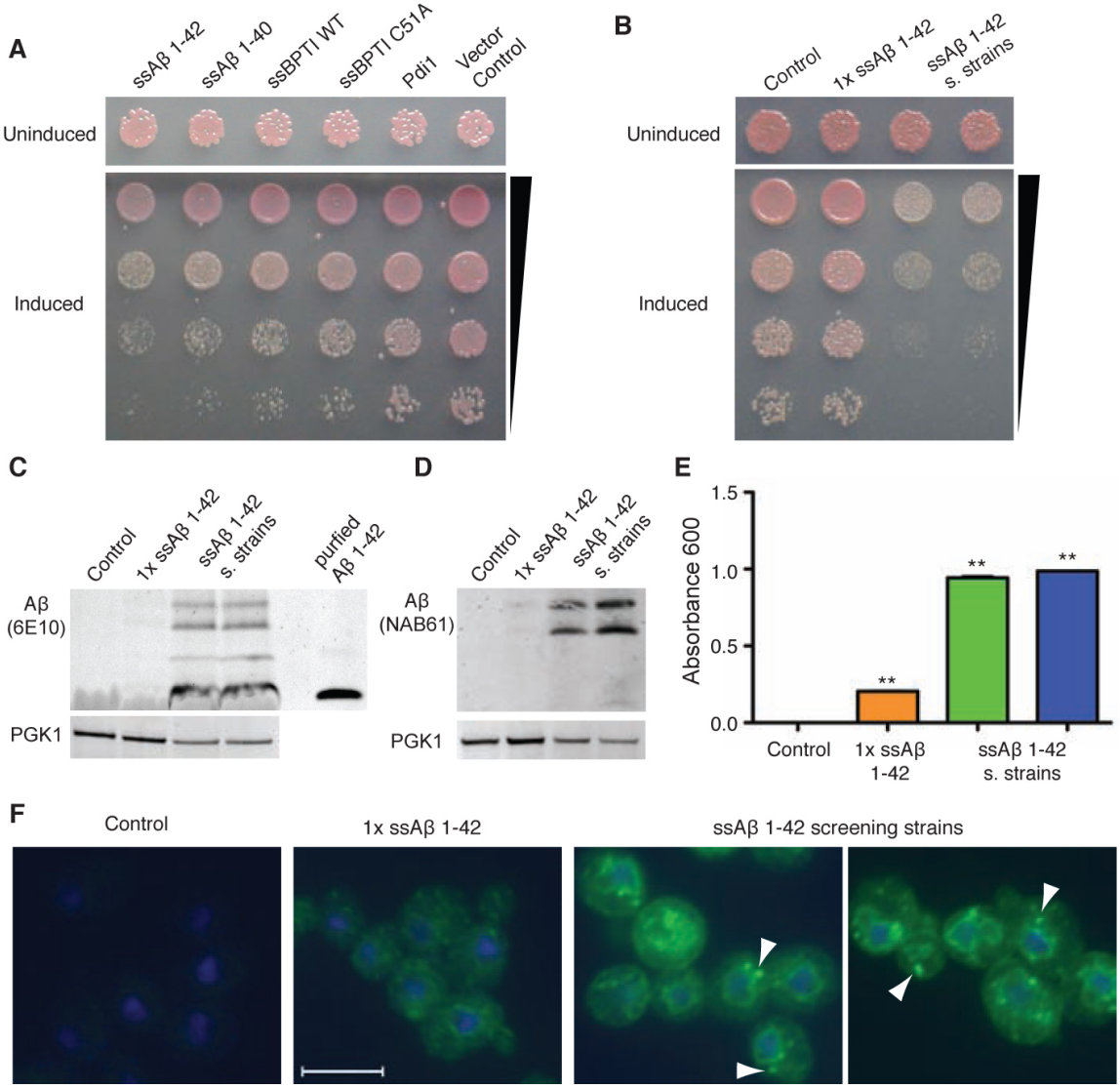

Figure C4.1: Expression of Aβ in the yeast secretory compartment.

(A) Comparison of ssAβ 1-42 toxicity with ssAβ 1-40, ssBPTI (WT and C51A) and Pdi1. ssAβ 1-42 was more toxic than ssAβ 1-40 and other proteins, all targeted to the secretory pathway with the signal sequence of Kar2. Proteins were expressed using the inducible *GAL1* promoter and a high copy number plasmid. Strains carrying the plasmids were serially diluted and spotted on inducing (galactose) and non-inducing (glucose) media. **(B)** Construction of stable ssAβ 1-42 strains for a genetic screen. A single

integrated genomic copy of ssAβ 1-42 was not toxic, but the integration of several copies of the construct resulted in robust toxicity. **(C)** Aβ 1-42 expression was detected by immunoblot analysis using the 6E10 Aβ-specific antibody. Samples were not boiled before loading on the gel. See Supplemental Figure C4.1 for the loss of oligomeric forms after boiling in LDS. **(D)** Immunoblot with NAB61, an antibody specific for soluble Ab oligomers, detects oligomers in unboiled samples. **(E)** An indirect ELISA assay using a monoclonal Aβ oligomer-specific antibody (OMAB) detects significant levels of Aβ oligomers in the 1xAβ strain and, more so, in the screening strains (n=5; error bars to small to be visible; ** = $p<0.01$, based on Dunnett's test). **(F)** Immunostaining for ssAβ 1-42 reveals localization to the ER/secretory compartment. Aβ was detected in the ER (ring surrounding the nucleus, stained blue with DAPI) and in small foci throughout the cell (arrowheads). The scale bar is 5μm and all figures are on the same scale.

Screen for genetic modifiers of Aβ toxicity

We transformed a screening strain with an overexpression library of 5532 full length ORFs (~90% of yeast ORFs) regulated by the same inducible promoter used for Aβ expression. The transformed strains were arrayed in media that prevented induction of either Aβ or the putative modifiers, and then plated (four replicates each) onto media that supported different levels of mitochondrial respiration under inducing conditions (see Supplemental Table C4.1 for further details). Plasmids that decreased or increased growth in cells expressing Aβ (Supplemental Figure C4.3) were retested in an independently generated Aβ screening strain and filtered to remove genes that affected expression from the *GAL1* promoter (Supplemental Figure C4.4) or affected growth in the absence of Aβ.

We identified 23 suppressors and 17 enhancers of Aβ toxicity (Supplemental Table C4.1). Only a few modifiers were strongly affected by the state of respiration (Supplemental Table C4.1). The screen hits comprised a wide range of cellular functions. Numerous hits had sequence similarity to human genes and twelve had very clear human homologs (determined by HomoloGene or by analogous functionality [*SLA1* – SH3KBP1] (STAMENOVA*, et al.* 2004))(Table C4.1). We focused further analysis on these, as their high degree of functional conservation made them more likely to be relevant to Aβ toxicity in other model organisms and, ultimately, in humans.

Yeast Aβ Suppressors	Cellular Function	Human Homolog	*C. elegans* Homolog
YAP1802	Endocytosis	*PICALM*	*unc-11**
INP52	Endocytosis	*SYNJ1*	*unc-26**
SLA1	Endocytosis	*SH3KBP1*	*Y44E3A.4**
RTS1	Phosphatase regulation	*PPP2R5C*	*pptr-2**
ADE12	Adenylosuccinate synthesis	*ADSSL1*	*C37H5.6b**
CRM1	Nuclear protein export	*XPO1*	*xpo-1**
GRR1	Ubiquitination	*FBXL2*	*C02F5.7*
VPS9	Vesicle transport	*RABGEF1*	*rabx-5*
Yeast Aβ Enhancers			
PBS2	Osmotic stress response	*MAP2K4*	*mkk-4**
KEM1	RNA processing	*XRN1*	*xrn-1*
MVP1	Vacuolar sorting	*SNX8*	*lst-4*
PMT2	Mannosylation	*POMT2*	-

(* Genes tested in the *C. elegans* model)

Table C4.1: Modifiers of Aβ toxicity with clear human homologs.

Yeast genes with clear human and nematode homologs were identified in an unbiased screen of 5,532 single copy plasmids carrying yeast ORFs under the control of the *GAL1* promoter. PICALM, one of three hits involved in endocytosis, is a risk factor for sporadic AD.

Notably, three of the twelve have functions related to clathrin-mediated endocytosis (*YAP1802*, *SLA1* & *INP52*; *P*=3.89e-4) and seven are functionally associated with the cytoskeleton (*YAP1802*, *SLA1*, *INP52, CRM1, GRR1, KEM1 & RTS1*; *P*=6.06e-8). Importantly, none had been identified in our previous screen for modifiers of α-syn toxicity (COOPER*, et al.* 2006; GITLER*, et al.* 2009), establishing their specificity for the type of toxicity caused by our ssAβ construct.

Modifiers of Aβ toxicity are associated with AD susceptibility

Remarkably, several human homologs of the yeast hits have strong connections to AD or Aβ toxicity in other experimental systems and human patients.

The *PBS2* homolog *MAP2K4*, part of the JNK pathway, is activated in response to Aβ oligomer administration to cultured cortical neurons (BOZYCZKO-COYNE*, et al.* 2001). Synaptojanin, the *INP52* homolog, has also been shown to modulate the toxicity of Aβ oligomers, although through a reduction in its activity rather than an increase as in our screen (BERMAN*, et al.* 2008).

Most strikingly, the human homolog of *YAP1802*, *PICALM*, is a confirmed risk factor for sporadic AD (HAROLD*, et al.* 2009; LAMBERT*, et al.* 2009). Indeed, initial reports that *PICALM* is associated with AD susceptibility at a genome-wide level of significance have been replicated in 12 independent AD case-control samples (BERTRAM*, et al.* 2010). *PICALM* is currently the third ranked AD risk factor on Alzgene (BERTRAM*, et al.* 2007).

To assess the potential clinical relevance of other modifiers of Aβ toxicity, we asked whether the eleven screen hits with highly conserved human homologs show

evidence of association with susceptibility for AD or AD-related pathologic burden. First, we examined association with AD susceptibility using data from a published family-based GWAS (BERTRAM, *et al.* 2008) performed on the National Institute of Mental Health (NIMH) Genetics Alzheimer's Disease Initiative Study (BLACKER, *et al.* 1997). Using a family-based association test, we discovered a suggestive association of *XPO1* (*CRM1* homolog, rs6545886, *P*=0.003) with AD susceptibility (See supporting online material for methodological details, Supplemental Table C4.2).

Next, we leveraged genotyping with extensive clinical and pathological data from two large epidemiological studies of aging, cognition, and AD: the Religious Orders Study (ROS) and the Rush Memory and Aging Project (MAP)(See supporting online material for methodological details, Supplemental Tables C4.3-6) (*36-38*). Using a quantitative summary measure of global AD pathologic burden available in these cohorts, counting both amyloid plaques and NFTs, we found that two additional loci identified by our yeast screen, *ADSSL1* (*ADE12* homolog, rs1128880, *P*=0.001) and *RABGEF1* (*VPS9* homolog, rs17566701, *P*=0.002) showed evidence of association with AD neuropathology (Supplemental Table C4.6). Both loci also harbored suggestive association signals with episodic memory decline (Supplemental Table C4.5).

C. elegans model of Aβ toxicity

The connection between *PICALM* and Aβ toxicity in our yeast model, together with these other suggestive connections, encouraged us to establish a new genetic model to directly test the effects of Aβ toxicity modifiers in a neuronal setting. The

nematode *C. elegans* has been previously employed to investigate Aβ toxicity (COHEN*, et al.* 2006; LINK 1995) in body wall muscle cells. To test our genetic modifiers in neurons, we first created stable transgenic lines that express Aβ 1-42 in glutamatergic neurons, a neuronal subtype particularly vulnerable in AD. The Aβ transgene was integrated into worm chromosomal DNA to ensure the same extent of Aβ 1-42 expression in all glutamatergic neurons. We used the *eat-4* promoter, which controls expression of the BNPI vesicular glutamate transporter and, again, targeted Aβ to the secretory pathway without a retention signal.

C. elegans is renowned for its highly stereotypical cell lineages. Wild-type worms invariably have five glutamatergic neurons in their tails. These are conveniently visualized in transgenic animals that also carry an *eat-4*-regulated GFP transgene. Expression of ssAβ resulted in the loss of these GFP-marked glutamatergic neurons in an age-related manner: at day three only 48% of worms had five intact glutamatergic neurons, and at day seven only 25% did (Figure C4.2B). To test the genetic modifiers, we established three independent stable transgenic lines for each gene (Table C4.1). Again the *eat-4* promoter was used to control expression. First, we tested the *C. elegans* homologs of the three yeast genes involved in clathrin-mediated endocytosis, including the homologs of Synaptojanin and the AD risk factor *PICALM*. All three, the worm *YAP1802*/*PICALM* homolog, the worm *INP52*/Synaptojanin homolog, and the worm *SLA1*/*SH3KBP1* homolog, increased the percentage of worms with five intact glutamatergic neurons (Figure C4.2A & B).

Next, we tested hits involved in a diverse array of other cellular pathways. The yeast *RTS1* gene encodes a phosphatase regulatory subunit that controls several stress-response pathways. The *ADE12* gene product catalyzes the first step in the synthesis of adenosine monophosphate from inosine 5-monophosphate. The *C. elegans* homologs of *RTS1/PPP2R5C* and *ADE12*/ADSSL1 suppressed the Aβ-induced loss of glutamatergic neurons (Figure C4.2A). We were unable to clone the worm homolog of *CRM1,* which encodes a highly conserved nuclear export receptor. However, expression of the highly homologous human *XPO1* gene significantly protected nematode glutamatergic neurons from Aβ toxicity (Figure C4.2A). Finally, we asked if the effects of a genetic enhancer also translated to the neuronal environment. Indeed, the *C. elegans* homolog of *PBS2/MAP2K4,* a MAP kinase involved in stress responses, increased neuronal loss (Figure C4.2A & B). We were unable to clone the worm homologs of *GRR1* and *VPS9* (Table C4.1).

Every gene we tested *in C. elegans* modified Aβ toxicity in the same direction (suppression vs. enhancement) in glutamatergic neurons as they did in yeast. The effect of each of the candidate genes was statistically robust ($p < 0.05$) for both the modest neuronal toxicity evinced at three days and the more severe toxicity at seven days. In contrast, expression of two control proteins, mCherry and LacZ, had no effect (Figure C4.2A). The modifiers did not alter the levels of Aβ mRNA, as determined by semi-quantitative RT-PCR (Supplemental Figure C4.5). Thus, the effects of the genetic modifiers can be attributed to modification of Aβ toxicity itself.

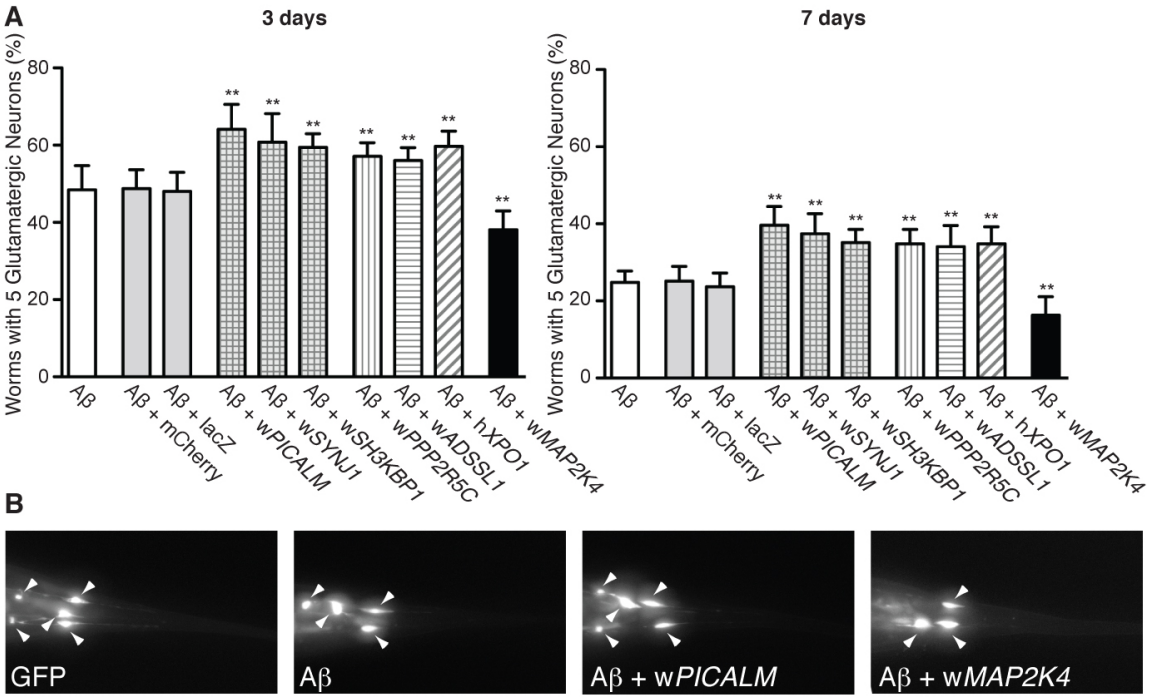

Figure C4.2: Hits from the screen modify the toxicity of Aβ in *C. elegans* glutamatergic neurons in the same direction as they do in yeast.

(A) A new animal model of Aβ toxicity. Aβ 1-42, carrying a signal sequence targeting it to the secretory compartment, was expressed in glutamatergic neurons that were also expressing GFP. Neuronal death increased from 50% at day 3 to 75% at day 7, establishing that this worm model exhibits age-dependent neurodegeneration. Control genes mCherry and lacZ had no effect on Aβ-induced neurodegeneration. Bar patterns indicate distinct functional categories (crosshatches for endocytic genes). The genetic modifiers tested influenced Aβ toxicity significantly ($p < 0.05$, Student's t-Test). XPO1 was derived from human cDNA. Each gene was tested in three independently established transgenic lines. **(B)** Representative examples of worms scored in Figure

C4.2A at the third day of development. Arrowheads indicate neuronal cell bodies, marked by transgenic expression of GFP.

***PICALM* suppresses the toxicity of soluble Aβ oligomers in rat cortical neurons**

Next, we asked if the toxicity elicited by targeted expression of Aβ 1-42 in the secretory compartment of yeast and in nematode glutamatergic neurons correlated with the toxicity of soluble Aβ 1-42 oligomers externally applied to neuronal cells. Oligomeric Aβ 1-42 species are found naturally in AD and thought to be causal in disease. Oligomeric species generated using synthetic peptide are increasingly employed with tissue culture cells and primary neuronal cultures to investigate Aβ proteotoxicity (BERMAN*, et al.* 2008; BOZYCZKO-COYNE*, et al.* 2001; KAYED*, et al.* 2003). Whether the acute toxicities observed in such cell cultures (massive cellular death after as little as 24 hrs) are subject to modification by the same human genetic risk factors that alter disease onset after many decades of life has only begun to be explored (TROMMER*, et al.* 2005).

To analyze a neuronal population particularly relevant to AD, we prepared primary cultures from rat cortical neurons. Soluble Aβ oligomers prepared from synthetic peptide were extremely toxic to these cells (Figure C4.3, GFP control infections). Transfection with lentivirus engineered to express *PICALM* rescued toxicity in a dose-dependent manner (Figure C4.3). *RAB1*, a gene that we have previously shown to protect neurons from α-syn induced toxicity (COOPER*, et al.* 2006), was unable to diminish the cell death induced by Aβ oligomers (Figure C4.3). Thus, the efficacy of a gene identified in yeast as a modifier of Aβ toxicity is recapitulated in neurons.

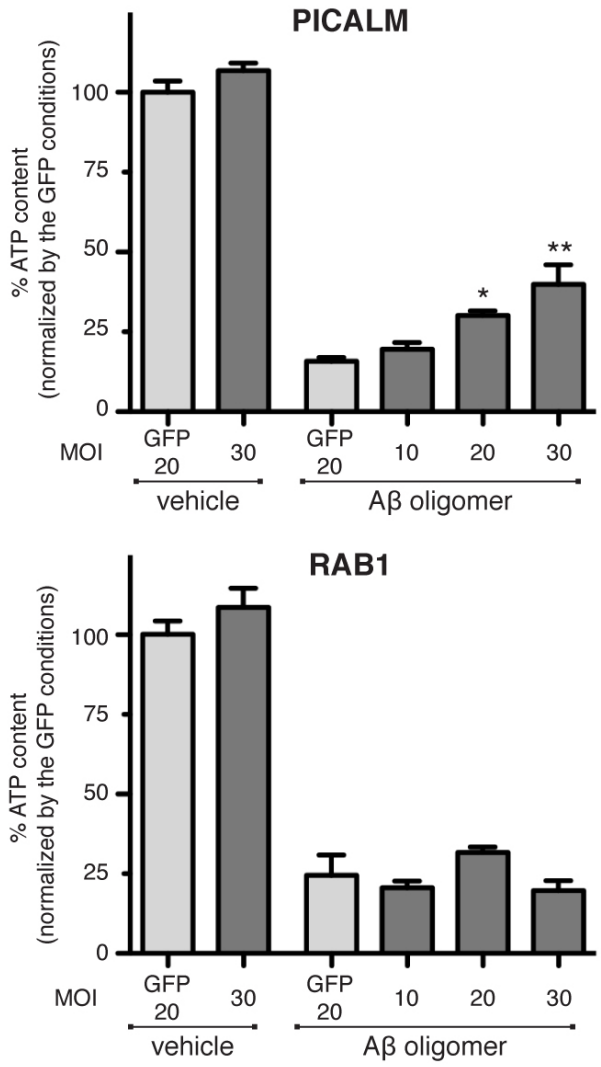

Figure C4.3: PICALM protects cultured rat cortical neurons from exogenously applied Aβ oligomers.

Cortical neuron cultures prepared from rat embryos at embryonic day 18 were cultured for 5 days, transduced, cultured for 13 days, and then incubated for 20 hours with 750nM of soluble Aβ oligomers prepared from synthetic peptide (See Supplemental Materials for details). Cell viability was assessed by ATP content. Infection with a PICALM lentiviral construct diminished toxicity in a dose-dependent, statistically significant manner. The GFP control and RAB1, a suppressor of neuronal α-syn toxicity,

had no significant effect. Data are representative of three independent experiments and shown as mean +/- SEM (*, $p<0.05$; **, $p<0.01$, based on Dunnett's test).

Effect of Aβ on endocytosis and trafficking

Having validated our approach to the discovery of Aβ toxicity modifiers, we returned to yeast to investigate the mechanistic connections between Aβ and the three modifiers that affect the same cellular process, clathrin-mediated endocytosis. The member of this class with a clear risk association to AD, *PICALM*, has been postulated to affect disease through modifications of APP trafficking. However, our cells express Aβ 1-42 directly, establishing a link between *PICALM* and Aβ toxicity itself.

Endocytosis might modulate Aβ toxicity simply by shunting toxic Aβ species to cellular compartments where they are inherently less toxic or are more subject to degradation. On the other hand, Aβ might specifically impair the endocytic machinery, with an increase in this function then being required to ameliorate that defect. To assay the impact of Aβ on the trafficking of a substrate of endocytosis we examined Ste3, a mating pheromone receptor that is targeted to the plasma membrane. In the absence of its mating hormone ligand, Ste3 is constitutively endocytosed and degraded in the vacuole (MALDONADO-BAEZ*, et al.* 2008). As expected from previous work, a Ste3-YFP fusion was primarily localized to the vacuole in our control strain. In Aβ -expressing strains Ste3-YFP was instead found in foci surrounding the vacuole. Thus, Aβ caused an explicit defect in the endocytic trafficking of this receptor (Figure C4.4A).

All three of the Aβ toxicity modifiers that function in endocytic trafficking, Yap1802, Inp52 and Sla1, reversed the defect in Ste3-YFP trafficking. Since the proteins encoded by these genes function in multi protein complexes, and since several other gene products modified Aβ toxicity in ways that might impinge on endocytic trafficking,

one would not expect a complete phenotypic reversal from the overexpression of any one protein. Indeed, vacuolar localization was restored in some cells, but by no means all (Figure C4.4A & Supplemental Figure C4.6).

Next, we monitored endocytic trafficking in a yeast strain in which clathrin light chain was endogenously tagged with GFP (Clc1-GFP). As expected, the control strain exhibited only a few faint foci of Clc1-GFP (SUN, *et al.* 2007). Aβ dramatically perturbed clathrin localization, increasing the number and brightness of foci but decreasing their size (Figure C4.4B & Supplemental Figure C4.7A). This confirmed the effect of Aβ on endocytic trafficking. Further, the small foci of Clc1-GFP in the Aβ strain suggested an effect on the processing of endocytic intermediates.

Yap1802 and Sla1 promote clathrin assembly (MALDONADO-BAEZ, *et al.* 2008), while Inp52 facilitates fission and uncoating of clathrin vesicles (STEFAN, *et al.* 2005). This suggested that the genetic modifiers might ameliorate endocytic trafficking in distinct ways. Indeed, Yap1802, the yeast *PICALM* homolog, increased the number of clathrin-containing foci (Figure C4.4B). Sla1 subtly increased them (Supplemental Figure C4.7B). Inp52, the homolog of Synaptojanin, decreased them (Figure C4.4B). Thus, all three endocytic modifiers attenuate the Aβ induced trafficking defect by increasing flux through the endocytic pathway. Yap1802 and Sla1 did so by increasing the assembly of clathrin-coated vesicles, Inp52 by increasing processing of those vesicles.

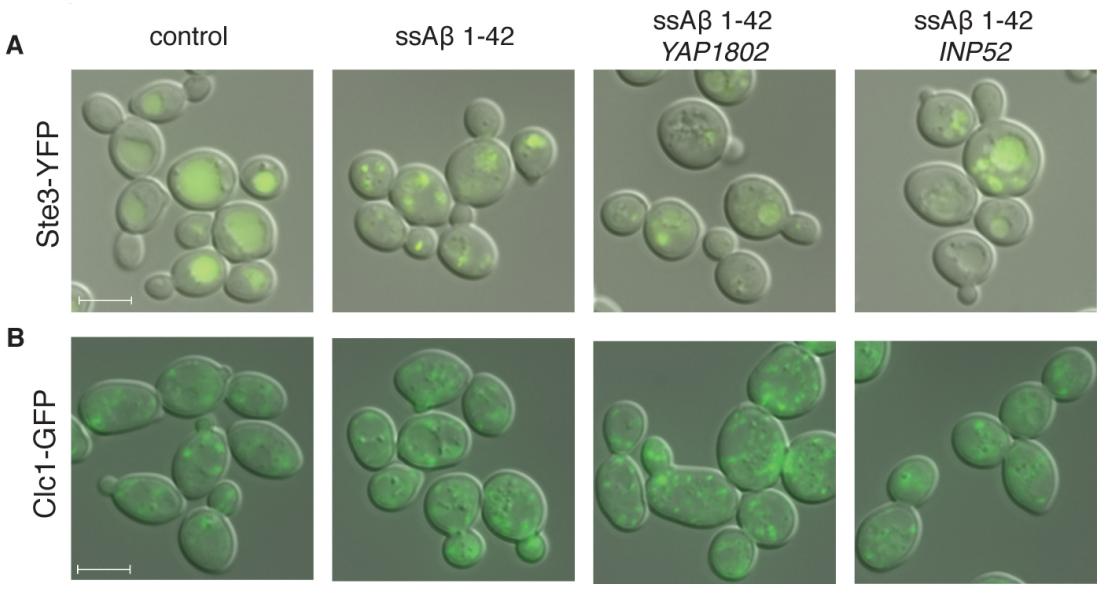

Figure C4.4: Aβ causes defects in endocytosis and receptor protein trafficking.

(A) Aβ 1-42 caused a defect in the trafficking of Ste3-YFP, a hormonal receptor protein. In controls Ste3-YFP was trafficked to the vacuole; in contrast Aβ expression resulted in the accumulation of Ste3-YFP in cytoplasmic foci. Co-expression of *YAP1802, INP52* and *SLA1* (Supplemental Figure C4.6) suppressed this effect. Ste3-YFP was expressed from a construct integrated in either a control or a screening strain using the constitutive *GPD* promoter. **(B)** Expression of ssAβ 1-42 in a strain with GFP-tagged clathrin light chain (Clc1-GFP) resulted in an increase of Clc1-GFP foci, representing endocytic intermediates. Co-expression of *YAP1802* enhanced, and *INP52* reversed, the effect of Aβ. *SLA1* subtly enhanced foci formation (Supplemental Figure C4.7B). The screening strain, with integrated copies of ssAβ 1-42, was mated to cells expressing Clc1-GFP strain and transformed with single copy control and test plasmids. *INP52*, *YAP1802, SLA1* and ssAβ were expressed using the inducible *GAL1* promoter. Scale bars are 5μm and all figures are on the same scale.

Conclusions and Perspectives

The treatments available for Alzheimer's disease are few and their efficacy limited. The complexity of deciphering how best to rescue neuronal function in the context of the whole brain is of staggering proportions. Our model enabled us to conduct an unbiased screen of the entire yeast genome for Aβ toxicity modifiers. We connected a diverse group of genes and pathways to Aβ toxicity in a manner that has clear relevance to neurons and human disease. These connections are conserved across a billion years of evolution and can counteract both the extracellular administration of Aβ oligomers to cortical neurons and the targeted expression of Aβ in the secretory compartment of yeast and nematode neurons. This confirms previous suggestions that the toxic conformers of Aβ are related to very ancient problems in protein homeostasis (COHEN, *et al.* 2006; KAYED, *et al.* 2003).

Of the twelve most highly conserved modifiers, three affected clathrin-mediated endocytosis (Table C4.1), establishing this process as a key point of vulnerability to Aβ toxicity. Neurons would naturally be particularly vulnerable to such a defect as they must constantly recycle neurotransmitters and receptors (JUNG, *et al.* 2007). Indeed, as this manuscript was being submitted, two GWAS analyses identified *CD2AP* as a novel AD risk factor (HOLLINGWORTH, *et al.* 2011; NAJ, *et al.* 2011). This protein functions in a complex with SH3KBP1 (also known as CIN85) (GAIDOS, *et al.* 2007), the functional homolog of our Aβ modifier *SLA1*, linking actin dynamics to endocytosis. In total, four AD risk factors (*PICALM*, *BIN1*, *CD2AP*, and *CD33*) are involved in endocytosis

(HOLLINGWORTH, *et al.* 2011; NAJ, *et al.* 2011); a process we establish is affected by Aβ toxicity.

Yeast cells to not express a recognizable homolog of Tau, a microtubule associated protein that is a key component of Aβ toxicity in AD. It is notable, however, that seven of the twelve conserved modifiers are functionally associated with the cytoskeleton, suggesting a more deeply rooted connection between the cytoskeleton and Aβ toxicity, likely involving its roles in vesicle trafficking. The connections between Aβ toxicity and the modifiers with more diverse cellular functions are at present unclear. However, if the associations we uncovered in human GWAS analyses for SNPs in *XPO1*, *ADSSL1* and *RABGEF1* prove valid, the high degree of conservation in these genes should make their roles in AD risk also accessible to analysis in yeast.

In recent years a number of neuronal models of AD have emerged, offering an unprecedented opportunity for preclinical evaluation of therapeutic strategies. Our yeast model provides a new tool to funnel genetic leads into these systems. It should also provide a means for screening large chemical libraries for compounds that might target the basic underlying cellular toxicities of Aβ 1-42. Combined with genetic analyses, this may facilitate a personalized medical approach to this profoundly devastating and complex disease.

Acknowledgements

We are grateful to numerous members of the Lindquist lab for comments on this manuscript. We also thank Lori Chibnik and Brendan Keenan for helpful discussions

concerning the human genetic analyses. We thank Dane Wittrup (BPTI), Virginia Lee (NAB61), Marc Vidal (worm and human ORFS) and Chris Link (*C. elegans* ssAβ) for generously providing constructs. SL is an Investigator of the HHMI. We thank Jason Corneveaux, Matthew Huentelman, and other Translational Genomics investigators for their contribution to genotyping of the human study cohorts. This work was supported by an HHMI Collaborative Innovation Award (to SL and GAC) and a NRSA fellowship F32 NS067782-02 (to JLG). RET is funded by the Cure Alzheimer's Fund. The authors also thank the participants of the Religious Orders Study and the Rush Memory and Aging Project, which were supported by NIH grants K08AG034290, P30AG10161, R01AG15819, and R01AG17917 (to JMS, DAB, DAE, and PLD). AO is supported by the Kempe foundation and Alzheimerfonden.

Author contributions

I created and characterized the Aβ strains used in this study using a construct created by Kent Matlack. I carried out the genetic screen with help from Haesun Han. Jessica Goodman performed western analysis on the Aβ strains and collaborated with Anders Olofsson and Malin Lindhagen-Persson on the Aβ ELISA experiments. Shusei Hamamichi carried out the *C. elegans* experiments in lab of Guy and Kim Caldwell. Chee Yeun Chung and Valeriya Baru conducted the Aβ cortical neuron experiments using Aβ oligomers generated by Jessica. I aided the design of the *C. elegans* and cortical neuron experiments and created several of the constructs used. Antonio Parrado and Rudolph Tanzi carried out the familial AD genetics analysis. Joshua Shulman and Phil DeJager

carried out the sporadic AD genetic analysis using data sets generated in part buy Eric Reiman, Denis A. Evans and David A. Bennett. Susan Lindquist and I wrote the paper receiving numerous helpful comments from Kent, Jessica, Shu and Joshua.

References

Berman, D.E., Dall'Armi, C., Voronov, S.V., McIntire, L.B., Zhang, H., Moore, A.Z., Staniszewski, A., Arancio, O., Kim, T.W., & Di Paolo, G. (2008) Oligomeric Amyloid-Beta Peptide Disrupts Phosphatidylinositol-4,5-Bisphosphate Metabolism. *Nat Neurosci* 11(5):547-554.

Bertram, L., Lange, C., Mullin, K., Parkinson, M., Hsiao, M., Hogan, M.F., Schjeide, B.M., Hooli, B., Divito, J., Ionita, I., Jiang, H., Laird, N., Moscarillo, T., Ohlsen, K.L., Elliott, K., Wang, X., Hu-Lince, D., Ryder, M., Murphy, A., Wagner, S.L., Blacker, D., Becker, K.D., & Tanzi, R.E. (2008) Genome-Wide Association Analysis Reveals Putative Alzheimer's Disease Susceptibility Loci in Addition to Apoe. *Am J Hum Genet* 83(5):623-632.

Bertram, L., Lill, C.M., & Tanzi, R.E. (2010) The Genetics of Alzheimer Disease: Back to the Future. *Neuron* 68(2):270-281.

Bertram, L., McQueen, M.B., Mullin, K., Blacker, D., & Tanzi, R.E. (2007) Systematic Meta-Analyses of Alzheimer Disease Genetic Association Studies: The Alzgene Database. *Nat Genet* 39(1):17-23.

Blacker, D., Haines, J.L., Rodes, L., Terwedow, H., Go, R.C., Harrell, L.E., Perry, R.T., Bassett, S.S., Chase, G., Meyers, D., Albert, M.S., & Tanzi, R. (1997) Apoe-4 and Age at Onset of Alzheimer's Disease: The Nimh Genetics Initiative. *Neurology* 48(1):139-147.

Bozyczko-Coyne, D., O'Kane, T.M., Wu, Z.L., Dobrzanski, P., Murthy, S., Vaught, J.L., & Scott, R.W. (2001) Cep-1347/Kt-7515, an Inhibitor of Sapk/Jnk Pathway Activation, Promotes Survival and Blocks Multiple Events Associated with Abeta-Induced Cortical Neuron Apoptosis. *J Neurochem* 77(3):849-863.

Cohen, E., Bieschke, J., Perciavalle, R.M., Kelly, J.W., & Dillin, A. (2006) Opposing Activities Protect against Age-Onset Proteotoxicity. *Science* 313(5793):1604-1610.

Cooper, A.A., Gitler, A.D., Cashikar, A., Haynes, C.M., Hill, K.J., Bhullar, B., Liu, K., Xu, K., Strathearn, K.E., Liu, F., Cao, S., Caldwell, K.A., Caldwell, G.A., Marsischky, G., Kolodner, R.D., Labaer, J., Rochet, J.C., Bonini, N.M., & Lindquist, S. (2006) Alpha-Synuclein Blocks Er-Golgi Traffic and Rab1 Rescues Neuron Loss in Parkinson's Models. *Science* 313(5785):324-328.

Gaidos, G., Soni, S., Oswald, D.J., Toselli, P.A., & Kirsch, K.H. (2007) Structure and Function Analysis of the Cms/Cin85 Protein Family Identifies Actin-Bundling Properties and Heterotypic-Complex Formation. *J Cell Sci* 120(Pt 14):2366-2377.

Gitler, A.D., Bevis, B.J., Shorter, J., Strathearn, K.E., Hamamichi, S., Su, L.J., Caldwell, K.A., Caldwell, G.A., Rochet, J.C., McCaffery, J.M., Barlowe, C., & Lindquist, S. (2008) The Parkinson's Disease Protein Alpha-Synuclein Disrupts Cellular Rab Homeostasis. *Proc Natl Acad Sci U S A* 105(1):145-150.

Gitler, A.D., Chesi, A., Geddie, M.L., Strathearn, K.E., Hamamichi, S., Hill, K.J., Caldwell, K.A., Caldwell, G.A., Cooper, A.A., Rochet, J.C., & Lindquist, S. (2009) Alpha-Synuclein Is Part of a Diverse and Highly Conserved Interaction Network That Includes Park9 and Manganese Toxicity. *Nat Genet* 41(3):308-315.

Hardy, J. & Selkoe, D.J. (2002) The Amyloid Hypothesis of Alzheimer's Disease: Progress and Problems on the Road to Therapeutics. *Science* 297(5580):353-356.

Harold, D., Abraham, R., Hollingworth, P., Sims, R., Gerrish, A., Hamshere, M.L., Pahwa, J.S., Moskvina, V., Dowzell, K., Williams, A., Jones, N., Thomas, C., Stretton, A., Morgan, A.R., Lovestone, S., Powell, J., Proitsi, P., Lupton, M.K., Brayne, C., Rubinsztein, D.C., Gill, M., Lawlor, B., Lynch, A., Morgan, K., Brown, K.S., Passmore, P.A., Craig, D., McGuinness, B., Todd, S., Holmes, C., Mann, D., Smith, A.D., Love, S., Kehoe, P.G., Hardy, J., Mead, S., Fox, N., Rossor, M., Collinge, J., Maier, W., Jessen, F., Schurmann, B., van den Bussche, H., Heuser, I., Kornhuber, J., Wiltfang, J., Dichgans, M., Frolich, L., Hampel, H., Hull, M., Rujescu, D., Goate, A.M., Kauwe, J.S., Cruchaga, C., Nowotny, P., Morris, J.C., Mayo, K., Sleegers, K., Bettens, K., Engelborghs, S., De Deyn, P.P., Van Broeckhoven, C., Livingston, G., Bass, N.J., Gurling, H., McQuillin, A., Gwilliam, R., Deloukas, P., Al-Chalabi, A., Shaw, C.E., Tsolaki, M., Singleton, A.B., Guerreiro, R., Muhleisen, T.W., Nothen, M.M., Moebus, S., Jockel, K.H., Klopp, N., Wichmann, H.E., Carrasquillo, M.M., Pankratz, V.S., Younkin, S.G., Holmans, P.A., O'Donovan, M., Owen, M.J., & Williams, J. (2009) Genome-Wide Association Study Identifies Variants at Clu and Picalm Associated with Alzheimer's Disease. *Nat Genet* 41(10):1088-1093.

Hebert, L.E., Scherr, P.A., Bienias, J.L., Bennett, D.A., & Evans, D.A. (2003) Alzheimer Disease in the Us Population: Prevalence Estimates Using the 2000 Census. *Arch Neurol* 60(8):1119-1122.

Hollingworth, P., Harold, D., Sims, R., Gerrish, A., Lambert, J.C., Carrasquillo, M.M., Abraham, R., Hamshere, M.L., Pahwa, J.S., Moskvina, V., Dowzell, K., Jones, N., Stretton, A., Thomas, C., Richards, A., Ivanov, D., Widdowson, C., Chapman, J., Lovestone, S., Powell, J., Proitsi, P., Lupton, M.K., Brayne, C., Rubinsztein, D.C., Gill, M., Lawlor, B., Lynch, A., Brown, K.S., Passmore, P.A., Craig, D., McGuinness, B., Todd, S., Holmes, C., Mann, D., Smith, A.D., Beaumont, H., Warden, D., Wilcock, G., Love, S., Kehoe, P.G., Hooper, N.M., Vardy, E.R., Hardy, J., Mead, S., Fox, N.C., Rossor, M., Collinge, J., Maier, W., Jessen, F., Ruther, E., Schurmann, B., Heun, R., Kolsch, H., van den Bussche, H., Heuser, I., Kornhuber, J., Wiltfang, J., Dichgans, M., Frolich, L., Hampel, H., Gallacher, J., Hull, M., Rujescu, D., Giegling, I., Goate, A.M., Kauwe, J.S., Cruchaga, C., Nowotny, P., Morris, J.C., Mayo, K., Sleegers, K., Bettens, K., Engelborghs, S., De Deyn, P.P., Van Broeckhoven, C., Livingston, G., Bass, N.J., Gurling, H., McQuillin, A., Gwilliam, R., Deloukas, P., Al-Chalabi, A., Shaw, C.E., Tsolaki, M., Singleton, A.B., Guerreiro, R., Muhleisen, T.W., Nothen, M.M., Moebus, S., Jockel, K.H., Klopp, N., Wichmann, H.E.,

Pankratz, V.S., Sando, S.B., Aasly, J.O., Barcikowska, M., Wszolek, Z.K., Dickson, D.W., Graff-Radford, N.R., Petersen, R.C., van Duijn, C.M., Breteler, M.M., Ikram, M.A., Destefano, A.L., Fitzpatrick, A.L., Lopez, O., Launer, L.J., Seshadri, S., Berr, C., Campion, D., Epelbaum, J., Dartigues, J.F., Tzourio, C., Alperovitch, A., Lathrop, M., Feulner, T.M., Friedrich, P., Riehle, C., Krawczak, M., Schreiber, S., Mayhaus, M., Nicolhaus, S., Wagenpfeil, S., Steinberg, S., Stefansson, H., Stefansson, K., Snaedal, J., Bjornsson, S., Jonsson, P.V., Chouraki, V., Genier-Boley, B., Hiltunen, M., Soininen, H., Combarros, O., Zelenika, D., Delepine, M., Bullido, M.J., Pasquier, F., Mateo, I., Frank-Garcia, A., Porcellini, E., Hanon, O., Coto, E., Alvarez, V., Bosco, P., Siciliano, G., Mancuso, M., Panza, F., Solfrizzi, V., Nacmias, B., Sorbi, S., Bossu, P., Piccardi, P., Arosio, B., Annoni, G., Seripa, D., Pilotto, A., Scarpini, E., Galimberti, D., Brice, A., Hannequin, D., Licastro, F., Jones, L., Holmans, P.A., Jonsson, T., Riemenschneider, M., Morgan, K., Younkin, S.G., Owen, M.J., O'Donovan, M., Amouyel, P. & Williams, J. (2011) Common Variants at Abca7, Ms4a6a/Ms4a4e, Epha1, Cd33 and Cd2ap Are Associated with Alzheimer's Disease. *Nat Genet*.

Ittner, L.M., Ke, Y.D., Delerue, F., Bi, M., Gladbach, A., van Eersel, J., Wolfing, H., Chieng, B.C., Christie, M.J., Napier, I.A., Eckert, A., Staufenbiel, M., Hardeman, E., & Gotz, J. (2010) Dendritic Function of Tau Mediates Amyloid-Beta Toxicity in Alzheimer's Disease Mouse Models. *Cell*.

Jung, N. & Haucke, V. (2007) Clathrin-Mediated Endocytosis at Synapses. *Traffic* 8(9):1129-1136.

Kayed, R., Head, E., Thompson, J.L., McIntire, T.M., Milton, S.C., Cotman, C.W., & Glabe, C.G. (2003) Common Structure of Soluble Amyloid Oligomers Implies Common Mechanism of Pathogenesis. *Science* 300(5618):486-489.

Khurana, V. & Lindquist, S. (2010) Modelling Neurodegeneration in Saccharomyces Cerevisiae: Why Cook with Baker's Yeast? *Nat Rev Neurosci* 11(6):436-449.

Knobloch, M., Konietzko, U., Krebs, D.C., & Nitsch, R.M. (2007) Intracellular Abeta and Cognitive Deficits Precede Beta-Amyloid Deposition in Transgenic Arcabeta Mice. *Neurobiol Aging* 28(9):1297-1306.

Kowalski, J.M., Parekh, R.N., & Wittrup, K.D. (1998) Secretion Efficiency in Saccharomyces Cerevisiae of Bovine Pancreatic Trypsin Inhibitor Mutants Lacking Disulfide Bonds Is Correlated with Thermodynamic Stability. *Biochemistry* 37(5):1264-1273.

LaFerla, F.M. (2010) Pathways Linking Abeta and Tau Pathologies. *Biochem Soc Trans* 38(4):993-995.

Lambert, J.C., Heath, S., Even, G., Campion, D., Sleegers, K., Hiltunen, M., Combarros, O., Zelenika, D., Bullido, M.J., Tavernier, B., Letenneur, L., Bettens, K., Berr, C., Pasquier, F., Fievet, N., Barberger-Gateau, P., Engelborghs, S., De Deyn, P., Mateo, I., Franck, A., Helisalmi, S., Porcellini, E., Hanon, O., de Pancorbo, M.M., Lendon, C., Dufouil, C., Jaillard, C., Leveillard, T., Alvarez, V., Bosco, P., Mancuso, M., Panza, F., Nacmias, B., Bossu, P., Piccardi, P., Annoni, G., Seripa, D., Galimberti, D., Hannequin, D., Licastro, F., Soininen, H., Ritchie, K., Blanche, H., Dartigues, J.F., Tzourio, C., Gut, I., Van Broeckhoven, C., Alperovitch, A., Lathrop,

M., & Amouyel, P. (2009) Genome-Wide Association Study Identifies Variants at Clu and Cr1 Associated with Alzheimer's Disease. *Nat Genet* 41(10):1094-1099.

Lee, E.B., Leng, L.Z., Zhang, B., Kwong, L., Trojanowski, J.Q., Abel, T., & Lee, V.M. (2006) Targeting Amyloid-Beta Peptide (Abeta) Oligomers by Passive Immunization with a Conformation-Selective Monoclonal Antibody Improves Learning and Memory in Abeta Precursor Protein (App) Transgenic Mice. *J Biol Chem* 281(7):4292-4299.

Lewis, J., Dickson, D.W., Lin, W.L., Chisholm, L., Corral, A., Jones, G., Yen, S.H., Sahara, N., Skipper, L., Yager, D., Eckman, C., Hardy, J., Hutton, M., & McGowan, E. (2001) Enhanced Neurofibrillary Degeneration in Transgenic Mice Expressing Mutant Tau and App. *Science* 293(5534):1487-1491.

Li, S., Hong, S., Shepardson, N.E., Walsh, D.M., Shankar, G.M., & Selkoe, D. (2009) Soluble Oligomers of Amyloid Beta Protein Facilitate Hippocampal Long-Term Depression by Disrupting Neuronal Glutamate Uptake. *Neuron* 62(6):788-801.

Lindhagen-Persson, M., Brannstrom, K., Vestling, M., Steinitz, M., & Olofsson, A. (2010) Amyloid-Beta Oligomer Specificity Mediated by the Igm Isotype--Implications for a Specific Protective Mechanism Exerted by Endogenous Auto-Antibodies. *PLoS One* 5(11):e13928.

Link, C.D. (1995) Expression of Human Beta-Amyloid Peptide in Transgenic Caenorhabditis Elegans. *Proc Natl Acad Sci U S A* 92(20):9368-9372.

Luheshi, L.M., Tartaglia, G.G., Brorsson, A.C., Pawar, A.P., Watson, I.E., Chiti, F., Vendruscolo, M., Lomas, D.A., Dobson, C.M., & Crowther, D.C. (2007) Systematic in Vivo Analysis of the Intrinsic Determinants of Amyloid Beta Pathogenicity. *PLoS Biol* 5(11):e290.

Maldonado-Baez, L., Dores, M.R., Perkins, E.M., Drivas, T.G., Hicke, L., & Wendland, B. (2008) Interaction between Epsin/Yap180 Adaptors and the Scaffolds Ede1/Pan1 Is Required for Endocytosis. *Mol Biol Cell* 19(7):2936-2948.

Naj, A.C., Jun, G., Beecham, G.W., Wang, L.S., Vardarajan, B.N., Buros, J., Gallins, P.J., Buxbaum, J.D., Jarvik, G.P., Crane, P.K., Larson, E.B., Bird, T.D., Boeve, B.F., Graff-Radford, N.R., De Jager, P.L., Evans, D., Schneider, J.A., Carrasquillo, M.M., Ertekin-Taner, N., Younkin, S.G., Cruchaga, C., Kauwe, J.S., Nowotny, P., Kramer, P., Hardy, J., Huentelman, M.J., Myers, A.J., Barmada, M.M., Demirci, F.Y., Baldwin, C.T., Green, R.C., Rogaeva, E., George-Hyslop, P.S., Arnold, S.E., Barber, R., Beach, T., Bigio, E.H., Bowen, J.D., Boxer, A., Burke, J.R., Cairns, N.J., Carlson, C.S., Carney, R.M., Carroll, S.L., Chui, H.C., Clark, D.G., Corneveaux, J., Cotman, C.W., Cummings, J.L., Decarli, C., Dekosky, S.T., Diaz-Arrastia, R., Dick, M., Dickson, D.W., Ellis, W.G., Faber, K.M., Fallon, K.B., Farlow, M.R., Ferris, S., Frosch, M.P., Galasko, D.R., Ganguli, M., Gearing, M., Geschwind, D.H., Ghetti, B., Gilbert, J.R., Gilman, S., Giordani, B., Glass, J.D., Growdon, J.H., Hamilton, R.L., Harrell, L.E., Head, E., Honig, L.S., Hulette, C.M., Hyman, B.T., Jicha, G.A., Jin, L.W., Johnson, N., Karlawish, J., Karydas, A., Kaye, J.A., Kim, R., Koo, E.H., Kowall, N.W., Lah, J.J., Levey, A.I., Lieberman, A.P., Lopez, O.L., Mack, W.J., Marson, D.C., Martiniuk, F., Mash, D.C., Masliah, E., McCormick, W.C., McCurry, S.M., McDavid, A.N., McKee, A.C., Mesulam, M., Miller, B.L., Miller, C.A., Miller, J.W., Parisi, J.E., Perl, D.P., Peskind, E., Petersen, R.C., Poon, W.W., Quinn, J.F., Rajbhandary, R.A.,

Raskind, M., Reisberg, B., Ringman, J.M., Roberson, E.D., Rosenberg, R.N., Sano, M., Schneider, L.S., Seeley, W., Shelanski, M.L., Slifer, M.A., Smith, C.D., Sonnen, J.A., Spina, S., Stern, R.A., Tanzi, R.E., Trojanowski, J.Q., Troncoso, J.C., Van Deerlin, V.M., Vinters, H.V., Vonsattel, J.P., Weintraub, S., Welsh-Bohmer, K.A., Williamson, J., Woltjer, R.L., Cantwell, L.B., Dombroski, B.A., Beekly, D., Lunetta, K.L., Martin, E.R., Kamboh, M.I., Saykin, A.J., Reiman, E.M., Bennett, D.A., Morris, J.C., Montine, T.J., Goate, A.M., Blacker, D., Tsuang, D.W., Hakonarson, H., Kukull, W.A., Foroud, T.M., Haines, J.L., Mayeux, R., Pericak-Vance, M.A., Farrer, L.A. & Schellenberg, G.D. (2011) Common Variants at Ms4a4/Ms4a6e, Cd2ap, Cd33 and Epha1 Are Associated with Late-Onset Alzheimer's Disease. *Nat Genet*.

Outeiro, T.F. & Lindquist, S. (2003) Yeast Cells Provide Insight into Alpha-Synuclein Biology and Pathobiology. *Science* 302(5651):1772-1775.

Roberson, E.D., Scearce-Levie, K., Palop, J.J., Yan, F., Cheng, I.H., Wu, T., Gerstein, H., Yu, G.Q., & Mucke, L. (2007) Reducing Endogenous Tau Ameliorates Amyloid Beta-Induced Deficits in an Alzheimer's Disease Mouse Model. *Science* 316(5825):750-754.

Selkoe, D.J. & Wolfe, M.S. (2007) Presenilin: Running with Scissors in the Membrane. *Cell* 131(2):215-221.

Shorter, J. & Lindquist, S. (2004) Hsp104 Catalyzes Formation and Elimination of Self-Replicating Sup35 Prion Conformers. *Science* 304(5678):1793-1797.

Stamenova, S.D., Dunn, R., Adler, A.S., & Hicke, L. (2004) The Rsp5 Ubiquitin Ligase Binds to and Ubiquitinates Members of the Yeast Cin85-Endophilin Complex, Sla1-Rvs167. *J Biol Chem* 279(16):16017-16025.

Stefan, C.J., Padilla, S.M., Audhya, A., & Emr, S.D. (2005) The Phosphoinositide Phosphatase Sjl2 Is Recruited to Cortical Actin Patches in the Control of Vesicle Formation and Fission During Endocytosis. *Mol Cell Biol* 25(8):2910-2923.

Su, L.J., Auluck, P.K., Outeiro, T.F., Yeger-Lotem, E., Kritzer, J.A., Tardiff, D.F., Strathearn, K.E., Liu, F., Cao, S., Hamamichi, S., Hill, K.J., Caldwell, K.A., Bell, G.W., Fraenkel, E., Cooper, A.A., Caldwell, G.A., McCaffery, J.M., Rochet, J.C., & Lindquist, S. (2009) Compounds from an Unbiased Chemical Screen Reverse Both Er-to-Golgi Trafficking Defects and Mitochondrial Dysfunction in Parkinson's Disease Models. *Dis Model Mech* 3(3-4):194-208.

Sun, Y., Carroll, S., Kaksonen, M., Toshima, J.Y., & Drubin, D.G. (2007) Ptdins(4,5)P2 Turnover Is Required for Multiple Stages During Clathrin- and Actin-Dependent Endocytic Internalization. *J Cell Biol* 177(2):355-367.

Thayanidhi, N., Helm, J.R., Nycz, D.C., Bentley, M., Liang, Y., & Hay, J.C. (2010) Alpha-Synuclein Delays Endoplasmic Reticulum (Er)-to-Golgi Transport in Mammalian Cells by Antagonizing Er/Golgi Snares. *Mol Biol Cell* 21(11):1850-1863.

Thinakaran, G. & Koo, E.H. (2008) Amyloid Precursor Protein Trafficking, Processing, and Function. *J Biol Chem* 283(44):29615-29619.

Trommer, B.L., Shah, C., Yun, S.H., Gamkrelidze, G., Pasternak, E.S., Stine, W.B., Manelli, A., Sullivan, P., Pasternak, J.F., & LaDu, M.J. (2005) Apoe Isoform-Specific Effects on Ltp: Blockade by Oligomeric Amyloid-Beta1-42. *Neurobiol Dis* 18(1):75-82.

Vossel, K.A., Zhang, K., Brodbeck, J., Daub, A.C., Sharma, P., Finkbeiner, S., Cui, B., & Mucke, L. (2010) Tau Reduction Prevents Abeta-Induced Defects in Axonal Transport. *Science* 330(6001):198.

Walsh, D.M., Tseng, B.P., Rydel, R.E., Podlisny, M.B., & Selkoe, D.J. (2000) The Oligomerization of Amyloid Beta-Protein Begins Intracellularly in Cells Derived from Human Brain. *Biochemistry* 39(35):10831-10839.

Winslow, A.R., Chen, C.W., Corrochano, S., Acevedo-Arozena, A., Gordon, D.E., Peden, A.A., Lichtenberg, M., Menzies, F.M., Ravikumar, B., Imarisio, S., Brown, S., O'Kane, C.J., & Rubinsztein, D.C. (2010) Alpha-Synuclein Impairs Macroautophagy: Implications for Parkinson's Disease. *J Cell Biol* 190(6):1023-1037.

Materials and Methods

Constructs, strains and growth conditions

The ssAβ1-42 construct consists of attB sites for Gateway cloning the Kar2 signal sequence and the Aβ1-42 sequence. The Aβ sequence was codon optimized for expression in yeast. The entire construct was synthesized and cloned into the Gateway entry vector pDONR221.

Sequence of the ssAβ construct: ACAAGTTTGTACAAAAAAGCAGGCTTCACAAA (Gateway flanking region)

ATGTTTTTCAACAGACTAAGCGCTGGCAAGCTGCTGGTACCACTCTCCGTGGTCCTGTACGCCCT

TTTCGTGGTAATATTACCTTTACAGAATTCTTTCCACTCCTCCAATGTTTTAGTTAGAGGT (Kar2 signal sequence)

GATGCTGAATTTAGACATGATTCTGGTTATGAAGTTCATCATCAAAAATTGGTTTTTTTTGCTGA

AGATGTTGGTTCTAATAAAGGTGCTATTATTGGTTTGATGGTTGGTGGTGTTGTCATTGCTTAA

(Aβ1-42)

ACCCAGCTTTCTTGTACAAAGTGGT (Gateway flanking region)

The same approach was used to generate the ssAβ1-40 construct.

The BPTI WT and C51A constructs were the kind gift of Dane Wittrup (KOWALSKI, *et al.* 1998). The original BPTI construct do contain a signal sequence, but we replaced it with the Kar2 signal sequence in order to target them in the same manner as Aβ. The Kar2ss sequence and Gateway flanking regions were added to the BPTI ORFs using overlap extension PCR.

The Pdi1 gene is part of the overexpression library used in the screen. The Pdi1 gene was gateway cloned into the pDONR221 entry vector. The Aβ and BPTI constructs as well as Pdi1 were cloned into the pAG Gal p426 vector (ALBERTI, *et al.* 2007). Constructs were transformed into W303 Mat α, can1-100, his3-11,15, leu2-3,112, trp1-1, ura3-1, ade2-1 using a standard lithium acetate transformation protocol.

To generate ssAβ1-42 screening strains the ssAβ1-42 construct was moved to a pAG Gal p305 expression vector (ALBERTI, *et al.* 2007). The plasmid was digested using BstX1, gel purified and transformed into W303. The transformation was carried out in duplicate and the level of growth of 16 transformants each was tested on synthetic deficient media lacking leucine with galactose. Two strains from the independent transformations where chosen as screening strains based on their robust yet intermediate toxicity that would allow for the identification of both suppressors and enhancers. Several transformants that showed no toxicity were chosen as 1xssAβ controls. The control strain for wild type yeast growth is carrying a Gal inducible YFP integrated in the same fashion as the ssAβ1-42 constructs.

For spotting assays strains were grown over night at 30°C in 3ml SD media lacking the relevant amino acids and containing glucose. Cell concentrations (OD_{600})

were adjusted in a 96-well plate to that of the strain with the lowest concentration. Cells were then 5-fold serially diluted and spotted on SD media containing glucose (Uninduced) and galactose (Induced). Plates were incubated at 30°C for 2 (glucose) or 3 days (galactose).

Cell lysis

Strains were grown in synthetic deficient media lacking leucine and uracil (SD-Leu-Ura) with raffinose overnight at 30°C. Cultures were the diluted into inducing media containing galactose (OD600 0.2) and grown for 8h. Cells were spun down for 5min at 3,000rpm. For preparation of yeast lysates, yeast pellets were resupsended in 200 μL of yeast lysis buffer (50 mM HEPES pH 7.5, 150 mM NaCl, 2.5 mM EDTA, 1% v/v Triton-X 100 with protease inhibitors). To this solution, 200 μL of glass beads (Aldrich) were added, and the yeast were bead beated for 3 minutes on maximum speed at 4°C. Afterwards, the sample was retrieved by puncturing a hole in the bottom of the eppendorf tube and spinning the samples into a new tube at 6,000 rpm for 15 seconds. The supernatant was transferred to a new tube, and this solution was used as the lysate.

Western Blot Protocol

For the western blot, the protein concentrations in the yeast lysates were normalized using the results from a BCA assay (Pierce). After normalization, samples were loaded on a 4-12% Bis-Tris gel (Invitrogen) and run at 150 V for approximately 50 minutes. Subsequently, the samples were transferred to 0.2 micron PVDF membrane (Bio-Rad).

After the transfer was completed, the membrane was blocked with 5% milk in PBS overnight. The membrane was briefly washed with PBS before the primary antibody, 6E10 (Covance) was added at a 1:1,000 dilution in 5% milk in PBS. The primary antibody was allowed to incubate for 2.5 hours, after which the blot was washed 4 x 5 minutes with PBS. The anti-mouse secondary (DyLight, Rockland) was added at a 1:10,000 dilution in 5% milk in PBS for 1 hour. The blot was washed 4 x 5 minutes with PBS. The blot was scanned using the Licor Odyssey Scanner.

For detection of oligomers using the NAB61 antibody, the antibody was diluted 1:500 in 5% milk in PBS and incubated with the blot. Subsequently, the blot was washed 4 x 5 minutes with PBS. The anti-mouse secondary (DyLight, Rockland) was added at a 1:10,000 dilution in 5% milk in PBS for 1 hour. The blot was washed 4 x 5 minutes with PBS. The blot was scanned using the Licor Odyssey Scanner.

Indirect ELISA Protocol

The indirect ELISA using the OMAB oligomer specific antibody was performed as described in Lindhagen-Persson *et al*. (LINDHAGEN-PERSSON*, et al.* 2010). Briefly, the oligomer specific monoclonal OMAB antibody (Agrisera AB, Vännäs, Sweden) was diluted to a concentration corresponding to 5 ug/ml and was coated to a 96 well polystyrene microtiterplate (F96 Nunc immunosorp, Denmark) overnight. Unspecific sites were blocked using 5% dry milk dissolved in PBS. Frozen yeast lysates were thawed on ice and centrifuged at 20,000 g for 5 minutes followed 3 serial dilutions in PBS. The plate coated with OMAB antibody was washed with water and 100 μl of the samples

was applied in 5 replicates. The samples were incubated at room temp for 25 minutes, and the plate was subsequently washed 4 x with PBS containing 0.15% Tween 20. Bound Aβ was detected using a polyclonal rabbit anti-Aβ antibody (antibody AS08 357, Agrisera AB, Vännäs Umeå) that was dissolved in blocking buffer at a 1:2,000 dilution. The rabbit antibody was allowed to incubate for 30 minutes, after which the plate was washed with PBS containing 0.15% Tween 20. A secondary anti-rabbit IgG-HRP (GE-healthcare, Buckinghamshar, UK) dissolved in blocking buffer was used to detect bound rabbit IgG. Before addition of the detection reagent, excess secondary anti-rabbit IgG-HRP was removed by washing with PBS containing 0.15% Tween 20. The plate was developed using 100 μl EC-blue® (Medicago, Uppsala, Sweden). Measurements were made at 400 nm and 600 nm, and the absorption ratio between 600nm and 400 nm was used to calculate the level of binding. Statistical significance was determined using the paired t-test.

Immunostaining

Strains were pregrown in raffinose media over night and then induced in galactose media for 8 hours (5ml OD_{600} 0.2). Cells were spun down and resuspended in 1mL3.7% formaldehyde (37% formaldehyde in 0.1M KPi (potassium phosphate buffer) pH6.4) after removal of supernatant. Cells were fixed over night at 4°C. After the fixation cells were washed three time in 1mL 0.1M KPi pH 6.4 and then resuspended in 1mL 1.2M sorbitol-citrate buffer (1L: 218.6g sorbitol, 17.40g anyhydorus K_2HPO_4, 7g citric acid; filter sterilize). Cells were spun down again and resuspended in 200μl of digestion mix

(200μL 1.2M sorbitol-citrate, 20μL glusolase and 2μL 10mg/mL zymolase). Cells were incubated in the digestion mix for 45min at 30°C . During the incubation 5μL 0.1% polylysine was added to each well of a 30 well slide (Thermo ER-212W). After 5min of incubation the slides was washed with distilled water and allowed to air dry completely. Digested cells were spun down at 3,000 rpm for 3min and gently resuspended in 1mL sorbitol-citrate. Cells were spun down again and then resuspended in a volume of sorbitol citrate dependent on cell pellet size (15-50μL). Five μL of cells was added to each well and incubated for 10min. Cells were removed from the side of the well using a vacuum tip. If the cell density was low, as revealed by light microscopy, more cells were added. The slides were then incubated in ice-cold methanol for 3min, followed by 10sec in ice-cold acetone. Acetone was shook off and slides air-dried. As the primary antibody 4μL of 1:200 6E10 in PBS/BSA (1% BSA, 0.04M K_2HPO_4, 0.01M KH_2PO_4, 0.15M NaCl, 0.1% NaN3; for 100mL: 1g BSA, 4mL 1M K_2HPO_4, 1mL 1M KH2PO4, 15mL 1M NaCl, 1mL 10% NaN3, sterilized water to 100mL) were added to each well. Slide was incubated over night at room temperature in a wet chamber. After the incubation the antibody was removed using a vacuum tip and each well was washed 3 times with PBS/BSA. Then 4μL of the secondary antibody, 1:100 anti-mouse FITC, was added to each well and incubated for 2 hours. Subsequently, each well was washed 4 times with PBS/BSA. One μL of DAPI-MOUNT was added to each well prior to adding the coverslip and sealing the slide with nail polish.

For co-immunostaining cells were processed as described above but incubated with 1:200 6E10 and 1:100 rabbit anti-GFP in PBS/BSA and subsequently 1:100 anti-

mouse Alexa Fluor 594 and 1:100 anti-rabbit Alexa Fluor 488 in PBS/BSA simultaneously. The GFP-tagged strains are part of the yeast GFP library (HOWSON*, et al.* 2005).

Images were taken on a Zeiss Aviovert. Final images were assembled from the different channels (GFP, DAPI and dsRed) in Adobe Photoshop. Brightness and contrast were adjusted equally for all images.

Screen for modifiers of Aβ toxicity

The overexpression library screened contains ~5800 full-length sequence verified yeast ORFs in the galactose-inducible Gateway expression plasmid pBY011 (*CEN*, *URA3*, AmpR) (OUTEIRO*, et al.* 2003). The library is arrayed in 96-well format. Plasmid DNA was prepared by pin inoculation into deep well 96-well plates containing 1.8mL LB-AMP, growth over night at 37°C and 96-well mini preps using a Qiagen BioRobot 8000. The DNA was transformed into a ssAβ screening strain (ssAβ1-42 p305) carrying a Gal4-ER-VP16 plasmid (*CEN*, *HIS3*, AmpR), which allows for expression from GAL promoters on carbon sources other than galactose in the presence of estradiol in the yeast media (QUINTERO*, et al.* 2007). Neither estradiol nor the Gal4-ER-VP16 plasmid had an effect on Aβ toxicity on its own. Transformations were carried out using a standard lithium acetate transformation protocol adapted for a 96-well format and automation using a Tecan Evo 150 liquid handling robot. Transformants were grown in synthetic deficient media lacking histidine, leucine, and uracil (SD-His-Leu-Ura) with glusose overnight. The cells were then diluted in water and spotted on SD-His-Leu-Ura agar plates containing glucose alone (control), galactose alone, glucose plus 1μM estradiol (Sigma E1024) or

glycerol plus 1μM estradiol using a Singer RoToR pinning robot and long 96-well pins. Putative enhancers and suppressors were identified after 2-4 days of growth at 30°C. Putative screen hits were cherry picked from the plasmid library, retransformed into two independent derived ssAβ screening strains and retested on the three screening conditions in two independently derived strains. We eliminated hits that have known effects on GAL induction and genes whose overexpression has previously been shown to be toxic. To further exclude false-positive suppressors we used flow cytometry to measure the expression of YFP in their presence. To further exclude false-positive enhancers that cause a general inhibition when overexpressed we examined their effects in the YFP control strain, which has no growth impairment. The identity of confirmed modifiers was verified by sequencing.

Flow cytometry

A strain carrying an integrated YFP was transformed with the putative Aβ suppressors. The resulting strains were grown in glucose media in a 96-well format, diluted into the various inducing media (galactose, glucose +1μM estradiol, glycerol + 1μM estradiol) [5μL culture added to 120μL media], and incubated over night at 30°C with mild shaking. These overnight cultures were diluted 20fold into water and YFP levels were measured using a Guava flow cytometer. Each strain was measured 3 times and 5000 cells were counted for each well. The whole experiment was repeated 3 times. Values are averages of these 3 experiments and reported in percent of the vector control strain YFP levels.

Analysis of ROS and MAP data sets

We leveraged available genotyping, and extensive clinical and pathological data from two large epidemiological studies of aging, cognition, and AD: the Religious Orders Study (ROS) and the Rush Memory and Aging Project (MAP). These studies enlisted more than 2,300 older persons, without dementia at baseline, who were clinically evaluated annually and who agreed to brain donation upon death. Nearly 900 autopsies have been completed. Recent studies in these cohorts demonstrate how intermediate AD-related cognitive and pathological phenotypes can enhance power for genetic association analysis (*6-8*). For our study, we utilized a combined cohort of 1,593 ROS and MAP subjects with longitudinal neuropsychiatric assessments and genome-wide genotyping, and a nested pathological cohort including 651 brain autopsies (Table S3).

We initially determined whether the modifiers correspond to loci that impact susceptibility for episodic memory decline, a cardinal feature of AD. In ROS and MAP, rate-of-change in memory performance is characterized based on repeated assessment of 7 neuropsychiatric tests, and our analyses were additionally adjusted for age, gender and years of education. We implemented a locus-based association test for memory decline, considering all common single nucleotide polymorphisms (SNPs) at each candidate locus, including both directly genotyped and imputed variants, based on the HapMap reference (FRAZER*, et al.* 2007) (Table S4 & S5). We tested if the observed associations were significant, by performing a permutation procedure to compute an empirical *P*-value (P_{perm}), adjusting for the multiple tests performed at each locus. Aside from *PICALM* (*rs7128598*, *p-value*=1.6x10^{-4}, P_{perm}=0.012), several other loci harbored

SNPs suggesting association with memory decline, but these results did not remain significant following permutation (Table S5).

We investigated whether our modifiers are associated with the development of AD neuropathology. These analyses used a quantitative summary measure of global AD pathologic burden, based on counts of amyloid plaques and NFTs on brain tissue sections. The relation of SNPs with this continuous measure of pathology were tested using linear regression, adjusting for age at the time of death. Notably, these analyses indicate association of 2 additional loci identified by our yeast screen, *ADSSL1* (*rs1128880*, *P*=0.001, *Pperm*=0.031) and *RABGEF1* (*rs17566701*, *P*=0.002, *Pperm*=0.038) with AD neuropathology (Table S6). Both of these loci also harbored suggestive association signals with episodic memory decline in the larger clinical cohort, showing a statistical trend toward significance following the permutation procedure (Table S5).

Soluble Oligomer Preparation for Cortical Cell Culture

Soluble oligomers were prepared as in Kayed *et al.* *(KAYED, et al. 2003)*. In brief, lyophilized Ab 1-42 (American Peptide Company) was resuspended in 200μL of HFIP (1,1,1,3,3,3-Hexafluoro-2-propanol, Aldrich), and this solution was bath sonicated for 30 minutes. Subsequently, 100μL of the HFIP solution was added to 900μL of ddH2O in a siliconized eppendorf tube. This solution was incubated at room temperature for 10-20 minutes. After the room temperature incubation, the HFIP in the sample was evaporated using a gentle stream of N_2 for approximately 20 minutes. The samples were

allowed to incubate at room temperature for 48 hours, after which they were frozen and stored at -80°C.

Rat primary cortical cultures

Cultures were prepared based on Lesuisse and Martin (LESUISSE, *et al.* 2002). Embryos were harvested by cesarean section from anesthetized pregnant Sprague-Dawley rats at embryonic day 18. Cerebral cortices were isolated and dissociated with Accumax digestion for 20 min at 37°C and triutration with Pasteur pipette. Poly-ornithine and lamine-coated 96-well plates were seeded with $4x10^4$ cells in neurobasal medium (Life Technologies) supplemented with B27 (Life Technologies), 0.5mM glutamine, 25μM β–mercaptoethanol, penicillin (100 IU/mL) and streptomycin (100μg/mL). One third of the medium was changed every 3 to 4 days. Aβ oligomer (final concentration 750 nM) or vehicle was added to the lentivirus-transduced cultures in 96-well plates at DIV 18. As a surrogate marker of cell viability, cellular ATP content was measured after 20 hours of Aβ oligomer incubation using ViaLight Plus kit (Lonza).

Lentivirus production and transduction to rat primary cortical cultures

pLENTI6/V5 DEST (Invitrogen) lentivirus expression vector was used to generate lentivirus encoding *GFP*, *PICALM* and *RAB1*. Lentiviral constructs were packaged into virus via lipid-mediated transient transfection of the expression constructs and packaging plasmids (pMD2.G and psPAX2) to 293 cells. Lentivirus was purified and concentrated using Lenti-X Maxi Purification kit and LentiX Concentrator (Clontech)

according to the manufacturer's protocol. Lentivirus titer was determined using QuickTiter Lentivirus titer kit (Lentivirus- Associated HIV p24; Cell Biolabs) according to the manufacturer's protocol. Rat cortical cultures were transduced with various multiplicities of infection (MOI) of lentivirus at DIV 5.

Microscopy of Clc1-GFP and Ste3-YFP

We created our own version of the Ste3 localization assay (MALDONADO-BAEZ*, et al.* 2008) by generating a *GPD*-driven Ste3-YFP construct, using the Ste3 plasmid from our ORF library and a *GPD* p303 vector from the pAG collection (ALBERTI*, et al.* 2007), and integrating it into an ssAβ 1-42 screening strain as well as a control strain. For all microscopy experiments strain were pre-cultured in raffinose media and then induced in galactose media. We tested the effect of selected modifiers by transforming these strains with the modifiers and analyzing them in the same fashion.

To examine the effects of Aβ on endocytosis we used the clathrin light chain (Clc1)-GFP strain from the GFP library (HOWSON*, et al.* 2005). In experiments to examine the effects of Aβ alone we transformed the GFP-fusion strain with the ssAβ 1-42 construct on a multi copy vector and the corresponding vector control. We also used GFP-fusion strain of other endocytic proteins (Abp1, Sla1 and Sla2) and observed similar Aβ-induced changes in localization as with Clc1-GFP (data not shown); yet the fluorescence of these fusions was rather low.

To test the effects of screen hits on the Clc1-GFP Aβ phenotype, we mated the Clc1-GFP fusion strain to a set of Aβ screening strains carrying individual modifiers. We

used this approach as expression of two genes from plasmids, one with varying copy number, can lead to inconsistent results when examining individual cells; as it is the case for microscopy. Furthermore, the GFP-fusion strains on their own are incompatible with integration constructs due to their complete deletion of auxotrophic markers. While Aβ toxicity was reduced in the resulting diploid, ssAβ 1-42 expression resulted in the same Clc1-GFP phenotype.

For both assays, we found that modifiers alone had no effect on localization. Expression was induced for 16h and GFP or YFP fluorescence monitored using a Zeiss Axiovert microscope. Brightness and contrast were adjusted equally for all images.

***C. elegans* experiments:**

Plasmid & Constructs

The following cDNAs were cloned into pDONR221 using Gateway Technology (Invitrogen, San Diego, CA): *ssA*β *1-42* (Chris Link, University of Colorado); *gfp* and *lacZ* (Andy Fire, Stanford University); *mCherry*; *C13G3.3*, *C32E8.10*, and *C37H5.6* (Worm ORFeome collection from Marc Vidal) (LAMESCH*, et al.* 2004); XPO1 (human ORFeome collection from Marc Vidal) (LAMESCH*, et al.* 2007); and *JC8.10*, *Y44E3A.4*, and *F42G10.2*. *JC8.10*, *Y44E3A.4*, and *F42G10.2* were isolated from our *C. elegans* cDNA library. The cDNAs were verified by DNA sequencing, and subsequently cloned into pDEST-EAT-4. pDEST-EAT-4 was generated by PCR amplification of a *eat-4* promoter, double digestion of the promoter and pDEST-UNC-54 using *BplI* and *KpnI*, and replacement of a *unc-54* promoter in pDEST-UNC-54 with a *eat-4* promoter via ligation reaction.

Nematode Strains

Nematodes were maintained following standard procedures (BRENNER 1974). To make a worm ssAβ 1-42 model UA162 [*baEx*107; P*eat-4*::ssAβ 1-42, P*eat-4*::gfp, P*myo-2*::mCherry], 50 μg/mL of P*eat-4*::ssAβ 1-42 and P*eat-4*::gfp as well as 2.5 μg/mL of P*myo-2*::mCherry were injected into wildtype N2 (Bristol) worms. This strain was integrated by using Spectrolinker XL-1500 (Spectronics Corporation, Westbury, NY) and outcrossed three times to N2 worms to generate UA166 [*baIn*l32; P*eat-4*::ssAβ 1-42, P*eat-4*::gfp, P*myo-2*::mCherry]. For neuroprotection analysis, three stable lines of UA163 [*baEx*108; [P*eat-4*::C13G3.3, rol-6 (su1006)], UA164 [*baEx*109; [P*eat-4*::C32E8.10, rol-6 (su1006)], and UA165 [*baEx*110; [P*eat-4*::C37H5.6, rol-6 (su1006)] were made and crossed with UA166 [*baIn*l32; P*eat-4*::ssAβ 1-42, P*eat-4*::gfp, P*myo-2*::mCherry] to generate UA167 {[*baIn*l32; P*eat-4*::ssAβ 1-42, P*eat-4*::gfp, P*myo-2*::mCherry]; *baEx*108; [P*eat-4*::C13G3.3, rol-6 (su1006)]}, UA168 {[*baIn*l32; P*eat-4*::ssAβ 1-42, P*eat-4*::gfp, P*myo-2*::mCherry]; *baEx*109; [P*eat-4*::C32E8.10, rol-6 (su1006)]}, and UA169 {[*baIn*l32; P*eat-4*::ssAβ 1-42, P*eat-4*::gfp, P*myo-2*::mCherry]; *baEx*110; [P*eat-4*::C37H5.6, rol-6 (su1006)]}. Furthermore, three stable lines of UA170 {[*baIn*l32; P*eat-4*::ssAβ 1-42, P*eat-4*::gfp, P*myo-2*::mCherry]; *baEx*111; [P*eat-4*::JC8.10, rol-6 (su1006)]}, UA171 {[*baIn*l32; P*eat-4*::ssAβ 1-42, P*eat-4*::gfp, P*myo-2*::mCherry]; *baEx*112; [P*eat-4*::Y44E3A.4, rol-6 (su1006)]}, UA172 {[*baIn*l32; P*eat-4*::ssAβ 1-42, P*eat-4*::gfp, P*myo-2*::mCherry]; *baEx*113; [P*eat-4*::XPO1, rol-6 (su1006)]}, UA173 {[*baIn*l32; P*eat-4*::ssAβ 1-42, P*eat-4*::gfp, P*myo-2*::mCherry]; *baEx*114; [P*eat-4*::F42G10.2, rol-6 (su1006)]}, UA174

{[*baIn*l32; P*eat-4*::ssAβ 1-42, P*eat-4*::gfp, P*myo-2*::mCherry]; *baEx*115; [P*eat-4*::mCherry, rol-6 (su1006)]}, and UA175 {[*baIn*l32; P*eat-4*::ssAβ 1-42, P*eat-4*::gfp, P*myo-2*::mCherry]; *baEx*116; [P*eat-4*::lacZ, rol-6 (su1006)]} were generated by directly injecting 50 μg/mL of putative ssAβ 1-42 toxicity modifiers and *rol-6* into UA166 [*baIn*l32; P*eat-4*::ssAβ 1-42, P*eat-4*::gfp, P*myo-2*::mCherry].

Neuroprotection Analysis

For analysis of putative ssAβ 1-42 toxicity modifiers, the transgenic worms were age-synchronized (LEWIS*, et al.* 1995), transferred onto NGM plates, and grown at 20°C for 3 or 7 days. For each trial, 30 worms were transferred to a 2% agarose pad, immobilized with 2 mM levamisole, and scored. Worms were considered rescued when all five glutamatergic neurons were intact and had no visible signs of degeneration. Each stable line was analyzed three times (for a total of 90 worms/transgenic line). Three separate transgenic lines were analyzed per gene (for a total of 270 animals/gene). Imaging and statistics were performed as described previously (HAMAMICHI*, et al.* 2008).

Semi-quantitative RT-PCR

RNA isolation and semi-quantitative RT-PCR were performed as described previously (HAMAMICHI*, et al.* 2008). Briefly, total RNAs were isolated from 50 L3-staged worms, amplified using SuperScript III RT (Invitrogen) with oligo dT primers, and treated with amplification grade RNase-free DNase I (Invitrogen) as well as RNase H (Invitrogen) following the manufacture's protocol. The following primers were designed for the PCR:

cdk-5	Primer 1:	5’ ggg-gat-gat-gag-ggt-gtt-cca-agc 3’
	Primer 2:	5’ ggc-gac-cgg-cat-ttg-aga-tct-ctg-c 3’

The trangenes were PCR amplified by using primer sequences specific to *unc-54* 3’UTR and each respective open reading frame.

unc-54 3’UTR	Primer 1:	5’ gac-tta-gaa-gtc-aga-ggc-acg-ggc 3’
ssAb 1-42	Primer 2:	5’ atg-cat-aag-gtt-ttg-ctg-gca-ctg-ttc-ttt-atc 3’
C13G3.3	Primer 2:	5’ gag-aaa-cag-gca-atg-gga-aac-ccg-c 3’
C32E8.10	Primer 2:	5’ gct-gct-cca-ttc-gga-tat-cca-aat-gc 3’
C37H5.6	Primer 2:	5’ gga-gta-acg-act-gga-cgt-aaa-cgt-cg 3’
JC8.10	Primer 2:	5’ gat-cga-cct-cgt-cca-cca-tca-gc 3’
Y44E3A.4	Primer 2:	5’ cac-tga-tca-ggt-cgc-cga-act-gc 3’
F42G10.2	Primer 2:	5’ cat-gac-gcc-ggt-tgt-cag-ccg 3’
XPO1	Primer 2:	5’ gtg-aca-gac-act-tca-cat-act-gct-gg 3’
mCherry	Primer 2:	5’ gat-gaa-ctt-cga-gga-cgg-cgg-c 3’
lacZ	Primer 2:	5’ gcc-tta-ctg-ccg-cct-gtt-ttg-acc 3’

Alberti, S., Gitler, A.D., & Lindquist, S. (2007) A Suite of Gateway Cloning Vectors for High-Throughput Genetic Analysis in Saccharomyces Cerevisiae. *Yeast* 24(10):913-919.

Bertram, L., Lange, C., Mullin, K., Parkinson, M., Hsiao, M., Hogan, M.F., Schjeide, B.M., Hooli, B., Divito, J., Ionita, I., Jiang, H., Laird, N., Moscarillo, T., Ohlsen, K.L., Elliott, K., Wang, X., Hu-Lince, D., Ryder, M., Murphy, A., Wagner, S.L., Blacker, D., Becker, K.D., & Tanzi, R.E. (2008) Genome-Wide Association Analysis Reveals Putative Alzheimer's Disease Susceptibility Loci in Addition to Apoe. *Am J Hum Genet* 83(5):623-632.

Blacker, D., Haines, J.L., Rodes, L., Terwedow, H., Go, R.C., Harrell, L.E., Perry, R.T., Bassett, S.S., Chase, G., Meyers, D., Albert, M.S., & Tanzi, R. (1997) Apoe-4 and Age at Onset of Alzheimer's Disease: The Nimh Genetics Initiative. *Neurology* 48(1):139-147.

Brenner, S. (1974) The Genetics of Caenorhabditis Elegans. *Genetics* 77(1):71-94.

Chen, J.X. & Yan, S.S. (2010) Role of Mitochondrial Amyloid-Beta in Alzheimer's Disease. *J Alzheimers Dis* 20 Suppl 2:S569-578.

Frazer, K., Ballinger, D., Cox, D., Hinds, D., Stuve, L., Gibbs, R., Belmont, J., Boudreau, A., Hardenbol, P., Leal, S., Pasternak, S., Wheeler, D., Willis, T., Yu, F., Yang, H., Zeng, C., Gao, Y., Hu, H., Hu, W., Li, C., Lin, W., Liu, S., Pan, H., Tang, X., Wang, J., Wang, W., Yu, J., Zhang, B., Zhang, Q., Zhao, H., Zhou, J., Gabriel, S., Barry, R., Blumenstiel, B., Camargo, A., Defelice, M., Faggart, M., Goyette, M., Gupta, S.,

Moore, J., Nguyen, H., Onofrio, R., Parkin, M., Roy, J., Stahl, E., Winchester, E., Ziaugra, L., Altshuler, D., Shen, Y., Yao, Z., Huang, W., Chu, X., He, Y., Jin, L., Liu, Y., Sun, W., Wang, H., Wang, Y., Xiong, X., Xu, L., Waye, M., Tsui, S., Xue, H., Wong, J., Galver, L., Fan, J., Gunderson, K., Murray, S., Oliphant, A., Chee, M., Montpetit, A., Chagnon, F., Ferretti, V., Leboeuf, M., Olivier, J., Phillips, M., Roumy, S., Sallee, C., Verner, A., Hudson, T., Kwok, P., Cai, D., Koboldt, D., Miller, R., Pawlikowska, L., Taillon-Miller, P., Xiao, M., Tsui, L., Mak, W., Song, Y., Tam, P., Nakamura, Y., Kawaguchi, T., Kitamoto, T., Morizono, T., Nagashima, A., Ohnishi, Y., Sekine, A., Tanaka, T., Tsunoda, T., Deloukas, P., Bird, C., Delgado, M., Dermitzakis, E., Gwilliam, R., Hunt, S., Morrison, J., Powell, D., Stranger, B., Whittaker, P., Bentley, D., Daly, M., de Bakker, P., Barrett, J., Chretien, Y., Maller, J., McCarroll, S., Patterson, N., Pe'er, I., Price, A., Purcell, S., Richter, D., Sabeti, P., Saxena, R., Schaffner, S., Sham, P., Varilly, P., Stein, L., Krishnan, L., Smith, A., Tello-Ruiz, M., Thorisson, G., Chakravarti, A., Chen, P., Cutler, D., Kashuk, C., Lin, S., Abecasis, G., Guan, W., Li, Y., Munro, H., Qin, Z., Thomas, D., McVean, G., Auton, A., Bottolo, L., Cardin, N., Eyheramendy, S., Freeman, C., Marchini, J., Myers, S., Spencer, C., Stephens, M., Donnelly, P., Cardon, L., Clarke, G., Evans, D., Morris, A., Weir, B., Mullikin, J., Sherry, S., Feolo, M., Skol, A., Zhang, H., Matsuda, I., Fukushima, Y., Macer, D., Suda, E., Rotimi, C., Adebamowo, C., Ajayi, I., Aniagwu, T., Marshall, P., Nkwodimmah, C., Royal, C., Leppert, M., Dixon, M., Peiffer, A., Qiu, R., Kent, A., Kato, K., Niikawa, N., Adewole, I., Knoppers, B., Foster, M., Clayton, E., Watkin, J., Muzny, D., Nazareth, L., Sodergren, E., Weinstock, G., Yakub, I., Birren, B., Wilson, R., Fulton, L., Rogers, J., Burton, J., Carter, N., Clee, C., Griffiths, M., Jones, M., McLay, K., Plumb, R., Ross, M., Sims, S., Willey, D., Chen, Z., Han, H., Kang, L., Godbout, M., Wallenburg, J., L'Archeveque, P., Bellemare, G., Saeki, K., An, D., Fu, H., Li, Q., Wang, Z., Wang, R., Holden, A., Brooks, L., McEwen, J., Guyer, M., Wang, V., Peterson, J., Shi, M., Spiegel, J., Sung, L., Zacharia, L., Collins, F., Kennedy, K., Jamieson, R. & Stewart, J. (2007) A Second Generation Human Haplotype Map of over 3.1 Million Snps. *Nature* 449(7164):851-861.

Gibson, G.E. & Shi, Q. (2010) A Mitocentric View of Alzheimer's Disease Suggests Multi-Faceted Treatments. *J Alzheimers Dis* 20 Suppl 2:S591-607.

Hamamichi, S., Rivas, R.N., Knight, A.L., Cao, S., Caldwell, K.A., & Caldwell, G.A. (2008) Hypothesis-Based Rnai Screening Identifies Neuroprotective Genes in a Parkinson's Disease Model. *Proc Natl Acad Sci U S A* 105(2):728-733.

Howson, R., Huh, W.K., Ghaemmaghami, S., Falvo, J.V., Bower, K., Belle, A., Dephoure, N., Wykoff, D.D., Weissman, J.S., & O'Shea, E.K. (2005) Construction, Verification and Experimental Use of Two Epitope-Tagged Collections of Budding Yeast Strains. *Comp Funct Genomics* 6(1-2):2-16.

Kayed, R., Head, E., Thompson, J.L., McIntire, T.M., Milton, S.C., Cotman, C.W., & Glabe, C.G. (2003) Common Structure of Soluble Amyloid Oligomers Implies Common Mechanism of Pathogenesis. *Science* 300(5618):486-489.

Kowalski, J.M., Parekh, R.N., & Wittrup, K.D. (1998) Secretion Efficiency in Saccharomyces Cerevisiae of Bovine Pancreatic Trypsin Inhibitor Mutants Lacking

Disulfide Bonds Is Correlated with Thermodynamic Stability. *Biochemistry* 37(5):1264-1273.

Lamesch, P., Li, N., Milstein, S., Fan, C., Hao, T., Szabo, G., Hu, Z., Venkatesan, K., Bethel, G., Martin, P., Rogers, J., Lawlor, S., McLaren, S., Dricot, A., Borick, H., Cusick, M.E., Vandenhaute, J., Dunham, I., Hill, D.E., & Vidal, M. (2007) Horfeome V3.1: A Resource of Human Open Reading Frames Representing over 10,000 Human Genes. *Genomics* 89(3):307-315.

Lamesch, P., Milstein, S., Hao, T., Rosenberg, J., Li, N., Sequerra, R., Bosak, S., Doucette-Stamm, L., Vandenhaute, J., Hill, D.E., & Vidal, M. (2004) C. Elegans Orfeome Version 3.1: Increasing the Coverage of Orfeome Resources with Improved Gene Predictions. *Genome Res* 14(10B):2064-2069.

Lesuisse, C. & Martin, L.J. (2002) Long-Term Culture of Mouse Cortical Neurons as a Model for Neuronal Development, Aging, and Death. *J Neurobiol* 51(1):9-23.

Lewis, J.A. & Fleming, J.T. (1995) Basic Culture Methods. *Methods Cell Biol* 48:3-29.

Lindhagen-Persson, M., Brannstrom, K., Vestling, M., Steinitz, M., & Olofsson, A. (2010) Amyloid-Beta Oligomer Specificity Mediated by the Igm Isotype--Implications for a Specific Protective Mechanism Exerted by Endogenous Auto-Antibodies. *PLoS One* 5(11):e13928.

Maldonado-Baez, L., Dores, M.R., Perkins, E.M., Drivas, T.G., Hicke, L., & Wendland, B. (2008) Interaction between Epsin/Yap180 Adaptors and the Scaffolds Ede1/Pan1 Is Required for Endocytosis. *Mol Biol Cell* 19(7):2936-2948.

Outeiro, T.F. & Lindquist, S. (2003) Yeast Cells Provide Insight into Alpha-Synuclein Biology and Pathobiology. *Science* 302(5651):1772-1775.

Quintero, M.J., Maya, D., Arevalo-Rodriguez, M., Cebolla, A., & Chavez, S. (2007) An Improved System for Estradiol-Dependent Regulation of Gene Expression in Yeast. *Microb Cell Fact* 6:10.

Stefan, C.J., Padilla, S.M., Audhya, A., & Emr, S.D. (2005) The Phosphoinositide Phosphatase Sjl2 Is Recruited to Cortical Actin Patches in the Control of Vesicle Formation and Fission During Endocytosis. *Mol Cell Biol* 25(8):2910-2923.

Supplemental Information

(beginning on next page)

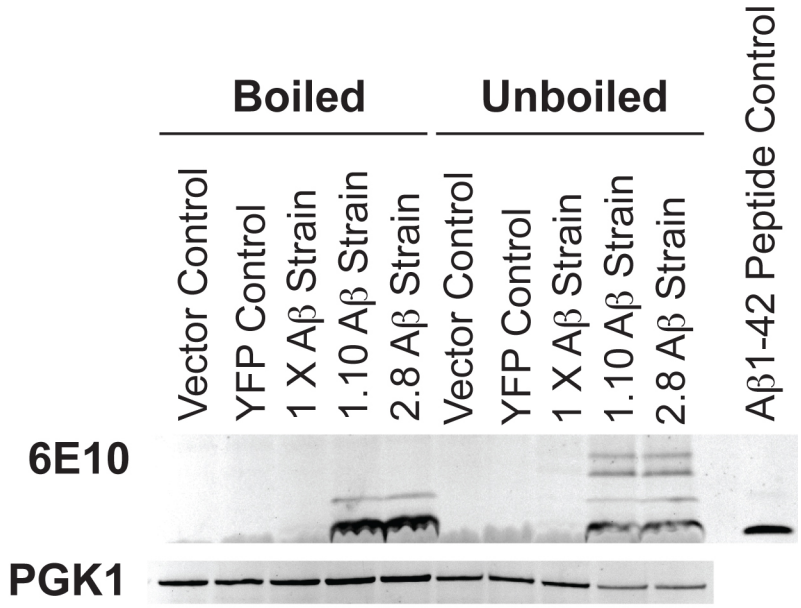

Supplemental Figure C4.1: Immunoblot analysis of strains expressing Aβ.

Aβ 1-42 expression was detected by immunoblot analysis using the 6E10 Aβ-specific antibody. Samples were loaded with and without prior boiling in LDS sample buffer. We detected higher molecular weight species of Aβ corresponding to trimers and tetramers only in the unboiled samples indicating that these species are non-covalent Aβ oligomers.

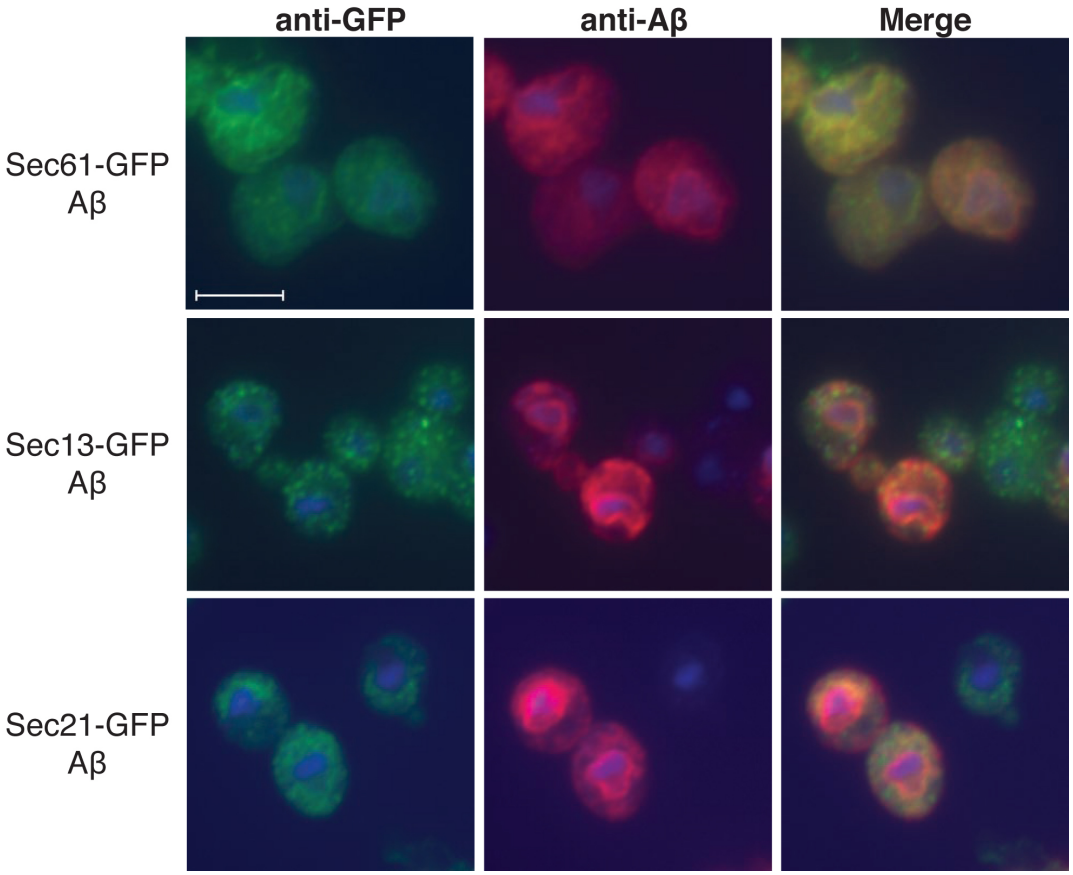

Supplemental Figure C4.2: Localization of Aβ to the endoplasmic reticulum and vesicular compartment.

To establish that our targeting scheme for Aβ was effective, we immunostained cells for Aβ and an ER marker, as well as two markers for ER-Golgi vesicles. ssAβ was expressed in the indicated GFP-tagged strains using a *GAL1*-driven high copy number plasmid. Sec61, an ER marker, is a component of the ER protein transport channel. Aβ co-localized with Sec61. Sec13, part of the COPII vesicle coat, and Sec21, part of the COPI vesicle coat, are markers for ER-Golgi vesicles. Aβ showed weak co-localization with Sec21, but no co-localization with Sec13. The scale bar is 5μM and all figures are on the same scale.

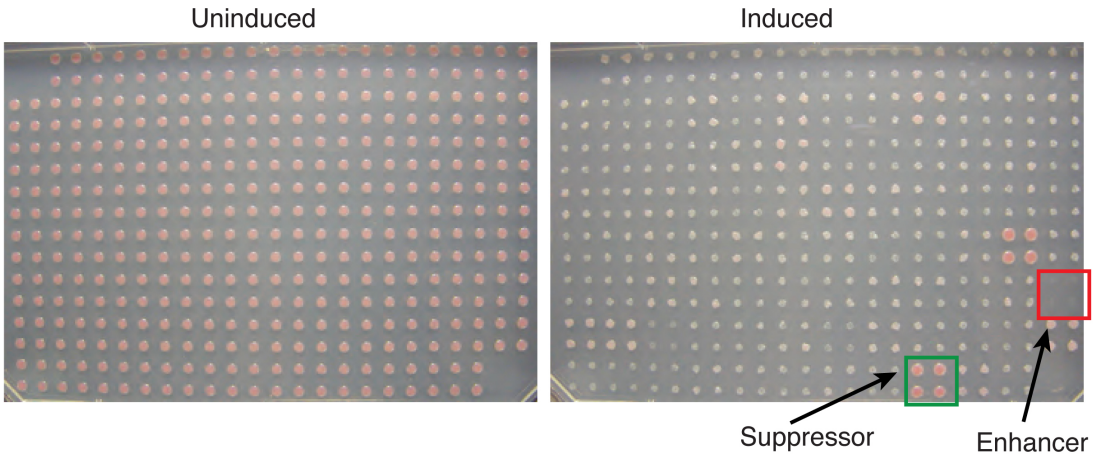

Supplemental Figure C4.3: Example of a screening plate.

Yeast strains carrying the ssAβ construct and the Gal4-ER-VP16 transcription factor were transformed with a plasmid library containing a genome-wide collection of ORFs. Each transformant was spotted 4 times in a square array using a Singer RoToR robot on media containing galactose, glucose and estradiol, glycerol and estradiol or glucose alone as a non-inducing growth control. Enhancers resulted in decreased growth and suppressors in increased growth, examples are boxed. Empty quadrants on the plate are the result of empty wells in the plasmid library.

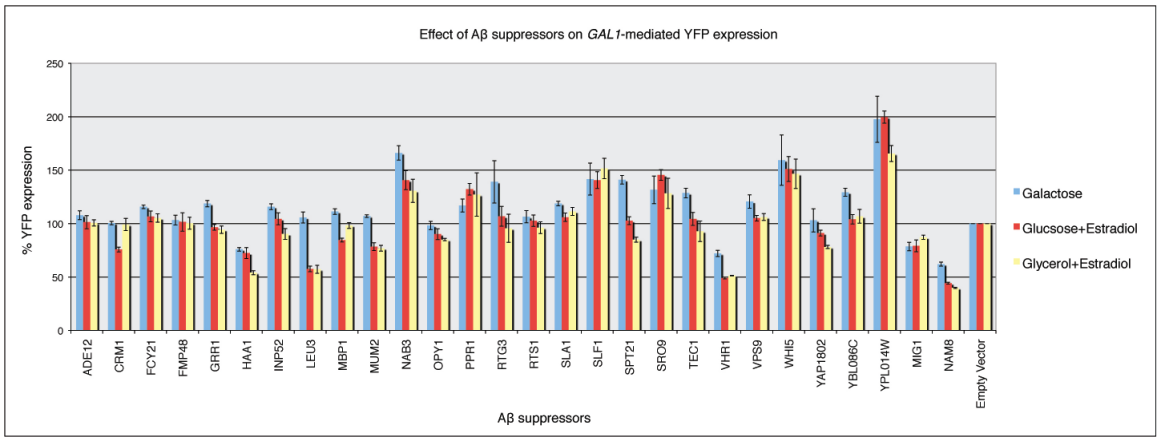

Supplemental Figure C4.4: Effect of suppressors on YFP expression levels.

Putative suppressors may decrease Aβ toxicity by decreasing *GAL1*-mediated expression. We assessed whether any of the identified suppressors affected *GAL1*-mediated expression by assaying the expression of Yellow Fluorescent Protein (YFP) under the control of a *GAL1* promoter. Putative suppressors were transformed into a strain carrying an integrated *GAL1*-controlled YFP construct and the Gal4-ER-VP16 transcription factor. The effect of putative hits on YFP expression levels was quantified using flow cytometry after overnight growth in one of three media conditions: galactose, glucose with estradiol or glycerol with estradiol. Hits that significantly decreased the levels of YFP in comparison to the vector control were eliminated as false positives (i.e. *HAA1, LEU3 and VHR1*). We did not eliminate suppressors that showed activity on all three media conditions, even if YFP expression levels were lower on one of the growth conditions.

Galactose	Glucose + Estradiol	Glycerol + Estradiol	Category	Systematic Name	Gene Name	Description	Human Homolog (HomoloGene prediction)	Human Homolog (pBlast)	Blast p-value
Suppressor	Suppressor	Suppressor	biosynthetic process	YNL220W	ADE12	Adenylosuccinate synthase, catalyzes the first step in synthesis of adenosine monophosphate from inosine 5'monophosphate during purine nucleotide biosynthesis.	ADSSL1	ADSSL1	3.00E-146
Suppressor	Suppressor	Suppressor	DNA replication	YBR057C	MUM2	Cytoplasmic protein essential for meiotic DNA replication and sporulation; interacts with Orc2p, which is a component of the origin recognition complex.			
Suppressor	Suppressor	Suppressor	endocytosis	YGR241C	YAP1802	Protein involved in clathrin cage assembly; binds Pan1p and clathrin; homologous to Yap1801p, member of the AP180 protein family.	PICALM	PiCALM	4.00E-26
-	Suppressor	Suppressor	endocytosis	YBL007C	SLA1	Cytoskeletal protein binding protein required for assembly of the cortical actin cytoskeleton; interacts with proteins regulating actin dynamics and proteins required for endocytosis; found in the nucleus and cell cortex; has 3 SH3 domains.	SH3KBP1 (functional homolog)	SH3RF3	6.00E-07
Suppressor	Suppressor	Suppressor	endocytosis	YNL106C	INP52	Polyphosphatidylinositol phosphatase, dephosphorylates a number of phosphatidylinositols (PIs) to PI; involved in endocytosis; hyperosmotic stress causes translocation to actin patches; synaptojanin-like protein with a Sac1 domain.	SYNJ1	SYNJ1	4.00E-125
Enhancer	Enhancer	Enhancer	endocytosis	YPL032C	SVL3	Protein of unknown function, mutant phenotype suggests a potential role in vacuolar function; green fluorescent protein (GFP)-fusion protein localizes to the cell periphery, cytoplasm, bud, and bud neck.			
Suppressor	Suppressor	Suppressor	kinase	YGR052W	FMP48	Putative protein of unknown function; the authentic, non-tagged protein is detected in highly purified mitochondria in high-throughput studies; induced by treatment with 8-methoxypsoralen and UVA irradiation.		MARK4	3.00E-21
Enhancer	Enhancer	Enhancer	kinase	YAL017W	PSK1	One of two PAS domain containing S/T protein kinases; coordinately regulates protein synthesis and carbohydrate metabolism and storage in response to a unknown metabolite that reflects nutritional status.		PASK	3.00E-50
Enhancer	-	Enhancer	kinase	YJL128C	PBS2	MAP kinase kinase that plays a pivotal role in the osmosensing signal-transduction pathway, activated under severe osmotic stress.	MAP2K4	MAP2K2	8.00E-69
Enhancer	Enhancer	-	kinase	YBL105C	PKC1	Protein serine/threonine kinase essential for cell wall remodeling during growth; localized to sites of polarized growth and the mother-daughter bud neck; homolog of the alpha, beta, and gamma isoforms of mammalian protein kinase C (PKC).		PKN2	5.00E-98
Enhancer	Enhancer	Enhancer	mannosyltransferase	YAL023C	PMT2	Protein O-mannosyltransferase, transfers mannose residues from dolichyl phosphate-D-mannose to protein serine/threonine residues; acts in a complex with Pmt1p, can instead interact with Pmt5p in some conditions; target for new antifungals.	POMT2	POMT2	6.00E-124
Enhancer	Enhancer	Enhancer	nuclear migration	YPL269W	KAR9	Karyogamy protein required for correct positioning of the mitotic spindle and for orienting cytoplasmic microtubules, localizes at the shmoo tip in mating cells and at the tip of the growing bud in small-budded cells through anaphase.			
Suppressor	Suppressor	Suppressor	protein transport	YGR218W	CRM1	Major karyopherin, involved in export of proteins, RNAs, and ribosomal subunits from the nucleus; exportin.	XPO1	XPO1	0.00E+00
Enhancer	Enhancer	Enhancer	response to mercury ion	YNL042W	BOP3	Protein of unknown function, potential Cdc28p substrate; overproduction confers resistance to methylmercury.			
Enhancer	Enhancer	Enhancer	RNA processing	YGL173C	KEM1	Evolutionarily-conserved 5'-3' exonuclease component of cytoplasmic processing (P) bodies involved in mRNA decay; plays a role in microtubule-mediated processes, filamentous growth, ribosomal RNA maturation, and telomere maintenance.	XRN1	XRN1	0.00E+00
Suppressor	Suppressor		signal transduction	YOR014W	RTS1	B-type regulatory subunit of protein phosphatase 2A (PP2A); homolog of the mammalian B' subunit of PP2A.	PPP2R5C	PPP2R5C	3.00E-153
Enhancer	Enhancer	Enhancer	signal transduction	YAL009W	SPO7	Putative regulatory subunit of Nem1p-Spo7p phosphatase holoenzyme, regulates nuclear growth by controlling phospholipid biosynthesis, required for normal nuclear envelope morphology, premeiotic replication, and sporulation.			
Enhancer	Enhancer	Enhancer	signal transduction	YGR070W	ROM1	GDP/GTP exchange protein (GEP) for Rho1p; mutations are synthetically lethal with mutations in Rom2, which also encodes a GEP.		NET1	5.00E-14
Enhancer	Enhancer	Enhancer	signal transduction	YLR332W	MID2	O-glycosylated plasma membrane protein that acts as a sensor for cell wall integrity signaling and activates the pathway; interacts with Rom2p, a guanine nucleotide exchange factor for Rho1p.			
Enhancer	Enhancer	Enhancer	signal transduction	YBL061C	SKT5	Activator of Chs3p (chitin synthase III), recruits Chs3p to the bud neck via interaction with Bni4p.		SEL1L2	9.00E-10
Suppressor	Suppressor	Suppressor	transcription factor	YOR083W	WHI5	Repressor of G1 transcription that binds to SCB binding factor (SBF) at SCB target promoters in early G1; phosphorylation of Whi5p by the CDK, Cln3p/Cdc28p relieves repression and promoter binding by Whi5.			
Suppressor	Suppressor	Suppressor	transcription factor	YLR014C	PPR1	Zinc finger transcription factor containing a Zn(2)-Cys(6) binuclear cluster domain, positively regulates transcription of genes involved in uracil biosynthesis.			
Suppressor	Suppressor	Suppressor	transcription factor	YBR083W	TEC1	Transcription factor required for full Ty1 expression, Ty1-mediated gene activation, and haploid invasive and diploid pseudohyphal growth; TEA/ATTS DNA-binding domain family member.		TEAD2	1.00E-10
-	Suppressor	Suppressor	transcription factor	YBL103C	RTG3	Basic helix-loop-helix-leucine zipper (bHLH/Zip) transcription factor that forms a complex with another bHLH/Zip protein, Rtg1p, to activate the retrograde (RTG) and TOR pathways.		MITF	6.00E-09
Suppressor	Suppressor	Suppressor	transcription factor	YDL056W	MBP1	Transcription factor involved in regulation of cell cycle progression from G1 to S phase, forms a complex with Swi6p that binds to MluI cell cycle box regulatory element in promoters of DNA synthesis genes.		DAPK1	1.00E-08
Enhancer	Enhancer	Enhancer	transcription factor	YIL122W	POG1	Putative transcriptional activator that promotes recovery from pheromone induced arrest; inhibits both alpha-factor induced G1 arrest and repression of CLN1 and CLN2 via SCB/MCB promoter elements; potential Cdc28p substrate; SBF regulated.			
Suppressor	Suppressor	Suppressor	transcription regulation	YMR179W	SPT21	Protein with a role in transcriptional silencing; required for normal transcription at several loci including HTA2-HTB2 and HHF2-HHT2, but not required at the other histone loci.			
-	Suppressor	Suppressor	transcription regulation	YPL190C	NAB3	Single stranded RNA binding protein; acidic ribonucleoprotein; required for termination of non-poly(A) transcripts and efficient splicing.			
-	Suppressor	Suppressor	translation regulation	YDR515W	SLF1	involved in the copper-dependent mineralization of copper sulfide complexes on cell surface in cells cultured in copper salts.		LARP1	4.00E-08
Suppressor	Suppressor	Suppressor	translation regulation	YCL037C	SRO9	Cytoplasmic RNA-binding protein that associates with translating ribosomes; involved in heme regulation of Hap1p as a component of the HMC complex, also involved in the organization of actin filaments; contains a La motif.		LARP1B	3.00E-12
Enhancer		Enhancer	translation regulation	YMR257C	PET111	Mitochondrial translational activator specific for the COX2 mRNA; located in the mitochondrial inner membrane.			

Enhancer	Enhancer	Enhancer	translation regulation	YLR139C	SLS1	Mitochondrial membrane protein that coordinates expression of mitochondrially-encoded genes; may facilitate delivery of mRNA to membrane-bound translation machinery.			
-	-	Suppressor	transport	YER060W	FCY21	Putative purine-cytosine permease.			
Enhancer	Suppressor	Suppressor	transport	YJR090C	GRR1	F-box protein component of the SCF ubiquitin-ligase complex; involved in carbon catabolite repression, glucose-dependent divalent cation transport, high-affinity glucose transport, morphogenesis, and sulfite detoxification.	FBXL2	FBXL20	4.00E-24
-	Suppressor	Suppressor	transport	YML097C	VPS9	A guanine nucleotide exchange factor involved in vesicle-mediated vacuolar protein transport; specifically stimulates the intrinsic guanine nucleotide exchange activity of Vps21p/Rab5: similar to mammalian ras inhibitors; binds ubiquitin.	RABGEF1	RABGEF1	4.00E-24
-	Suppressor	Suppressor	unknown	YBL086C	YBL086C	Protein of unknown function; green fluorescent protein (GFP)-fusion protein localizes to the cell periphery.			
Suppressor	Suppressor	Suppressor	unknown	YPL014W	YPL014W	Putative protein of unknown function; green fluorescent protein (GFP)-fusion protein localizes to the cytoplasm and to the nucleus.			
Suppressor	Suppressor	Suppressor	unknown	YBR129C	OPY1	Protein of unknown function, overproduction blocks cell cycle arrest in the presence of mating pheromone; the authentic, non-tagged protein is detected in highly purified mitochondria in high-throughput studies.			
-	Enhancer	Enhancer	vacuole	YDR229W	IVY1	Phospholipid-binding protein that interacts with both Ypt7p and Vps33p, may partially counteract the action of Vps33p and vice versa, localizes to the rim of the vacuole as cells approach stationary phase.			
Enhancer	Enhancer	-	vacuole	YMR004W	MVP1	Protein required for sorting proteins to the vacuole; overproduction of Mvp1p suppresses several dominant VPS1 mutations; Mvp1p and Vps1p act in concert to promote membrane traffic to the vacuole.	SNX8	SNX8	6.00E-21

Supplemental Table C4.1: Suppressors and enhancers of Aβ toxicity identified in the yeast screen.

We constructed yeast strains with an intermediate level of Aβ expression and corresponding toxicity that allowed us to identify in the same screen genes that alleviated or enhanced toxicity when overexpressed (see Materials and Methods). Aβ toxicity is likely to be influenced by mitochondrial function in neurons (CHEN, *et al.* 2010; GIBSON, *et al.* 2010). We took advantage of the fact that the extent to which yeast rely on mitochondrial respiration is carbon source dependent, thereby allowing us to test the full library of ORFs at different levels of respiration. In glucose, cells ferment and respiration remains low until all glucose is converted to ethanol. In galactose respiration is moderately active. In glycerol, cells are completely dependent on respiration for growth. To determine if the effect of putative modifiers on Aβ toxicity depended on the level of mitochondrial respiration, we conducted our screen on the three different carbon sources mentioned: glucose, galactose and glycerol. The expression of both ssAβ and the library of yeast ORFs were under control of the *GAL1* promoter. To induce expression in glucose and glycerol, we employed a chimeric Gal4-Estrogen Receptor-VP16 transcription factor that enables induction of the *GAL1* promoter through the addition of the estrogen estradiol (QUINTERO, *et al.* 2007). We plated the ssAβ strains carrying two plasmids, the Gal4-ER-VP16 transcription factor on one and individual yeast ORFs on the other, on media containing galactose, glucose + estradiol, or glycerol + estradiol. We also plated cells on glucose alone as a non-inducing growth control.

Suppressors increased growth relative to a vector control on the indicated conditions; enhancers decreased it (see Fig. S3 for an example of a screening plate). The function and localization of the gene products identified as modifiers are based on Saccharomyces Genome Database (SGD) gene summaries.

Only a few of the modifiers, specifically *SLA1, RTG3, NAB3, SLF1, FCY21, VPS9, GRR1, YBL086c, IVY1, PBS2, PKC1* and *MVP1,* were strongly affected by the state of mitochondrial respiration. However, the fact that most of the suppressors and enhancers were reproduced on all three media indicates the robustness of their affects on Aβ toxicity.

Gene	SNP	Chr.	Position[1]	MAF[2]	Fams[3]	FBAT-GEE[4]
PICALM	rs10501603	11	85,359,564	0.23	172	0.03
PICALM	rs615887	11	85,367,689	0.24	159	0.01
PICALM	rs597446	11	85,452,707	0.39	215	0.03
PICALM	rs568755	11	85,483,910	0.32	193	0.04
PICALM	rs659023	11	85,502,507	0.35	206	0.29
PPP2R5	rs11625483	14	101,321,490	0.38	206	0.86
PPP2R5	rs1746598	14	101,333,217	0.08	77	0.72
PPP2R5	rs8016207	14	101,366,968	0.18	149	0.98
PPP2R5	rs8015021	14	101,379,446	0.08	63	0.21
PPP2R5	rs10873529	14	101,481,601	0.28	179	0.14
ADSSL1	rs4983386	14	104,281,252	0.46	239	0.29
XPO1	rs7563678	2	61,653,462	0.4	216	0.17
XPO1	rs778755	2	61,692,688	0.45	216	0.07
XPO1	rs17010833	2	61,714,960	0.05	48	0.42
XPO1	rs6545886	2	61,733,522	0.11	109	0.003
SYNJ1	rs845022	21	32,920,977	0.42	187	0.61
SYNJ1	rs845006	21	32,953,727	0.06	60	0.68
SYNJ1	rs928754	21	33,006,701	0.48	195	0.6
FBXL20	rs755500	17	34,663,391	0.26	175	0.09
RABGEF1	rs12537474	7	65,749,172	0.08	136	0.64
XRN1	rs1552340	3	143,498,288	0.42	225	0.33

POMT2	rs8009261	14	76,810,128	0.44	210	0.56
POMT2	rs3783986	14	76,832,625	0.4	203	0.59
POMT2	rs1861889	14	76,833,554	0.08	72	0.66
POMT2	rs4899651	14	76,854,215	0.25	178	0.29
SNX8	rs7805462	7	2,122,849	0.32	192	0.62
MAP2K4	rs1468501	17	11,862,669	0.26	184	0.75
MAP2K4	rs976244	17	11,897,717	0.21	171	0.93
MAP2K4	rs9907196	17	11,925,064	0.2	167	0.98
MAP2K4	rs4791490	17	11,989,069	0.19	145	0.16
MAP2K4	rs7208899	17	12,075,716	0.06	54	0.94

[1]Physical position from Build 27 NCBI36/Hg18
[2]Minor allele frequency (MAF)
[3]Number of informative families from FBAT-GEE analysis
[4]P-value from family-based association test (FBAT)

Supplemental Table C4.2: Genome-wide FBAT-GEE association results from NIMH cohort.

To test for support for a genetic association between AD and our eleven candidate genes we revisited the family-based genome-wide association screen (GWAS) analysis (BERTRAM*, et al.* 2008) performed on the National Institute of Mental Health (NIMH) Genetics Alzheimer's Disease Initiative Study (BLACKER*, et al.* 1997). The sample consisted of 1,217 participants from 439 families of self-reported European ancestry. Genotyping was prepared with the GeneChip Human Mapping 500K Array Set from Affymetrix. Within the eleven gene regions, plus a 50kb window proximally and distally, 133 SNPs passed quality control assessment (using PLINK v1.07) and were tested for association using a family-based association test (FBAT v3.6) approach.

The FBAT method is similar in design to a classic transmission disequilibrium test method in which the genotype distribution in the affected is compared to its expected distribution under the null hypothesis. To optimize statistical power, age of onset and

AD affection status were tested together as a combined outcome variable, by use of the multivariate extension of the FBAT-approach, FBAT-GEE (Generalized Estimating Equation). We assumed an additive genetic model to test for association between our outcome variable and genotype.

Table S2 contains a subset of tested SNPs from the genome-wide FBAT-GEE association analysis that was pruned based on linkage disequilibrium. Pruning was performed with the "indep" command in PLINK which reduces a set of SNPs into a subset that are in approximate linkage equilibrium with each other. Selection of the subset is based on the variance inflation factor $1/(1-R^2)$, R^2 is the multiple correlation coefficient for a SNP being regressed on all other SNPs concurrently. Additional features of the pruning are described on the PLINK website under the LD-base SNP pruning sections.

The association for the *XPO1* SNP rs6545886 is robust to a Bonferroni adjustment for the 4 independent SNPs tested at each locus (Padj=0.003 * 4 = 0.012).

	Clinical	**Pathological**
n	1593	651
age[1]	85	87.9
female (%)	69.4	62.4
AD[2] **(%)**	22.1	40.9

[1]Age at last evaluation (clinical) or death (pathological)
[2]Clinical diagnosis of Alzheimer's disease based on NINCDS criteria (probable or possible)

Supplemental Table C4.3: Cohort demographics and characteristics.

Clinical, pathological and genotype data from the Religious Orders Study and Rush Memory and Aging Project were used to clinically validate significance of our screen results. Age indicates the time of last evaluation for the clinical cohort, and time of death for the pathology cohort. AD clinical diagnosis was based on NINCDS criteria, inclusive of probable and possible AD.

YEAST GENE	HUMAN HOMOLOG	Chr	Hg18 Coordinates[1]	Size (kb)	SNPs tested (n)
YAP1802	*PICALM*	11	85296132 - 85507756	211	187
RTS1	*PPP2R5C*	14	101295924 - 101513830	218	144
ADE12	*ADSSL1*	14	104211578 - 104334692	123	42
CRM1	*XPO1*	2	61508572 - 61668922	160	45
INP52	*SYNJ1*	21	32872943 - 33072148	199	109
GRR1	*FBXL20*	17	34620365 - 34861402	241	80
VPS9	*RABGEF1*	7	65793077 - 65963883	171	78
KEM1	*XRN1*	3	143458138 - 143699543	241	66
PMT2	*POMT2*	14	76761051 - 76906970	146	148
MVP1	*SNX8*	7	2211164 - 2370625	160	67
PBS2	*MAP2K4*	17	11814859 - 12037776	223	114

[1]Based on RefSeq gene consensus, plus a 50kb window both proximally and distally.

Supplemental Table C4.4: Human loci tested for associations with intermediate AD cognitive and neuropathologic phenotypes.

We comprehensively evaluated both genotyped and imputed common variation at human homologs for 11 out of 12 of the top results of our yeast screen. We were unable to evaluate the human functional homolog of Sla1, SH3KBP1, due to imprecise imputation on the X chromosome. At each locus, all SNPs from the quality-controlled, genome-wide genotyping dataset were extracted from RefSeq-based genomic

coordinates, inclusive of a 50kb genomic window, both proximal and distal. The size of each locus analyzed and the resultant number of SNPs tested is shown.

YEAST GENE	HUMAN HOMOLOG	best SNP[1]	A1[2]	Frq	Beta (95% CI)	P	P_{perm}[3]
YAP1802	*PICALM*	rs7128598	G	0.25	-0.016 (-0.025 to -0.008)	1.59E-04	**0.012**
RTS1	*PPP2R5C*	rs10873529	G	0.27	0.009 (0.001 to 0.017)	0.029	0.614
ADE12	*ADSSL1*	rs11851852	T	0.03	-0.033 (-0.055 to -0.011)	0.003	0.072*
CRM1	*XPO1*	rs967968	C	0.47	0.010 (0.003 to 0.017)	0.007	0.079*
INP52	*SYNJ1*	rs13339977	T	0.02	0.026 (0.001 to 0.052)	0.045	0.559
GRR1	*FBXL20*	rs11657409	T	0.27	-0.009 (-0.018 to 0.0004)	0.062	0.476
VPS9	*RABGEF1*	rs13224487	G	0.01	0.045 (0.012 to 0.077)	0.007	0.076*
KEM1	*XRN1*	rs6440083	G	0.29	0.011 (0.003 to 0.019)	0.005	0.062*
PMT2	*POMT2*	rs2042045	A	0.34	-0.010 (-0.018 to -0.003)	0.009	0.299
MVP1	*SNX8*	rs4721548	G	0.44	-0.006 (-0.014 to 0.001)	0.086	0.816
PBS2	*MAP2K4*	rs7221795	A	0.08	-0.017 (-0.030 to -0.004)	0.012	0.230

[1]Strongest SNP association observed at each locus.
[2]minor/reference allele
[3]Empirically-determined P-value from permutation test. Significant results (P<0.05) boldfaced; Suggestive results (P<0.1) asterisked.

Supplemental Table C4.5: Locus associations with episodic memory decline.

Using PLINK software, each locus-based SNP set was evaluated for associations with rate-of-change in episodic memory performance within the combined ROS and MAP clinical cohort, based on repeated assessments of 7 neuropsychiatric tests. Linear regression analyses were adjusted for baseline age, gender, and years of education. For each locus, this analysis defines the strongest, independent marker SNP. For each such SNP, the minor/reference allele (A1), allele frequency (Frq), effect size (Beta & 95% CI), as well as P-value (P) are shown. In order to determine if the observed locus association is significance, a permutation test was performed, in which phenotype labels were

permuted 1000 times, in order to determine an empirical P-value (P_{perm}), adjusting for the number of SNPs tested at each locus. The results was considered significant for $P_{perm}<0.05$ (bold); whereas $P_{perm}<0.1$ was interpreted as suggestive (asterisk). Of the 11 loci evaluated, PICALM was found to be associated with decline in episodic memory performance, and several additional loci showed suggestive association signals.

YEAST GENE	HUMAN HOMOLOG	best SNP[1]	A1[2]	Frq	Beta (95% CI)	P	P_{perm}[3]
YAP1802	*PICALM*	rs7950477	T	0.02	0.219 (0.068 to 0.371)	0.005	0.157
RTS1	*PPP2R5C*	rs6575881	T	0.005	-0.364 (-0.680 to -0.048)	0.024	0.548
ADE12	*ADSSL1*	rs1128880	G	0.48	0.098 (0.039 to 0.156)	0.001	**0.031**
CRM1	*XPO1*	rs2518934	C	0.44	-0.042 (-0.085 to 0.0002)	0.052	0.357
INP52	*SYNJ1*	rs7284048	A	0.08	0.056 (-0.024 to 0.137)	0.172	0.951
GRR1	*FBXL20*	rs16968748	G	0.02	-0.165 (-0.335 to 0.006)	0.059	0.513
VPS9	*RABGEF1*	rs17566701	T	0.48	-0.067 (-0.111 to -0.024)	0.002	**0.038**
KEM1	*XRN1*	rs13101141	A	0.06	-0.045 (-0.137 to 0.046)	0.331	0.970
PMT2	*POMT2*	rs2287385	A	0.16	0.077 (0.021 to 0.133)	0.007	0.244
MVP1	*SNX8*	rs3807428	A	0.05	-0.095 (-0.190 to -0.001)	0.048	0.630
PBS2	*MAP2K4*	rs12603093	C	0.25	0.040 (-0.009 to 0.089)	0.107	0.916

[1]Strongest SNP association observed at each locus.
[2]minor/reference allele
[3]Empirically-determined P-value from permutation test. Significant results (P<0.05) boldfaced; Suggestive results (P<0.1) asterisked.

Supplemental Table C4.6: Locus associations with global AD pathology.

Using PLINK software, each locus-based SNP set was evaluated for associations with a quantitative measure of global AD pathology within the combined ROS and MAP autopsy cohort, based on averaged counts of neuritic plaques, diffuse plaques, and neurofibrillary tangles from 5 brain regions. Linear regression analyses were adjusted for age at the time of death. For each locus, this analysis defines the strongest, independent

marker SNP. For each such SNP, the minor/reference allele (A1), allele frequency (Frq), effect size (Beta & 95% CI), as well as P-value (P) are shown. In order to determine if the observed locus association is significance, a permutation test was performed, in which phenotype labels were permuted 1000 times, in order to determine an empirical P-value (P_{perm}), adjusting for the number of SNPs tested at each locus. The results was considered significant for $P_{perm}<0.05$ (bold). ADSSL1 and RABGEF1 were each found to harbor significant signals of association with the global AD pathology measure.

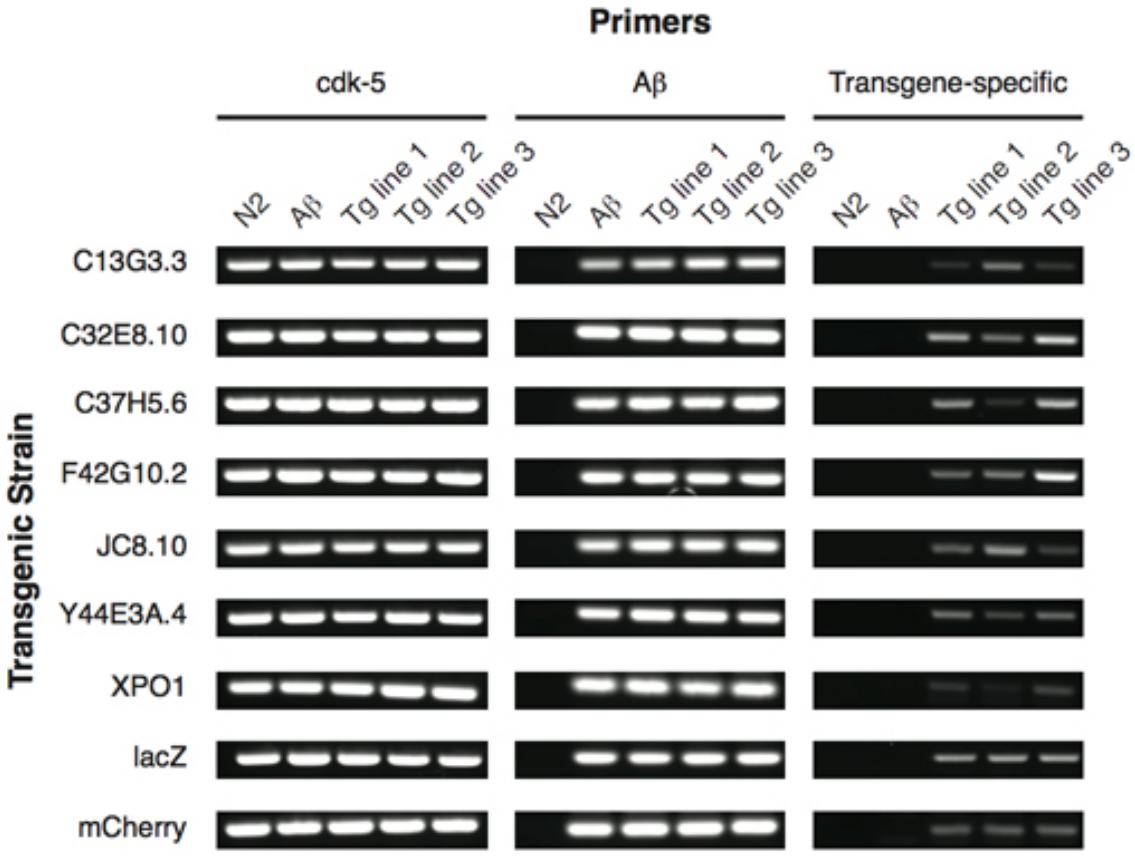

Supplemental Figure C4.5: Analysis of transgene expression in worm strains.

We conducted semi-quantitative RT-PCR to ensure that transgenes did not influence ssAβ 1-42 expression in *C. elegans*. We could not measure Aβ levels by western blot analysis as we expressed Aβ in only specific cells per animal. The PCR was conducted by using primers designed to amplify *cdk-5* (control), Aβ, and indicated transgenic modifiers of Aβ induced neurodegeneration. For all primers, a N2 wildtype strain served as both a positive (*cdk-5*) and negative (Aβ and transgenes) control. The ssAβ transgene of the Aβ strain (UA166) was integrated into worm chromosomal DNA to maintain steady Aβ expression level in the entire organism (see Materials and Methods). Using UA166 strain, 9 additional transgenic strains expressing homologs of Aβ toxicity modifiers identified in yeast were generated. Expression levels of the corresponding modifiers varied since the transgenes remained as extrachromosomal arrays. To address the discrepancies, we generated 3 independent lines for each of the 9 transgenic strains. Importantly, co-expression of the modifiers did not change the ssAβ expression level.

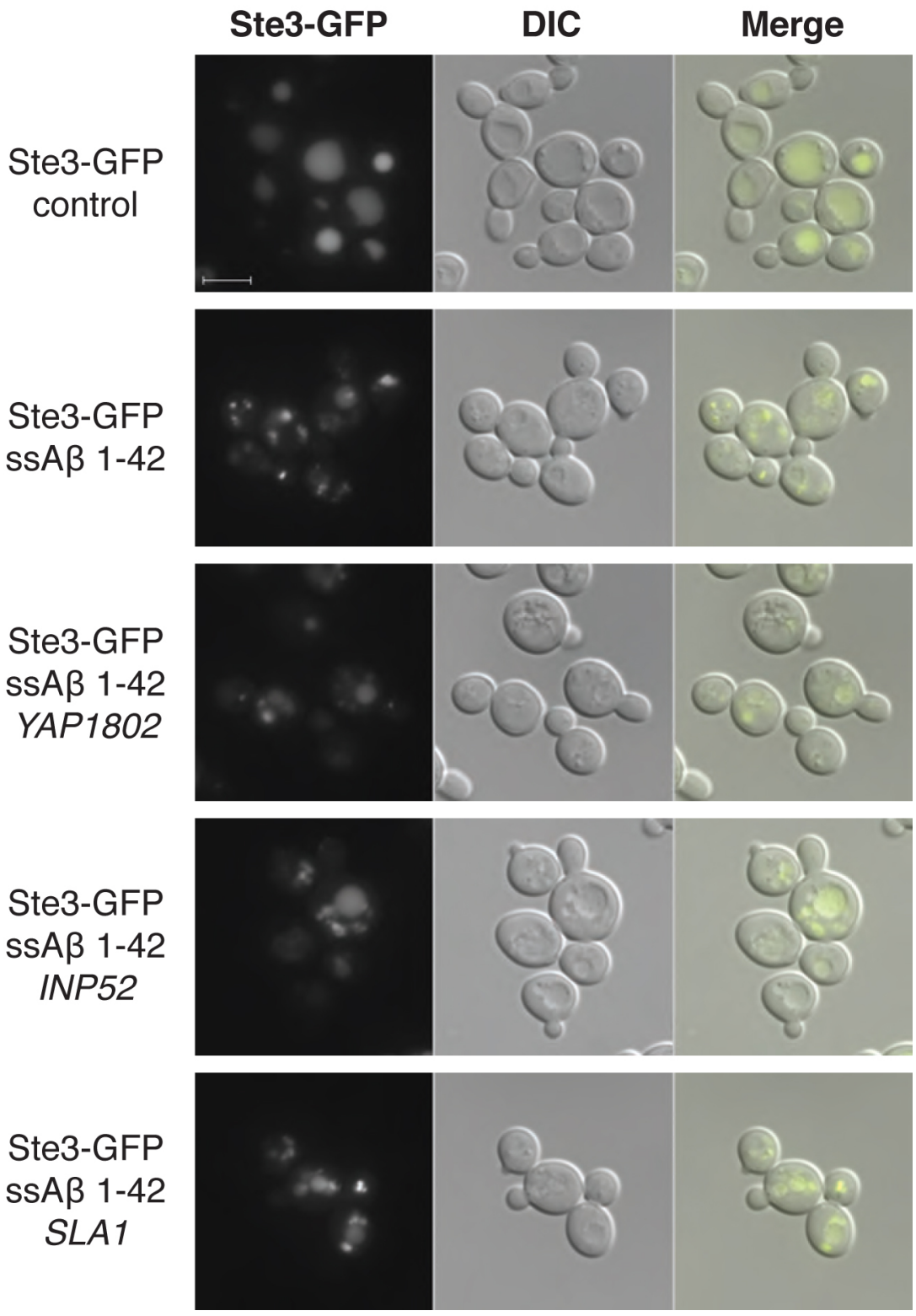
Ste3-GFP
DIC
Merge
Ste3-GFP control
Ste3-GFP ssAβ 1-42
Ste3-GFP ssAβ 1-42 YAP1802
Ste3-GFP ssAβ 1-42 INP52
Ste3-GFP ssAβ 1-42 SLA1

Supplemental Figure C4.6: Aβ toxicity modifiers modulate the Aβ-induced change in Ste3-YFP trafficking.

To examine the effect of Aβ on endocytosis and protein trafficking, we created our own version of the Ste3 localization assay (MALDONADO-BAEZ, *et al.* 2008). The mating pheromone receptor Ste3p is constitutively targeted to the plasma membrane, but in the absence of its ligand it is endocytosed and degraded in the vacuole. We generated a Ste-YFP under the control of the constitutive *GPD* promoter and integrated into a control and an ssAβ 1-42 screening strain. ssAβ 1-42 expression changed Ste3-YFP localization from mostly vacuolar to cytoplasmic foci surrounding the vacuole, clearly showing that Aβ causes a defect in Ste3-YFP trafficking. We then examined the effects of modifiers involved in endocytosis. The endocytic genes *YAP1802, INP52* and *SLA1* reversed the effect induced by Aβ. *SLA1* functions, as *YAP1802*, in clathrin assembly. As such these endocytic suppressors reversed the effect of Aβ by increasing endocytic trafficking.

Interestingly, modifiers that had little effect on growth of ssAβ 1-42 strains under these growth conditions, such as *SLA1* (Table S1), still modulated the Aβ induced phenotypes. The scale bar is 5μM and all figures are on the same scale.

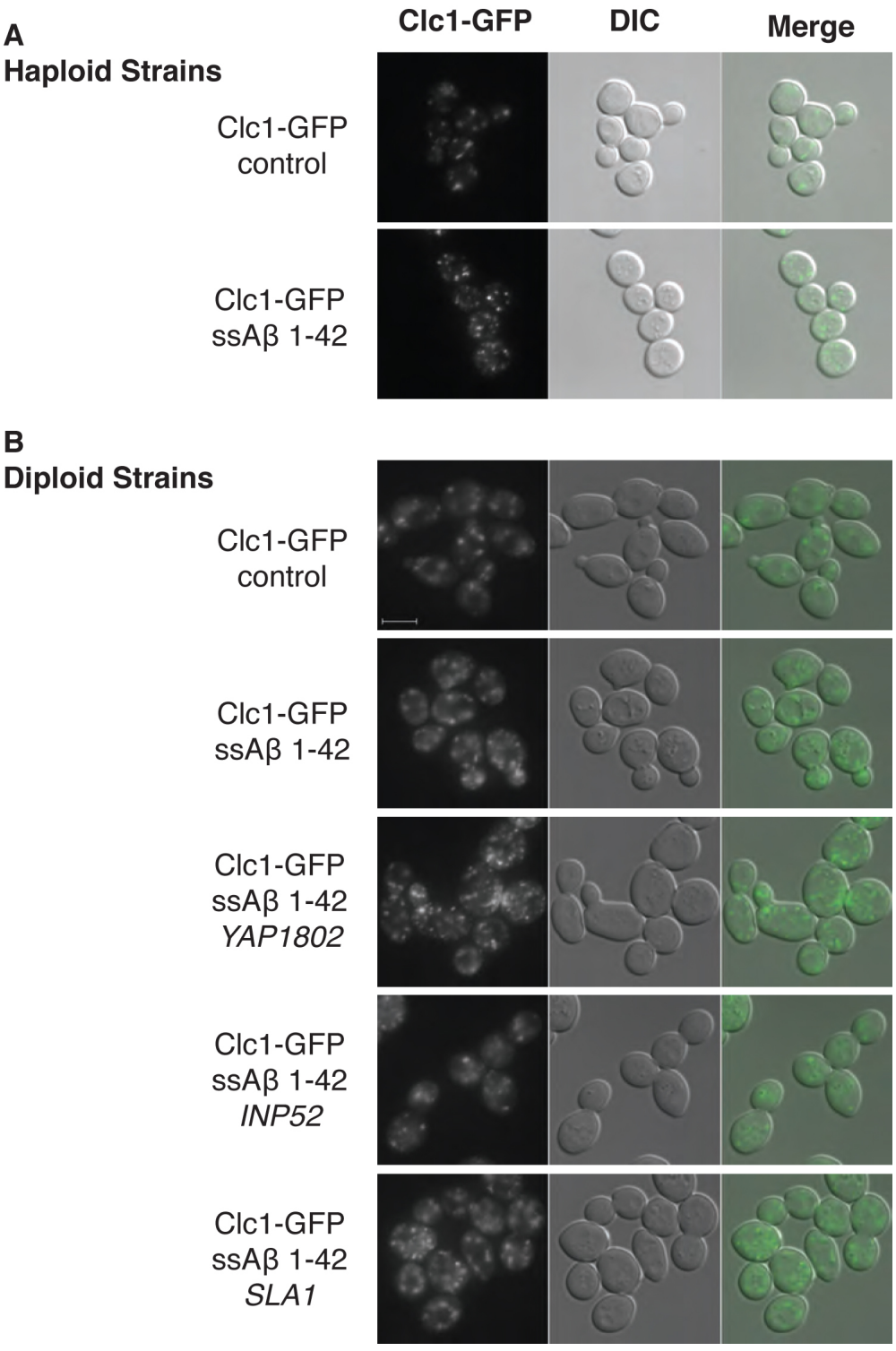

Supplemental Figure C4.7: Aβ toxicity modifiers modulate the Aβ-induced change in clathrin localization.

(A) We expressed ssAβ 1-42 in strain carrying a haploid clathrin light chain GFP fusion (Clc1-GFP). ssAβ 1-42 expression resulted in an increase in the number and brightness of Clc1-GFP foci, while also decreasing their size. Since this GFP-fusion strain, part of the GFP library (HOWSON*, et al.* 2005), is incompatible with our ssAβ 1-42 integration construct, we used a *GAL*-driven multi copy vector.

(B) Next, we examined the effects of suppressors with annotated functions in endocytosis on this Aβ-induced phenotype. But expression of ssAβ 1-42 from a multi copy vector, whose numbers can vary from cell to cell, and expression of the modifiers from an additional plasmid resulted in a large variation in the observed phenotypes. To achieve robust Aβ toxicity in the Clc1-GFP background, we hence mated one of the ssAβ 1-42 screening strains to the Clc1-GFP strain. While Aβ toxicity was attenuated in the diploid, it still induced the change in Clc1-GFP localization. We then tested the effects of the modifiers in this background. *YAP1802*, involved in clathrin cage assembly (MALDONADO-BAEZ*, et al.* 2008), enhanced the Aβ-induced phenotype; Clc1-GFP foci became more plentiful, brighter and smaller. In contrast, *INP52,* involved in clathrin vesicle fission and recycling (STEFAN*, et al.* 2005), reversed the Aβ-induced phenotype. *SLA1* increases the number of foci, consistent with its role in clathrin assembly, but the effect is subtle. Consequently, the Clc1-GFP foci likely represent endocytic intermediates that accumulate upon ssAβ 1-42 expression. *YAP1802* counteracts this defect by increasing vesicle formation, while *INP52* acts to complete the fission of otherwise stalled vesicles. As such both proteins result in an increased flux through the endocytic pathway. The scale bar is 5μM and all figures are on the same scale.

Appendix One:

Prion induction involves an ancient system for the sequestration of aggregated proteins and heritable changes in prion fragmentation

This work was previously published in *PNAS.*

Authors: Jens Tyedmers, Sebastian Treusch, Jijun Dong, J. Michael McCaffery, Brooke Bevis, Susan Lindquist

Abstract

When the translation termination factor Sup35 adopts the prion state, [*PSI*$^{+}$], the read-through of stop codons increases, uncovering hidden genetic variation and giving rise to new, often beneficial phenotypes. Evidence suggests that prion induction involves a process of maturation, but this has never been studied in detail. To do so, we used a visually tractable prion model consisting of the Sup35 prion domain fused to GFP (PrD-GFP) and overexpressed it to achieve induction in many cells simultaneously. PrD-GFP first assembled into Rings as previously described. Rings propagated for many generations before the protein transitioned into a Dot structure. Dots transmitted the [*PSI*$^{+}$] phenotype through mating and meiosis, but Rings did not. Surprisingly, the underlying amyloid conformation of PrD-GFP was identical in Rings and Dots. However, by electron microscopy Rings consisted of very long uninterrupted bundles of fibers, whereas Dot fibers were highly fragmented. Both forms were deposited at the IPOD, a biologically ancient compartment for the deposition of irreversibly aggregated proteins, that we propose is the site of *de novo* prion induction. We find that oxidatively damaged proteins are also localized there, helping to explain how proteotoxic stresses increase the rate of prion induction. Curing PrD-GFP prions, by inhibiting Hsp104's fragmentation activity, reversed the induction process: Dot cells produced Rings before PrD-GFP reverted to the soluble state. Thus, formation of the genetically transmissible prion state is a two-step process that involves an ancient system for the asymmetric inheritance of damaged proteins and heritable changes in the extent of prion fragmentation.

Introduction

Prions are self-perpetuating protein conformations that store and transmit phenotypic information independently of nucleic acids. In fungi, they act as protein-based elements of heredity, stably propagating their altered protein conformations and associated phenotypes (CHERNOFF 2007; SHORTER, *et al.* 2005).

In *Saccharomyces cerevisiae*, seven prions are known (HALFMANN, *et al.* 2010) and evidence indicates that numerous other yeast proteins are capable of forming prions (ALBERTI, *et al.* 2009). The proteins have different molecular functions and produce different prion phenotypes. Although they share no sequence homology, their prion domains (PrDs) are enriched in asparagine and glutamine residues. These PrDs can adopt self-perpetuating prion conformations that are amyloids. They template the conversion of soluble prion proteins of the same type to the same conformation (CHERNOFF 2007; SHORTER, *et al.* 2005). The AAA+ ATPase Hsp104 shears amyloid fibers to generate prion seeds, also referred to as propagons (COX, *et al.* 2003), ensuring inheritance of the prion state from generation to generation (CHERNOFF, *et al.* 1995).

The protein determinant for the prion [*PSI*$^{+}$] is the translation termination factor Sup35. Sup35's PrD, NM, has an N-terminal amyloidogenic domain (N) and a solubilizing middle domain (M) (CHERNOFF 2007; SHORTER, *et al.* 2005). *In vitro,* purified PrD can form amyloid fibrils on its own (GLOVER, *et al.* 1997). *In vivo*, assembly of the prion reduces availability of soluble, functional termination factor. This causes stop codon read-through (CHERNOFF 2007; SHORTER, *et al.* 2005) and results in a large array of diverse phenotypes depending on the genetic background (TRUE, *et al.* 2000). Stressful conditions alter protein folding homeostasis and

increase the rate at which cells switch to the prion state, creating a bet-hedging strategy for survival in fluctuating environments (ALBERTI, *et al.* 2009; HALFMANN, *et al.* 2010; TYEDMERS, *et al.* 2008).

[*PSI*$^{+}$] propagation is well studied. However, the spontaneous *de novo* formation of [*PSI*$^{+}$] is rare and poorly understood. Overexpression of Sup35, or its PrD, dramatically increases the frequency of [*PSI*$^{+}$] induction (CHERNOFF, *et al.* 1993), offering an opportunity to investigate the process. During prion induction two distinct aggregation patterns are observed: ribbon and ring structures that extend throughout the cell and round dot structures (GANUSOVA, *et al.* 2006; ZHOU, *et al.* 2001). Dots correspond to the mature [*PSI*$^{+}$] prion state. The ring structures appear to be a hallmark of *de novo* [*PSI*$^{+}$] induction but their nature remains a mystery. This is the subject of our investigation.

Results

Expression of PrD-GFP in a Sup35 PrD deletion strain results in Rings and Dots

To study the *de novo* formation and inheritance of prion amyloid *in vivo* on a single-cell level, we employed a fusion of the PrD (NM) with GFP, which is soluble in [*prion*$^{-}$] cells but faithfully propagates with the wild-type Sup35 amyloid in [*PRION*$^{+}$] cells (PATINO, *et al.* 1996). To determine if this visually tractable protein is fully capable of forming a prion in its own right, we expressed it from the Sup35 promoter to maintain normal expression. When these cells were mated to [*psi*$^{-}$] cells the protein remained soluble. When mated to [*PSI*$^{+}$] cells it acquired the prion state (Supplemental Figure A1.1), was dominant in matings and segregated 4:0 in meiosis.

Thus, PrD-GFP fully recapitulates prion behavior. However, as expected, spontaneous switches to the prion state were too rare to be observed spontaneously.

To provide a robust system for studying prion induction, we placed the PrD-GFP fusion under the control of the GPD promoter, which increased its expression ~15 fold, and integrated a single copy into the genome, to keep expression uniform in each cell. We also deleted the PrD from the endogenous *SUP35* gene, making the translation termination domain immune from sequestration into the prion. This can be toxic when it happens excessively (CHERNOFF*, et al.* 1993; VISHVESHWARA*, et al.* 2009).

Soon after transformation, while cells were still in micro-colonies, they had the diffuse GFP-fluorescence of [*prion*$^-$] cells. In more mature colonies, a large fraction of cells displayed a large ring-, rod- or ribbon-like structure of PrD-GFP fluorescence (collectively referred to as "Rings" throughout this paper). This Ring pattern was inherited for many generations. After two to eight re-streaks, each representing ~25 generations, the aggregation pattern changed and PrD-GFP was exclusively found in one large focus per cell, hereafter referred to as Dots (Figure A1.1a). Rings and Dots were previously described during prion induction in cells transiently overexpressing PrD-GFP in the presence of wild-type Sup35 (GANUSOVA*, et al.* 2006; ZHOU*, et al.* 2001).

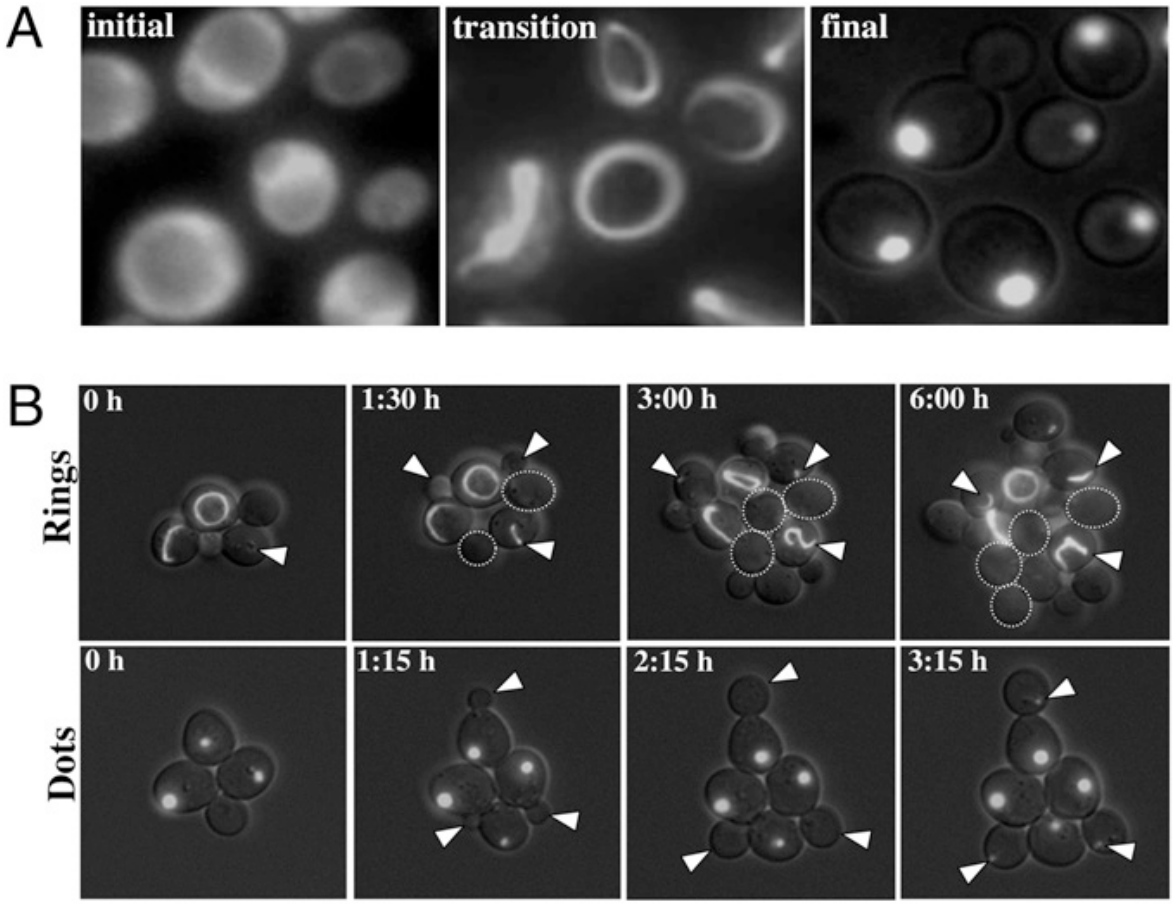

Figure A1.1: Expression of PrD-GFP at high levels produces self-propagating Ring assemblies that transition to a Dot assembly only after many generations.

(A) Cells constitutively expressing PrD-GFP under control of the GPD promoter are shown at different times; initial = immediately after transformation of the expression construct; intermediate = transformants after 3-5 days; final = transformants after ~ 10 days (hundreds of generations). **(B)** Haploid cells propagating either PrD-GFP Rings (upper panel) or Dots (lower panel). Cell divisions (arrows) were followed microscopically. Images represent a merge of several focal planes of GFP fluorescence overlaid with single DIC focal plane. A dotted line encircles progeny of Ring mothers that did not form any aggregates during the course of the experiment.

Propagation of Rings and Dots is independent of [*RNQ*$^{+}$]

When PrD-GFP was overexpressed in cells carrying a deletion of *RNQ1*, a factor required for efficient prion induction (DERKATCH*, et al.* 2001; OSHEROVICH*, et al.* 2001; SONDHEIMER*, et al.* 2000), it remained diffuse (ZHOU*, et al.* 2001)(Supplemental Figure A1.2). When cells containing Rings or Dots were mated to cells with a *RNQ* deletion and sporulated, haploid progeny with the deletion maintained their Rings and Dots (Supplemental Figure A1.3). Thus, as for the [*PSI*$^{+}$] prion itself (DERKATCH*, et al.* 2000), Dots and Rings require [*RNQ*$^{+}$] for their induction, but not their propagation.

Time-lapse microscopy establishes stable asymmetric inheritance of both aggregation states

We followed the propagation of PrD-GFP Rings and Dots for several cell divisions using time-lapse microscopy (Figure A1.1b). Both were faithfully propagated, but Rings were less stable, frequently giving rise to progeny with diffuse fluorescence (Figure A1.1b, upper panel, cells encircled by dotted line). Surprisingly, during cell division, Rings and Dots were retained in mother cells. Visible assemblies only became detectable in daughter cells after the dividing septum had formed. Cells with Rings initially gave rise to daughters with a single small focus, much like the initiating focus in Dot cells, but these generally expanded to form a typical Ring structure by the time the cell was ready for a new division (Figure A1.1b, upper panel).

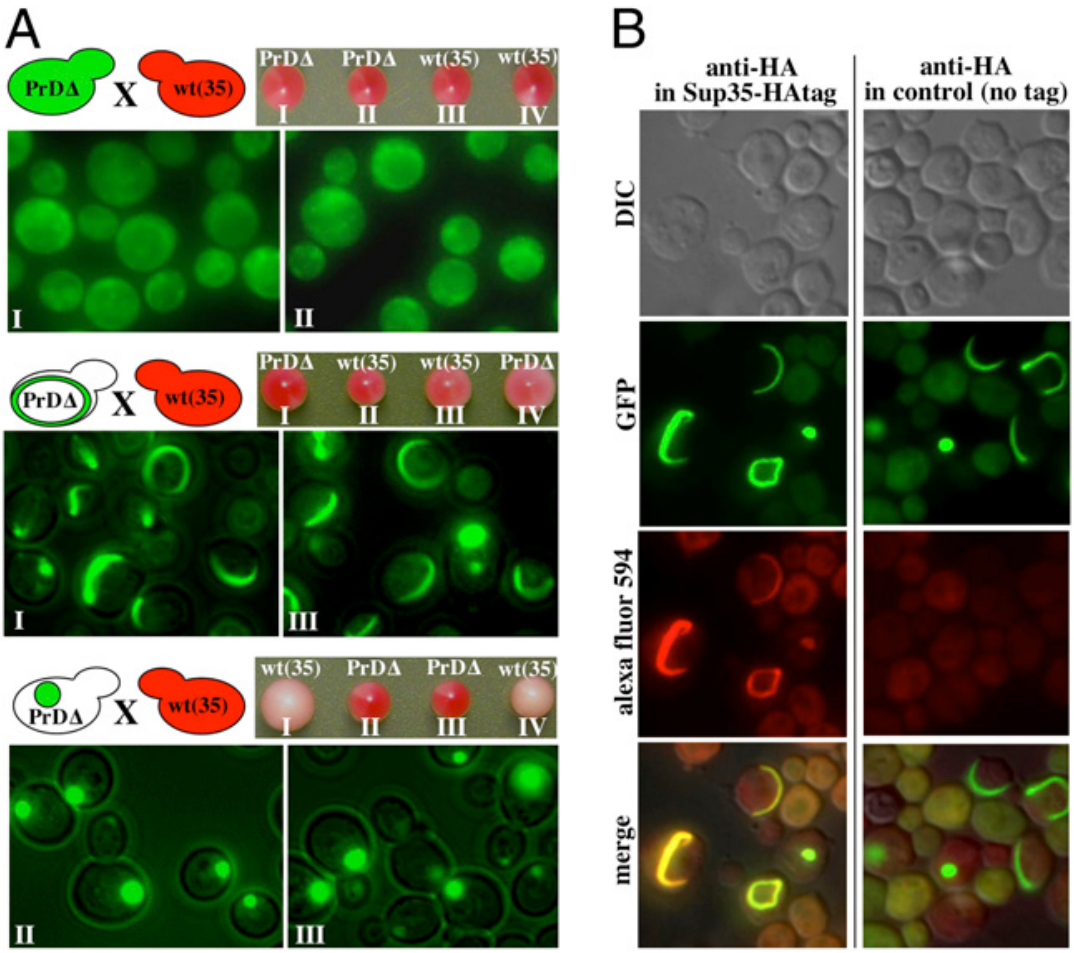

Figure A1.2: Cells with Rings do not induce the [*PSI*$^+$] prion state in a mating partner.

(A) Haploid strains carrying a PrD deletion of the endogenous SUP35 gene (PrDΔ) displaying diffuse PrD-GFP fluorescence, Rings or Dots were mated with a wild-type SUP35 [*psi*$^-$] strain. The resulting diploids were sporulated and tetrads were dissected. Spores with the PrD-GFP fusion were analyzed by fluorescence microscopy. Colony colors of the progeny, [*psi*$^-$] = red and [*PSI*$^+$] = light pink, revealed that Dots, but not Rings induced the prion state in wild-type SUP35.

(B) Sup35-HA co-localizes with PrD-GFP Rings and Dots. A [*psi*$^-$] strain carrying an inducible copy of PrD-GFP and a C-terminally HA-tagged Sup35 (SUP35-HA) was analyzed by immunofluorescence and fluorescence microscopy. Co-localization is shown in yellow in merged images.

PrD-GFP Dots can transmit the [*PSI*$^+$] phenotype but Rings cannot

Genetically, a defining feature of prions is dominance in crosses to mating partners. We first mated Ring and Dot cells to isogenic partners whose *RNQ1* gene had been deleted prior to PrD-GFP expression. As noted above, this kept their PrD-GFP protein in the diffuse non-prion state. After mating, diffuse PrD-GFP converted to the Ring or Dot form of its mating partner. When these diploids were sporulated, all haploid progeny of Dot matings contained Dots. Rings were also inherited, albeit less faithfully (Supplemental Figure A1.3).

Next we mated Ring and Dot cells to wild-type [*psi*$^-$] cells to determine if they could transmit the [*PSI*$^+$] phenotype. Both Rings and Dots were maintained in the diploids. All cells carried the *ade1-14* stop codon mutation (SHORTER*, et al.* 2005) but because one Sup35 allele carried a PrD deletion, the [*PSI*$^+$] read-through phenotype could not be detected in the diploid. However, after sporulation haploid progeny that received the wild-type *SUP35* gene and whose protein had acquired the [*PSI*$^+$] state, were expected to switch colony color from red to pink (Figure A1.2a).

In control matings, parents with diffuse PrD-GFP fluorescence produced only red [*psi*$^-$] progeny (Figure A1.2a, upper panel). Progeny of Dot parents that received only the wild-type Sup35 gene invariably gave rise to pink [*PSI*$^+$] colonies as expected for faithful transmission of the prion state from PrD-GFP to wild-type Sup35 (Figure A1.2a, lower panel). Also as expected, progeny carrying both wild-type Sup35 and the PrD-GFP over-expression construct were never recovered, due to excessive, toxic sequestration of Sup35 (CHERNOFF*, et al.* 1993; VISHVESHWARA*, et al.* 2009). Surprisingly, Ring cells produced no wild-type Sup35 progeny with the [*PSI*$^+$] phenotype (Figure A1.2a, middle). Furthermore, cells carrying both the PrD-GFP construct and

wild-type Sup 35 were readily obtained (for example, Figure A1.2a, middle, spore III). In these cells PrD-GFP maintained its initial Ring pattern, demonstrating that Rings generally propagated faithfully to progeny during meiosis.

A simple explanation might be that the PrD-GFP in Ring cells does not interact with WT Sup35. To test this we induced PrD-GFP Rings and Dots in cells with HA-tagged Sup35 protein as the only source of this essential protein. HA co-localized with both Rings and Dots (Figure A1.2b), eliminating this explanation.

In Ring and Dot cells PrD-GFP is in the same amyloid conformation

A common feature of prions is the ability to exist in several related, but distinct, amyloid conformations, known as "prion strains" (KING*, et al.* 2004; TANAKA*, et al.* 2004). These propagate with different polymerization and fragmentation efficiencies. Because they reach different equilibria between the soluble functional form and the amyloid, they produce distinct phenotypes (in *ade1-14* cells, colonies with different shades of pink) (KING*, et al.* 2004; TANAKA*, et al.* 2004; TANAKA*, et al.* 2006). Thus, another explanation for our results might be that Rings represent a different prion strain than Dots, one that is too "weak" to elicit a detectable phenotype. This occurs, for example, with the [ETA^+] variant of [PSI^+] (ZHOU*, et al.* 1999).

When crude cell lysates of all cell types were boiled in SDS they all produced a PrD-GFP band of the same intensity by SDS-PAGE, confirming that the protein was expressed at the same level (Figure A1.3a, top). When analyzed without boiling on semi-denaturing agarose gels the PrD-GFP protein of both Ring and Dot cells migrated as high molecular weight SDS-resistant complexes typical of prion amyloids (Figure A1.3a, bottom left).

Next, we tested the ability of Dots and Rings to seed polymerization of purified soluble PrD, a defining characteristic of prions. Lysates of cells with diffuse fluorescence did not seed polymerization. But lysates of Ring and Dot cells had very similar seeding capacities (Figure A1.3a, bottom right): SDS-resistant species could be detected almost immediately and their sizes increased similarly during the course of the experiment.

Proteins from different prion strains transform [*psi*$^-$] cells to [*PSI*$^+$] in a phenotype-specific manner. To minimize manipulations, crude extracts were introduced directly into [*psi*$^-$] cells to test for such differences (KING*, et al.* 2004; TANAKA*, et al.* 2004). To our surprise, lysates from cultures with Rings and Dots both gave rise to the same strong [*PSI*$^+$] strain (Figure A1.3b): Dot lysates induced the strong prion phenotype in 71 transformants, the weak phenotype in only three. Ring lysates induced the strong phenotype in 101 transformants, the weak in only six.

Although the stability of amyloid structures makes it extremely unlikely that a weak conformation might convert to a strong one during our procedure (KING*, et al.* 2004; TANAKA*, et al.* 2004), we considered the possibility. We eliminated the sonication step prior to transformation and used several different lysis procedures without changing the outcome. More definitively, we performed many similar experiments with lysates from bona fide weak prion strains but never observed conversion of weak prion strains to strong. Thus, Rings and Dots do not represent different prion conformations or strains.

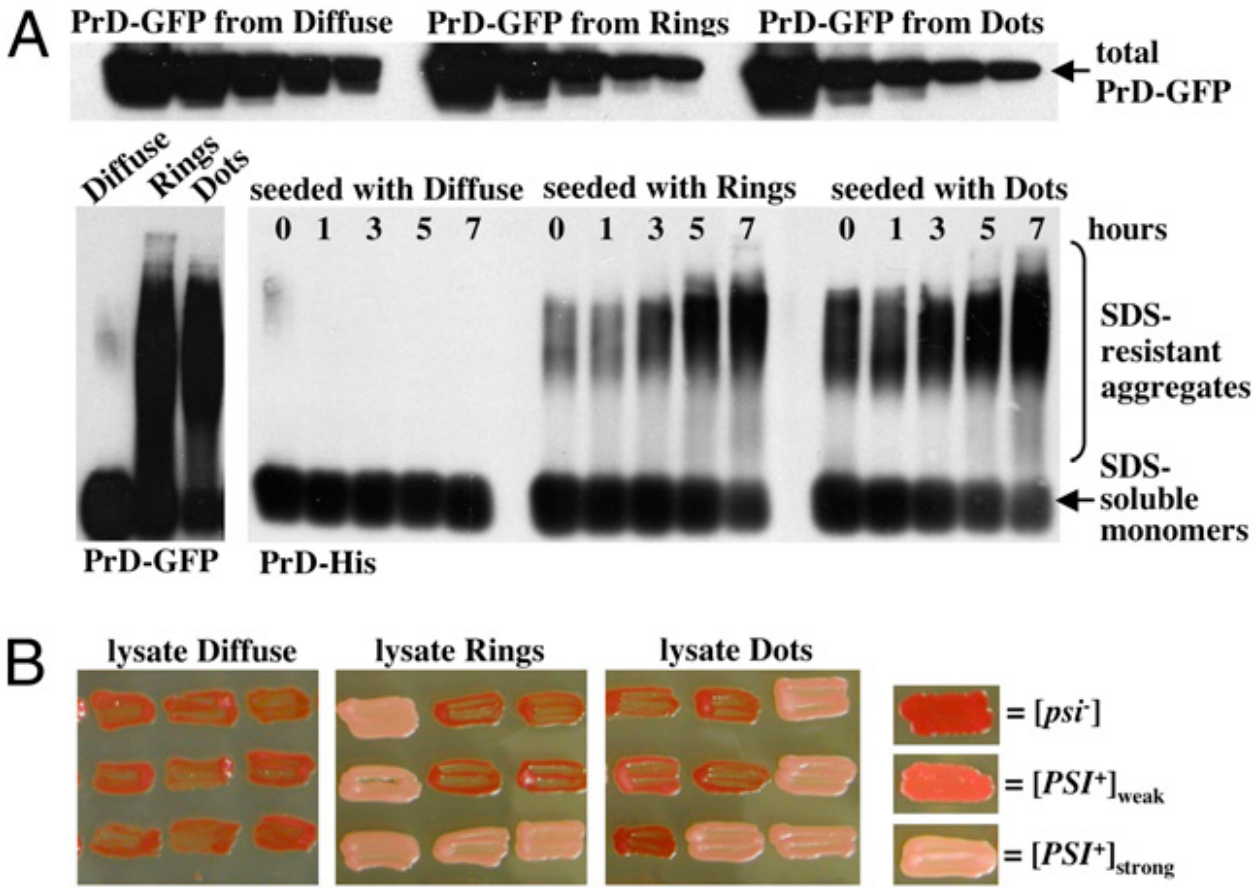

Figure A1.3: Cells with Rings and Dots contain PrD-GFP in the same prion conformation.

(A) Upper panel: crude lysates from cells displaying diffuse, Ring or Dot fluorescence were adjusted to equal protein concentrations and serial dilutions (1:2 steps) were loaded onto an SDS gel and analyzed by SDS-PAGE and Western Blotting with an anti-GFP antibody to reveal the amounts of PrD-GFP in the different lysates. **Lower panel left:** the three different lysates were analyzed by semi-denaturing agarose gel analysis (SDD-AGE) followed by Western Blotting with an anti-GFP antibody. Lysates from cells with Rings and Dots, but not diffuse PrD-GFP, contain SDS-resistant high molecular weight aggregates of PrD-GFP. **Lower panel right:** purified PrD-His was seeded with the three different lysates *in vitro* and analyzed by SDD-AGE and Western Blotting with an anti-His-tag antibody. SDS-resistant high molecular weight aggregates

were formed with comparable kinetics. **(B)** Protein transformations of a [*psi*$^-$] tester strain (red colony color) were performed with crude lysates from cells with diffuse PrD-GFP fluorescence or Rings and Dots. The prion status and strain of the transformants was determined by colony color. Both types of aggregates induced a strong [*PSI*$^+$] strain (light pink color) with similar efficiencies.

Aggregate formation occurs at a site specific to the deposition of insoluble aggregates

We asked if the differences in transmissibility of the [*PSI*$^{+}$] phenotype with Rings and Dots could be due to different cellular localizations. The vacuolar dye FM4-64 established that PrD-GFP Dots were localized adjacent to the vacuole (Figure A1.4a, left column). A single focus at the vacuole is characteristic of the pre-autophagosomal structure (PAS), which coordinates autophagosome formation and cytoplasm-to-vacuole vesicle trafficking (HE, *et al.* 2009). Colocalization of a PrD-YFP fusion and the CFP-tagged PAS markers ATG8 and ATG14 confirmed this localization (Figure A1.4a). Dots were directly adjacent to the PAS. Rings intersected it (Figure A1.4a).

Recently, a perivacuolar PAS-associated site for the deposition of irreversibly aggregated proteins was discovered and termed the IPOD for Insoluble PrOtein Deposit (KAGANOVICH, *et al.* 2008). It also accumulates the Ure2 and Rnq1 proteins in their prion forms (KAGANOVICH, *et al.* 2008). To extend this characterization, we used mass spectroscopy to identify proteins that were co-immuno-captured with PrD-GFP Dots but not with soluble PrD-GFP (Supplemental Figure A1.4 & Supplemental Table A1.1). Rnq1 was among them confirming the capture of bona fide IPOD substrates. We also found proteins known to be very sensitive to oxidative damage (CABISCOL, *et al.* 2000).

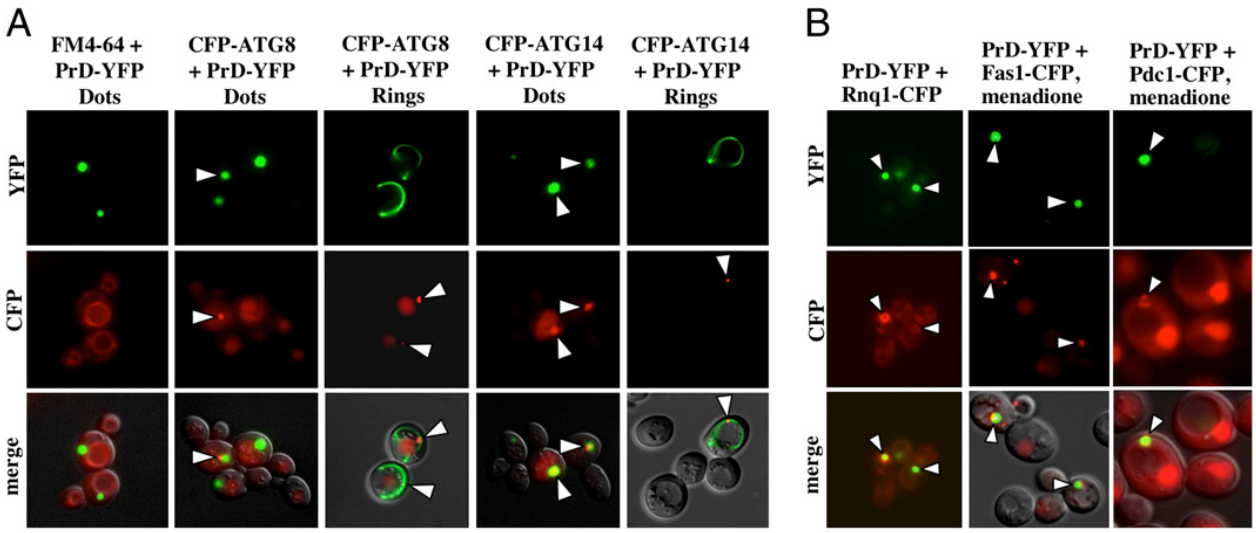

Figure A1.4: Prion aggregates localize to the IPOD compartment as shown using markers for the pre-autophagosomal structure (PAS) and additional IPOD substrates.

Cells carrying Dots were generated using a genomic copy of GPD-controlled PrD-YFP. Rings were induced using an analogous galactose-inducible construct. **(A)** FM4-64 visualization of the vacuolar membrane shows the perivacuolar localization of PrD-YFP Dots (left column). The localization of Rings and Dots to the pre-autophagosomal structure was visualized using centromeric plasmids expressing N-terminal CFP fusions of ATG8 or ATG14. **(B)** Co-localization of PrD-YFP Dots with known and newly identified substrates of the IPOD compartment (indicated by arrows). Genomic copies of PDC1 or FAS1 were tagged with CFP (columns 1 and 2), while the Rnq1-CFP fusion was expressed from a plasmid under control of the Cup1 promoter (column 3). Aggregation of Pdc1-CFP or Fas1-CFP was induced using 0.1 mM or 2 mM of menadione, respectively, for 4 hours prior to microscopy. The Rnq1-CFP expression was induced using 100 µM Cupper sulfate. Images represent one single optical plane.

CFP-tagged versions of Rnq1 and the two oxidation-sensitive proteins, Fas1 (fatty acid synthase) and Pdc1 (pyruvate decarboxylase1) (CABISCOL, *et al.* 2000) were used to confirm cellular co-localization by microscopy. RNQ1-CFP co-localized with PrD-YFP Dots constitutively (Figure A1.4b). Fas1 and Pdc1's partial colocalization with PrD-YFP Dots was most apparent after cells were treated with the oxidizing agent menadione (CABISCOL, *et al.* 2000) (Figure A1.4b). Thus, the previously reported polarisome-dependent asymmetric inheritance of oxidatively damaged proteins (AGUILANIU, *et al.* 2003; LIU, *et al.* 2010) occurs in part at the IPOD, which is also a site for prion accumulation.

Number of PrD-GFP amyloid fibers differs between Ring and Dot aggregates

Next we investigated the difference between Rings and Dots by transmission electron microscopy (TEM). We easily identified both forms by their highly ordered fibrous appearance, which closely resembled fibrils formed by Sup35 or PrD *in vitro* (GLOVER, *et al.* 1997; KRZEWSKA, *et al.* 2006). We confirmed that these assemblies were indeed PrD-GFP Rings and Dots by immuno-EM using an antibody against GFP (Supplemental Figure A1.5). We also found the typical electron-dense foci formed by amorphous aggregates of damaged proteins at this site further confirming the co-localizations described above (Supplemental Figure A1.6).

Rings and Dots were not separated from the surrounding cytoplasm by any compartmentalizing elements, such as membranes or cytoskeletal structures. Fibrils formed *in vitro* by the Sup35 PrD alone have an average diameter of ~ 11.5 nm, whereas fibrils of full-length Sup35 are ~ 25 nm (GLOVER, *et al.* 1997; KRZEWSKA, *et al.* 2006). In cross sections, Ring and Dot PrD-GFP fibrils had identical doughnut-like morphologies with a diameter of around 25 - 30

nm and an inner core of 6 - 12 nm (Supplemental Figure A1.5). This is consistent with the prion domain forming the inner core of the fiber, surrounded by GFP molecules.

However, there was one profound difference between the fibrils in the Rings and Dots, their length. Rings contained bundles of very long uninterrupted fibrils (Figure A1.5a, upper panel). Dots contained a profusion of short fibril bundles with diverse orientations in the same structure (Figure A1.5a, lower panel). Thus, Ring and Dot aggregates displayed an extreme difference in fragmentation and, consequently, in the number of fibril ends. The cell lysis procedure used in our protein transformation or seeding assays (Figure A1.3) would certainly fragment the very long fibrils of Ring cells, eliminating the sole difference between Rings and Dots.

In vivo, the only known protein with the capacity to sever PrD fibrils is the AAA+ ATPase Hsp104. Inhibition of Hsp104 increases the number of ring-bearing cells when PrD-GFP is overexpressed in the presence of wild-type Sup35 (ZHOU, *et al*. 2001). But the relationship between Hsp104 activity and Dots has never been examined. We inhibited Hsp104 activity in Dot cells by two different methods: incubation with 5 mM GdHCl, which selectively inhibits Hsp104's ATPase cycle (NESS, *et al*. 2002) (Figure A1.5b), or expression of a dominant negative mutant of Hsp104 (Supplemental Figure A1.7), which is incorporated into Hsp104 hexamers and blocks their activity. In both cases time-lapse microscopy revealed that pre-existing Dots never changed, but mother cells with Dots rapidly and invariably produced daughter cells with Rings. These Rings also remained intact. However, within just a few divisions, all Ring-containing cells gave rise to progeny with diffuse PrD-GFP fluorescence. Thus, the curing of Dots by Hsp104 inhibition mirrors their formation. The distinct states of prion maturation result from differences in the number of fiber fragments generated by Hsp104 and hence the number of prion seeds.

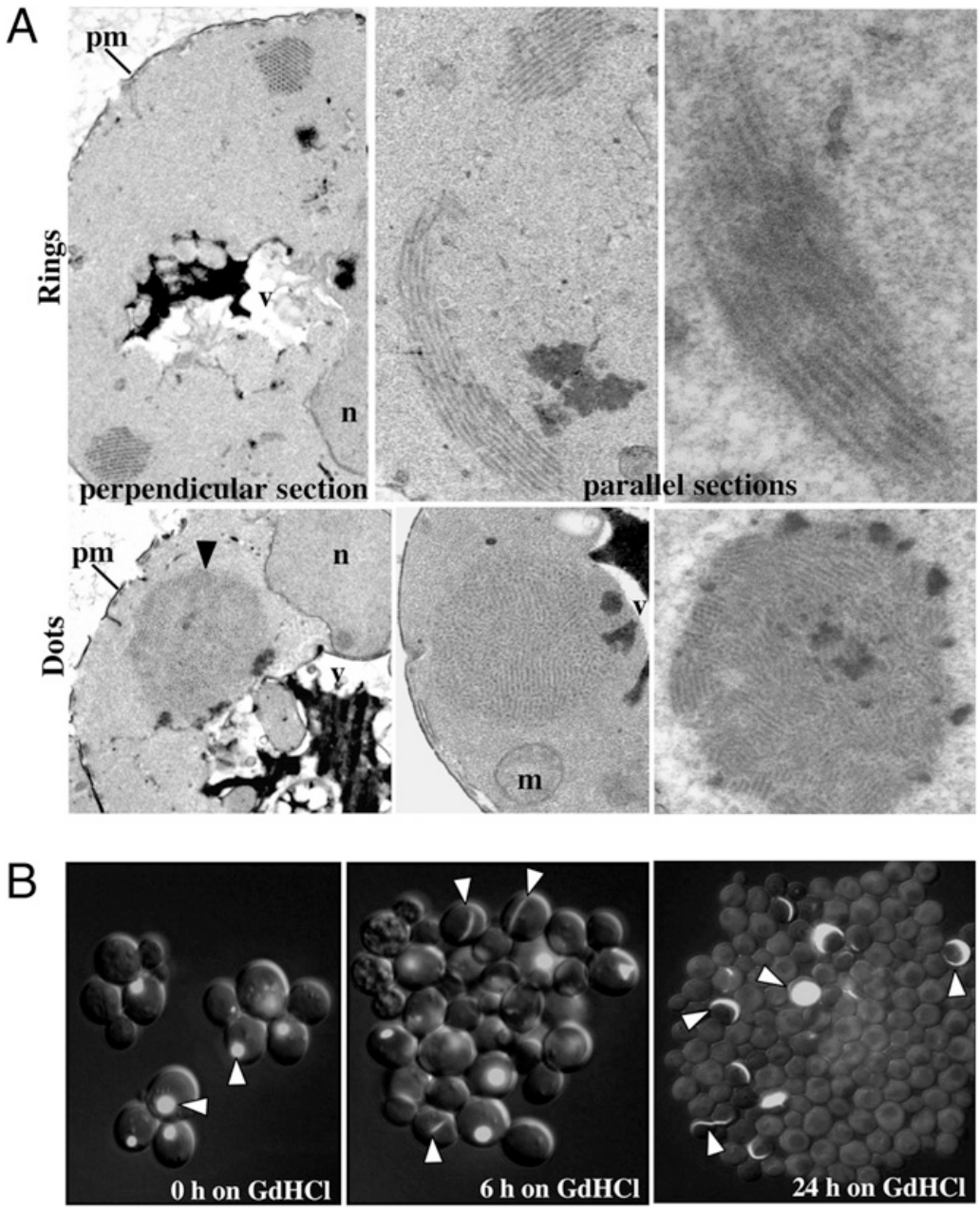

Figure A1.5: Electron microscopy of Ring and Dot cells reveals the different degrees of PrD-GFP fibril fragmentation.

(A) Upper panel: different magnifications of ultrathin cell section with a large Dot aggregate next to the vacuole; lower panel: perpendicular or parallel sections of a cell displaying PrD-GFP Rings. m: mitochondrion, n: nucleus, v: vacuole, pm: plasma membrane. **(B)** Time-lapse

microscopy of constitutively PrD-GFP expressing strain carrying a Dot aggregate. Cells were monitored for several hours in the presence of 5 mM GdHCl to inhibit Hsp104 activity. Upon inhibition of Hsp104, cells with Dot aggregates gave rise to progeny forming Ring aggregates. Progeny thereof ultimately displayed diffuse fluorescence. Images show different representative groups of cells at different time points (0, 6, 24 hours) and are an overlay of a single focal plane DIC image and a merge of fluorescence z-stack images.

Discussion

We find that prion induction by the Sup35 PrD involves a maturation process with a distinct, stable, and heritable intermediate. Surprisingly, this intermediate (Ring state) has all of the biochemical characteristics of the mature prion (Dot state), but distinct phenotypic properties. It does not confer a [*PSI*$^{+}$] phenotype on meiotic progeny whose only source of Sup35 is the wild-type protein, even when PrD-GFP Rings co-exist in the same cell. How might we resolve this seeming paradox and also decipher the nature of the prion induction process? Two other observations, we think, provide the key.

First, by electron microscopy, Ring fibrils are long and uninterrupted, Dot fibrils highly fragmented. Indeed, the degree of fiber fragmentation is the defining characteristic for the different structures, as blocking Hsp104's fragmentation activity reverts Dots to Rings before the assemblies are lost entirely. Second, the deposition of Rings and Dots occurs at a site specific for the compartmentalization of damaged proteins, known as the IPOD (KAGANOVICH*, et al.* 2008). In cells undergoing mitosis, Rings and Dots are retained in mother cells but re-form in their daughters at the IPOD immediately after septum formation. The most parsimonious explanation is that prion seeds, too small to be detected by fluorescence (KAWAI-NOMA*, et al.* 2006), are liberated by the activity of Hsp104 and transmitted to daughter cells.

Taking these observations together, we propose a model for prion induction that also explains the distinct phenotypes and heritable nature of Rings and Dots. Upon initial expression, PrD-GFP is soluble but the intrinsically unstructured Sup35 PrD has a high propensity to misfold. This misfolded protein is targeted to the IPOD. Because nucleated conformational conversion to the prion state requires an oligomeric intermediate (SERIO*, et al.*

2000), the high local concentration of PrD-GFP at the IPOD increases the likelihood of prion induction (GANUSOVA, *et al.* 2006). [*RNQ*$^{+}$] prions, which are required for [*PSI*$^{+}$] induction (DERKATCH, *et al.* 2001; OSHEROVICH, *et al.* 2001; SONDHEIMER, *et al.* 2000), are also located at the IPOD and ready to facilitate nucleation (this study and (DERKATCH, *et al.* 2004; KAGANOVICH, *et al.* 2008)).

Initially, only a few prion seeds form. Therefore, the rate at which soluble full length Sup35 is sequestered from translation is limited. Rings formed in this way can coexist with the wild-type protein without causing toxicity or creating a [*PSI*$^{+}$] phenotype (Figure A1.2a, middle panel, spore III). The small number of seeds creates long bundles of fibers, which appear as Rings confined only by the boundary of the cell. Inheritance of a small number of seeds by daughter cells perpetuates the Ring state.

Dots consist of short highly fragmented fibers. Increased fragmentation causes a larger number of prion seeds to be inherited by daughters, explaining the more stable inheritance of Dots relative to Rings and the ability to reliably transmit the prion state to all meiotic progeny. In this case polymerization is limited by the amount of soluble prion protein and not by the number of prion seeds. Thus, meiotic progeny inheriting PrD-GFP Dots, whose only source of the essential Sup35 is the wild-type protein, are inviable.

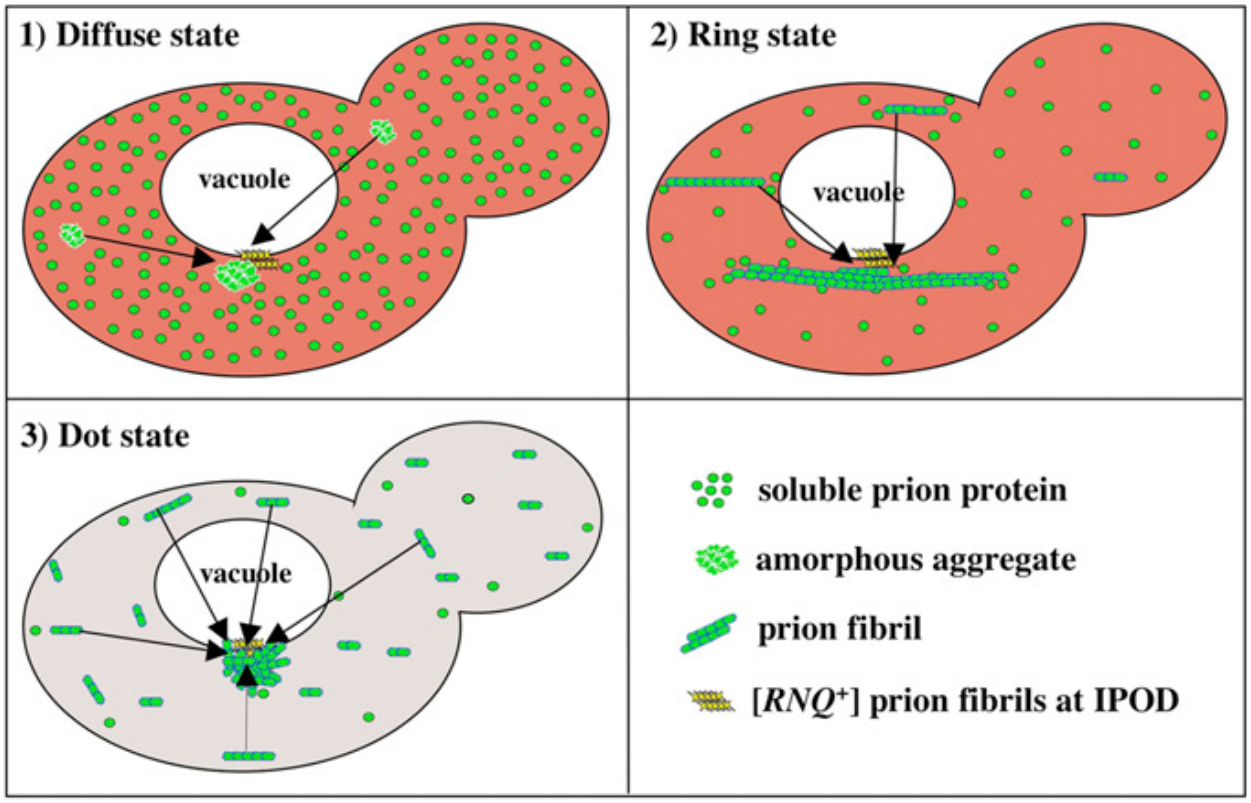

Figure A1.6: Schematic model for the induction and maturation of the PrD-GFP prion via a long-lived poorly fragmented fibril state.

The discussion of this appendix chapter contains a detailed description of this model for the maturation of the PrD-GFP prion.

A remaining question is how cells switch from the transitional Ring state to the mature prion state. One possibility is that a Ring-containing mother rarely but stochastically transmits a sufficiently large number of seeds to its daughter to create a profusion of shorter fibrils. Indeed, the number of wild type [*PSI*$^{+}$] propagons is known to be clonally diverse (Cox, *et al.* 2003). However, Ring and Dot cells contain the same quantity of the fibril fragmenting protein Hsp104 (Supplemental Figure A1.8), which plays a critical role in [*PSI*$^{+}$] inheritance (Borchsenius, *et al.* 2006; Borchsenius, *et al.* 2001; Chernoff, *et al.* 1995; Ness, *et al.* 2002; Wegrzyn, *et al.* 2001). With just a few initiating fibrils, one might expect them to be highly susceptible to Hsp104, but Hsp104's remodeling functions are tightly regulated in unstressed cells (Schirmer, *et al.* 2004). Thus, another explanation is a heritable switch in the activity of Hsp104. Speculatively, an inhibitor of Hsp104 might itself be a prion – the concentration of aggregated proteins at the iPOD could favor its switch to a heritable, non-functional state, converting Rings to highly fragmented mature prions.

However that specific detail may be resolved, many lines of evidence suggest that normal [*PSI*$^{+}$] induction, as well as the induction of other prions, involves a transitional state like the one we describe. For example, propagons of wild-type [*PSI*$^{+}$] are subject to biased retention in mother cells by a previously unknown mechanism (Cox, *et al.* 2003). Both Rings and Dots are observed in cells with wild-type Sup35 during "typical" laboratory prion inductions with overexpressed PrD (Ganusova, *et al.* 2006; Zhou, *et al.* 2001) and Rings behave as an immature transitional state with unstable inheritance. Further, in those cases where it has been examined, the induction of [*PSI*$^{+}$], [*URE3*] and [*RNQ*$^{+}$] by over-expression of their PrDs clearly involves a genetically unstable intermediate. Cells initially segregate both [*prion*$^{-}$] and [*PRION*$^{+}$]

clones and only later stabilize to reliably produce [*PRION*$^{+}$] colonies (DERKATCH*, et al.* 2001; DERKATCH*, et al.* 2000; FERNANDEZ-BELLOT*, et al.* 2000; OSHEROVICH*, et al.* 2001; SALNIKOVA*, et al.* 2005). Finally, in the absence of PrD over-expression, proteotoxic stresses, including oxidative stresses, increase the spontaneous induction of [*PSI*$^{+}$] (SIDERI*, et al.* 2010; TYEDMERS*, et al.* 2008). The more severe the stress the more efficient the induction. Co-localization of such damaged proteins at the IPOD could provide an opportunity for cross seeding akin to that provided by [*RNQ*$^{+}$]. Subsequently, in the absence of PrD overexpression, the fragmentation activity of Hsp104 would be sufficient to free most of the assembled protein from the IPOD, allowing direct cytoplasmic inheritance of prion propagons.

The concerted asymmetric retention of prion fibrils is tied to an ancient (but only recently discovered) system for the asymmetric inheritance of misfolded damaged proteins. Mitotic cells, ranging from bacteria, to yeast, to human embryonic stem cells, systematically retain and sequester damaged and misfolded proteins to one cell during division (AGUILANIU*, et al.* 2003; LINDNER*, et al.* 2008; RUJANO*, et al.* 2006). This is thought to ensure the fitness of the next generation by allowing one of the two mitotic products to start afresh with respect to protein damage – segregating an aging (soma-like) lineage from a rejuvenated (germ-like) lineage. We propose that the IPOD is not only a depository for damaged proteins, but plays a critical positive role in prion biology as the cellular site of *de novo* prion induction.

Acknowledgements

We thank K. Allendoerfer, K. K. Frederick, R. Krishnan, and S. Alberti for critical reading of the manuscript. We are grateful to E. Spooner (Whitehead Institute) for mass spectrometry and

M.J. Sa and A.W. Murray (Harvard University) for assistance with time-lapse microscopy. This work was supported by NIH GM025874 (S.L.), an EBMO Long Term fellowship (J.T.), a Human Frontiers Science Program Organization Long Term Fellowship (J.T.), and an American Heart Association fellowship (J.D.). S.L. is an Investigator of the Howard Hughes Medical Institute.

Author contributions

Jens Tyedmers performed the majority of experiments. Jijun Dong carried out the seeding and protein transformation experiments. Brooke Bevis designed the NM-YFP construct and conducted initial microscopy experiments. J. Michael McCaffery conducted the EM experiments. I helped with the interpretation of results and wrote the paper together with Jens and Susan Lindquist.

References

Aguilaniu, H., Gustafsson, L., Rigoulet, M., & Nystrom, T. (2003) Asymmetric Inheritance of Oxidatively Damaged Proteins During Cytokinesis. *Science* 299(5613):1751-1753.

Alberti, S., Halfmann, R., King, O., Kapila, A., & Lindquist, S. (2009) A Systematic Survey Identifies Prions and Illuminates Sequence Features of Prionogenic Proteins. *Cell* 137(1):146-158.

Borchsenius, A.S., Muller, S., Newnam, G.P., Inge-Vechtomov, S.G., & Chernoff, Y.O. (2006) Prion Variant Maintained Only at High Levels of the Hsp104 Disaggregase. *Curr Genet* 49(1):21-29.

Borchsenius, A.S., Wegrzyn, R.D., Newnam, G.P., Inge-Vechtomov, S.G., & Chernoff, Y.O. (2001) Yeast Prion Protein Derivative Defective in Aggregate Shearing and Production of New 'Seeds'. *Embo J* 20(23):6683-6691.

Cabiscol, E., Piulats, E., Echave, P., Herrero, E., & Ros, J. (2000) Oxidative Stress Promotes Specific Protein Damage in Saccharomyces Cerevisiae. *J Biol Chem* 275(35):27393-27398.

Chernoff, Y.O. (2007) Stress and Prions: Lessons from the Yeast Model. *FEBS Lett* 581(19):3695-3701.

Chernoff, Y.O., Derkach, I.L., & Inge-Vechtomov, S.G. (1993) Multicopy Sup35 Gene Induces De-Novo Appearance of Psi-Like Factors in the Yeast Saccharomyces Cerevisiae. *Curr Genet* 24(3):268-270.

Chernoff, Y.O., Lindquist, S.L., Ono, B., Inge-Vechtomov, S.G., & Liebman, S.W. (1995) Role of the Chaperone Protein Hsp104 in Propagation of the Yeast Prion-Like Factor [Psi+]. *Science* 268(5212):880-884.

Cox, B., Ness, F., & Tuite, M. (2003) Analysis of the Generation and Segregation of Propagons: Entities That Propagate the [Psi+] Prion in Yeast. *Genetics* 165(1):23-33.

Derkatch, I.L., Bradley, M.E., Hong, J.Y., & Liebman, S.W. (2001) Prions Affect the Appearance of Other Prions: The Story of [Pin(+)]. *Cell* 106(2):171-182.

Derkatch, I.L., Bradley, M.E., Masse, S.V., Zadorsky, S.P., Polozkov, G.V., Inge-Vechtomov, S.G., & Liebman, S.W. (2000) Dependence and Independence of [Psi(+)] and [Pin(+)]: A Two-Prion System in Yeast? *Embo J* 19(9):1942-1952.

Derkatch, I.L., Uptain, S.M., Outeiro, T.F., Krishnan, R., Lindquist, S.L., & Liebman, S.W. (2004) Effects of Q/N-Rich, Polyq, and Non-Polyq Amyloids on the De Novo Formation of the [Psi+] Prion in Yeast and Aggregation of Sup35 in Vitro. *Proc Natl Acad Sci U S A* 101(35):12934-12939.

Fernandez-Bellot, E., Guillemet, E., & Cullin, C. (2000) The Yeast Prion [Ure3] Can Be Greatly Induced by a Functional Mutated Ure2 Allele. *Embo J* 19(13):3215-3222.

Ganusova, E.E., Ozolins, L.N., Bhagat, S., Newnam, G.P., Wegrzyn, R.D., Sherman, M.Y., & Chernoff, Y.O. (2006) Modulation of Prion Formation, Aggregation, and Toxicity by the Actin Cytoskeleton in Yeast. *Mol Cell Biol* 26(2):617-629.

Glover, J.R., Kowal, A.S., Schirmer, E.C., Patino, M.M., Liu, J.J., & Lindquist, S. (1997) Self-Seeded Fibers Formed by Sup35, the Protein Determinant of [Psi+], a Heritable Prion-Like Factor of S. Cerevisiae. *Cell* 89(5):811-819.

Halfmann, R., Alberti, S., & Lindquist, S. (2010) Prions, Protein Homeostasis, and Phenotypic Diversity. *Trends Cell Biol* 20(3):125-133.

He, C. & Klionsky, D.J. (2009) Regulation Mechanisms and Signaling Pathways of Autophagy. *Annu Rev Genet* 43:67-93.

Kaganovich, D., Kopito, R., & Frydman, J. (2008) Misfolded Proteins Partition between Two Distinct Quality Control Compartments. *Nature* 454(7208):1088-1095.

Kawai-Noma, S., Ayano, S., Pack, C.G., Kinjo, M., Yoshida, M., Yasuda, K., & Taguchi, H. (2006) Dynamics of Yeast Prion Aggregates in Single Living Cells. *Genes Cells* 11(9):1085-1096.

King, C.Y. & Diaz-Avalos, R. (2004) Protein-Only Transmission of Three Yeast Prion Strains. *Nature* 428(6980):319-323.

Krzewska, J. & Melki, R. (2006) Molecular Chaperones and the Assembly of the Prion Sup35p, an in Vitro Study. *Embo J* 25(4):822-833.

Lindner, A.B., Madden, R., Demarez, A., Stewart, E.J., & Taddei, F. (2008) Asymmetric Segregation of Protein Aggregates Is Associated with Cellular Aging and Rejuvenation. *Proc Natl Acad Sci U S A* 105(8):3076-3081.

Liu, B., Larsson, L., Caballero, A., Hao, X., Oling, D., Grantham, J., & Nystrom, T. (2010) The Polarisome Is Required for Segregation and Retrograde Transport of Protein Aggregates. *Cell* 140(2):257-267.

Ness, F., Ferreira, P., Cox, B.S., & Tuite, M.F. (2002) Guanidine Hydrochloride Inhibits the Generation of Prion "Seeds" But Not Prion Protein Aggregation in Yeast. *Mol Cell Biol* 22(15):5593-5605.

Osherovich, L.Z. & Weissman, J.S. (2001) Multiple Gln/Asn-Rich Prion Domains Confer Susceptibility to Induction of the Yeast [Psi(+)] Prion. *Cell* 106(2):183-194.

Patino, M.M., Liu, J.J., Glover, J.R., & Lindquist, S. (1996) Support for the Prion Hypothesis for Inheritance of a Phenotypic Trait in Yeast. *Science* 273(5275):622-626.

Rujano, M.A., Bosveld, F., Salomons, F.A., Dijk, F., van Waarde, M.A., van der Want, J.J., de Vos, R.A., Brunt, E.R., Sibon, O.C., & Kampinga, H.H. (2006) Polarised Asymmetric Inheritance of Accumulated Protein Damage in Higher Eukaryotes. *PLoS Biol* 4(12):e417.

Salnikova, A.B., Kryndushkin, D.S., Smirnov, V.N., Kushnirov, V.V., & Ter-Avanesyan, M.D. (2005) Nonsense Suppression in Yeast Cells Overproducing Sup35 (Erf3) Is Caused by Its Non-Heritable Amyloids. *J Biol Chem* 280(10):8808-8812.

Schirmer, E.C., Homann, O.R., Kowal, A.S., & Lindquist, S. (2004) Dominant Gain-of-Function Mutations in Hsp104p Reveal Crucial Roles for the Middle Region. *Mol Biol Cell* 15(5):2061-2072.

Serio, T.R., Cashikar, A.G., Kowal, A.S., Sawicki, G.J., Moslehi, J.J., Serpell, L., Arnsdorf, M.F., & Lindquist, S.L. (2000) Nucleated Conformational Conversion and the Replication of Conformational Information by a Prion Determinant. *Science* 289(5483):1317-1321.

Shorter, J. & Lindquist, S. (2005) Prions as Adaptive Conduits of Memory and Inheritance. *Nat Rev Genet* 6(6):435-450.

Sideri, T.C., Stojanovski, K., Tuite, M.F., & Grant, C.M. (2010) Ribosome-Associated Peroxiredoxins Suppress Oxidative Stress-Induced De Novo Formation of the [Psi +] Prion in Yeast. *Proc Natl Acad Sci U S A*.

Sondheimer, N. & Lindquist, S. (2000) Rnq1: An Epigenetic Modifier of Protein Function in Yeast. *Mol Cell* 5(1):163-172.

Tanaka, M., Chien, P., Naber, N., Cooke, R., & Weissman, J.S. (2004) Conformational Variations in an Infectious Protein Determine Prion Strain Differences. *Nature* 428(6980):323-328.

Tanaka, M., Collins, S.R., Toyama, B.H., & Weissman, J.S. (2006) The Physical Basis of How Prion Conformations Determine Strain Phenotypes. *Nature* 442(7102):585-589.

True, H.L. & Lindquist, S.L. (2000) A Yeast Prion Provides a Mechanism for Genetic Variation and Phenotypic Diversity. *Nature* 407(6803):477-483.

Tyedmers, J., Madariaga, M.L., & Lindquist, S. (2008) Prion Switching in Response to Environmental Stress. *PLoS Biol* 6(11):e294.

Vishveshwara, N., Bradley, M.E., & Liebman, S.W. (2009) Sequestration of Essential Proteins Causes Prion Associated Toxicity in Yeast. *Mol Microbiol* 73(6):1101-1114.

Wegrzyn, R.D., Bapat, K., Newnam, G.P., Zink, A.D., & Chernoff, Y.O. (2001) Mechanism of Prion Loss after Hsp104 Inactivation in Yeast. *Mol Cell Biol* 21(14):4656-4669.

Zhou, P., Derkatch, I.L., & Liebman, S.W. (2001) The Relationship between Visible Intracellular Aggregates That Appear after Overexprzhession of Sup35 and the Yeast Prion-Like Elements [Psi(+)] and [Pin(+)]. *Mol Microbiol* 39(1):37-46.

Zhou, P., Derkatch, I.L., Uptain, S.M., Patino, M.M., Lindquist, S., & Liebman, S.W. (1999) The Yeast Non-Mendelian Factor [Eta+] Is a Variant of [Psi+], a Prion-Like Form of Release Factor Erf3. *Embo J* 18(5):1182-1191.

Material and Methods

Yeast strains, media, and constructs: Yeast strains BY4741 (Euroscarf) and 74D-694 (CHERNOFF, *et al.* 1995) were grown on standard synthetic media lacking particular amino acids/bases and containing either D-glucose (SD) or D-galactose (SGal) as carbon source. Sporulation was performed on 1% potassium acetate, 0.05% dextrose, 0.1% yeast extract, and 0.01% complete amino acid mix, Bio101. Expression of PrD-GFP (TYEDMERS, *et al.* 2008) was controlled by either the Gal1 or GPD promoter. The expression plasmid for RNQ1-CFP was described in (SONDHEIMER, *et al.* 2000). Gene deletions used primer sequences listed at the yeast deletion project website (http://www-sequence.stanford.edu/group/yeast_deletion_project/Deletion_primers_PCR_sizes.txt). Genomic C-terminal Cerulean fusions were confirmed by PCR. Plasmids coding for N-terminal Cerulean ATG8 or ATG14 fusions were generated using Gateway shuttle vectors (ALBERTI, *et al.* 2007) and the ORFs from the Open Biosystems mORF collection.

Seeding and transformation: The seeding efficiency of crude lysates from cells with diffuse fluorescence, Rings or Dots was tested with purified His-tagged protein using SDD-AGE as described (BAGRIANTSEV, *et al.* 2006). The same lysates were tested for transformation activity with a 74D-694-derived strain containing an *ADE1* mutation suppressible by [PSI^+] and a *URA3* plasmid as described (TANAKA, *et al.* 2004). Details are in supplementary methods.

Microscopy: Cells were grown in liquid culture to mid-log phase or on agar plates overnight and examined with an Axioplan microscope with a 100x objective (Zeiss) and narrow band pass filters for co-localization studies with different fluorescent proteins. Monoclonal HA antibody (Cell Signaling) and a secondary anti-mouse IgG antibody were coupled to alexa fluor 594 (Invitrogen). Unless indicated, images were taken in one representative focal plane. Photoshop was used for colorization, linear adjustments of brightness and contrast, and for creation of composite and merged images. Time-lapse microscopy was performed on agarose pads of ~ 20 x 20 x 1 mm, prepared by pouring ultrapure agarose (2% w/v) in SD media directly onto a microscope slide. After addition of the cells, the pad was covered with a cover slide and sealed with melted VLAP wax (1:1:1 Vaseline : lanolin : paraffin). Every 60 – 90 min, we collected a stack of 12 – 15 optical sections spaced 0.4 µm apart. Representative fluorescence images were de-blurred using a simple deconvolution algorithm, and then projected to one image. For conventional and immunoelectron microscopy details see supplementary methods.

Electron Microscopy: For conventional EM, yeast cells were harvested by centrifugation and resuspended in fix (3 % glutaraldehyde/0.1 M sodium cacodylate/5mM $CaCl_2$, pH 6.8). Cells were fixed for 1 hour at room temperature, washed, and resuspended in 1.2 M sorbitol in phos-citrate buffer (0.1 M K_2HPO_4/0.033 M citric acid). The fixed cells were then treated with glucuronidase and zymolyase for 1h to remove the cell walls, as described previoulsy (BANTA*, et al.* 1988). Cells were embedded in 2% ultra-low gelling temperature (Sigma, type IX), stained with osmium/thiocarbohydrazide as previously described (BANTA*, et al.* 1988), and embedded in low-viscosity Spurr plastic resin for 48 h at 60°C. Sections (80 nm) were cut on a Leica UCT

ultramicrotome, stained with lead citrate and uranyl acetate, respectively; and examined at 80 kV using a Philips EM 410 transmission electron microscope. Images were collected with a Soft Imaging System Megaview III camera, and figures assembled in Adobe Photoshop with only linear adjustments in brightness and contrast.

For ImmunoEM, cells were fixed in suspension for 15 min by adding an equal volume of freshly prepared 8% formaldehyde contained in 100 mM PO_4 buffer (pH 7.4). The cells were pelleted, resuspended in fresh fixative (4% formaldehyde/100 mM PO_4, pH 7.4), and incubated for an extra 18 – 24 hours at 4 °C. The cells were washed briefly in PBS and resuspended in 2% low-gelling-temperature agarose. The agarose blocks were trimmed into pieces of 1 mm^3, cryoprotected by infiltration with 2.3 M sucrose/20 % polyvinyl pyrrolidone (10,000)/PBS (pH 7.4) for 2 h, mounted on cryopins, and rapidly frozen in liquid nitrogen. Ultrathin cryosections were cut on a Leica UCT ultramicrotome equipped with an FC-S cryoattachment and collected onto formvar/carbon-coated nickel grids. The grids were washed through several drops of 1’ PBS containing 2.5% FCS and 10 mM glycine (pH 7.4) and then blocked in 10% FCS for 30 min and incubated overnight in 10 mg/ml chicken anti-GFP antibody (Abcam Antibodies) and a 1:200 dilution of rabbit anti-a-1,6 mannose serum. After washing, the grids were incubated for 2 h in 12-nm Au donky anti-rabbit conjugate or 6 nm Au donky anti-chicken (Jackson ImmunoResearch). The grids were washed through several drops of PBS followed by several drops of ddH2O. Grids were then embedded in an aqueous solution containing 3.2% polyvinyl alcohol (10K)/0.2% methyl cellulose (400 centiposes)/0.1% uranyl acetate.

Immunofluorescence

Fixation and spheroblasting: An overnight culture was grown in selective media to saturation and used to inocculate of fesh culture. 8 ml of cells were harvested at an OD_{600} of 0.6 and placed onto a bottle top filter (0.2 µm pores). After the liquid was removed by vacuum, cells were immediately resuspended in 5 ml of 4% formaldehyde in 50 mM KPO4, pH 6.5, 1 mM $MgCl_2$ and incubated for 2 h at room temperature in a 15 ml screw cap tube. Cells were collected by centrifugation for 3 min at 1000 x g, washed in 50 mM KPO4, pH 6.5, 1 mM MgCl2 containing a protease inhibitor cocktail (Roche 1 836 170) and resuspended in the same buffer to an OD_{600} of 10. 0,6 µl 2-mercapto-ethanol and 7 µl of a 1mg/ml zymolyase T100 solution were added to 100 µl of cells and incubated for 30 min at 30°C. Spheroblasts were washed by centrifugation for 2 min at 1000 x g and resuspended carefully in 100 µl of 50 mM KPO_4, pH 6.5, 1 mM $MgCl_2$ containing a protease inhibitor cocktail (Roche 1 836 170)

Adhesion of cells to microscope slide: Wells on a cover slide were created using an adhesive courier document pouch and a rotating-head hole puncher, coated with 0,1 % polylysine (Sigma #P-1524) and washed 3 x with water before 10 µl spheroblasts/well were added. After 3 min of adhesion, excess liquid was removed and the coverslip was dried completely before it was immersed in precooled (- 20) acetone for 5 min. After blotting away excess solvent, the cover slip was dried before blocking and antibody incubation steps followed.

Antibody incubation: For blocking, each well was incubated with a drop of PBS-block (1% milk powder, 0,1% BSA, 0,1% octyl glucoside) for 30 min before the primary antibody (monoclonal mouse anti-HA-tag antibody (6E2) from cell signaling, lot 1B # 2367) in PBS-block was added and incubated for 60 min at room temperature in a humid chamber. Each well was washed 8 x with PBS-block before the secondary antibody (alexa fluor 594 anti-mouse IgG A11062, lot

#57764a from invitrogen) was added and incubated for 30 min in the dark. Subsequently, cells were washed 8 times, excess liquid was removed and 5 µl of mounting media/well was added before the cover slip was inverted onto a slide and sealed with nail polish.

Cell lysis of strains displaying diffuse-, Ring- or Dot-shaped aggregates for PrD-seeding reactions and protein transformations: Strains carrying PrD-GFP under control of a Gal-inducible promoter and displaying diffuse, Ring- or Dot-shaped aggregation patterns of PrD-GFP were grown in SGal media to an OD between 1 -2. For the Ring cultures this yielded the largest fraction of cells displaying Ring aggregates (~ 70 %). Harvested cell pellets were frozen before resuspension in chilled lysis buffer (50 mM Tris-HCl, pH7.4, 200 mM NaCl, 2mM TCEP, 5 % glycerol, 1 mM EDTA, 4 mM PMSF, 5 ug/ml aprotinin, 5 ug/ml leupeptin and 1 tablet of complete protease inhibitor cocktail (Roche)). An equal volume of glass beads was added to the pellet suspension and crude lysates were generated by bead-beating for 10 minutes on a Qiagen tissue-lyser . Crude lysates were pre-cleared at 500 rcf for 2 min at 4 ^{o}C. The total amount of PrD-GFP in different lysates was assessed by immunoblotting with a GFP antibody.

Protein Transformation: Yeast cells with an *ADE1* mutation suppressible by [*PSI*$^{+}$] (*MAT*α *leu2-3, -112 his3-11 trp1-1 ura3-1 ade1-14 can1-100* [*pin*-] [*psi*-] [*ure-o*]) were co-transformed with PrD-GFP from crude lysates of cells with diffuse, Ring- or Dot- fluorescence and a *URA3* plasmid as described (TANAKA*, et al.* 2006) and summarized here. Yeast cells were grown in 50 ml YPD at 30 °C to OD_{600} ~ 0.5 – 0.6. Cells were recovered by centrifugation at 3000 x g for 5min at 25°C, washed once with sterile distilled water, once with 1 M sorbitol, and then with SCE buffer (1M

sorbitol, 10 mM EDTA, 10 mM DTT, 100 mM sodium citrate, pH 5.8). After resuspension in 1ml of SCE buffer, cells were incubated with lyticase (200 units/ml) for 30 min at 30 °C. Spheroblasts were recovered and washed with 1M sorbitol followed by STC buffer (1 M sorbitol, 10 mM $CaCl_2$, 10 mM TrisHCl, pH 7.5) and finally resuspended in 1ml STC buffer. Twenty-five microliters of crude lysates (2 mg/mL total protein concentration) of yeast cells displaying diffuse, Ring or Dot fluorescence of PrD-GFP was mixed with a URA3 plasmid and salmon sperm DNA.Spheroblasts were added to the protein solution and incubated for 30 min at 25 °C. Fusion of spheroblasts with plasmid/protein complexes was induced by addition of 9 volumes of PEG-buffer (20% PEG 8000, 10 mM $CaCl_2$, 10 mM TrisHCl, pH 7.5), and incubation for 30 min at 25 °C. Spheroblasts were recovered and resuspended in SOS buffer (1M sorbitol, 0.25% yeast extract, 0.5% bacto-peptone, 7mM $CaCl_2$,) and incubated for 30 min at 30 °C. Recovered transformants were mixed with 7 ml URA dropout top agar (2.5% agar at 45 ^{o}C containing 1M sorbitol) and immediately poured onto URA dropout plates (containing 1M sorbitol). After incubation at 30 ^{o}C for 4-5 days, approximately 100 Ura^{+} colonies were randomly chosen and streaked onto modified YEPD plates containing 1/4 of the standard amount of yeast extract to enhance color phenotypes of [PSI^{+}] and [psi^{-}] states.

Seeding efficiency of cell lysates displaying different PrD-GFP aggregation patterns: Equilibrated crude lysates from cells displaying diffuse, Ring or Dot fluorescence of PrD-GFP were added to reaction tubes containing 5 µM of purified His-tagged PrD in 1xCRBB buffer (5 mM potassium phosphate, pH 7.4, 150 mM NaCl, 5 µg/ml aprotinin and 5 µg/ml leupeptin). The reactions were incubated at RT without agitation. Polymerization time points were harvest by

adding 2% SDS sample buffer (2x TAE, 20 % glycerol, 8 % SDS (w/v), bromophenol bue) and snap freezing them. Formation of SDS resistant aggregates was assessed by SDD-AGE and probing with a His antibody (BAGRIANTSEV*, et al.* 2006).

Immunoprecipitation: Cells expressing PrD-GFP under control of the GPD-promoter displaying diffuse PrD-GFP fluorescence ([prd-gfp-]) or Dots ([PrD-GFP+]) were grown in selective media to an OD of ~ 0,6, harvested, washed with water and finally resuspended in spheroblasting buffer (1 M sorbitol , 0.1 EDTA, 0.5 mg/ml zymolyase T-100 (Seikagaku), 20 mM DTT) and incubated the cells for 30 min at 30 ºC to remove the cell wall. After pelleting the spheroblasts, they were resuspended in IP buffer (50 mM Hepes, pH 7.5, 150 mM NaCl, 2.5 mM EDTA, 1 % Triton X-100, 40 mM NEM, 1 mM PMSF, 1 Roche inhibitor mix tablet/5 ml). Glass beads were added and beated in a bead beater for 2 min at 4 ºC. Lysates were incubated with an anti-GFP antibody and incubated for 1.5 hours at 4 ºC. Subsequently, BSA-blocked Dynal beads were added to the lystes and further incubated for 4 h at 4 ºC. After rigorous washing with IP-buffer, proteins bound to the beads were eluted with Laemmli sample buffer (50 mM Tris-HCl, pH 6.8, 2 % BME, 2 % SDS, 10 % glycerol) followed by SDS-PAGE and Coomassie brilliant blue staining.

Mass spectrometry: Proteins present in bands that were cut out of the gel, fragmented by trypsin digest and separated by HPLC (Waters NanoAcquity) using a 0.075 micron diameter column with a flow rat of 250 nl/min. The eluant from this was introduced into a linear ion trap tandem mass spectrometer (Thermo LTQ) equipped with a nanospray source. The resulting CID spectra were searched against a protein database using SEQUEST.

Alberti, S., Gitler, A.D., & Lindquist, S. (2007) A Suite of Gateway Cloning Vectors for High-Throughput Genetic Analysis in Saccharomyces Cerevisiae. *Yeast* 24(10):913-919.

Bagriantsev, S.N., Kushnirov, V.V., & Liebman, S.W. (2006) Analysis of Amyloid Aggregates Using Agarose Gel Electrophoresis. *Methods Enzymol* 412:33-48.

Banta, L.M., Robinson, J.S., Klionsky, D.J., & Emr, S.D. (1988) Organelle Assembly in Yeast: Characterization of Yeast Mutants Defective in Vacuolar Biogenesis and Protein Sorting. *J Cell Biol* 107(4):1369-1383.

Chernoff, Y.O., Lindquist, S.L., Ono, B., Inge-Vechtomov, S.G., & Liebman, S.W. (1995) Role of the Chaperone Protein Hsp104 in Propagation of the Yeast Prion-Like Factor [Psi+]. *Science* 268(5212):880-884.

Sondheimer, N. & Lindquist, S. (2000) Rnq1: An Epigenetic Modifier of Protein Function in Yeast. *Mol Cell* 5(1):163-172.

Tanaka, M., Chien, P., Naber, N., Cooke, R., & Weissman, J.S. (2004) Conformational Variations in an Infectious Protein Determine Prion Strain Differences. *Nature* 428(6980):323-328.

Tanaka, M. & Weissman, J.S. (2006) An Efficient Protein Transformation Protocol for Introducing Prions into Yeast. *Methods Enzymol* 412:185-200.

Tyedmers, J., Madariaga, M.L., & Lindquist, S. (2008) Prion Switching in Response to Environmental Stress. *PLoS Biol* 6(11):e294.

Supplemental Materials

(starting on next page)

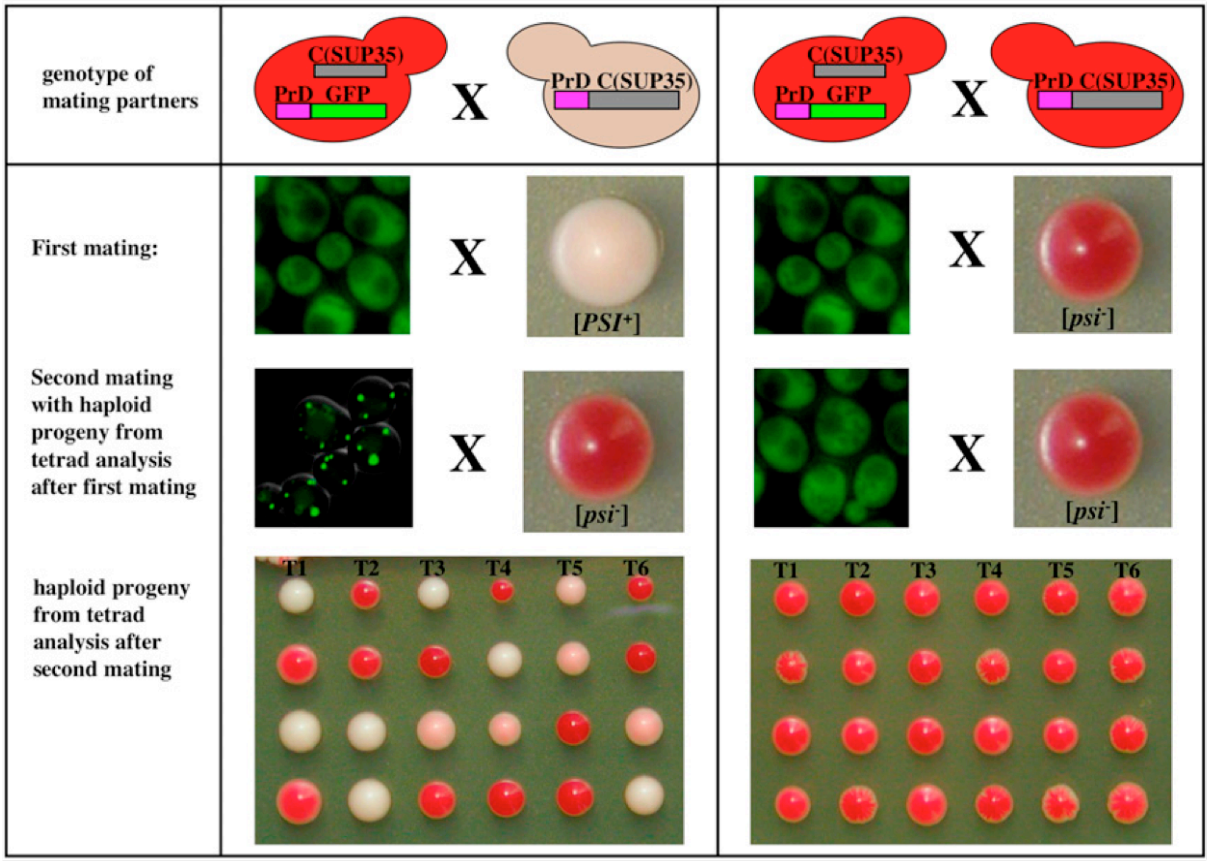

Supplemental Figure A1.1: PrD-GFP is a prion on its own right.

To reveal whether PrD-GFP can act as an independent prion, haploid strains with a deletion of PrD in the en- dogenous SUP35 gene (C(SUP35)) that expressed PrD-GFP under control of the Sup35 promoter (concentrations comparable to wild-type Sup35 (PrD-C(SUP35)) and displayed diffuse GFP fluorescence were used. A first mating involved a mating partner with wild-type Sup35 in [PSI+] to induce the prion conformation in PrD-GFP (left panel). A similar mating with a [psi-] strain served as a control (right panel). Haploid progeny from the first mating that contained the PrD-GFP fusion and the C(SUP35) allele was analyzed by fluorescence microscopy and revealed that only mating of PrD-GFP with a [PSI+] strain resulted in formation of PrD-GFP aggregates (left panel, middle). Subsequently, this progeny was mated to a [psi-] strain wild

type for SUP35 and revealed that PrD-GFP in its ag- gregated state could transmit the prion state to the wild-type SUP35 protein in a mating partner (bottom, left panel).

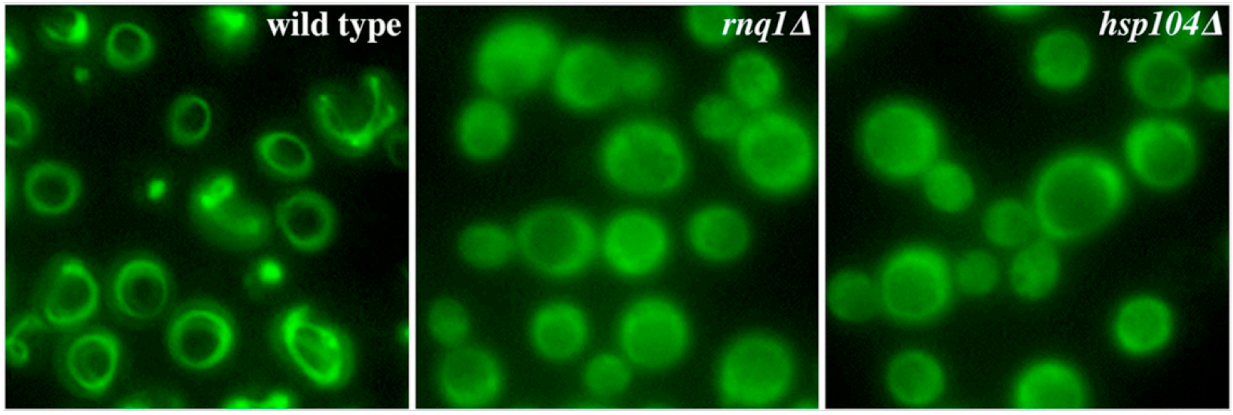

Supplemental Figure A1.2: The formation of Ring aggregates and Dot aggregates requires HSP104 and RNQ1.

Constitutive expression PrD-GFP under control of the GPD promoter (compare with Fig. A) results in Ring- and Dot aggregates in a control strain (wild type), but only diffuse fluorescence or in a strain with the deletion of RNQ1 (rnq1Δ) or HSP104 (hsp104Δ).

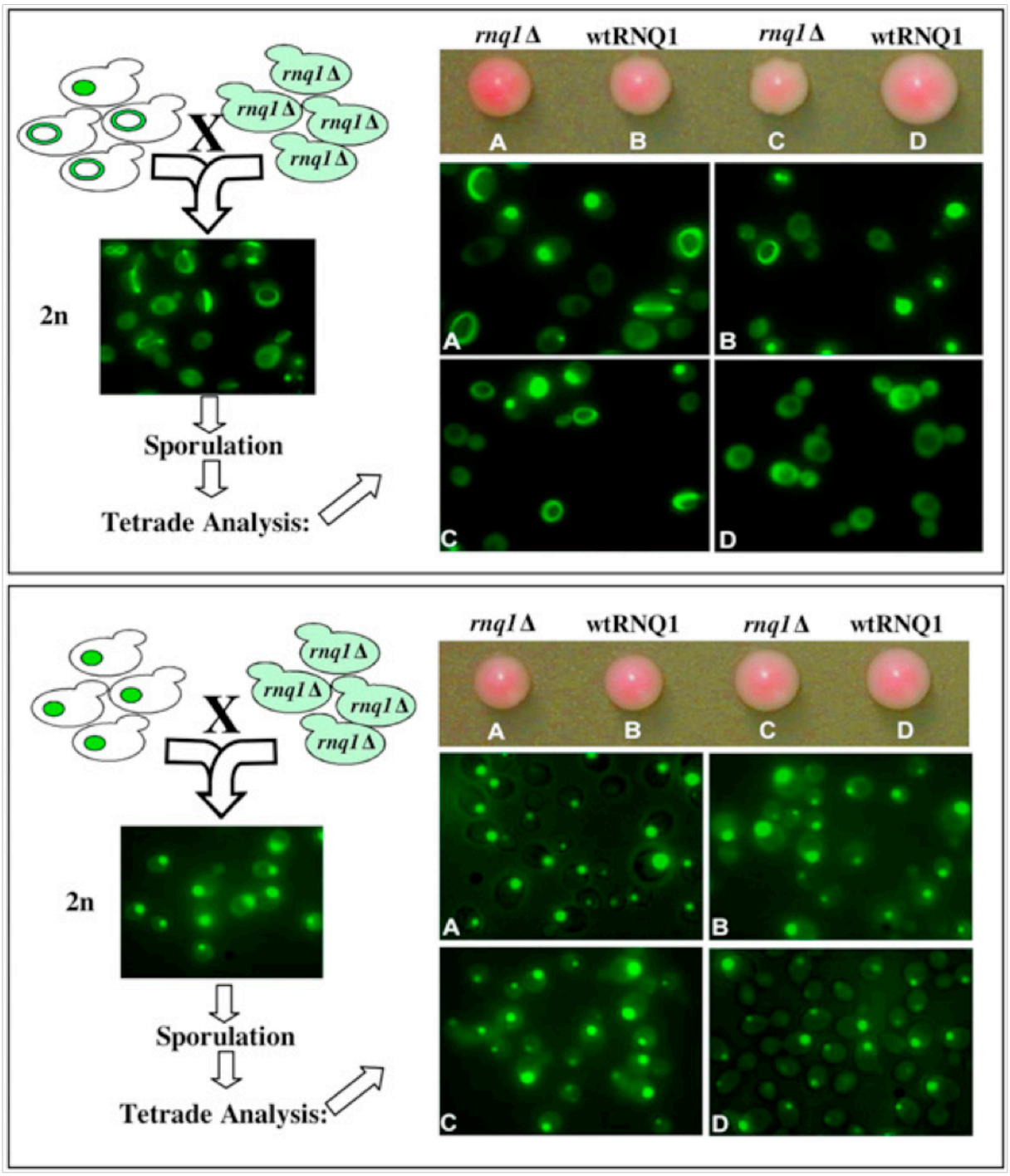

Supplemental Figure A1.3: **Both Ring and Dot aggregates can propagate in the absence of Rnq1.**

Haploid strains carrying a PrD deletion in the endogenous SUP35 gene that expressed PrD-GFP under control of the GPD promoter and displayed mostly Rings (A) or only Dots (B) were mated to an equivalent strain that carried ad- ditionally a deletion of RNQ1 and displayed diffuse PrD-GFP fluorescence (compare with Fig. S2). The resulting diploids were analyzed by fluorescence mi- croscopy and displayed mostly Ring-aggregates (A, left) or only Dots (B, left). After sporulation and tetrad analysis, spores were genotyped by PCR to detect segregation of wild-type RNQ1 (wtRNQ1) and the corresponding deletion (rnq1Δ) and analyzed for PrD-GFP-fluorescence. Rings and Dots both propagated also in the absence of RNQ1.

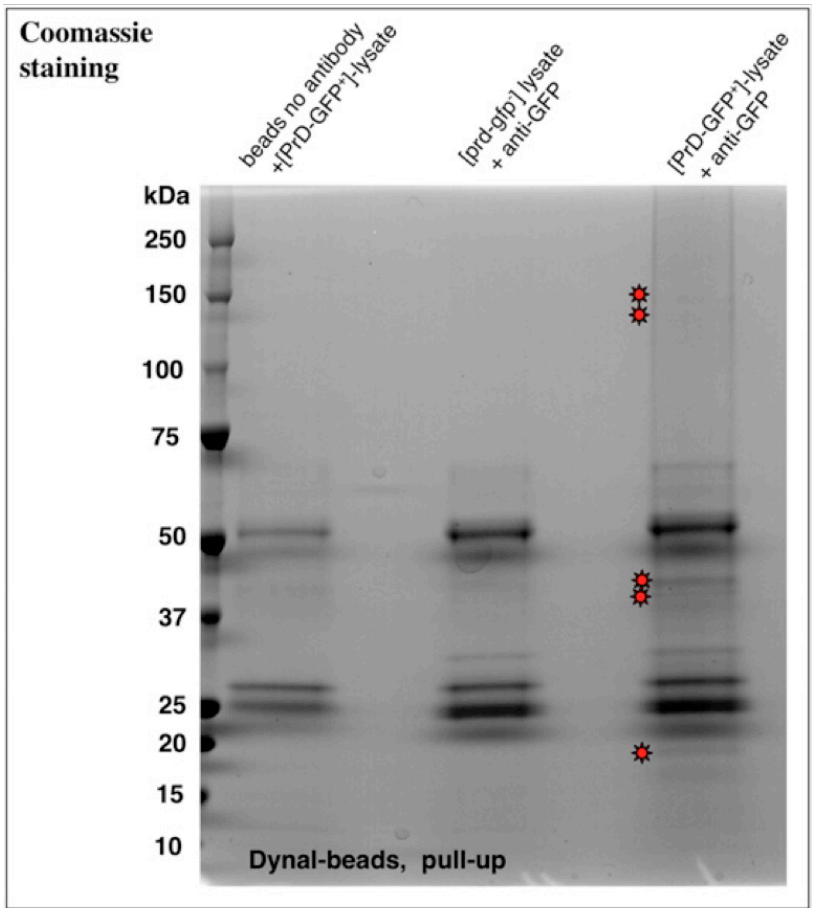

Supplemental Figure A1.4: Co-purification of proteins with PrD-GFP from cell lysates with Dot aggregates.

Coomassie stain of eluate fractions from immuno-precipitations with lysates from cells expressing PrD-GFP and displaying Dots ([PrD-GFP+]-lysates) or diffuse fluorescence ([prd-gfp-]-lysate) were incubated with no antibody (control, left lane) or antibodies against GFP (middle and right lanes). Magnetic Dynal beads coated with protein A were used to isolate antibody–protein complexes from the lysates. Stars indicate protein bands occurring specifically when lysates from cells with PrD-GFP in Dot aggregates were used. Size ranges of ~10 kDa steps were cut out of the gel from eluates of cells with diffuse fluorescence (control) and Dot fluorescence and analyzed by mass spectrometry.

Table S1. Proteins copurifying specifically with PrD-GFP Dots

METABOLIC ENZYMES AND RIBOSOMAL PROTEINS Rpl30, Rps9bp, Rpl21ap, Rpl11, Rpl4a, Rpl5	
Ade1p	Phosphoribosyl amino imidazole succinocarbozamide synthetase
Rhr2	DL-glycerol-3-phosphatase
Adh1	Alcohol dehydrogenase
Oye2	NAPDH dehydrogenase (old yellow enzyme), isoform 2
Sam2	*S*-adenosylmethionine synthetase
Eno1	Enolase I
Eno2	Enolase II
Glc7	Lactoylglutathione lyase (glyoxalase I)
Glo1	Lactoylglutathione lyase (glyoxalase I)
Sah1	Putative *S*-adenosyl-L-homocysteine hydrolase
Cdc19	Pyruvate kinase
Pdc1	Pyruvate decarboxylase
Ded81	Asparaginyl-tRNA synthetase
Tkl1	Transketolase 1
Ade3	Cytoplasmic trifunctional enzyme C1-tetrahydrofolate synthase
CHAPERONES	
Sis1	Type II HSP40 co-chaperone that interacts with the HSP70 protein Ssa1p
Ydj1	Protein chaperone; member of the DnaJ family
Cph1	Cytoplasmic peptidyl-prolyl cis-trans isomerase
CYTOSKELETON	
Nap1	Regulation of microtubule dynamics during mitosis; controls bud morphogenesis
Bni1	Formin, nucleates the formation of linear actin filaments
Arc19	Subunit of the ARP2/3 complex, motility and integrity of cortical actin patches
PROTEASOME	
Pre3	20S proteasome β-type subunit,
Pre1	20S proteasome β-type subunit
OTHER	
Rnq1	[PIN(+)] prion
Ypt1	Ras-like small GTPase, involved in the ER-to-Golgi step of the secretory pathway
Sgn1	Cytoplasmic RNA-binding protein; may have a role in mRNA translation

Supplemental Table A1.1: Table of proteins present only in protein bands isolated from Dot cell lysates but not cell lysates with diffuse PrD-GFP fluorescence. At least two different peptides of each listed protein were identified by mass spectrometry.

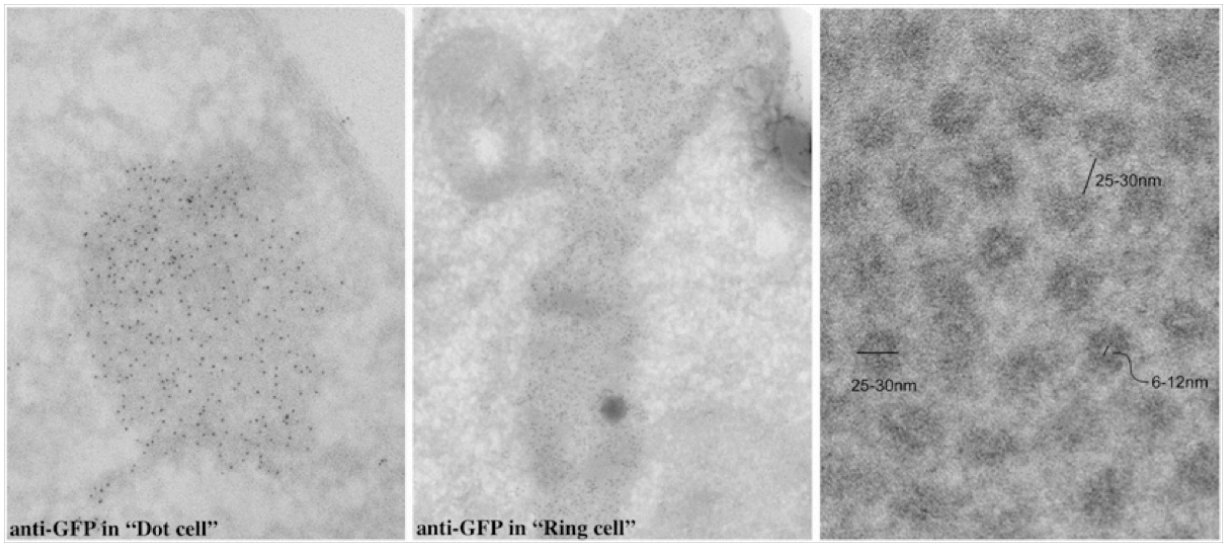

Supplemental Figure A1.5: Characterization of PrD-GFP in Ring- or Dot aggregates by immuno-EM and determination of the dimensions in PrD-GFP fibrils.

(A) Ultrathin sections of a cell with Dots (left) or Rings (right) were analyzed by immuno-EM with an antibody against GFP labeled with immunogold and confirmed that PrD-GFP is present in areas with accumulated fibrils. **(B)** Magnification of perpendicular section of a Ring aggregate allows measuring the diameter of the inner core of the fibril (6–12 nm), the entire fibril (25–30 nm), and the spacing between two fibrils (25–30 nm). Identical measures were found for bundles of fibrils from Dot aggregates.

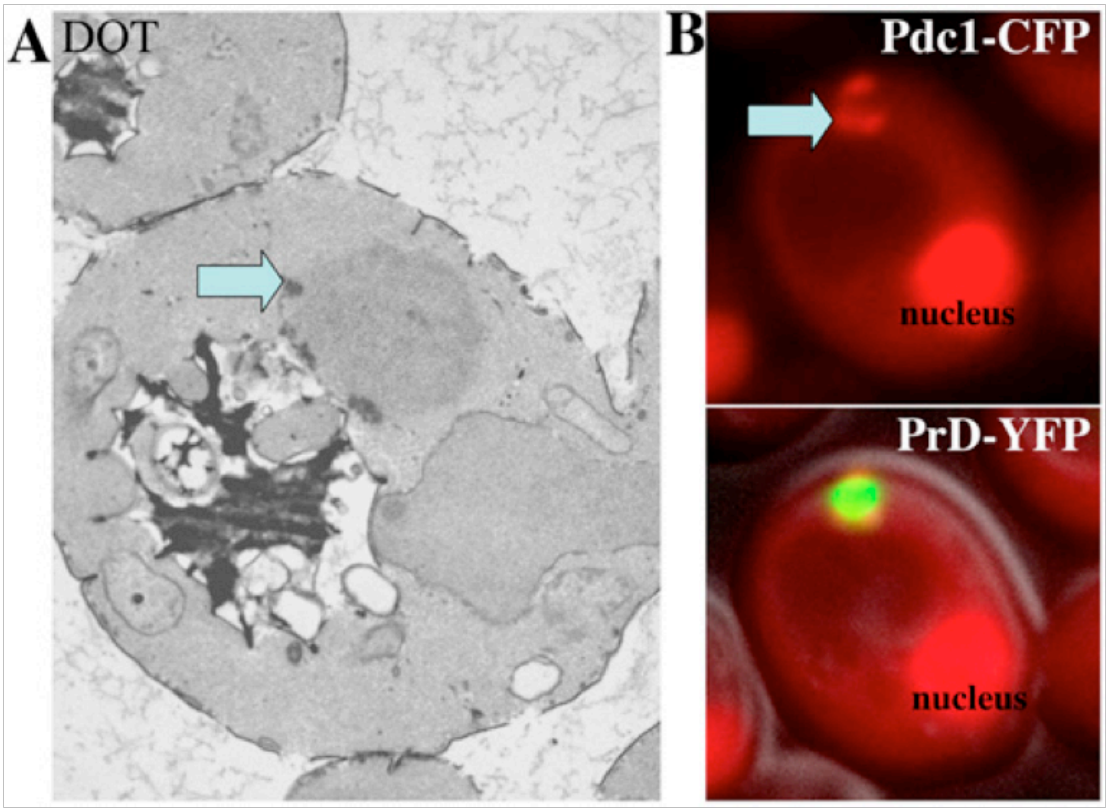

Supplemental Figure A1.6: Prion fibril accumulations at the IPOD are partially surrounded by electron-dense material typical for amorphously aggregated proteins.

A different cutout of the same DOT-cell as shown in the electron micrograph in Fig. 5A Lower Left is compared with a magnification of Fig. 4B, right column. The latter displays a fluorescence microscopy image of cells expressing PrD-YFP and Pdc1-CFP after incubation with low concentrations of menadione (0.1 mM) for 4 h.

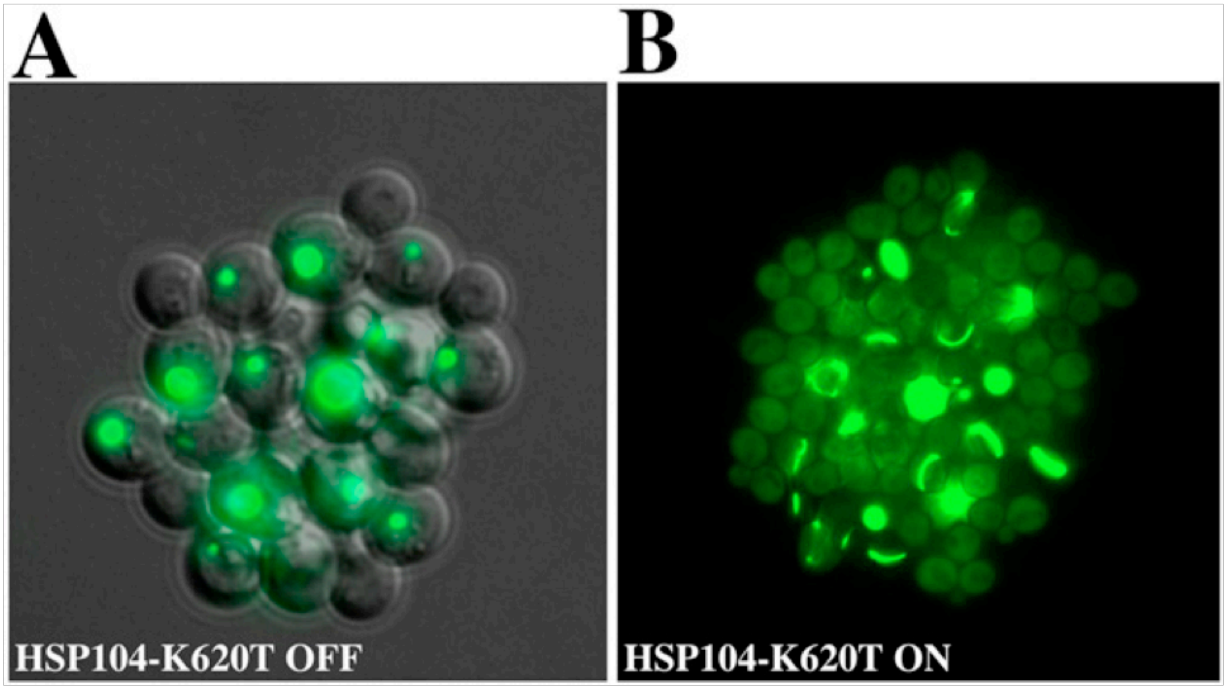

Supplemental Figure A1.7: **Expression of the dominant negative HSP104 mutant K620T induces the formation of PrD-GFP Rings in the progeny of Dot-containing cells.**

A haploid strain with a deletion of PrD in the endogenous SUP35 gene that expressed PrD-GFP under control of the GPD promoter and propagated the Dot state was transformed with a plasmid coding for the dominant negative HSP104 mutant HSP104-K620T [Parsell DA, Sanchez Y, Stitzel JD, Lindquist S (1991) Nature 353:270–273] under control of a glucocorticoid inducible promoter [Schirmer EC, Lindquist S (1998) Methods Enzymol 290:430–444]. Cells were placed on an agarose pad on a microscope slide either lacking (A) or containing (B) 10 µM deoxycorticosterone to induce expression of the HSP104 mutant and allowed to divide for several hours. The images represent a merge of several focal planes taken at the end (12 h) of time-lapse microscopy experiments.

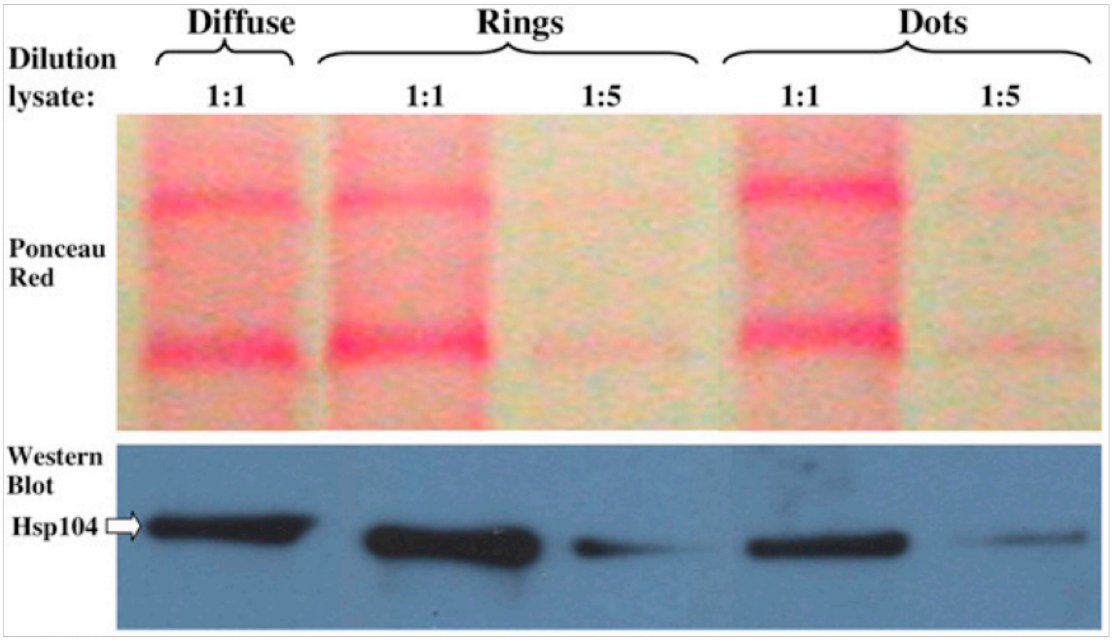

Supplemental Figure A1.8: **Similar levels of Hsp104 in cells with diffuse PrD-GFP fluorescence, PrD-GFP Rings or Dots.**

Different dilutions of cell lysates from cells displaying diffuse, Ring or Dot fluorescence were subjected to SDS/PAGE followed by Western blot analysis onto PVDF membranes. The PVDF membranes were stained with Ponceau-S (Upper) to control for loading and subsequently incubated with an antibody against Hsp104 (Lower).

Appendix Two:

Identification of malaria

Hsp40 chaperone inhibitors in yeast

This chapter was previously submitted as an R03 research grant.

Abstract

Our laboratory has used yeast to model the cellular defects caused by the human proteins implicated in neurodegenerative diseases. Furthermore, we have studied the reliance of fungal pathogens on the protein folding machinery to evolve drug resistance. Recently, we have begun to apply the lessons we learned from these two research areas to the investigation of the malaria pathogen *Plasmodium falciparum*.

The genome of *P. falciparum* is very AT-rich and consequently encodes an unusual amount of asparagine-rich proteins, predicted to be non-globular and of low complexity and thus likely to impose unique demands on the protein folding machinery. Strikingly, *P. falciparum* also shows a marked expansion of the heat shock protein 40 (Hsp40) family of co-chaperones. During its life cycle in its human host *P. falciparum* infects and remodels red blood cells. We propose that during this process the parasite relies on a greatly expanded class of Hsp40 co-chaperones.

We have developed assays to assess the function of Pf Hsp40s in yeast and we seek to identify small molecules that inhibit the functions of those chaperones. In particular we focus on a Pf Hsp40 that has been shown to be crucial to parasite proliferation. Compounds inhibiting the function of this Hsp40 in yeast will be tested in established parasite survival and host cell remodeling assays to elucidate the role of this Hsp40 in the parasite life cycle.

Specific Aims

The induction of heat shock proteins (Hsps) is one the most highly conserved homeostatic mechanisms known and is observed in all organisms, from bacteria to man. These

proteins have diverse molecular functions but all are related to solving problems in protein folding. When pathogens enter their hosts the sudden change in temperature, and ensuing fevers in the host, create a crisis in protein folding that causes an extreme dependence on Hsps.

Plasmodium falciparum causes the most severe form of human malaria and is responsible for the majority of casualties. The genome of *P. falciparum* is very AT-rich and consequently encodes an unusual amount of asparagine-rich proteins, predicted to be non-globular and of low complexity and thus likely to impose unique demands on the protein folding machinery. Strikingly, *P. falciparum* also shows a marked expansion of the heat shock protein 40 (Hsp40) family of co-chaperones. During its life cycle in its human host Pf infects and remodels red blood cells. We propose that during this process the parasite relies on the greatly expanded class of Hsp40 co-chaperones to not only remodel the infected red blood cells but also to cope with the misfolding of asparagine-rich proteins.

We have developed assays to assess the function of Pf Hsp40s, using yeast as a convenient discovery platform, and seek to identify small molecules that inhibit the functions of these proteins. For the purpose of this grant we focus on the Pf Hsp40, PFA0660w, which has been shown to be essential for parasite proliferation, but also provide preliminary results for other Pf Hsp40s. The compounds suppressing PFA0660w function will be used as probes to investigate the role of the Hsp40 PFA0660w in parasite biology and to explore their potential as therapeutic targets.

<u>Specific Aim 1 (Primary HTS assay): Identification of small molecules that inhibit the activity of the Pf Hsp40 PFA0660w</u>

Plasmodium Falciparum exports several Hsp40s to remodel its red blood host cell. Of those the Hsp40 PFA0660w (GeneID: 813268) has been suggest to be required for parasite survival. Expression of this Hsp40 is very toxic in yeast, and this toxicity depends upon its functional interaction with yeast Hsp70interaction. This toxicity provides us with an assay of PFA0660w function that can be easily used to screen for inhibitors. In conjunction with the Outreach Lab at the Broad Institute, a designated MLPCN center, we have adapted this phenotypic assay for a 384-well based small molecule screen and have already completed initial tests of assay robustness. We propose to screen the MLPCN small molecule collection for specific inhibitors of Hsp40 PFA0660w activity.

According to listings available on Pubchem no screens specifically targeting Pf Hsp40 function have been performed to date. The proposed screen would be carried out at the Broad Institute MLPCN screening center.

Specific Aim 2 (Secondary assay): Elimination of identified small molecules toxic to human cells

While yeast survival screens are particularly suited to the discovery of target-specific small molecules that are non-cytotoxic, we will specifically eliminate compounds that are inherently toxic to human cells. To do so, we will test the effect of the small molecules identified under Aim 1 on the survival of non-transformed human fibroblasts. Compound cytotoxicity will be assessed using commercially available MTT cell proliferation and ToxiLight assay kits. This kit provides a quantitative measurement of cytotoxicity based on the detection of Adenylate Kinase released to the cell culture medium due to a loss in cell integrity.

Specific Aim 3 (Secondary assay): Testing the efficacy of identified small molecules on parasites in culture

To test the effect of identified Hsp40 inhibitors on *P. falciparum* we will use a previously established high-throughput growth assay (BANIECKI*, et al.* 2007). The assay takes advantage of the fact that the parasite proliferates within DNA-less red blood cells. Consequently the fluorescent DNA staining dye DAPI can be used to measure DNA content and hence growth of blood-stage parasites. The assay is both simple and robust and has previously been used by the Broad Institute screening platform.

Specific Aim 4 (Tertiary assay): Mechanism determination using established *in vitro* chaperone assays

Lastly, we will test the ability of the small molecules identified to interfere with Hsp40 function in *in vitro* chaperone assays. Specifically, we will test if the compounds can interfere with the ability of Hsp40s to stimulate the ATPase activity of the human Hsp70 and facilitate the refolding of firefly luciferase in cooperation with the Hsp70. Both of these tests are hallmark *in vitro* assays for co-chaperone function and have been shown to be adaptable to testing modulators of Hsp40 function (FEWELL*, et al.* 2004; LU*, et al.* 1998). Using these assays we will be able to easily determine the specificity of any compound capable of inhibiting *Pf* Hsp40 dependent ATPase stimulation or luciferase refolding by also testing its effect on human Hsp40 co-chaperone function.

Significance

Malaria afflicts more than 500 million people annually (WHO 2007). It is caused by eukaryotic intracellular parasites that are spread from person to person through the bites of infected mosquitoes. Of these parasites *Plasmodium falciparum* causes the most severe form of human malaria and is responsible for the majority of casualties (RASTI, *et al.* 2004). The genome of *P. falciparum* is very AT-rich and encodes an extremely unusual number of asparagine-rich proteins. These are predicted to be non-globular and of low complexity and thus likely to impose unique demands on the protein folding machinery (ARAVIND, *et al.* 2003). Strikingly, *P. falciparum* also shows a marked expansion of the heat shock protein 40 (Hsp40) family of co-chaperones (Figure A2.1) (BOTHA, *et al.* 2007; PAVITHRA, *et al.* 2007). Hsp40s are defined by the presence of a J domain that can regulate the activity of Hsp70 chaperones. Hsp70 chaperones facilitate the folding of nascent polypetide chains, as well as the disassembly of protein structures and translocation of proteins across membranes (WALSH, *et al.* 2004). Hsp40s determine the activity of Hsp70s by stimulating Hsp70 ATPase activity and hence stabilizing their interaction with substrate proteins (QIU, *et al.* 2006). We hypothesize that these Hsp40s are crucial for *P. falciparum* pathobiology and propose to identify inhibitors of their molecular functions.

Severe malaria occurs once *P. falciparum* infects human red blood cells and starts to proliferate within them. The parasite remodels its host cell, especially the host cell membrane, in order to avoid clearance in the spleen. To accomplish these modifications, the parasite exports a wide range of proteins across its surrounding vacuolar membrane into the erythrocyte. . The “exportome” consists of 396 proteins, which ultimately allow for the

remodeling of the infected erythrocyte and thus its adherence to host endothelium (SARGEANT, *et al.* 2006). Cytoadherence of infected red blood cells is a crucial component of malaria pathogenesis as it not only circumvents splenic clearance, a part of the host immune response, but also leads to occlusion of the microvasculature in various tissues and organs (MILLER, *et al.* 2002; RASTI, *et al.* 2004).

Among the proteins exported to modify the host cell is a special group of protein folding assistants, known as the Hsp40 co-chaperones. Importantly, Hsp40 co-chaperones have undergone a marked expansion in the *P. falciparum* genome (BOTHA, *et al.* 2007; PAVITHRA, *et al.* 2007). Of the expanded number of Hsp40 co-chaperones, 19, about half, are predicted to be exported to the erythrocyte (BOTHA, *et al.* 2007). Several of these exported chaperones have very recently been shown to be essential for remodeling of the red blood cell and/or parasite viability (MAIER, *et al.* 2008). Hsp40s confer specificity to the refolding machinery by binding to particular unfolded proteins and expedite their folding by stimulating the ATPase activity of Hsp70 chaperones. No members of the Hsp70 family encoded by *P. falciparum* have been shown to be exported; as such the exported Hsp40s have been suggested to interact with the human host Hsp70 (BOTHA, *et al.* 2007; CHARPIAN, *et al.* 2008; SARGEANT, *et al.* 2006). The *Pf* proteome also has a vastly increased frequency of proteins that show an extreme bias toward a few amino acids, most notably asparagines (N), and are predicted to form non-globular, low-complexity structures. The abundance of these proteins distinguishes *Plasmodium* from most other eukaryotes (ARAVIND, *et al.* 2003). We recently characterized a specific role for the yeast Hsp40 protein Sis1 in the folding and detoxification of a N-rich prion protein (DOUGLAS, *et al.* 2008). As such, we hypothesize that the extreme abundance of N-rich proteins and the unusual

expansion of Hsp40 proteins encoded by the *P. falciparum* genome are related, with the asparagine-rich proteins requiring Hsp40s for their proper folding and function.

P. falciparum exports four Sis1-homologs, Type 2 Hsp40 chaperones, to the red blood cell (BOTHA*, et al.* 2007). Type 2 Hsp40 chaperones are defined as containing the canonical Hsp40 J-domain, GF region and C-terminal domain. Of the four Sis1-homologs, PFA0660w (GeneID: 813268) is the only one that appears to be essential for growth of the parasite in red blood cells (MAIER*, et al.* 2008). Several Type 4 Hsp40 proteins, defined by the presence of a J-domain without a complete HPD motive, are also exported. Three of these, PF11_0034, PF11_0509 and PF10_0381, appear to be essential or required for the adhesion of infected red blood cells to the endothelium.

We believe that targeting the critical interaction of *Pf* Hsp40s, and especially that of the essential PFA0660w, with the chaperone machinery of the erythrocyte will provide an entirely new therapeutic strategy and an important tool for investigating the unique biology of the parasite.

Preliminary Studies

Expression of Pf Hsp40s in *Saccharomyces cerevisiae*

To identify inhibitors of Hsp40 function we first designed phenotypic assays for *P. falciparum* Hsp40 function in *Saccharomyces cerevisiae.* Since *Plasmodium Falciparum* exhibits a different codon bias than Saccharomyces cerevisiae, we recoded the four Type 2 Hsp40s and the three Type 4 Hsp40s to facilitate their expression in yeast. Expression of the codon-optimized PFA0660w, via an inducible promoter, resulted in severe growth inhibition (Figure

A2.2). Expression of PFE0055c and PF11_0034 also resulted in moderate toxicity. Next, we asked if toxicity of the two Type 2 Hsp40s, PFA0660w and PFE0055c, depended on their functional interaction with yeast Hsp70. Hsp40s contain a J-domain with a conserved triptych HPD sequence motif that is essential for their stimulation of the ATPase domain of a partner Hsp70 (WALSH*, et al.* 2004). We found that mutations of the HPD motives in the J-domains of PFA0660w and PFE0055c alleviated toxicity (Figure A2.3). We conclude that the toxicity of PFA0660w and PFE0055c in yeast represents a readout of their chaperone function.

To further establish that the *P. falciparum* Type 2 Hsp40s could function as chaperones in yeast we tested if they could complement the loss of the essential yeast Hsp40 Sis1. We utilized a strain deleted for Sis1 whose growth was maintained by a counter-selectable plasmid carrying Sis1. We constitutively expressed the four *P. falciparum* Sis1 homologs, selected against the presence of the Sis1 plasmid and assayed strain growth. Of the four Sis1 homologs only PFE0055c could complement for Sis1 (Figure A2.4). As expected the HPD mutant of PFE055c could not maintain growth. Consequently, PFE0055c can function as a Hsp40 co-chaperone in yeast.

Development of a PFA0660w growth assay

Screening for small molecule suppressors of toxicity eliminates compounds that are toxic on their own. Since PFA0660w appears to be essential and induced a very robust toxicity in yeast, we adapted the PFA0660w growth assay to a 384-well format to in order to screen for inhibitors of PFA0660w function. Toxicity of PFA0660w expression in liquid media was comparable to that seen on agar plates. Assay design and validation was carried out with the

help of the Broad Institute's Outreach Lab. In particular assay validation was carried out using the Outreach Labs small molecule 384-well pilot screen plates: two plates of natural products, two plates of biologically active compounds and one plate of commercially available compounds.

Briefly, small molecules were pinned to 384-well clear bottom polystyrene plates containing 20µl of media, then 20µl of media containing the PFA0660w harboring yeast strain were overlaid; yielding 40µl media per well with a final compound concentration of 10µM. The media used was standard synthetic yeast media containing galactose as a carbon source to induce the expression of PFA0660w. After the addition of the yeast containing media, plates were grown in a humidified chamber for three days at 30 °C. The cultures do not require mixing during the 3-day incubation period. Cells were then resuspended by mild vortexing of the plates and cell density was measured based on absorbance at 600nm using a plate reader.

The assay was not affected by 10µM DMSO and was used as a negative control. Two-percent glucose, which represses the expression of PFA0660w in our inducible yeast system, was used as a positive control. The assay showed great between-plate and day-to-day robustness. The Z factor ranged between .766 and .857 for different pilot screen plates screened on different days.

Validation of the PFA0660w assay using a collection of putative anti-malaria compounds

The screening platform at the Broad Institute has previously conducted a small molecule screen for inhibitors of parasite proliferation in red blood cell culture. This screen was based on a similar assay described under Aim 3 but did not encompass the large MLPCN compound

collection that we propose to screen using our more directed and certainly cheaper yeast-based assay. To test whether our PFA0660w assay could result in the identification of compounds that show activity against *P. falciparum* in culture we screened the collection of putative anti-malarials identified by the Broad.

This screen of 460 compounds resulted in 13 hits, of which 10 reproduced in individual retests. The compounds suppressing PFA0660w toxicity did not affect our galactose-based expression system and did not suppress the growth defect caused by the expression of another unrelated protein under identical assay conditions. In fact, three of these hits showed such strong rescue of PFA0660w toxicity (average screen Z-scores ranging from 5.4 to 8.7) that we will use them as positive controls in the future.

This specific validation screen proves that our yeast based PFA0660w growth assay is capable of identifying small molecules with anti-malarial activity. Yet following their identification in the Broad screen this subset of compounds was not pursued as anti-malarials, as they either exhibited low IC50s or were toxic to human fibroblasts. As our screen of this small collection resulted in several positives, we are likely to identify further compounds with anti-malaria activity by screening a larger collection of compounds, some of which may have better IC50s than the compounds previously identified.

Research Design and Methods

Specific Aim 1 (Primary HTS assay): Identification of small molecules that inhibit the activity of the Pf Hsp40 PFA0660w

The yeast strain W303 harboring a single copy vector with codon optimized PFA0660w under the control of the inducible Gal1 promoter will be pre-grown in non-inducing raffinose media over night. Cultures will be diluted to an OD of 0.2 and grown for 4 hours to yield mid-log cultures ideal for reproducible galactose induction. Meanwhile, compound will be transferred into 20µl of yeast media in 384-well clear bottom polystyrene plates using a pinning robot transferring 100nl of compound per well. 20µl per well of the mid-log cultures of the PFA0660w yeast strain will then be overlaid using a peristaltic pump driven plate filler. The plates do not require mixing once the yeast cultures have been added. Plates will then be incubated for 3 days at 30 °C in a humidified chamber to prevent evaporation of the liquid media. After the incubation period the cells, which will have grown at the bottom of the plates, will be briefly re-suspended by vortexing the plates in a plate vortexer. Cell density in each well will then be measured as OD 600nm using a plate reader with an attached plate stacker.

Small molecules will be called as hits if their Z scores are higher than 2. Hits will be cherry picked and tested non-specific effects in yeast growth assays such as suppression of galactose induction. Briefly, a strain expressing a toxicity inducing protein unrelated to PFA0660w will be used to test for unspecific effects of the hits on yeast growth assays. This control assay is identical to the PFA0660w screen in setup and execution.

Yeast strains and media can easily be supplied to the MLPCN screening center. Their cost is negligible compared to the baseline cost per well screened.

<u>Specific Aim 2 (Secondary assay): Elimination of identified small molecules toxic to human cells</u>

Identified hits cytotoxic to human cells but not to yeast cells may result in false positives in the later malaria parasite assay. As such we will eliminate compounds that are toxic to non-transformed human fibroblasts. All small molecules identified under Aim 1 as specifically suppressing the toxicity of PFA0660w expression will be tested unless they have been previously annotated as being cytotoxic.

We will examine compound cytotoxicity using two commercially available assays: the ATCC MTT cell proliferation assay and the Lonza ToxiLight BioAssay. The MTT assay measures cell proliferation based on the ability of metabolically active cells to reduce the yellow tetrazolium MTT. The ToxiLight assay provides a quantitative measurement of cytotoxicity based on the detection of Adenylate Kinase released to the cell culture medium due to a loss in cell integrity. Serial dilutions of the compounds, centered on the screening concentration of 10μM, will be added to primary human fibroblasts seeded in 96-well plates. After an incubation of 24 hours the MTT and ToxiLight assays will be performed to measure cell proliferation and viability. The amount of serial dilutions per compound will be determined based on the number and availability of small molecules to be tested.

<u>Specific Aim 3 (Secondary assay): Testing the efficacy of identified small molecules on parasites in culture</u>

To determine if the identified suppressors of PFA0660w toxicity have anti-malaria activity, we will test their effects on the proliferation of blood-stage *P. falciparum*. We will use a previously established high-throughput growth assay (BANIECKI*, et al.* 2007) that has been in use at the Broad Institute screening facility. This simple and robust assay uses the fluorescent DNA

staining dye DAPI to measure DNA content and hence growth of blood-stage parasites. Compounds will be added to media containing 96 or 384-well plates, depending on the number of hits to be tested. Synchronized ring-stage parasite cultures will be added to plates with and without the compounds. Following 72 h of incubation, DAPI will be added to detect and quantify the amount of parasites present using a fluorescence plate reader.

Specific Aim 4 (Tertiary assay): Mechanism determination using established *in vitro* chaperone assays.

Finally, we will test the ability of the identified small molecules to directly interfere with Hsp40 function using *in vitro* chaperone assays. Activity of Hsp40s can be monitored *in vitro* based on their ability to stimulate the ATPase activity of Hsp70 chaperone and their ability to facilitate the refolding of denatured luciferase.

We not only codon optimized PFA0660w for its expression in yeast, but also made sure that it would be fit to be expressed and purified from *E. Coli*. Purified PFA0660w and human Hsp70 will be incubated with [^{32}P] ATP in the presence or absence of the small molecules for 10min at 30 °C. ADP formation will be measured using thin layer chromatography on polyethyleneimine cellulose plates(13). To measure luciferase refolding the chaperones PFA0660w and human Hsp70 will be incubated with chemically denatured luciferase in the presence or absence of the compounds for 30 min at 25 °C. The refolding of luciferase can be monitored using a standard luminometer.

Compounds capable of inhibiting chaperone activity in these assays will be further tested to determine their specificity to PFA0660w. By repeating the assays using a human

Hsp40 co-chaperone instead of PFA0660w we will be able to easily determine if any compounds effect is specific to PFA0660w.

Future Plan

Compounds that suppress PFA0660w toxicity in yeast and show activity against malaria parasites in culture will be used to probe the role of the PFA0660w co-chaperone in the life cycle of the parasite. For example administration of the compounds to synchronized *P. falciparum* cultures will allow us to determine at which stage of the parasite life cycle PFA0660w is essential for parasite survival. Furthermore, we will use the identified compounds to study how the exported PFA0660w affects the malarial and host proteome in red blood cells. In particular we will examine effects on the rigidity of parasite-infected red blood cells and their adherence to endothelial surface proteins (MAIER*, et al.* 2008).

References

Aravind, L., Iyer, L.M., Wellems, T.E., & Miller, L.H. (2003) Plasmodium Biology: Genomic Gleanings. *Cell* 115(7):771-785.

Baniecki, M.L., Wirth, D.F., & Clardy, J. (2007) High-Throughput Plasmodium Falciparum Growth Assay for Malaria Drug Discovery. *Antimicrob Agents Chemother* 51(2):716-723.

Botha, M., Pesce, E.R., & Blatch, G.L. (2007) The Hsp40 Proteins of Plasmodium Falciparum and Other Apicomplexa: Regulating Chaperone Power in the Parasite and the Host. *Int J Biochem Cell Biol* 39(10):1781-1803.

Charpian, S. & Przyborski, J.M. (2008) Protein Transport across the Parasitophorous Vacuole of Plasmodium Falciparum: Into the Great Wide Open. *Traffic* 9(2):157-165.

Douglas, P.M., Treusch, S., Ren, H.Y., Halfmann, R., Duennwald, M.L., Lindquist, S., & Cyr, D.M. (2008) Chaperone-Dependent Amyloid Assembly Protects Cells from Prion Toxicity. *Proc Natl Acad Sci U S A* 105(20):7206-7211.

Fewell, S.W., Smith, C.M., Lyon, M.A., Dumitrescu, T.P., Wipf, P., Day, B.W., & Brodsky, J.L. (2004) Small Molecule Modulators of Endogenous and Co-Chaperone-Stimulated Hsp70 Atpase Activity. *J Biol Chem* 279(49):51131-51140.

Lu, Z. & Cyr, D.M. (1998) Protein Folding Activity of Hsp70 Is Modified Differentially by the Hsp40 Co-Chaperones Sis1 and Ydj1. *J Biol Chem* 273(43):27824-27830.
Maier, A.G., Rug, M., O'Neill, M.T., Brown, M., Chakravorty, S., Szestak, T., Chesson, J., Wu, Y., Hughes, K., Coppel, R.L., Newbold, C., Beeson, J.G., Craig, A., Crabb, B.S., & Cowman, A.F. (2008) Exported Proteins Required for Virulence and Rigidity of Plasmodium Falciparum-Infected Human Erythrocytes. *Cell* 134(1):48-61.
Miller, L.H., Baruch, D.I., Marsh, K., & Doumbo, O.K. (2002) The Pathogenic Basis of Malaria. *Nature* 415(6872):673-679.
Pavithra, S.R., Kumar, R., & Tatu, U. (2007) Systems Analysis of Chaperone Networks in the Malarial Parasite Plasmodium Falciparum. *PLoS Comput Biol* 3(9):1701-1715.
Qiu, X.B., Shao, Y.M., Miao, S., & Wang, L. (2006) The Diversity of the Dnaj/Hsp40 Family, the Crucial Partners for Hsp70 Chaperones. *Cell Mol Life Sci* 63(22):2560-2570.
Rasti, N., Wahlgren, M., & Chen, Q. (2004) Molecular Aspects of Malaria Pathogenesis. *FEMS Immunol Med Microbiol* 41(1):9-26.
Sargeant, T.J., Marti, M., Caler, E., Carlton, J.M., Simpson, K., Speed, T.P., & Cowman, A.F. (2006) Lineage-Specific Expansion of Proteins Exported to Erythrocytes in Malaria Parasites. *Genome Biol* 7(2):R12.
Walsh, P., Bursac, D., Law, Y.C., Cyr, D., & Lithgow, T. (2004) The J-Protein Family: Modulating Protein Assembly, Disassembly and Translocation. *EMBO Rep* 5(6):567-571.
WHO (2007) Malaria Fact Sheet. *World Health Organization Website*.

Figures

(Starting on next page)

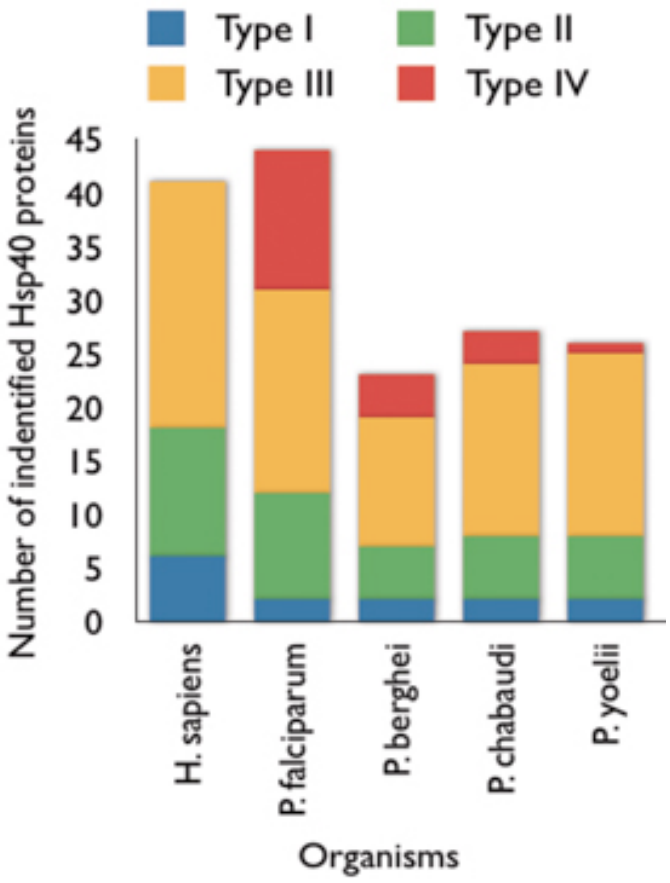

Figure A2.1: The *Plasmodium falciparum* genome has an increased abundance of Hsp40 chaperones.

Enrichment of Hsp40 chaperones in *P. falciparum* in comparison to humans and other *Plasmodia* species. Hsp40 type is determined based on the Hsp40 domains conserved. Adapted from Botha et al. *IJBCB* 2004.

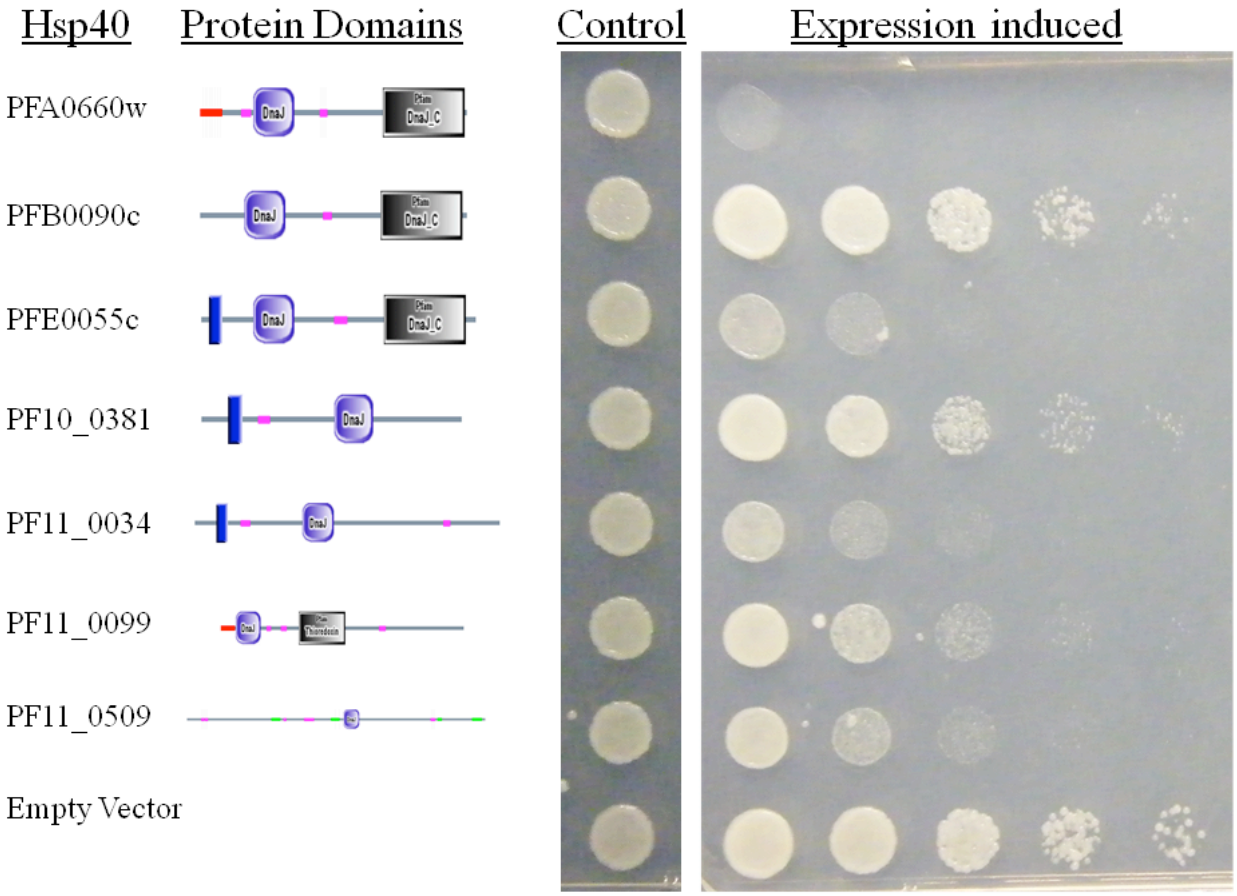

Figure A2.2: Expression of codon-optimized *P. falciparum* Hsp40s in yeast.

PFA0660w, PFB0090c, PFE0055c and PF11_0099 are Type 2 Hsp40s. PF10_0381, PF11_0034 and PF11_0509 are Type 4 Hsp40s. Proteins domains as determined by SMART are shown. Expression of PFA0660w was very toxic, while expression of PFE0055c and PF11_0034 was also moderately toxic.

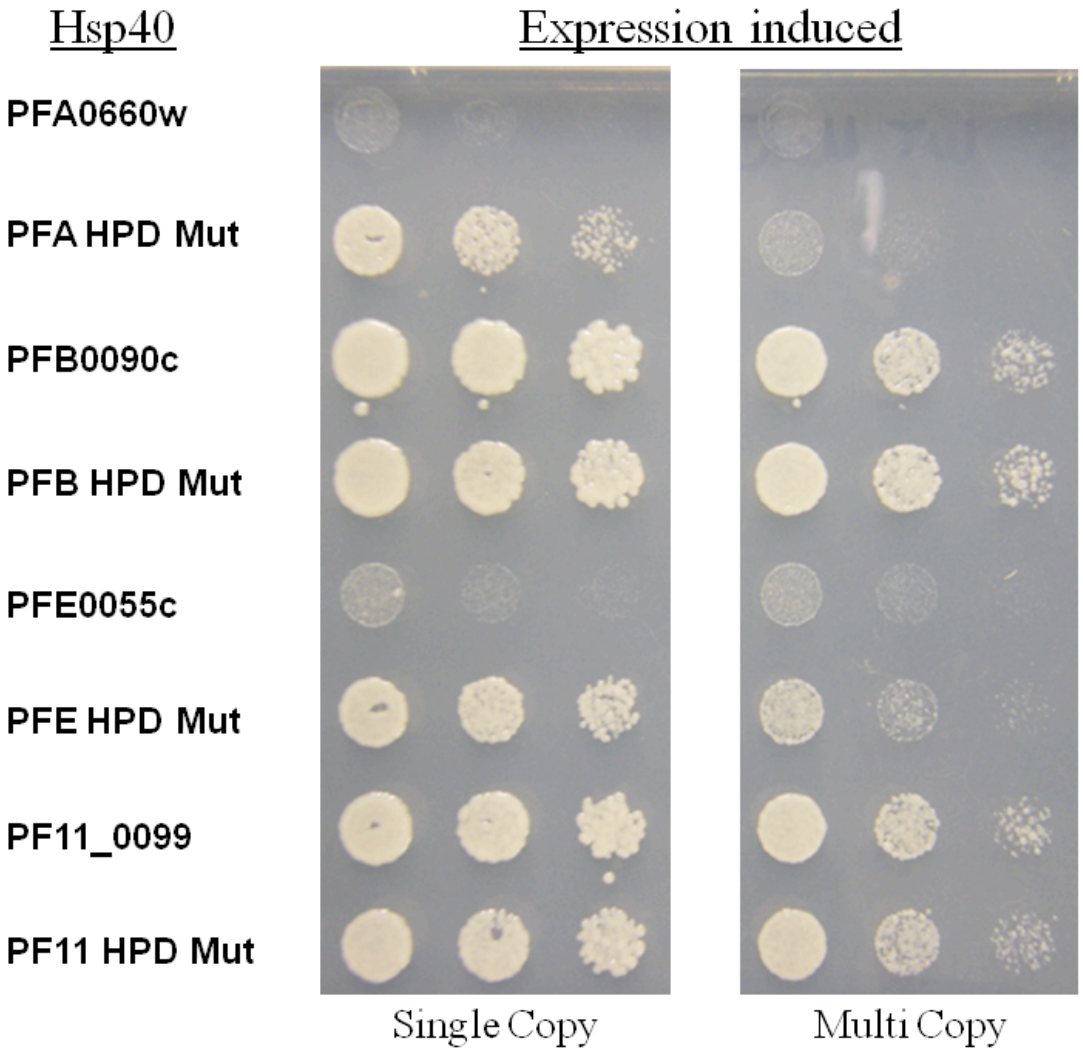

Figure A2.3: Toxicity of *P. falciparum* Hsp40s depends on chaperone function.

To determine if the toxicity of the Type 2 Hsp40s depended on their ability to interact with Hsp70 we introduced mutations in their HPD motives. The conserved HPD motive within the J-domain is required for the ability of Hsp40 co-chaperones to stimulate the ATPase activity of Hsp70s. Mutations in the HPD motives of the Hsp40s PFA0660w and PFE0550c markedly reduced their toxicity. This indicates that their toxicity is at least partially dependent on their ability to functionally interact with yeast Hsp70s.

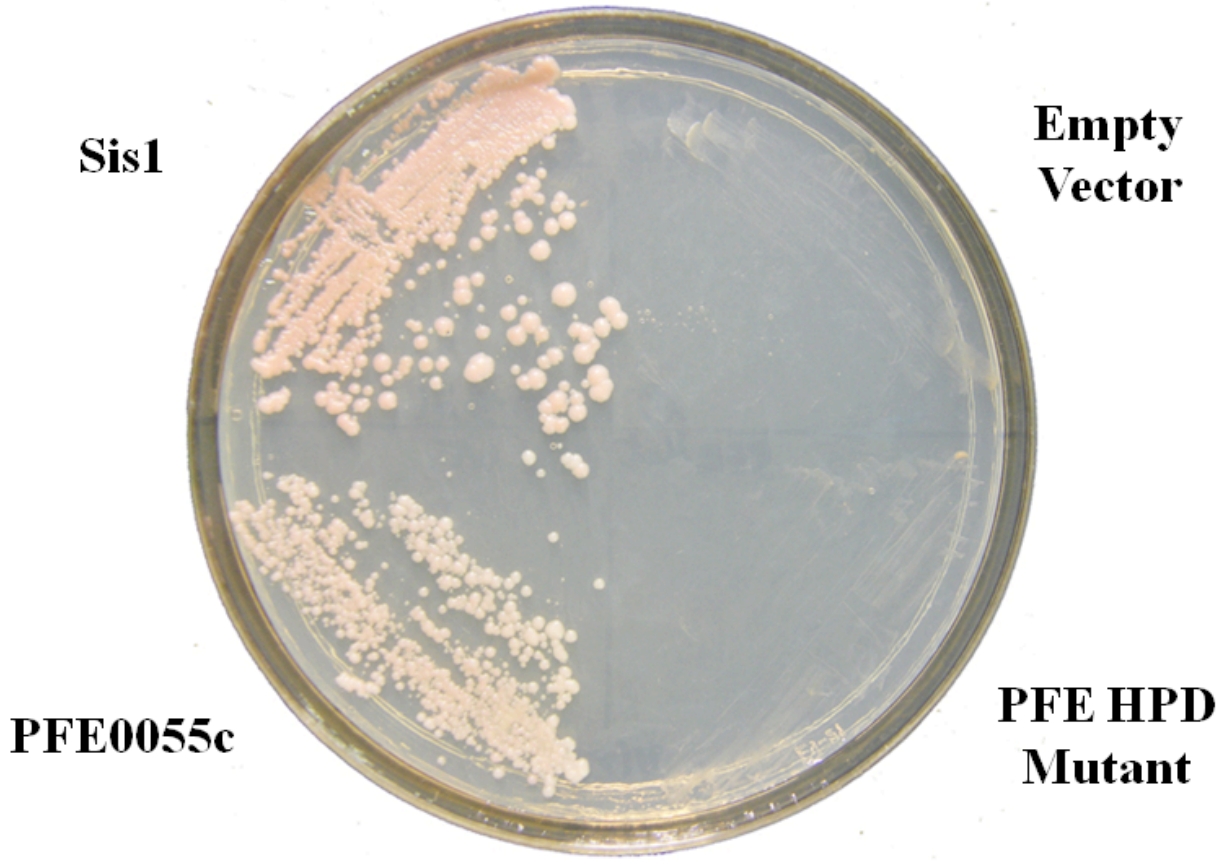

Figure A2.4: The *P. falciparum* Hsp40 PFE055c can complement the loss of the essential yeast Hsp40 Sis1.

To determine if the recoded Type 2 Hsp40s could function as chaperones in yeast we tested if they could complement the loss of the essential yeast Hsp40 Sis1. After loss of Sis1 only the expression of PFE0055c could support a moderate level of growth. As expected, the non-functional HPD mutant of PFE0055c could not complement.

Appendix Three:

Future Directions

Rnq1 and asymmetric inheritance of damaged proteins

The IPOD (insoluble protein deposit) appears to play an important role in the asymmetric inheritance of irreversible misfolded and damaged proteins as it is preferentially retained in the aging mother cell (TYEDMERS, *et al.* 2010). Rnq1 amyloid is one of the key species targeted to the IPOD (KAGANOVICH, *et al.* 2008; TYEDMERS, *et al.* 2010) and can induce the amyloid formation of other proteins (DERKATCH, *et al.* 2001). Yet it remains unclear how the IPOD is formed or how misfolded proteins are specifically targeted to it. As shown by the analysis of Rnq1 toxicity suppressors containing prion domains, the amyloid conversion of these proteins must either occur at the IPOD or facilitate the targeting of these proteins to the IPOD. This raises the question whether Rnq1 plays a role in the asymmetric inheritance of protein damage. Rnq1 could interact with misfolded proteins thereby facilitating their amyloid formation and localization to the IPOD. Intriguingly, once the amyloid conversion of a misfolded protein had occurred, the self-templating properties would turn capture of the remaining misfolded protein of the same amino acid sequence into a self-enabled process.

The fact that the Hsp104 chaperone is required for the asymmetric inheritance of damaged proteins supports the notion that amyloid formation may play an important role in asymmetric inheritance (ERJAVEC, *et al.* 2007). Hsp104 is required for the maintenance and inheritance of amyloid-based yeast prions (CHERNOFF, *et al.* 1995; SHORTER, *et al.* 2005) and has been shown to facilitate amyloid formation *in vitro* (SHORTER, et al. 2004). It has not been investigated whether Rnq1 is needed for Hsp104's effect on asymmetric inheritance and longevity. In some regards it appears unlikely that

Rnq1 would be required. Hsp104 overexpression can suppress the aging defect of a *SIR2* mutant strain and Hsp104 overexpression has not been shown to influence the *in vivo* prion properties of Rnq1 (ERJAVEC*, et al.* 2007). Furthermore, I observed that Hsp104-GFP fusions in part localize to the IPOD even in cells that should be prion minus due to prior inhibition of Hsp104 (this is to some extent indicated in (KAGANOVICH*, et al.* 2008)). The latter itself seems worthy of additional investigation. Hsp104 could potentially be the "founding" component of the IPOD that, in a manner similar to the one described for Rnq1 above, captures misfolded proteins and triggers their self-propagating ordered amyloid assembly. Yet, given Rnq1's ability to induce the amyloid formation of other proteins, Rnq1 could very well act in concert with Hsp104.

Hence, it would be interesting to investigate how Rnq1 and its prion status affect yeast longevity. As accumulation of damaged proteins during aging could induce [*RNQ*$^{+}$] formation it would be important to abrogate Rnq1's prion forming ability for control experiments. Unfortunately, simply using a complete deletion of *RNQ1* might give rise to "side effects". It has been shown that promoter of the neighboring and divergently transcribed ORF *BIK1* extends into the *RNQ1* ORF and that deletion of *RNQ1* results in the down-regulation of *BIK1* expression (STRAWN*, et al.* 2006). Hence, it would be best to create either a targeted deletion of just the Rnq1 prion domain or to introduce a premature stop codon into the *RNQ1* ORF that prevents Rnq1 prion domain translation. Longevity of [*RNQ*$^{+}$] and [*rnq*-] strains could then be compared to that of a strain unable to form Rnq1 amyloid or any other type of Rnq1 aggregate. If Rnq1's ability to form

amyloid is found to confer increased longevity, it could then be tested if moderately expressing solely the prion domain of Rnq1 had the same effect.

Chapter Three raises the question whether the core spindle pole body (SPB) component Spc42 assembly can serve as a sensor of protein damage that delays cell cylce progression to ensure asymmetric inheritance. The effect of Rnq1 overexpression on Spc42 localization and cell viability is very profound. Cells arrested due to Rnq1 toxicity may be able to reinitiate mitosis and rebud to some extend, but progeny of these cells are likely to be aneuploid due to chromosome missegregation. Therefore, if Spc42 assembly serves as a sensor of protein damage, physiological effects ought to be more subtle than those induced by Rnq1 overexpression. But as the dosage of Spc42 appears to be tightly regulated (JASPERSEN*, et al.* 2004), protein damage would only have to alter Spc42 assembly and localization slightly to delay spindle duplication.

I attempted to use a Spc42-GFP fusion to monitor Spc42 assembly, but this approach did not allow me to detect small changes in the rate or amount of Spc42 assembly. I was able to observe that various proteotoxic conditions resulted in what appeared to misoriented spindles (late stage dividing cells in which the SPBs were not properly segregated to the mother and daughter cells), but I could not reliably detect overt mislocalizations of Spc42. The amount of Spc42 molecules per cell is relatively low, making it difficult to detect Spc42-GFP in anything but clear foci. As such a more sensitive assay for measuring Spc42 assembly or detecting its localization throughout the cell is needed to further explore this question. FRET between Spc42 and other interacting SPB components, for instance Spc29, may provide a reliable readout of

proper SPB assembly. Fluorescence correlation spectroscopy, which has been previously used to monitor the dynamics of yeast prion protein oligomers *in vivo* (KAWAI-NOMA, et al. 2006), could be used to measure the rate of movement of a Spc42-GFP fusion throughout the cell.

Another approach to examine how misfolded proteins can influence Spc42 assembly and localization would be to determine the molecular basis of the Rnq1::Spc42 interaction. Spc42 is a highly phosporylated coiled-coil protein and SPB assembly appears to be governed largely by coiled-coil interactions (DONALDSON*, et al.* 1996; ZIZLSPERGER*, et al.* 2010). Intriguingly, a recent study investigated the role of coiled-coils in the aggregation and conformational switching of prion proteins and polyQ proteins (FIUMARA*, et al.* 2010). Decreasing or enhancing the propensity to form coiled-coils altered the extent of aggregation accordingly. A region within Rnq1's prion domain was predicted to form a coiled-coil and furthermore proteins interacting with mutant huntingtin were also shown to contain coiled coil domains (FIUMARA*, et al.* 2010). This suggests that the interaction between Rnq1 and Spc42 may be mediated by a transient coiled-coil formation within the prion domain of Rnq1 as it undergoes its transition to the amyloid state.

The Keating lab at MIT has analyzed the coiled-coil interactions between various SPB components (ZIZLSPERGER*, et al.* 2010; ZIZLSPERGER*, et al.* 2008). Their *in vitro* assays could easily be extended to include the predicted coiled-coils predicted within Rnq1 and other proteins prone to aggregate. We have previously shown that overexpression of just the Rnq1 prion domain itself is not toxic (DOUGLAS*, et al.* 2008). As such the

formation of the predicted coiled-coil within the Rnq1 prion domain may require certain sequence contexts, but it should be possible to engineer a coiled-coil starting with the predicted amino acid sequence. These experiments would not only allow us to determine which precise protein contacts determine the Rnq1::Spc42 interaction, but would answer how specific this type of interaction is. Does the Rnq1 coiled-coil mimic coiled-coils formed by other SPB components? Can other proteins prone to misfold and aggregate form similar coiled-coils? The results could then be used to design further experiments aimed at investigating how and under which conditions coiled-coil interactions with misfolded proteins may impede SPB assembly.

Yeast model of Abeta toxicity

The identification of genetic modifiers of Abeta toxicity using our yeast model opens the door for a wide range of additional investigations. Since many of them are already ongoing I will discuss them rather briefly.

First of all, it will be important to determine if screen hits besides PICALM can suppress the toxicity of Abeta oligomers on primary cortical neurons. Subsequently, it will be interesting to investigate how the various genetic suppressors function to counteract toxic Abeta species. Jessica Goodmann, a postdoc in the lab, is characterizing the oligomeric species formed by Abeta expressed in yeast. If any of these oligomeric species are proteotoxic, we may find that our genetic suppressors alter the ratios of the Abeta species formed. For the genes that can counteract Abeta oligomer toxicity in

neuron cultures, one could test how they influence the binding and internalization of labeled Abeta oligomers to and into neuronal cells.

We also have begun to collaborate with Li-Heui Tsai's group to test the genetic suppressors of Abeta toxicity in mouse models of AD. We (in particular Shu Hamamichi in collaboration with Damien Rei and Johannes Graeff of the Tsai lab) hope to test if the suppressors can ameliorate the neuronal degeneration and behavioral phenotypes observed in AD mouse models such as 5xFAD mice. 5xFAD mice exhibit intraneuronal Abeta accumulation, which may be especially interesting from the perspective of our yeast model, amyloid plaque formation, neurodegeneration, and memory loss (OAKLEY, *et al.* 2006). We will administer select genetic suppressors, beginning with PICALM, using AVV vectors and will later score the extent of neuron loss and memory decline.

Furthermore, we hope to discern if rare mutations in the homologs of our alpha-synuclein and Abeta screen hits contribute to Alzheimer's and Parkinson's disease (COOPER, *et al.* 2006; YEGER-LOTEM, *et al.* 2009). Vikram Khurana and I have assembled lists of hit homologs to be sequenced for Parkinson's and Alzheimer's disease, respectively. This analysis will require intricate multi-plexing of sequencing runs and computational analyses to filter out false positives. Our effort is aided by Whitehead fellow Yaniv Erlich. Yaniv is an expert on high-throughput sequencing analysis aimed at the identification of rare disease variants (EDVARDSON, *et al.* 2010; ERLICH, *et al.* 2009). Vikram and Sue are currently procuring funding and clinical samples to be sequenced.

Finally, our yeast model may enable us to determine how clioquinol and other metal chelators can detoxify Abeta in a cellular setting. It was found that yeast exposure

to clioquinol induces a metal starvation response in yeast, but those experiments used highly toxic concentrations of clioquinol (Li*, et al.* 2010). Kent Matlack and I have performed gene expression analysis to decipher the responses elicited by concentrations of clioquinol capable of suppressing Abeta toxicity. Elena Nabieva has begun to compare these results to the gene expression profile elicited by Abeta expression. The hope is that these microarray data will pinpoint particular genes that are required for the efficacy of clioquinol-based suppression. We will then test if the effect of clioquinol on Abeta toxicity can be mimicked by genetic manipulation of these genes.

References

Chernoff, Y.O., Lindquist, S.L., Ono, B., Inge-Vechtomov, S.G., & Liebman, S.W. (1995) Role of the Chaperone Protein Hsp104 in Propagation of the Yeast Prion-Like Factor [Psi+]. *Science* 268(5212):880-884.

Cooper, A.A., Gitler, A.D., Cashikar, A., Haynes, C.M., Hill, K.J., Bhullar, B., Liu, K., Xu, K., Strathearn, K.E., Liu, F., Cao, S., Caldwell, K.A., Caldwell, G.A., Marsischky, G., Kolodner, R.D., Labaer, J., Rochet, J.C., Bonini, N.M., & Lindquist, S. (2006) Alpha-Synuclein Blocks Er-Golgi Traffic and Rab1 Rescues Neuron Loss in Parkinson's Models. *Science* 313(5785):324-328.

Derkatch, I.L., Bradley, M.E., Hong, J.Y., & Liebman, S.W. (2001) Prions Affect the Appearance of Other Prions: The Story of [Pin(+)]. *Cell* 106(2):171-182.

Donaldson, A.D. & Kilmartin, J.V. (1996) Spc42p: A Phosphorylated Component of the S. Cerevisiae Spindle Pole Body (Spd) with an Essential Function During Spb Duplication. *J Cell Biol* 132(5):887-901.

Douglas, P.M., Treusch, S., Ren, H.Y., Halfmann, R., Duennwald, M.L., Lindquist, S., & Cyr, D.M. (2008) Chaperone-Dependent Amyloid Assembly Protects Cells from Prion Toxicity. *Proc Natl Acad Sci U S A* 105(20):7206-7211.

Edvardson, S., Shaag, A., Zenvirt, S., Erlich, Y., Hannon, G.J., Shanske, A.L., Gomori, J.M., Ekstein, J., & Elpeleg, O. (2010) Joubert Syndrome 2 (Jbts2) in Ashkenazi Jews Is Associated with a Tmem216 Mutation. *Am J Hum Genet* 86(1):93-97.

Erjavec, N., Larsson, L., Grantham, J., & Nystrom, T. (2007) Accelerated Aging and Failure to Segregate Damaged Proteins in Sir2 Mutants Can Be Suppressed by

Overproducing the Protein Aggregation-Remodeling Factor Hsp104p. *Genes Dev* 21(19):2410-2421.

Erlich, Y., Chang, K., Gordon, A., Ronen, R., Navon, O., Rooks, M., & Hannon, G.J. (2009) DNA Sudoku--Harnessing High-Throughput Sequencing for Multiplexed Specimen Analysis. *Genome Res* 19(7):1243-1253.

Fiumara, F., Fioriti, L., Kandel, E.R., & Hendrickson, W.A. (2010) Essential Role of Coiled Coils for Aggregation and Activity of Q/N-Rich Prions and Polyq Proteins. *Cell* 143(7):1121-1135.

Jaspersen, S.L. & Winey, M. (2004) The Budding Yeast Spindle Pole Body: Structure, Duplication, and Function. *Annu Rev Cell Dev Biol* 20:1-28.

Kaganovich, D., Kopito, R., & Frydman, J. (2008) Misfolded Proteins Partition between Two Distinct Quality Control Compartments. *Nature* 454(7208):1088-1095.

Kawai-Noma, S., Ayano, S., Pack, C.G., Kinjo, M., Yoshida, M., Yasuda, K., & Taguchi, H. (2006) Dynamics of Yeast Prion Aggregates in Single Living Cells. *Genes Cells* 11(9):1085-1096.

Li, C., Wang, J., & Zhou, B. (2010) The Metal Chelating and Chaperoning Effects of Clioquinol: Insights from Yeast Studies. *J Alzheimers Dis*.

Oakley, H., Cole, S.L., Logan, S., Maus, E., Shao, P., Craft, J., Guillozet-Bongaarts, A., Ohno, M., Disterhoft, J., Van Eldik, L., Berry, R., & Vassar, R. (2006) Intraneuronal Beta-Amyloid Aggregates, Neurodegeneration, and Neuron Loss in Transgenic Mice with Five Familial Alzheimer's Disease Mutations: Potential Factors in Amyloid Plaque Formation. *J Neurosci* 26(40):10129-10140.

Shorter, J. & Lindquist, S. (2004) Hsp104 Catalyzes Formation and Elimination of Self-Replicating Sup35 Prion Conformers. *Science* 304(5678):1793-1797.

Shorter, J. & Lindquist, S. (2005) Prions as Adaptive Conduits of Memory and Inheritance. *Nat Rev Genet* 6(6):435-450.

Strawn, L.A. & True, H.L. (2006) Deletion of Rnq1 Gene Reveals Novel Functional Relationship between Divergently Transcribed Bik1p/Clip-170 and Sfi1p in Spindle Pole Body Separation. *Curr Genet* 50(6):347-366.

Tyedmers, J., Treusch, S., Dong, J., McCaffery, J.M., Bevis, B., & Lindquist, S. (2010) Prion Induction Involves an Ancient System for the Sequestration of Aggregated Proteins and Heritable Changes in Prion Fragmentation. *Proc Natl Acad Sci U S A* 107(19):8633-8638.

Yeger-Lotem, E., Riva, L., Su, L.J., Gitler, A.D., Cashikar, A.G., King, O.D., Auluck, P.K., Geddie, M.L., Valastyan, J.S., Karger, D.R., Lindquist, S., & Fraenkel, E. (2009) Bridging High-Throughput Genetic and Transcriptional Data Reveals Cellular Responses to Alpha-Synuclein Toxicity. *Nat Genet* 41(3):316-323.

Zizlsperger, N. & Keating, A.E. (2010) Specific Coiled-Coil Interactions Contribute to a Global Model of the Structure of the Spindle Pole Body. *J Struct Biol* 170(2):246-256.

Zizlsperger, N., Malashkevich, V.N., Pillay, S., & Keating, A.E. (2008) Analysis of Coiled-Coil Interactions between Core Proteins of the Spindle Pole Body. *Biochemistry* 47(45):11858-11868.